(2)

Chemical Technology Division

ANL-92/9

ANL Technical Support Program for DOE Environmental Restoration and Waste Management

Annual Report
October 1990–September 1991

by J. K. Bates, C. R. Bradley, W. L. Bourcier, E. C. Buck, J. C. Cunnane, N. L. Dietz, W. L Ebert, J. W. Emery, R. C. Ewing, X. Feng, T. J. Gerding, M. Gong, W.-T. Han, J. C. Hoh, J. J. Mazer, L. E. Morgan, J. K. Nielsen, S. A. Steward, M. Tomozawa, L.-M. Wang, and D. J. Wronkiewicz

Argonne National Laboratory, Argonne, Illinois 60439
operated by The University of Chicago
for the United States Department of Energy under Contract W-31-109-Eng-38

MASTER

ARGONNE NATIONAL LABORATORY
Chemical Technology Division
9700 South Cass Avenue
Argonne, Illinois 60439

ANL--92-9

DE92 011753

Erratum for ANL-92/9

ANL TECHNICAL SUPPORT PROGRAM FOR DOE ENVIRONMENTAL RESTORATION AND WASTE MANAGEMENT

ANNUAL REPORT
OCTOBER 1990 - SEPTEMBER 1991

Please substitute the attached pages for the corresponding pages in the above report, which you should have recently received in the mail. In the original version, the four contributors from Lawrence Livermore National Laboratory were inadvertently omitted from the list of authors. Our sincere apologies to these individuals for this oversight.

May 1992

Distribution Category:
High Level Radioactive Waste
Disposal in Tuff
(UC-814)

ANL-92/9

ARGONNE NATIONAL LABORATORY
9700 South Cass Avenue
Argonne, Illinois 60439

ANL TECHNICAL SUPPORT PROGRAM FOR DOE ENVIRONMENTAL RESTORATION AND WASTE MANAGEMENT

ANNUAL REPORT
OCTOBER 1990 - SEPTEMBER 1991

by

J. K. Bates, C. R. Bradley, W. L. Bourcier,* E. C. Buck, J. C. Cunnane, N. L. Dietz, W. L. Ebert, J. W. Emery, R. C. Ewing,** X. Feng, T. J. Gerding, M. Gong, W.-T. Han,*** J. C. Hoh, J. J. Mazer, L. E. Morgan,* J. K. Nielsen,* S. A. Steward,* M. Tomozawa,*** L.-M. Wang,** and D. J. Wronkiewicz

Chemical Technology Division

March 1992

*Lawrence Livermore National Laboratory, Livermore, CA.
**University of New Mexico, Albuquerque, NM.
***Rensselaer Polytechnic Institute, Troy, MI.

ANL TECHNICAL SUPPORT PROGRAM FOR DOE ENVIRONMENTAL RESTORATION AND WASTE MANAGEMENT

ANNUAL REPORT
OCTOBER 1990 - SEPTEMBER 1991

by

J. K. Bates, C. R. Bradley, W. L. Bourcier,* E. C. Buck, J. C. Cunnane, N. L. Dietz, W. L. Ebert, J. W. Emery, R. C. Ewing,** X. Feng, T. J. Gerding, M. Gong, W.-T. Han,*** J. C. Hoh, J. J. Mazer, L. E. Morgan,* J. K. Nielsen,* S. A. Steward,* M. Tomozawa,*** L.-M. Wang,** and D. J. Wronkiewicz

ABSTRACT

A program has been established for DOE Environmental Restoration and Waste Management (EM) to evaluate factors that are likely to affect waste glass reaction during repository disposal, with emphasis on an unsaturated environment typical of what may be expected for the proposed Yucca Mountain repository site. This report covers progress in FY 1991 on the following tasks:

1. A critical review of those parameters that affect the reactivity of glass in an unsaturated environment is in progress. This effort involves a search of the literature to identify the important parameters. Temperature and glass compositions are the first parameters examined in detail.

2. An interface between waste producers and the repository program is being implemented.

3. A series of tests has been started to evaluate the reactivity of fully radioactive glasses in a high-level waste repository environment and compare it to the reactivity of synthetic glasses of similar composition.

4. The effect of radiation upon the durability of waste glasses at a high glass surface area-to-liquid volume (SA/V) ratio and high gas-to-liquid volume ratio will be assessed. These tests address both vapor and high SA/V liquid conditions.

5. A series of tests is being performed to compare the extent of reaction of nuclear waste glasses at various SA/V ratios. Such differences in the SA/V ratio may significantly affect glass durability.

6. Analytical electron microscopy (AEM), infrared spectroscopy, and nuclear resonant profiling are being used to assess the glass/water reaction pathway by identifying intermediate phases that appear on the reacting glass. Additionally, colloids from the leach solutions are being studied using AEM.

*Lawrence Livermore National Laboratory, Livermore, CA.
**University of New Mexico, Albuquerque, NM.
***Rensselaer Polytechnic Institute, Troy, MI.

Reproduced from the best available copy.

Available to DOE and DOE contractors from the
Office of Scientific and Technical Information
P.O. Box 62
Oak Ridge, TN 37831
Prices available from (615) 576-8401, FTS 626-8401

Available to the public from the
National Technical Information Service
U.S. Department of Commerce
5285 Port Royal Road
Springfield, VA 22161

Distribution Category:
High-Level Radioactive Waste
Disposal in Tuff
(UC-814)

ANL-92/9

ARGONNE NATIONAL LABORATORY
9700 South Cass Avenue
Argonne, Illinois 60439

ANL TECHNICAL SUPPORT PROGRAM FOR DOE ENVIRONMENTAL RESTORATION AND WASTE MANAGEMENT

ANNUAL REPORT
OCTOBER 1990 - SEPTEMBER 1991

by

J. K. Bates, C. R. Bradley, W. L. Bourcier,* E. C. Buck, J. C. Cunnane, N. L. Dietz, W. L. Ebert, J. W. Emery, R. C. Ewing,** X. Feng, T. J. Gerding, M. Gong, W.-T. Han,*** J. C. Hoh, J. J. Mazer, L. E. Morgan,* J. K. Nielsen,* S. A. Steward,* M. Tomozawa,*** L.-M. Wang,** and D. J. Wronkiewicz

Chemical Technology Division

March 1992

*Lawrence Livermore National Laboratory, Livermore, CA.
**University of New Mexico, Albuquerque, NM.
***Rensselaer Polytechnic Institute, Troy, MI.

TABLE OF CONTENTS

TABLE OF CONTENTS (contd)

TABLE OF CONTENTS (contd)

LIST OF FIGURES

LIST OF FIGURES (contd)

LIST OF FIGURES (contd)

LIST OF FIGURES (contd)

LIST OF FIGURES (contd)

LIST OF TABLES

LIST OF TABLES (contd)

ANL TECHNICAL SUPPORT PROGRAM FOR DOE ENVIRONMENTAL RESTORATION AND WASTE MANAGEMENT

ANNUAL REPORT
OCTOBER 1990 - SEPTEMBER 1991

by

J. K. Bates, C. R. Bradley, W. L. Bourcier,* E. C. Buck, J. C. Cunnane, N. L. Dietz, W. L. Ebert, J. W. Emery, R. C. Ewing,** X. Feng, T. J. Gerding, M. Gong, W.-T. Han,*** J. C. Hoh, J. J. Mazer, L. E. Morgan,* J. K. Nielsen,* S. A. Steward,* M. Tomozawa,*** L.-M. Wang,** and D. J. Wronkiewicz

ABSTRACT

A program has been established for DOE Environmental Restoration and Waste Management (EM) to evaluate factors that are likely to affect waste glass reaction during repository disposal, with emphasis on an unsaturated environment typical of what may be expected for the proposed Yucca Mountain repository site. This report covers progress in FY 1991 on the following tasks:

1. A critical review of those parameters that affect the reactivity of glass in an unsaturated environment is in progress. This effort involves a search of the literature to identify the important parameters. Temperature and glass compositions are the first parameters examined in detail.

2. An interface between waste producers and the repository program is being implemented.

3. A series of tests has been started to evaluate the reactivity of fully radioactive glasses in a high-level waste repository environment and compare it to the reactivity of synthetic glasses of similar composition.

4. The effect of radiation upon the durability of waste glasses at a high glass surface area-to-liquid volume (SA/V) ratio and high gas-to-liquid volume ratio will be assessed. These tests address both vapor and high SA/V liquid conditions.

5. A series of tests is being performed to compare the extent of reaction of nuclear waste glasses at various SA/V ratios. Such differences in the SA/V ratio may significantly affect glass durability.

6. Analytical electron microscopy (AEM), infrared spectroscopy, and nuclear resonant profiling are being used to assess the glass/water reaction pathway by identifying intermediate phases that appear on the reacting glass. Additionally, colloids from the leach solutions are being studied using AEM.

*Lawrence Livermore National Laboratory, Livermore, CA.
**University of New Mexico, Albuquerque, NM.
***Rensselaer Polytechnic Institute, Troy, MI.

7. Technical review of AEM results is being provided.

8. A study on water diffusion of nuclear waste glasses is being performed.

9. A mechanistically based model is being developed to predict the performance of glass over repository-relevant time periods.

EXECUTIVE SUMMARY

This report provides an overview of progress during FY 1991 for the Technical Support Program that is part of the ANL Technology Support Activity for DOE, Environmental Restoration and Waste Management (EM). The purpose is to evaluate, before hot start-up of the Defense Waste Processing Facility (DWPF) and the West Valley Demonstration Project (WVDP), factors that are likely to affect glass reaction in an unsaturated environment typical of what may be expected for the candidate Yucca Mountain repository site. Specific goals for the testing program include the following:

- to review and evaluate available information on parameters that will be important in establishing the long-term performance of glass in a repository environment,
- to perform testing to further quantify the effects of important variables where there are deficiencies in the available data, and
- to initiate long-term testing that will bound glass performance under a range of conditions applicable to repository disposal.

The progress made in FY 1991 on each of the technical tasks is summarized below.

Critical Review of Parameters Affecting Glass Reaction in an Unsaturated Environment

The predicted repository environment at Yucca Mountain has been described by the Yucca Mountain Site Characterization Project (YMP) as hydrologically unsaturated with possible air exchange with the neighboring biospheres. We have identified several environmental conditions that can affect the durability of waste emplaced in such an unsaturated environment over repository-relevant time periods. To date, much of the information regarding what is known about these conditions has not been synthesized for use within the waste glass research community. Thus, the need to perform such a critical review was identified, and the review is currently underway.

The purpose of this task is to review the existing literature in order to evaluate the state of knowledge regarding the influence of each of the identified critical parameters on glass reaction. Each review will be issued as stand-alone documents, and these documents will be integrated into a summary compendium document.

The technical approach used to perform this task has been to assemble all known and pertinent sources of scientific literature and then objectively and critically consider the current state of knowledge as to how each critical parameter affects nuclear waste glass reaction. A synthesis of existing data will be performed, where possible, to provide a framework for comparing the results obtained from different studies. All reviewed references used in the critical reviews have been collected in a computerized data

base. A preliminary critical review had been previously performed to provide a foundation for subsequent detailed reviews of each parameter. The first review report, detailing the effects of temperature on waste glass performance, has been completed. This report concluded that reaction mechanisms for waste glass dissolution in water are complex and involve multiple simultaneous reaction processes. The temperature dependence of each of the individual reaction processes can be described by the Arrhenius equation, a relationship derived from empirical observations. In cases where the reaction mechanism changes as a function of time or temperature (i.e., the dominant reaction process changes), the Arrhenius equation is less useful in interpreting the temperature dependence of the overall reaction mechanism. Understanding the interplay of the reaction processes and their temperature dependences for nuclear waste glasses requires a clear understanding of the reaction mechanism, which has not yet been achieved. Until a better understanding of glass reaction mechanisms is available, caution should be exercised in using temperature as an accelerating parameter in waste glass tests. The next parameter to undergo a detailed critical review is the effect of glass composition on glass durability. This review is in progress. Models of glass structure are being used to help understand how water may interact with glass.

Waste Producer/Repository Program Interface

The Waste Producer/Repository Program Interface task was established to address the connection between the Waste Acceptance Preliminary Specifications (WAPS), specification 1.3, and the waste glass performance requirements in the repository.

A strawman position paper was developed which outlined interim (i.e., prior to repository licensing) positions on waste glass performance and the connection between WAPS 1.3 and performance requirements. However, attempts to establish an interface between the waste producers and the repository program which could resolve the technical issues associated with the strawman position were not successful. The scope of the task was, therefore, changed to include preparation of a "white paper" or "compendium" which will describe the scientific basis for evaluating the behavior of waste glass under a range of conditions associated with storage, transportation, and disposal.

Long-Term Testing of Fully Radioactive Glass

The objective of this task is to evaluate the performance of fully radioactive glasses, similar to those that will be produced by the DWPF, in meeting the performance objectives for glass storage in a high-level waste repository located in an unsaturated horizon. Specifically, long-term test data will be generated such that (1) reaction of fully radioactive glass can be compared with that of nonradioactive glass of the same nominal composition; (2) interactions between waste package components that must be accounted for in independent reaction path models are identified; and (3) the long-term behavior of glass is established under anticipated unsaturated disposal conditions, such that glass performance models can be validated. To meet these goals, tests with fully radioactive glass (SRL 165/42, 131/11, and 200R compositions) and simulated (nonradioactive glass) are being done in the following modes: batch, intermittent drip, and laboratory analogue.

To date, 212 of the planned long-term batch tests have been initiated, and 100 of them have been terminated. The longest tests have been in progress for more than 19 months. The solution analyses for the terminated tests are about 90% completed, and include determination of leachate pHs, cations, selected anions, total carbon, and actinides. The surface analyses on the samples from the terminated tests are in progress. These analyses consist of optical microscopy, scanning electron microscopy/electron diffraction spectroscopy (SEM/EDS), secondary ion mass spectrometry (SIMS), and transmission electron microscopy/electron diffraction spectroscopy (TEM/EDS).

The results available to date indicate that elemental releases to solution differ by up to 400% between the fully radioactive (R) and simulated (S) glasses. However, in general, differences in glass reactivity as measured by the release of boron, lithium, and sodium are less than a factor of two. The differences in reactivity are not large enough to alter the order of glass durability for the different compositions or to change the controlling glass dissolution mechanism. A radiation effect exists, mainly in terms of the influence on the leachate pH, which, in turn, affects the glass reaction mechanism and rate. The differences in reactivity between fully radioactive and the simulated glasses can be reasonably explained if the controlling reaction mechanism is taken into account. The differences are glass-composition and leaching-mechanism dependent. Lithium is found to be the fastest element released to solution in an ion-exchange-dominated glass reaction process, while lithium is released more slowly compared to boron and sodium in a matrix-dissolution-dominated process, where boron and sodium are usually among the most concentrated species in solution.

The durability order measured by the major element release to solution for both simulated and fully radioactive glasses is the same: SRL 165/42 > 131/11 > 200. Surface layer examination of the reacted glasses indicate of that the durability order, as defined by the thickness of the reacted layers, is the same as is derived from the solution data. The TEM results show that the thickness of the reacted layers ranges from a few nanometers for monolith SRL 165/42 glass to about 200 nm for 200S and 200R powders. The TEM survey of 131/11S glass samples reacted at SA/V = 2000 m^{-1} for 30, 70, and 140 days showed that they form an outer reaction layer that is partially crystallized. Beneath this layer, there are etch pits, which are typically 50 to 100 nm in diameter. This surface layer becomes thicker as one progresses from 30 to 140 days. The composition and spacing results are consistent with a smectite clay.

The ongoing batch tests will be continued as tests are scheduled to be completed through eight years. Data generated from solution analyses will be combined with surface layer studies to more completely compare the reactivity of the radioactive and nonradioactive glasses and to provide a data base for validation of glass performance models.

A series of intermittent drip tests using 200R glass has been started following the Unsaturated Test Procedure. The tests are being done with prehydrated and as-cast glass to represent bounding conditions that may exist during disposal. To date, the first sampling period has been completed. While the solution analyses are not complete, it is clear that the elemental release from the prehydrated glass is dominated by glass reaction, and the small volume of liquid that has contacted the glass during the testing period has become highly concentrated in both cations and anions released from the glass. Analyses are in progress measuring the size and actinide distribution of particulate material in the test solutions.

Two laboratory analogue tests have been started. In these tests, a glass monolith is suspended in a closed cavity in a tuff rock core and subjected to unsaturated flow conditions. The effluent from the rock core is monitored for radionuclide content, and the glass is studied at the termination of the test. Two tests are in progress: one with prehydrated glass and one with as-cast glass.

Effect of Radiation on Glass Reaction at Large SA/V

The objective of this task is to determine if radiation will have any significant effects on glass behavior under the high surface-area-to-liquid-volume ratio (SA/V) conditions expected at a geologically unsaturated repository site. These tests examine (1) the effect of radiation on the environment of a moist air system, (2) glass reaction in a radiolytic field, and (3) the influence of radiation and radiolytic products on the formation and stability of glass alteration phases.

Results to date indicate that nitrate and nitrite yields during gamma irradiation are inversely related to temperature. Alpha yields are similar to those obtained with gamma radiation, once the attenuation of alpha particles by thin films of water on the active foil source is taken in to account.

Glass wafers exposed to an irradiation field react five to ten times faster than their nonradioactive counterparts. Despite this advanced reaction rate, detailed microscopic examinations indicate a remarkable similarity between secondary minerals that form in the irradiated and nonirradiated tests. This observation indicates that the surficial fluid chemistry, especially the solution pH, appears to have remained similar on the irradiated and nonirradiated samples. In the irradiated tests, the increase in glass reaction products has apparently neutralized the formation of radiolytic products.

Cation release trends from irradiation tests with monoliths immersed in EJ-13 water (90°C, SA/V = 340 m^{-1}) generally display parabolic release patterns for Si, Ca, Mg, Na, K, Li, and B; however, for some samples, Ca, Mg, B, Si, and U may decrease in concentration after one year. Parabolic trends probably reflect a decrease in rate of glass dissolution as solution concentrations near saturation levels, while the later decrease in concentration may result from the precipitation of phases that have relatively low solubilities.

Relationship between High SA/V Experiments and MCC-1

A series of static leach tests is being performed to assess the effect of SA/V on the mechanism and rate of glass reaction. A clear understanding of the effects of this test variable is necessary to interpret the results of tests used to compare glass durability, monitor production consistency, and project the long-term glass behavior in possible repository environments using computer simulation.

The SA/V ratios tested include 10 m^{-1} (used in the MCC-1 test) and 2000 m^{-1} (used in PCT), as well as 340 and 20,000 m^{-1}. Reference waste glasses designated as SRL 131 and SRL 202 are doped with actinide elements to monitor their release behavior. These glasses are reacted in a J-13 groundwater solution in steel reaction vessels at 90°C for times between three days and about seven years. An SRL 202 glass doped with uranium is reacted in Teflon vessels with J-13 solution or deionized water to assess the effects of the vessel material and the leachant on the reaction. Leachates are analyzed for pH, anions, carbon, cations, and actinides in unfiltered and filtered aliquots. The reacted solids are analyzed using scanning electron microscopy with X-ray analysis, analytical electron microscopy, secondary ion mass spectrometry, and X-ray diffraction.

Tests have been completed through 364 days with actinide-doped glasses and through 56 days with uranium-doped glass. Results show the effects of SA/V to be beyond simple dilution. The pH values increased with SA/V, and filterable colloids were generated at high SA/V. The measured rate of reaction was higher at high SA/V. Analysis of the reacted solids is in progress to characterize differences in the reaction path that may have occurred at the different SA/V ratios.

Analytical Electron Microscopy, Infrared Spectroscopy, and Resonant Nuclear Profiling

This task includes the use of analytical electron microscopy (AEM), infrared spectroscopy (IR), and resonant nuclear profiling (RNP) to examine the structure of reacted glasses. The AEM is being performed at ANL, and peer review of the results is being conducted by the University of New Mexico (UNM); IR and RNP are being conducted at Rensselaer Polytechnic Institute (RPI).

The analytical support staff at ANL collaborates with other members of the Technical Support Program and scientists from other DOE laboratories to investigate and identify reaction products that are produced during glass corrosion. These structural studies provide information necessary to understand the reaction processes. This information will contribute to the development of the models needed for prediction of glass behavior. This year, approximately 70 bulk samples were mounted in about 250 epoxy blocks, producing over 500 TEM grids, each holding about 40 sections. The analyses of these sections helped in the interpretation of results from each of the experimental tasks. An example is given where the process that controls the reaction of SRL 165-based glass is described. The AEM results were essential in monitoring the growth of the reaction layer and in providing evidence as to how the layer can contribute to colloidal material in solution.

AEM has also been used to study colloids in the leach solutions. Techniques have been developed based on wicking solutions through TEM grids which thereby isolates the colloidal species. These species can then be identified and compared to the composition and structure of the reacted layers. In addition, a study of the formation of colloids in nuclear waste glass reactions was conducted. The results showed that plutonium and americium were released predominantly as colloids, but neptunium was released as soluble material.

AEM analysis of the reacted glass samples is an important component of the ANL Technical Support Program. The objectives of the work at the UNM is to provide peer review input by performing AEM and SEM analysis on samples similar to those studied at ANL. Two samples have been examined from the task "Effect of Radiation on Glass Reaction at Large SA/V." The results show a complex layer structure and the formation of several secondary phases. The identification of phases enhanced the ANL results by finding new phases that form within the layer structure and confirmed the sample preparation method provides minimal damage to the sample.

Experiments were conducted at RPI to study the difference of water into three simulated nuclear waste glasses. This information is necessary to help define the rate-controlling processes of glass reaction. The reaction of the glass types decreased in the order SRL 131U > SRL 202U > SRL 165U.

Modeling Tasks at Lawrence Livermore National Laboratory

The purpose of this task is to develop a model for glass dissolution and validate it using experimental results. This model will be used to evaluate glass performance in repository environments. As part of this objective, we have performed experiments designed to quantify the effects of glass composition and solution composition on glass durability, and have incorporated this information into the model.

Progress in developing the glass dissolution model was made in the following areas: (1) rate parameters generated by the flow-through tests have been incorporated into the model; (2) the glass dissolution model was incorporated into Gt, an alternate reaction path code having the additional capability to simulate rock-centered flow-through scenarios; (3) thermodynamic data for observed alteration minerals was added to the database; (4) the EQ3/6 data base was reformatted for use by Gt; and (5) the model was used to simulate glass performance in three different repository scenarios including glass only, glass plus hostrock plus container, and glass plus hostrock plus container plus cement.

Several sets of flow-through glass dissolution tests were completed which provided the pH dependence of the glass dissolution rate for SRL 165 glass and a simple SRL 165 glass analog. We found that the five-component analog glass behaves nearly identically to the SRL 165 glass which indicates that the primary controls on glass dissolution rate depend mainly on the major components of the glass. This will simplify future experiments aimed at quantifying the effect of glass composition on glass durability by reducing the number of compositional components that need to examined. The flow tests also showed a lack of dependence of glass dissolution rate on dissolved calcium and magnesium in solution.

I. INTRODUCTION

The High-Level Nuclear Waste Technical Support Program at Argonne National Laboratory (ANL) is part of the technology support activity performed for DOE's Environmental Restoration and Waste Management (EM). This program was initiated in 1989, and its purpose is to evaluate, before hot start-up of the Defense Waste Processing Facility (DWPF) and the West Valley Demonstration Project (WVDP), factors that will likely affect glass reaction in an unsaturated environment. The need for such a program recognizes that the long-term prediction of glass performance in a repository environment and the relationship between the release of radionuclides from a glass waste package and performance assessment of the repository are tasks that must be addressed, but that the completion of such tasks will not be finalized until application for a repository license, which will be several years after the production of waste for storage and disposal begins. The Technical Support Program at ANL also recognizes that the modeling and performance assessment programs must have a firm basis that (1) accounts for important physical parameters that will affect glass reaction in an unsaturated environment and (2) relates the mechanistic basis of glass reaction to conditions that will exist in an unsaturated environment.

The goals of the ANL Technical Support Program are to (1) review parameters that will be important to evaluating glass performance, (2) perform testing to further quantify the effects of important variables, (3) initiate long-term testing that will bound glass performance under a range of conditions that may be important to storage of waste in an unsaturated environment, and that can be used to validate models generated to predict long-term performance, and (4) to develop and demonstrate the applicability of models to predict glass performance. The information developed in this program, when combined with data generated by the glass waste producers and by the Yucca Mountain Project (YMP), will form the basis for a well-founded program that will ultimately qualify vitrified high-level waste for repository disposal.

The physical parameters or processes that are important for controlling glass reaction in an unsaturated environment were identified and evaluated previously [BATES-1]. These include (1) glass composition, (2) radiation, (3) temperature, (4) surface area of glass/volume of liquid (SA/V), (5) the effect of unsaturated conditions on glass reaction, and (6) the effect of alteration layers on glass reaction. This year, modeling of glass performance has also been included as an important factor to evaluate. Prior to hot facility startup, these items will be critically evaluated such that their role in glass performance will be established. This year, review of each of the physical parameters was initiated, while testing and modeling were conducted to augment the reviews. In this report, progress in each active area is reviewed after a general background description applicable to all areas is presented.

II. BACKGROUND

Work in each area is governed by a Task Plan, which enables the work to be planned according to the quality guidelines of the ANL Technical Support Program and allows all program activities to be coordinated. The Task Plans outline work to be done in an activity, but do not restrict the flexibility to make adjustments based on knowledge gained as the test results are evaluated. Plans have been written for the following tasks: "Critical Review of Parameters Affecting Glass Reaction in an Unsaturated Environment," "Waste Producer/Repository Program Interface," "Long-Term Testing of Fully Radioactive Glass," "Effect of Radiation on Glass Reaction at Large SA/V," "Relationship between High SA/V Experiments and MCC-1," "Analytical Electron Microscopy Support," "Technical Review of Analytical Electron Microscopy of Glass Reaction," "Water Diffusion Study of Simulated Nuclear Waste Glasses," and "Modeling Tasks at Lawrence Livermore National Laboratory." While these Task Plans are not formally published documents, copies of the Plans are available upon request. Ongoing work in each of these tasks is described in latter sections of this report.

An integral part of the testing program was the identification and preparation of glasses to be used. Several factors were considered in choosing glass compositions, including: (1) composition of "fully"[1] radioactive glasses available for testing; (2) the need to test a range of compositions based on glass durability, which may be a function of the test conditions; (3) the desire to use compositions similar to those already in use so that a comparative data base can be developed; (4) the necessity to test both radioactive and nonradioactive compositions (for comparative and technique-development purposes); and (5) minimization of testing time and cost.

The compositions of fully radioactive glasses are set by glass availability and include (1) 165 sludge-only based glass, designated 165/42 (the glass frit is 165 type and the sludge is from tank 42); (2) 131 sludge-only based glass, designated 131/11 (the glass frit is 131 type and the sludge is from tank 11); and (3) 200 frit-based glass, 200R [the glass frit is 200 type, the sludge is from tanks 8 and 12 and the precipitate hydrolysis aqueous (PHA) feed is simulated]. These glasses were produced by Westinghouse Savannah River Co. (WSRC) over the past several years and represent glasses developed as the process engineering matured. The base frits used in these glasses (131, 200, and 165) represent the expected durability range from least to most durable based on hydration theory [JANTZEN]. The sludge from tanks 11 and 42 is rich in aluminum, and the final compositions of the 131/11 and 165/42 compositions do not represent glasses expected to be produced by the DWPF. However, the composition of 200R glass is similar to the expected blend composition identified in the Waste Compliance Plan (WCP) [WCP] and, therefore, is a fair simulation of a production glass.

The extent to which a glass composition falls within the range of production compositions influences the use of the glass in testing. The 131/11 and 165/42 compositions, although they may not be produced, are useful for comparative testing with a simulated nonradioactive glass of the same

---

[1] The term "fully radioactive glass" is used to designate glasses made containing actual waste taken from the waste storage tanks at the Westinghouse Savannah River Site. The glass may not contain the complete complement of radionuclides anticipated to exist in the final DWPF product, because the glass contains only radionuclides contained in the sludge component of the waste.

composition to demonstrate whether any differences in reactivity exist between production and simulated glasses. The 200R glass is also useful for comparative testing, but because of its similarity to production glass, it is used in a more extensive test matrix to assess glass performance under unsaturated conditions (see Sec. V for details of testing these glasses). For each of these fully radioactive glasses, simulated glasses were produced with the same composition. Simulated glasses are designated as "S" glasses, e.g., 131/11S.

Because none of the "fully" radioactive glasses are exact representations of glasses identified in the WCP, we felt that another set of glasses should be produced for testing done in other tasks in this program and in other testing performed by the YMP. Concurrence of glass compositions to be tested was obtained from Lawrence Livermore National Laboratory (LLNL), the responsible agency for the YMP Glass Task. The compositions chosen are 131-, 165-, and 202-based glasses and are similar to compositions identified in the WCP. The actual compositions are based on the use of manufactured bulk frits as starting frits modified to match WCP glasses as closely as possible. Thus, the base 131 frit is 131 frit produced in the semiworks at WSRC, the base 165 frit is 165 black frit manufactured by Ferro Corp., and the base 202 frit is based on DWPF start-up frit. Each base frit is modified by the addition of chemical additives, including zeolite and actinide elements, to produce the glasses used in testing. If a glass contains uranium but no transuranic elements, it is designated a "U" glass, e.g., 131U. If a glass contains transuranic elements, it is designated an "A" glass, e.g., 131A.

At this time, testing has been initiated on all of the "fully" radioactive and simulated glass, and the glass compositions are shown in Table 1. The starting glasses are continuing to undergo analysis so the compositions shown in Table 1 are subject to change. However, the data presented in the subsequent sections of this report are based on the values in Table 1. A standard leachate was used throughout the testing program. The leachate is based on the equilibration of well water J-13 with tuff rock. The resulting water is termed EJ-13 water, and its composition is listed in Table 2.

Table 1. Composition of Glasses Used in Testing[a]

Element	Oxide Weight Percent								
	131/11R	131/11S	131A	200R	200S	202A	165/42R	165/42S	165A
Al	9.7	9.2	3.27	5.9	5.5	3.84	10.36	8.7	4.08
B	9.4	9.3	9.65	9.7	9.6	7.97	8.02	8.4	6.76
Ba	0.02	0.05	0.16	0.02	0.03	0.22	--	0.4	0.06
Ca	3.9	2.9	0.93	0.9	0.9	1.20	0.33	0.3	1.62
Cr	0.9	0.7	0.13	0.3	0.2	0.08	0.33	0.8	<0.01
Cu	0.02	0.04	0.02	0.1	0.1	0.40	0.03	0.06	--
Fe	4.8	5.1	12.66	9.0	8.8	11.41	5.89	6.1	11.74
K	0.06	0.1	3.86	3.5	3.3	3.71	0.05	0.08	0.19
Li	3.3	3.2	3.00	3.4	3.3	4.23	4.72	4.7	4.18
Ce	--	--	TBA[b]	--	--	TBA	--	--	--
Nd	--	--	TBA	0.1	--	TBA	--	--	--
La	--	--	TBA	0.06	0.01	TBA	--	--	--
Mg	1.4	1.6	1.31	1.6	1.7	1.32	1.02	1.0	0.70
Mn	1.7	1.7	2.43	1.6	1.5	2.21	1.94	1.8	2.79
Mo	--	--	--	0.01	0.02	0.05	--	--	--
Na	16.6	17.5	12.08	15.0	16.0	8.92	11.12	10.8	10.85
Ni	0.5	0.6	1.24	0.9	0.9	0.82	0.61	0.8	0.85
Pb	0.02	0.1	--	0.03	0.05	0.01	0.05	0.01	--
Si	45.5	45.8	43.76	45.5	45.4	48.95	TBA	52.4	52.86
Sr	0.02	0.02	0.01	0.01	0.02	0.03	0.04	0.01	0.11
Ti	1.5	1.7	0.65	0.08	0.1	0.91	--	0.08	0.14
Zn	0.02	0.05	0.02	0.02	0.04	0.02	0.03	0.1	0.04
Zr	0.08	0.1	0.22	0.06	0.09	0.10	0.83	1.4	0.66
Th	--	--	--	--	--	0.26	--	0.01	--
Ru	--	--	--	--	--	<0.05	--	--	--
U	0.25	0.26	TBA	1.8	1.9	1.93	TBA	0.1	0.92
Tc	--		0.02	--		0.02	--	--	0.02
^{237}Np	TBA		0.01			0.01	TBA	--	0.01
^{238}Pu	2.7E-4		2.1E-4			--	1.7E-4	--	--
^{239}Pu	TBA		TBA			TBA	--	--	0.01
^{241}Am	9.0E-5		2.4E-4			TBA	9.5E-5	--	0.0004
^{244}Cm	TBA		--			--		--	--
^{137}Cs	1.7E-8					--	1.1E-4	--	--

[a]The compositions reported are best values at this time. Glass analyses are ongoing and the compositions are upgraded with new data as they become available.

[b]TBA = to be analyzed.

Table 2. Composition of EJ-13 Leachant (pH = 8.1)

	Comp., mg/L
Al	1.1
B	0.17
Ca	5.4
Li	0.050
Mg	0.4
Na	53.9
Si	46.4
K	7.3
NO_3^-	11
F^-	2.3
HCO_3^-	100
Cl^-	8.4

III. CRITICAL REVIEW OF PARAMETERS AFFECTING GLASS REACTION IN AN UNSATURATED ENVIRONMENT

A. Introduction and Background

The predicted repository environment at Yucca Mountain has been described by the YMP as hydrologically unsaturated with possible air exchange with the neighboring biosphere [SCP]. We have identified several environmental conditions that can affect the durability of waste emplaced in such an unsaturated environment over repository-relevant time periods. To date, much of the information regarding what is known about these conditions has not been synthesized for use within the waste glass research community. Thus, the need to perform such a critical review was identified, and the review is currently underway.

During the projected lifetime of an unsaturated repository, large amounts of liquid water are not expected to come into contact the waste; however, water vapor or small volumes of transient water may contact the waste during the emplacement. We have identified the amount of water contacting the glass waste to be a primary parameter affecting waste glass durability. Other identified primary parameters include the effects of temperature, radiation fields, glass composition, and alteration phases resulting from glass hydration. Detailed critical reviews of how each of these parameters affects waste glasses will be performed as a part of this task.

B. Objectives

The purpose of the Critical Review Task is to review the existing literature in order to evaluate the state of knowledge regarding the influence of each of the identified critical parameters on glass reaction. Each review will be issued as stand-alone documents, and these documents will be integrated in a summary compendium document. The results from this task will be used to support startup of DWPF and WVDP.

C. Technical Approach

The technical approach has been to assemble all known and pertinent sources of scientific literature and then objectively and critically consider the current state of knowledge as to how each critical parameter affects nuclear waste glass reaction. When desirable, we have included reviews and discussions of studies of materials other than nuclear waste glasses, but this ancillary information is used to relate waste glass reaction to the parameter being reviewed. A synthesis of existing data will be performed, where possible, to provide a framework for comparing the results obtained from different studies.

All reviewed references used in the critical reviews have been collected in a computerized data base. The data base lists the reference, along with keywords and ANL reviewer's comments regarding the reference. The references in the data base include published journal articles, symposia proceedings, unpublished manuscripts, letters, and output from literature searches. The data base serves as a repository, as well as a resource, for all of the relevant information that will be used in the critical reviews. The data base has a word search capability that facilitates the review process and ensures that pertinent literature is not overlooked by the critical review authors.

D. Results and Discussion

A preliminary critical review was previously performed to provide a foundation for subsequent detailed reviews of each parameter [BATES-1]. The first such report, detailing the effects of temperature on waste glass performance, has been completed [MAZER-1]. This report concluded that reaction mechanisms for waste glass dissolution in water are complex and involve multiple simultaneous reaction processes. The temperature dependence of each of the individual reaction processes can be described by the Arrhenius equation, a relationship derived from empirical observations. In cases where the reaction mechanism changes as a function of time or temperature (i.e., the dominant reaction process changes), the Arrhenius equation is less useful in interpreting the temperature dependence of the overall reaction mechanism. Understanding the interplay of the reaction processes and their temperature dependences for nuclear waste glasses requires a clear understanding of the reaction mechanism, which has not yet been achieved. Until this understanding is attained, caution should be exercised in using temperature as an accelerating parameter.

The next parameter to undergo a detailed critical review is the effect of glass composition on glass durability. This review is in progress. Models of glass structure are used to help understand the fundamentals of how water may interact with glass. Brief reviews of models of glass dissolution are combined with this information to form a basis for analyzing theoretical and empirical models relating glass composition to glass durability. All available studies in this area are being obtained, and where possible, the available data will be presented in a manner that will allow a comparison of the results obtained in different studies.

E. Future Progress

Reviews of the remaining factors or parameters (radiation, SA/V ratio, surface layers, unsaturated environments, and models) are being initiated, and drafts of each report will be completed in the upcoming year. The process governing the execution of each review involves several steps. The author(s) initially produces an outline listing the expected content of each section. The outline is then internally reviewed and corrections and additions are made, as necessary. A draft of the manuscript is then prepared and submitted for internal review. After the comments from this review are addressed, the manuscript is then sent out for an external review by acknowledged experts in each field. After the comments from this review are received and incorporated into the manuscript, the final document is published and distributed.

IV. WASTE PRODUCER/REPOSITORY PROGRAM INTERFACE

A. Introduction and Background

The U.S. Nuclear Regulatory Commission (NRC) staff has repeatedly asked questions (see [LINEHAM], for example) concerning the adequacy of the performance, in a geologic repository, of the nuclear waste glass to be produced by the vitrification projects. The questions involved have been posed in different ways and include the connection between the Waste Acceptance Preliminary Specifications (WAPS), specification 1.3, and waste glass performance requirements in the repository. Because this issue will probably be raised during the Energy Systems Advisory Acquisition Board (ESAAB) review of the hot-startup decision for the DWPF and WVDP, it is important to develop a suitable response. The task described here includes activities intended to develop such a response.

The issues involved are complex, and development of a suitable response, in the DWPF and WVDP hot-startup time frames, is complicated by the following:

1. There is no regulatory performance standard or performance objective for the waste glass that can be used to assess the adequacy of the performance of the DWPF and WVDP products. (Note: Compliance with the WAPS cannot be used to indicate the adequacy of performance, since the WAPS are not linked to regulatory performance objectives, such as 10 CFR 60.113.)

2. Although the waste glass is part of the engineered barrier system (EBS), it will not be possible to assess the performance adequacy of the actual EBS in the time frame of the DWPF and WVDP hot startup because repository site selection and EBS design decisions will be made after the hot-startup decisions.

3. The issues involved are primarily related to repository licensing, which is the responsibility of the repository program in the Office of Civilian Radioactive Waste Management (OCRWM); thus, interim responses, prior to hot startup, have to be coordinated with this repository program.

Because of the growing concern that the hot-startup decisions could be complicated or delayed if a suitable interim (i.e., prior to the ESAAB hearings) response is not developed, a technical exchange meeting (with EM and OCRWM program representatives) was held at ANL on June 14 and 15, 1990, to address the adequacy of ongoing work to satisfy the hot-startup decision needs. This meeting resulted in several recommendations, which include the following:

1. To develop a strawman position paper which would provide an interim response to NRC questions concerning the adequacy of waste glass performance and the connection between WAPS 1.3 and waste performance.

2. To establish a continuing interface between the EM waste glass producers and the OCRWM repository program.

The recommendations were the basis upon which the task described herein was proposed and initiated in FY 1991.

At the time when the need for, and scope of, a continuing interface between the EM and the OCRWM repository program were first identified, there were several related activities sponsored by EM and OCRWM. On the EM side, a variety of experimental and modeling activities on waste glass behavior under possible disposal conditions (see, for example, the work described for other tasks in this report) were underway. On the OCRWM side, efforts were continuing on the development of waste glass dissolution submodels and assessment of EBS performance assessment, including an evaluation of the performance of waste glass by the Performance Assessment Scientific Support (PASS) Program and the Performance Assessment Calculational Exercises (PACE-90). At the outset, we envisioned that this task would involve technical exchange (e.g., presentations and technical exchange meetings) so that the waste glass performance assessment activities supported by OCRWM could benefit from the EM-supported work, and the EM-supported work could benefit from feedback provided by the performance assessment activities in identifying needs for additional information and waste glass testing. In addition, this task was intended to coordinate preparation of a joint EM/OCRWM position on responding to the waste glass performance issues and to coordinate external review of reports generated by the critical review task (Sec. III). As the task progressed, it became necessary to modify the scope. In particular, the original scope was modified to include the following:

1. An investigation of the potential significance of colloids in assessing nuclear waste glass behavior after disposal. The issue of the role of colloids in EBS performance assessment has been raised repeatedly and was considered to be an important technical issue for the interface between waste glass testing and EBS performance assessment with regard to source term assumptions. The objective of the study conducted under this task was to provide an initial basis for evaluating the need to consider the role of colloids in performance assessment studies of nuclear waste glass. This investigation was done in conjunction with ongoing work in the other experimental tasks.

2. Preparation of a "white paper" or "compendium" which would describe the scientific basis for evaluating the behavior of the waste glasses to be produced by the vitrification projects.

These scope changes are reflected in the discussion that follows.

B. Objectives

The initial objectives of this task were the following:

1. To initiate and coordinate interface activities between EM-supported waste glass testing and OCRWM-supported performance assessment in order to:

   - ensure that OCRWM-supported performance assessments on waste glass reflected, and were consistent with, the experimental results from EM-supported waste glass testing;
   - identify specific information for the EM-supported testing program that could be used in the OCRWM performance assessments;
   - obtain feedback from the performance assessments that could be used to refine and prioritize waste glass testing needs;
   - coordinate preparation of a joint EM/OCRWM position for responding to waste glass performance issues that are raised in connection with hot startup of DWPF and WVDP.

2. To coordinate external reviews of the critical review reports (Sec. III) produced within this program.

As the task progressed, the objectives were modified to include the following:

3. To investigate the formation and characteristics of colloids in nuclear waste glass reactions. The objective here was to provide an initial basis for evaluating the need to consider the role of colloids in performance assessment.

4. To prepare a "white paper" or "compendium" which will describe the scientific basis for evaluating the behavior of waste glasses under a range of conditions associated with storage, transportation, and disposal.

C. Status and Discussion

The task progress as it relates to each of the objectives is discussed in this section.

Interface between EM-Supported Testing and OCRWM-Supported Performance Assessment

An interface, of the type originally envisioned for this task, was not established for two reasons:

1. The OCRWM repository program did not accept our authority to initiate formal contacts to establish an interface; these had to be initiated by DOE/EM.

2. The OCRWM repository program activities related to waste glass performance assessment were terminated due to higher priority demands for the available resources.

A position statement for responding to waste glass performance issues was drafted and transmitted to the repository program. However, for the first reason cited above, this task was not able to effectively expedite agreement on a joint EM/OCRWM position. Comments were provided on the OCRWM-drafted position that was subsequently transmitted to the NRC.

An interface was established with the waste glass submodel development work through the modeling task of Lawrence Livermore National Laboratory (LLNL), described in Sec. XI. However, the termination of waste glass performance assessments at the EBS level rendered establishing an effective interface at this level impossible.

Establishment of an effective technical interface with the OCRWM performance assessment of the EBS continues to be an important objective. However, a formal EM/OCRWM interface agreement, documented, for example, in a memorandum of agreement (MOA), is needed.

External Review Coordination

An external review of the critical review report entitled "Temperature Effects on Waste Glass Performance" was completed. The review comments were incorporated in the published report [MAZER-1].

A QA procedure was prepared for the administration of the external reviews on the remaining critical review reports.

Formation and Characterization of Colloids in Nuclear Waste Glass Reactions

The results obtained on formation and characterization of colloids are discussed in Sec. VIII.

Preparation of "White Paper/Compendium" on Waste Glass Behavior

To summarize the scientific basis for responding to issues concerning the long-term behavior of nuclear waste glass, an effort has been initiated to prepare a white paper or compendium of information on waste glass behavior under a broad range of conditions associated with storage, transportation, and disposal. An annotated outline for this document has been prepared and transmitted to the Program Technical Support Office (PTSO) for review and comment.

D. Future Progress

As indicated by the above discussion, the scope of this task is continuing to evolve. The focus is shifting to the preparation of the white paper or compendium on waste glass behavior. The nature of the continuing interaction with the OCRWM repository program on issues related to waste glass behavior is not clear. For the preparation of the white paper/compendium document, it is expected that the repository program will perform some oversight and review functions. Because the repository program is unlikely to have any significant ongoing work in FY 1992 on waste glass performance assessment, it is also expected that serving as an interface between EM-supported testing and OCRWM-supported modeling will not be possible. However, establishment of an effective technical interface continues to be an important objective, and arrangements (e.g., the MOA referred to earlier) for a workable interface need to be formalized between EM and OCRWM.

The external review of the critical review report on the "Effects of Glass Composition on Waste Glass Performance" will be conducted and coordinated with the PTSO.

V. LONG-TERM TESTING OF FULLY RADIOACTIVE GLASS

A. Introduction and Background

Before glass can be stored in a waste repository, it is necessary to predict how the glass may behave in the repository. The behavior prediction will be based on the development of a model. Information that goes into the model includes data describing glass reaction mechanisms, rates of initial and final reaction, the affinity of the glass to react, and dependence of glass reaction on interactions with other components in the waste package. The model must be mechanistically, not empirically based. To demonstrate its predictive capability, the model must be validated. Validation tests include long-term tests that closely simulate the expected conditions for storage, including parameters related to the glass and the repository. This task addresses tests to be performed that will provide information that can be used to validate glass reaction models, and can be used to demonstrate an understanding of glass reaction processes that will occur in an unsaturated environment. The results will also indicate whether differences exist in the reaction of fully radioactive glass compared to nonradioactive glass of the same nominal composition. This is important to demonstrate because model development has generally been done using results from nonradioactive glass tests. The results of the radioactive and nonradioactive tests can be used to demonstrate glass reaction under potential repository conditions, but by themselves should not be used to predict glass reaction to repository time frames.

B. Objective and Rationale

The objective of this task is to evaluate the performance of fully radioactive glasses, similar to those that will be produced by the DWPF, in meeting the performance objectives for glass storage in a high-level waste repository, with emphasis on conditions that may be encountered in an unsaturated horizon. Specifically, long-term data will be generated such that (1) reaction of fully radioactive glass can be compared with that of nonradioactive glass with a similar nominal composition; (2) interactions between waste package components that must be accounted for in independent reaction path models are identified; and (3) the long-term behavior of glass is established under anticipated disposal conditions, such that validation of glass performance models can be achieved.

In the DWPF process, glass will be produced by combining sludge and supernatant waste components with nonradioactive frit. The glass produced in the DWPF will be radioactive, such that it must be processed and handled in remotely operated facilities. However, most testing to evaluate the performance of glass has been done using simulated nonradioactive analogs of the same composition as the radioactive glass. It must be demonstrated that the simulated experiments are adequate representations of reactions that will occur with the actual glass to be produced by the DWPF. The issues of concern are: (1) does the simulated glass react through the same controlling mechanism? (2) does the analog glass produce the same secondary phases and in the same sequences? (3) is there an effect due to radioactivity that is not adequately simulated using nonradioactive glass? and (4) is there an effect of using glasses that may not contain all the nonradioactive components that will be present in the sludge, supernate, and frit feeds to the DWPF? Nonradioactive glasses are generally produced from pure starting materials, and thus minor components that will be present in the DWPF glass may not be present in the simulated glass. The effect of minor components may be accentuated when glass is reacted under the high SA/V conditions expected in an unsaturated environment. Testing of radioactive glass has been performed by WSRC [BIBLER-1 to -6]. The present tests will extend the duration of testing to longer time periods and will generate results that permit comparison between radioactive and nonradioactive glasses for three different compositions. A comparison between the leaching of radioactive and

nonradioactive glasses was also done as part of the joint Japanese, Swiss, Swedish (JSS) Program. Results from that program [JSS] indicated that after one year there may be a factor of two difference in reaction. The present tests will extend the time period to assess glass performance under conditions which should approach the final rate-controlling processes.

C. Technical Approach

To determine the long-term performance of glass under disposal conditions, tests must be conducted such that the "final" reaction conditions (steady state) are achieved. An unsaturated environment presents a challenge in performing long-term testing because, over the duration of storage, the conditions are expected to change, perhaps significantly, with respect to the amount of water available to react with the glass and to transport radionuclides.

Tests to evaluate the performance of glass in an unsaturated environment must address the unique features of such an environment and must be performed for time periods of long enough duration so that the stage is reached where secondary phase formation (as opposed to supersaturated solution concentrations) controls the glass reaction. Relevant tests include static tests performed at high SA/V ratios, and high SA/V flow tests done to simulate the waste package environment. The information obtained from these tests must include the solution composition as a function of time, combined with a description of the glass alteration. To meet these goals, three types of tests are being performed:

(1) Long-term static tests (i.e., no water flow) at high SA/V with monoliths and powders. These tests provide temporal solution trends, plus easy identification of secondary phases combined with the distribution of radionuclides in the reacted glass layers.

(2) Long-term intermittent flow tests at high SA/V following a modified version of the Unsaturated Test Procedure [BATES-2] as applied to "aged" and fresh glass monoliths.

(3) Long-term repository environment tests following the laboratory analog procedure as applied to "aged" and fresh glass monoliths [BATES-3].

The tests are being performed with the three different general groups of glass compositions: 165-, 200-, and 131-frit based glasses (Table 1). A description of the tests in each test category, including status and results/discussion, is given below.

1. Long-Term Static Tests at High SA/V

The long-term static tests are being performed following the test matrix shown in Table 3. The matrix is divided into three sections, based on the glass type (165, 131, and 200). The tests in progress with the 165 and 131 glass types are identical except for the number of replicates. The tests done with the 131 glass type are not replicated due to the limited amount of 131/11 glass available for testing. The tests done with 165 and 200 type glasses are done in duplicate. The schedule allows for all long-term tests (>364 days) to be started at the same time (t = 0). The short-term tests (<280 days) are staggered such that, at the end of 280 days, all the TBD (to be determined) tests are started. Static tests are performed in the batch mode to allow for examination of solids at each test period so that the mass balance between the residual solids (reacted glass and secondary phases) and the solution composition can be documented. The tests are static, i.e., no exchange of leachant to promote conditions representative of an unsaturated site (little or no flow), and the reaction environment is disturbed as little as possible; thus, optimal conditions exist for secondary phase nucleation and growth.

Table 3. Test Matrix[a] for Long-Term Static Tests at High SA/V Ratios

	131 Glass Type[b]				200 Glass Type[c]						165 Glass Type[c]				
SA/V*t,	131/11		Simulated		200R			Simulated			165/42		Simulated		
day•m^{-1}	340	2000	340	2000	340	2000	20,000	340	2000	20,000	340	2000	340	2000	Blank[b]
Reaction Progress[d]															
1,020															3
2,380															7
4,760					14[e]			14							14
6,000						3			3						28
9,520	28		28								28		28		56
14,000															70
19,040					56			56							91
28,000						14			14						98
30,940	91		91								91		91		140
60,000		30		30								30		30	182
61,880					182			182							238
123,760	364		364		364			364			364		364		280
140,000		70		70		70			70			70		70	364
247,520	728		728		728			728			728		728		546
280,000		140		140			15			15		140		140	728
495,000	1456		1456		1456			1456			1456		1456		980
560,000		280		280		280			280			280		280	1456
990,080	2912		2912		2912			2912			2912		2912		1820
1,120,000		560		560		560	56		560	56		560		560	2912
1,960,000		980		980		980	98		980	98		980		980	TBD
3,649,000		1820		1820		1820	182		1820	182		1820		1820	TBD
7,280,000							364			364					TBD
10,920,000							546			546					TBD
14,560,000							728			728					
					TBD[f]	TBD	TBD	TBD	TBD	TBD	TBD	TBD	TBD	TBD	
					TBD	TBD	TBD	TBD	TBD	TBD					

[a]The entries in the table indicate the duration of a specific test in days. The tests done at 340 m^{-1} use monoliths, the tests done at 2000 and 20,000 m^{-1} use powder.

[b]Tests are single tests.

[c]Tests are duplicate.

[d]Reaction Progress in terms of SA/V*t (units of day•m^{-1}). No significance is implied to the use of this reaction progress indicator.

[e]The underlined tests were terminated.

[f]TBD = To be determined.

The text matrix for each glass composition and for blank tests is shown in Table 3. The detailed matrix description can be found in [BATES-4].

a. Status

To date, 212 of the planned long-term static tests have been initiated, and 88 of these have been terminated. The longest tests have been in progress for more than 17 months. The solution analyses for the terminated tests are about 90% completed and include determination of leachate pH, cations, selected anions, total carbon, and actinides. The surface analyses on the terminated samples are in progress and consist of analyses using optical microscopy, SEM/EDS, SIMS, and TEM/EDS.

b. Results and Discussion

For ease of comparison, the results are first presented in radioactive/nonradioactive glass pairs for each glass composition type tested. These pairs are compared with regard to normalized leachate concentrations, preliminary leach mechanism, formation of surface alteration layers, and SA/V dependence. At last, an overview about the performance comparison of radioactive/nonradioactive glasses over different compositions is presented.

All the leach tests were carried out with EJ-13 well water, and therefore, the results of the blank tests are presented first.

i. Blank Tests

The blank tests were carried out without glass but with EJ-13 well water (equilibrated with tuff rock). The average leachant composition of the blank tests was used for the blank correction calculations of the tests with glasses. The composition of the EJ-13 water used to initiate the blank tests is tabulated in Table 4a. The data analyzed from blank tests up to 240 days (Table 4b) show that the Si, Na, K, and Ca concentrations in the blanks were practically unchanged from the starting solution concentrations. The more soluble species, such as boron and lithium, in blank tests were always larger than or equal to the starting solution concentrations, and the concentration of magnesium in blank tests was lower than the starting EJ-13 solution. The pHs of the blank tests were equal to or slightly higher than the starting EJ-13. This pH increase associated with blank tests run in 304L stainless steel containers has also been observed in similar test conditions [FENG-1]. Since the major components of the blank tests were essentially constant with time, the average of those concentrations (Table 4b) was used for the calculation of the blank-corrected concentrations (cation only) for those tests with both fully radioactive and simulated glasses.

ii. 200-Type Glasses

The solution data for the monolith tests at SA/V = 340 m^{-1} and for the powder tests at SA/V = 2000 m^{-1} and 20,000 m^{-1} for the 200-type glasses show that the radioactive 200R reacts less than the corresponding nonradioactive 200S.[2] The leaching behavior of 200R and 200S is compared at SA/V = 2000 m^{-1} and 20,000 m^{-1} in Fig. 1. The 200R shows consistently lower leaching than 200S for all the elements. This includes the matrix elements boron and silicon and the alkalis lithium and sodium. The differences range from 60% to 400%. The pHs of the leachates in 200R are always lower than those in 200S (Figs. 1e and 1f). A separate study [WRONKIEWICZ] on the radiation effect indicates that

---

[2] In discussion that follows, "R" affixed to glass designation indicates fully radioactive, and "S" indicates simulated nonradioactive.

Table 4a. Average Concentration of Elements in EJ-13 Water (starting solution, pH = 8.14)

Element	Conc., ppb
Al	1060
B	170
Ca	5400
Fe	10
K	7383
Li	48
Mg	382
Na	53867
Ni	30
Si	46400
Sr	21

Table 4b. Average Concentrations of Elements in EJ-13 Water After Blank Tests (used for the calculation of the blank corrected concentrations of the tests with glasses)

Element	Conc., ppb	Element	Conc., ppb
Al	743	Sr	45
B	274	Ti	85
Ba	125	Zn	90
Ca	4695	Zr	192
Cr	125	F^-	3000
Cu	242	CHO^{2-}	<400
Fe	105	Cl^-	9300
K	6998	NO_2^-	<200
Li	84	NO_3^-	15800
Mg	182	HPO_4^{2-}	<600
Mn	80	SO_4^{2-}	24000
Na	52533	$C_2O_4^{2-}$	<600
Ni	188	Total Carbon	22000
Pb	148	Organic Carbon	4600
Si	44454	Inorganic Carbon	17400

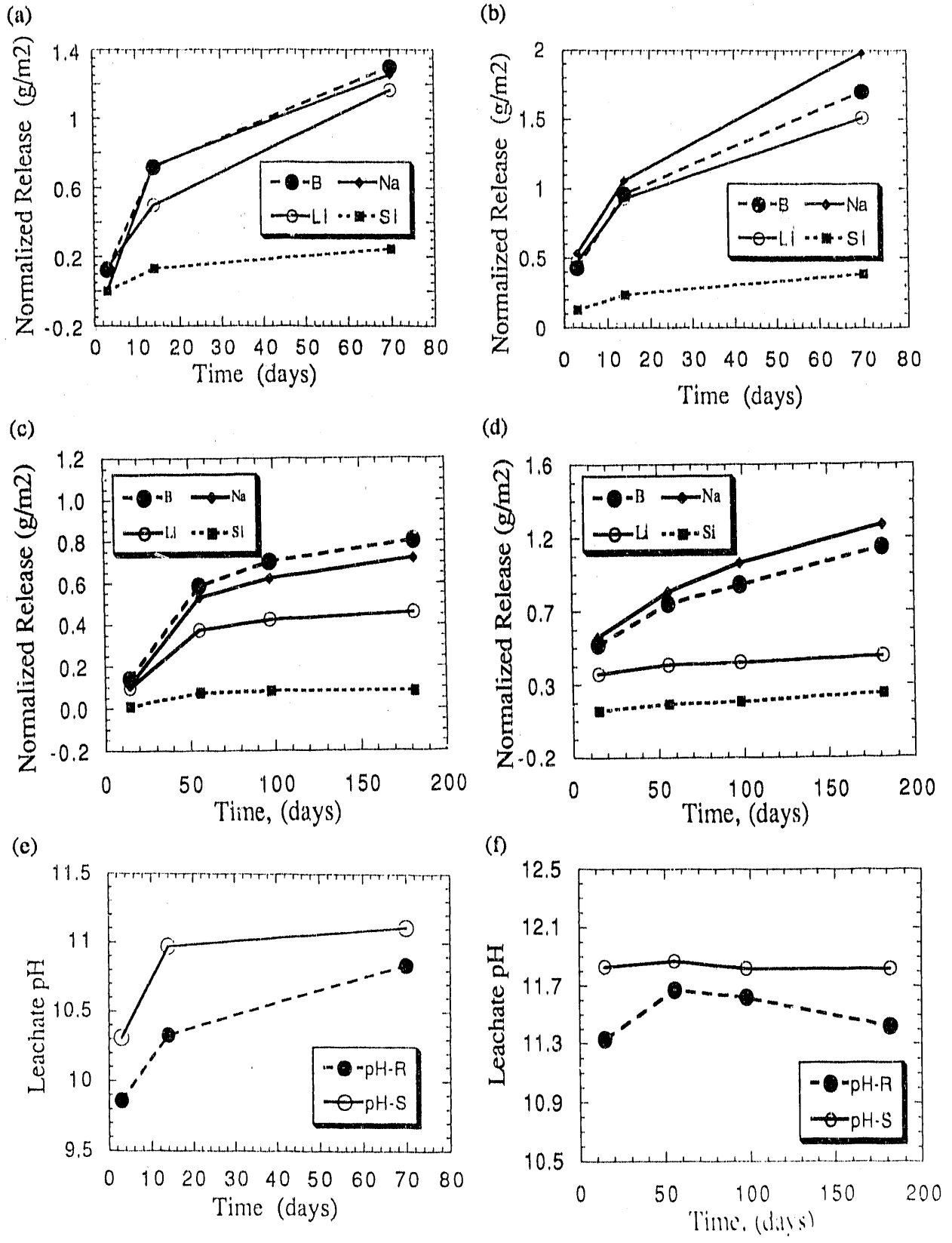

Fig. 1. Normalized Release among Different Elements for (a) 200R at SA/V = 2000 m^{-1}, (b) 200S at SA/V = 2000 m^{-1}, (c) 200R at SA/V = 20,000 m^{-1}, and (d) 200S at SA/V = 20,000 m^{-1}, and Leachate pH for (e) 200R and 200S at SA/V = 2000 m^{-1} and (f) 200R and 200S at SA/V = 20,000 m^{-1}

nitrogen-related acids and organic acids are produced when a humid atmosphere is exposed to β and γ radiation, and the acids produced tend to reduce the leachate pH. The pH difference for tests at SA/V = 20,000 m^{-1} is smaller than that at SA/V = 2000 m^{-1}. This is because the radiation effect is less dominant at the higher SA/V conditions.

Glass dissolution usually begins with a dealkalization step, characterized by the exchange of hydronium/alkali, followed by matrix dissolution step, which is characterized by a congruent release from the glass. The elemental concentrations measured in solution are a combination of these two release processes plus solubility-limited secondary phase formation that occurs at the glass surface. The short-term solution data for the 200-type glasses suggest that the dominant glass reaction process for both 200R and 200S is matrix dissolution, even at the shortest time tested. At later times or at high SA/V (20,000 m^{-1}), solubility effects also become important. Figures 1a to 1d illustrate the relative normalized release values for individual elements of both 200R and 200S glasses. Initially, a nearly congruent release of boron, sodium, and lithium is evident for both glasses. Silicon exhibits lower normalized release than those of boron, lithium, and sodium, since silicon exhibits a solubility-controlled formation of clay phases [BATES-5]. It is also interesting that the longer the term of the test, the greater the deviation from congruent release. The leachate of 200S at SA/V = 2000 m^{-1} has higher elemental concentrations than 200R and a greater separation in release values is observed between boron, sodium, and lithium (Fig. 1a. vs. Fig. 1b) for 200S. This divergence in normalized release values suggests that, as the solution approaches saturation, elements are being selectively incorporated into secondary phases. The ranking of glasses with respect to the normalized release values follows the order: 200S at 20,000 m^{-1} > 200R at 20,000 m^{-1} > 200S at 2000 m^{-1} > 200R at 2000 m^{-1} (Fig. 1), and the order of deviation from the congruent dissolution is also the same. The largest effect of solubility control is on the concentrations of lithium. The longer the reaction, the greater the normalized lithium release value deviates from those of boron and sodium. The lithium release is lower than the boron or sodium release. This suggests that lithium enrichment should occur in the surface clay phases.

If matrix dissolution is the dominant elemental release process for both 200R and 200S glasses, an explanation can then be offered for the finding that 200R leaches less than 200S. The rate for a glass reaction controlled by matrix dissolution depends on the concentration of the nucleophilic species, hydroxide. The pHs are lower in 200R solutions compared with the 200S solutions due to the radiation effect of 200R, and the hydroxide concentrations in 200R solutions are lower than those of 200S. It is the lower hydroxide concentrations that decrease the dissolution rate of 200R in comparison with 200S.

iii. 165/42-Type Glasses

In contrast to the dissolution results for the 200-type glasses discussed above, 165/42R shows a slightly greater reactivity than 165/42S, as shown in Figs. 2a and 2b. The differences range from 10% to 150%. The pHs in Fig 2c show an interesting "cross over," where the pH of the 165/42R is initially lower than that of 165/42S and becomes higher in the later part of the glass reaction. The relative elemental release values for each glass also differ from those in 200-type glasses, as shown in Fig. 2, where lithium has concentrations of four to ten times larger than those of boron, sodium, or silicon.

Although differences in normalized releases are observed between the fully radioactive and the simulated 165/42 glass, the solution kinetics analysis indicates that the dominant release process for both 165/42R and 165/42S is an ion-exchange reaction. The exchange of hydronium ions from solution for the alkalis in the glasses is the rate-determining step, and the rate of the glass

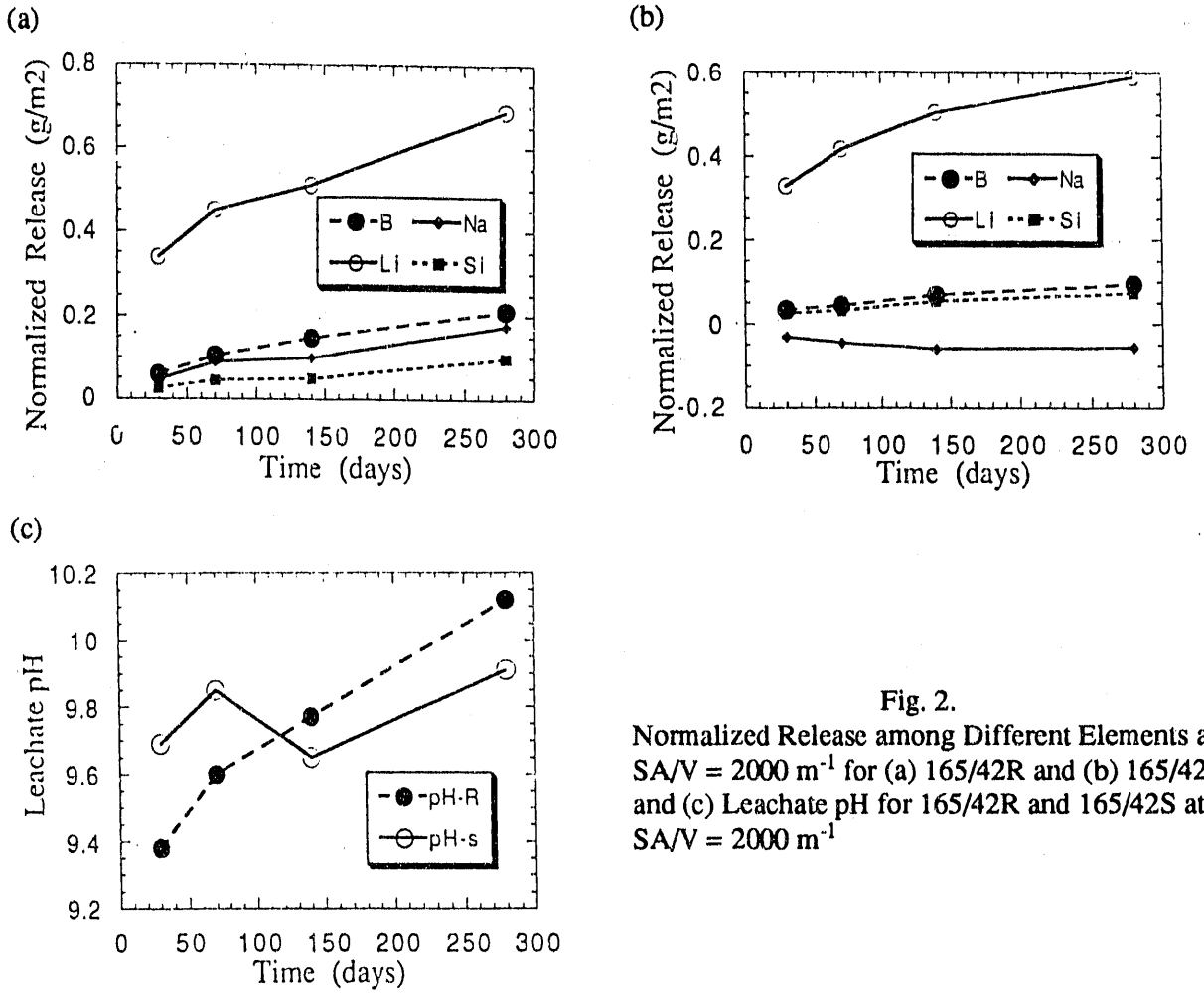

Fig. 2.
Normalized Release among Different Elements at SA/V = 2000 m^{-1} for (a) 165/42R and (b) 165/42S and (c) Leachate pH for 165/42R and 165/42S at SA/V = 2000 m^{-1}

reaction depends on the concentration of the hydronium ions. Since the pH is initially lower in 165/42R as a result of radiation effects, the leaching of 165/42R is faster than 165/42S due to the higher concentration of hydronium ion in 165/42R. We, therefore, observe slightly higher normalized releases in 165/42R compared to 165/42S. The main glass reaction process can be presented as:

$$\text{Glass-O}^{-}\text{R} + \text{H}_3\text{O}^{+}(\text{solution}) = \text{Glass-OH} + \text{R}^{+}(\text{solution}) + \text{H}_2\text{O} \qquad (1)$$

where R^+ represents the alkali element. As the reaction proceeds, hydronium ions are consumed more rapidly from the leachate of 165/42R. The pH of the leachate increases, and the pH "cross over" occurs (Fig. 2c). The relative elemental concentration levels (Fig. 2) also agree with a reaction mechanism controlled by ion exchange. Although lithium, sodium, and potassium in the glass have the same chance to exchange with hydronium ions, lithium is consistently released more rapidly in 165-based glass [EBERT-2] and has the least chance to be exchanged back to the glass surface because of its high hydration energy, its large hydrated radius, its low mobility in solution [FENG-2]. Additionally, lithium shows little tendency for 165-based glasses to be incorporated into the reacted layers under hydrothermal test conditions [EBERT-2]. The normalized release of lithium, therefore, is usually the greatest among all the elements in the leachate for an ion-exchange-controlled glass dissolution. The measurable concentrations of boron and silicon indicate that the glass dissolution is a collection of multiple processes,

since boron and silicon are usually released through matrix hydrolysis reactions. These multiple processes may include either (1) water diffusion, ion exchange, and matrix dissolution, or (2) hydrolysis, solution saturation, and secondary phase precipitation.

iv. 131-Type Glasses

Figure 3 compares the leach behavior between 131/11R and 131/11S at SA/V = 2000 m^{-1}. These data show that 131/11R has a lower reactivity than 131/11S. The differences are about 150% to 200% for boron and silicon, while lower differences of about 20-80% are observed for alkalis such as lithium and sodium. The pHs of the leachates in 131/11R are also lower than those in 131/11S beyond 70 days. The relative elemental releases demonstrate that lithium falls between sodium and boron for 131/11R and is lower than both sodium and boron for 131/11S.

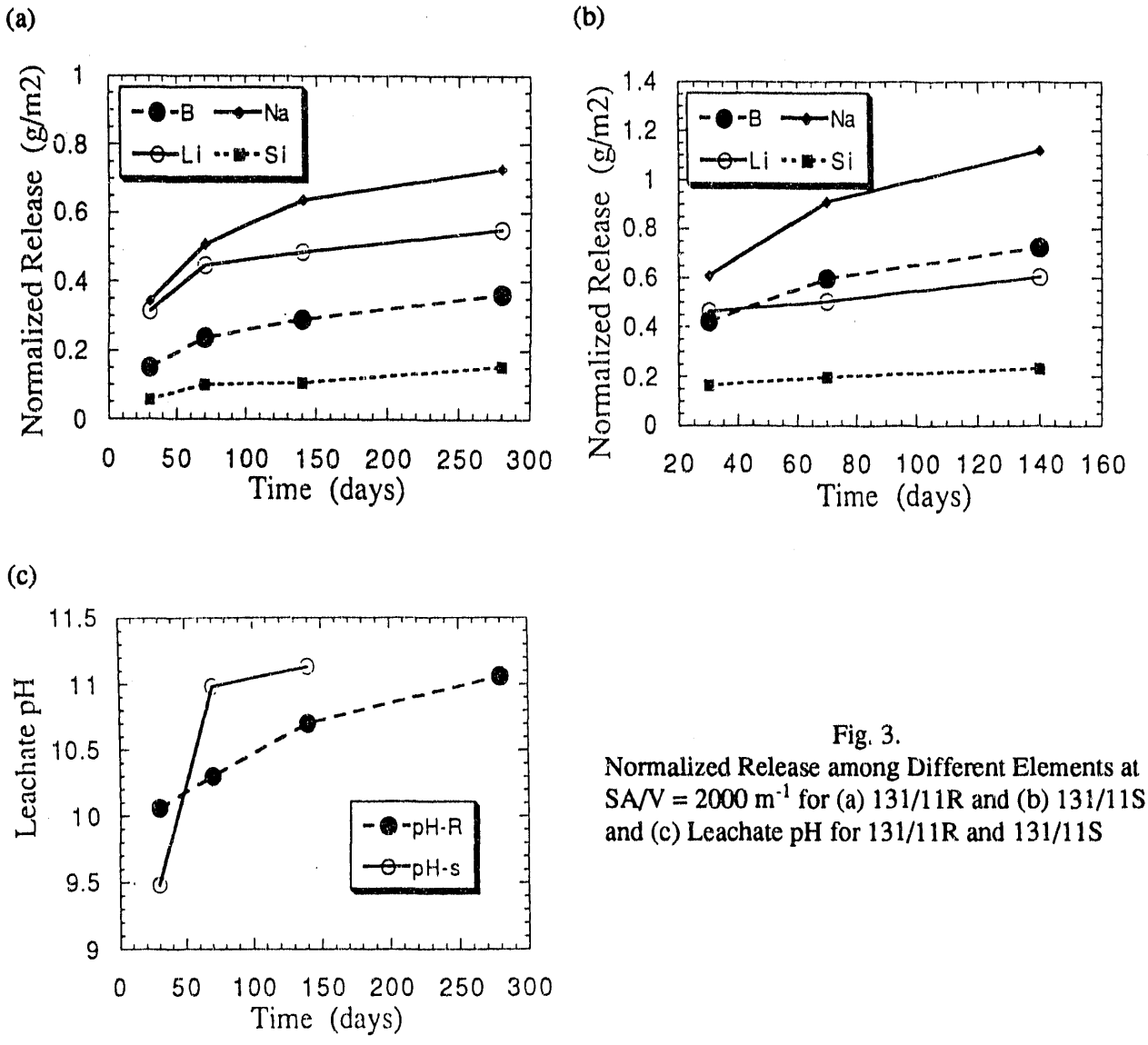

Fig. 3.
Normalized Release among Different Elements at SA/V = 2000 m^{-1} for (a) 131/11R and (b) 131/11S and (c) Leachate pH for 131/11R and 131/11S

The solution kinetics analysis suggests that matrix dissolution is the dominant glass reaction process at longer terms. The lower pHs for 131/11R are responsible for its lower elemental release rates compared with 131/11S, as discussed above for 200-type glasses. However, the solution data for 131-type glasses (as discussed below) also suggest that ion exchange plays an important role in glass reaction during the early stage of testing. As discussed above for 165/42 glass, the highest normalized release for an ion-exchange-controlled glass dissolution is usually for lithium. In the case of matrix dissolution, all the elements are released stoichiometrically. The concentration of released alkalis in solution may be reduced due to incorporation into in situ alteration layers and clay phases. However, the boron is usually very soluble and shows little tendency to be incorporated into alteration layers [SCHEETZ-1, -2]. Only minor amounts of boron have been found to participate in precipitation reactions, and the solution concentration of boron has been concluded to be a good indicator of glass reaction [SCHEETZ-2]. In matrix-dissolution-control glass dissolution, the concentration of boron is, therefore, usually higher than that of lithium and potassium but close to sodium. In fact, lithium is found to be the least concentrated species among boron, sodium, and lithium for 200-type glass, where matrix dissolution is the dominant process.

As shown in Fig. 3, the release of lithium for both 131/11R and 131/S is still higher than or close to boron, although lithium is no longer the highest release. This suggests that ion exchange has been an important process in the dissolution of 131/11 glasses. The boron release is close to sodium, and the highest release is for sodium not lithium, suggesting that matrix dissolution is now the dominant process. The solution data also indicate that 131/11S is less durable than 131/11R, and we expected that 131/11S would switch from an ion-exchange-dominated glass reaction to a matrix-dissolution-dominated process earlier than 131/11R. As a result, the concentration of boron, the most soluble product of matrix dissolution, surpasses the concentration of lithium, the indicator of ion-exchange-controlled process, earlier during the reaction progress. This is, indeed, the case, as shown in Fig. 3b, where boron release for 131/11S surpasses that of lithium, but not for 131/11R (Fig. 3a).

v. Durability of Different Glass Compositions for Radioactive and Simulated Glasses

The leach behavior of the radioactive and simulated glasses for each composition type was compared above. Also of interest is a comparison between the different glass types (131, 200, 165) for both the radioactive and the simulated glass to see whether there is a difference in the order of durability. Figure 4 presents this comparison for the simulated glass, and Fig. 5 is for the radioactive glasses. The order of glass durability for the simulated glasses arranged according to the normalized release of boron, silicon, sodium, and lithium is 165/42S > 131/11S > 200S. The pHs in Fig. 4e follow the same order as the glass durability for simulated glasses, i.e., the most durable glass, 165/42S, has the lowest pH values, while the least durable, 200S, has the highest pH values. The durability order for the radioactive glasses, as shown in Figs. 5a to 5d, is the same as that of the simulated glasses in terms of the boron, silicon, and sodium normalized releases. The pHs of those radioactive glasses in Fig. 5e also show exactly the same order as the corresponding nonradioactive glasses in Fig. 4e. However, the lithium release illustrated in Fig. 5e shows that 165/42R leached slightly faster than 131/11R. This is because the lithium release for 131/11R is much slower than that of boron or sodium, and it, therefore, does not represent a full measure of durability. This lithium anomaly is not seen in the simulated glass because 131/11S is much less durable than 165/42S, and this durability order is maintained even with the comparison between the fastest releasing element of 165/42S (an ion-exchange-dominated process), lithium, and the lowest released element of 131/11S (a matrix-dissolution-dominated process), lithium. Therefore, the durability order measured by the major element released into solution for both simulated and fully radioactive glasses is the same: 165/42 > 131/11 > 200.

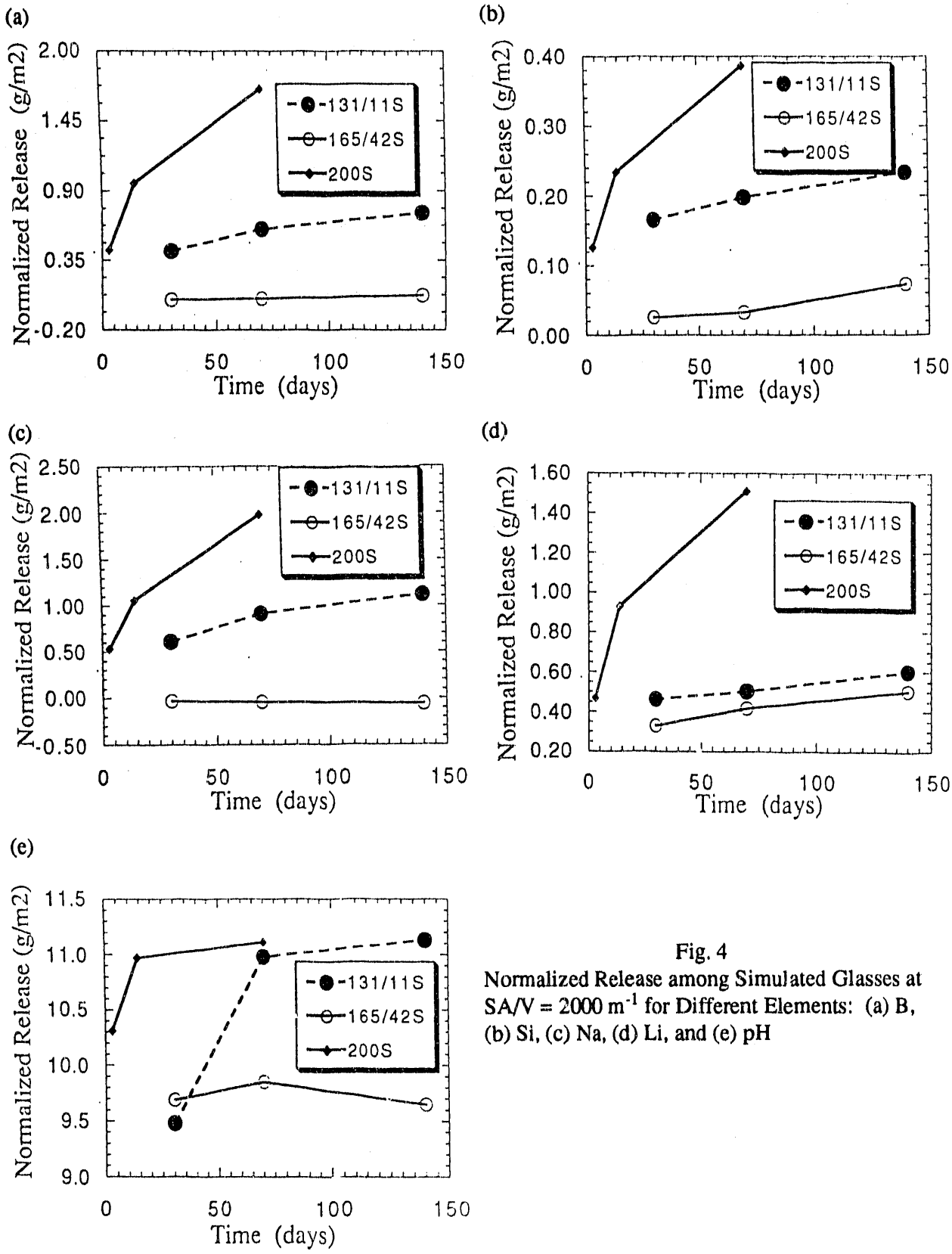

Fig. 4
Normalized Release among Simulated Glasses at SA/V = 2000 m^{-1} for Different Elements: (a) B, (b) Si, (c) Na, (d) Li, and (e) pH

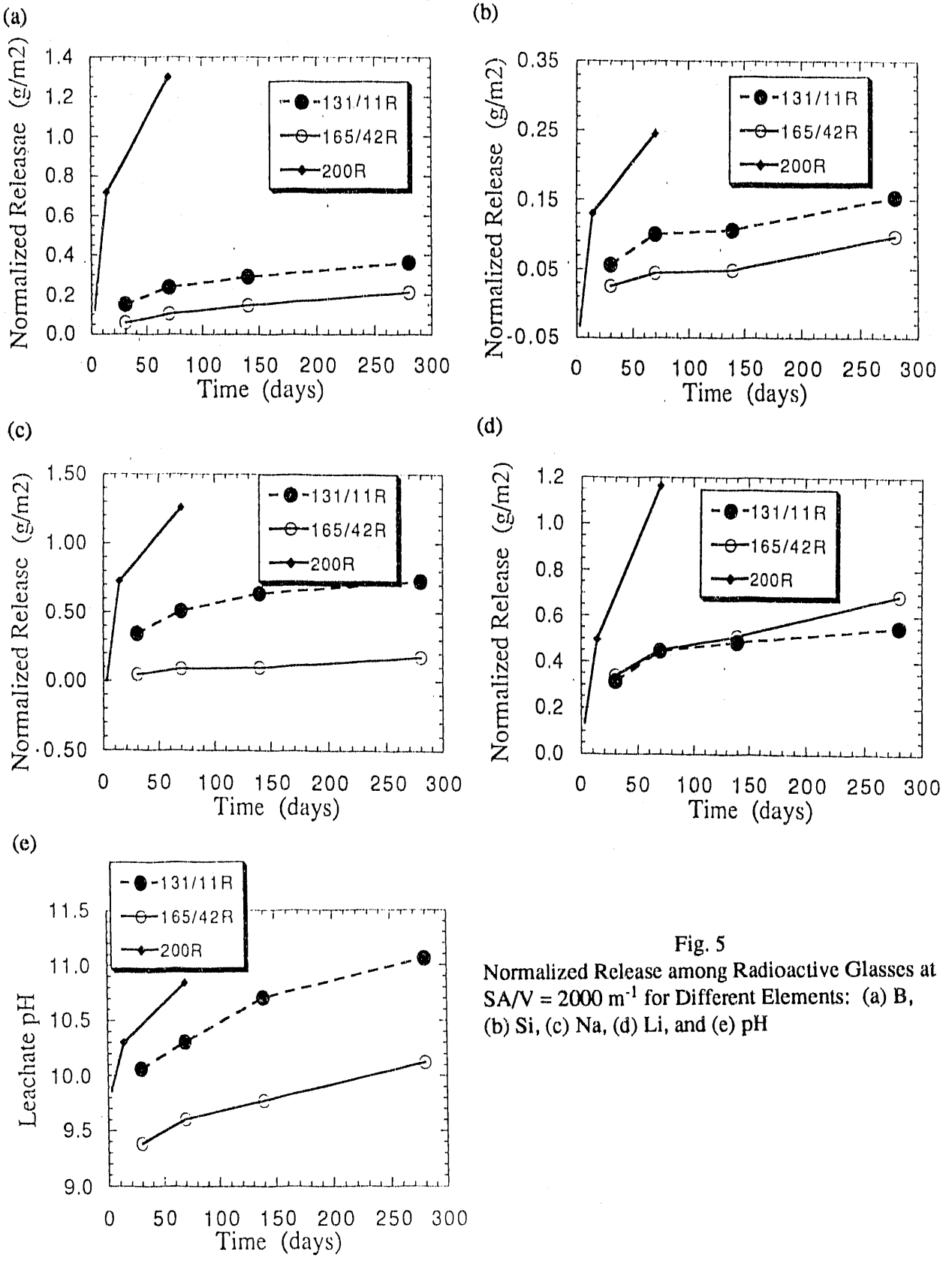

Fig. 5
Normalized Release among Radioactive Glasses at SA/V = 2000 m^{-1} for Different Elements: (a) B, (b) Si, (c) Na, (d) Li, and (e) pH

vi. Reacted Layer Analysis

In this section, the glass reactivity will be examined based on a description of the reacted layers. Temporal trends in layer formation, degree of crystallinity, and secondary phase formation will be compared between the simulated and radioactive glass types. The analysis of the reacted layers so far has been performed only on the simulated glass samples. However, a laboratory for preparation of the radioactive samples has been established, and analysis of these samples is underway. The results presented in this section are preliminary, and further comparison will be done when more results are available.

131-Type Glasses - All the reacted glass samples were surveyed by TEM and selected results are presented here. The TEM survey of 131/11S samples (SA/V = 2000 m^{-1}) reacted for 30, 70, and 140 days (Figs. 6a to 6c) shows an outer reaction layer that is partially crystallized. Beneath this layer are etch pits, which are typically 50 to 100 nm in diameter. This surface layer (etch pits plus outer layer) becomes thicker as one progresses from 30 to 140 days, and the etch pits become more extensive with time. Analysis of the outer layer shows that it is primarily composed of Si, Na, Al, Fe, and Mg, and is just beginning to crystallize. Lattice images show microcrystalline regions where only a few lattice planes are evident (Fig. 6). From this image a basal spacing of 12-13 Å is measured. This general composition and spacing are consistent with a smectite clay. The layer of glass encompassing the pitted region and extending about 200 nm into the glass is depleted of sodium, but otherwise has a composition similar to the bulk glass. The concentrations of elements lighter than sodium also may be modified, but this is not detectable with EDS.

200-Type Glasses - The reaction progress for 200S glass tested at SA/V = 2000 m^{-1} for 3, 14, and 70 days is shown in Figs. 7a to 7c. The thickness of the reacted layers and the degree of crystallinity increase with time. The layers are still in contact with glass shards at 3 days and a gel layer is present. Gradually, however, the layer becomes separated from the glass (Figs. 7b and 7c). The development of the reacted layers of 200S glasses at SA/V = 20,000 m^{-1} and 340 m^{-1} is similar to that for 2000 m^{-1}, in that the layer becomes thicker with time and gradually becomes physically disassociated with the glass.

165-Type Glasses - Compared with 131/11S and 200S glasses, this glass type is much more durable, as shown in Fig. 8a and 8b, where the reacted layers are very thin for those 165/42S glass samples (SA/V = 2000 m^{-1}) reacted for 30 and 70 days. The reacted layers became thicker as reaction time increased to 140 and 280 days. Etch pits are also observed under the layers for the longer time samples. More detailed TEM analysis on those samples is underway. Additionally, SIMS analyses are being performed to monitor the depletion of alkali elements in the base glass region.

Composition and SA/V Dependence of the Reacted Layers - Table 5 is a summary of TEM analysis results for the reacted layers. As shown, the reacted layer thickness ranges from a few nanometers for monolithic 165/42S glasses to about 200 nm for 200S glass. The thickness of the reacted layers at the same SA/V and reaction time is different for each composition. The 200-type glasses exhibited the largest thickness, and the 165-type showed the least reaction and the thinnest reacted layers. The durability measured by reacted layer thickness is 165/42S > 131/11S > 200S. This durability order agrees with that derived from solution analysis discussed above.

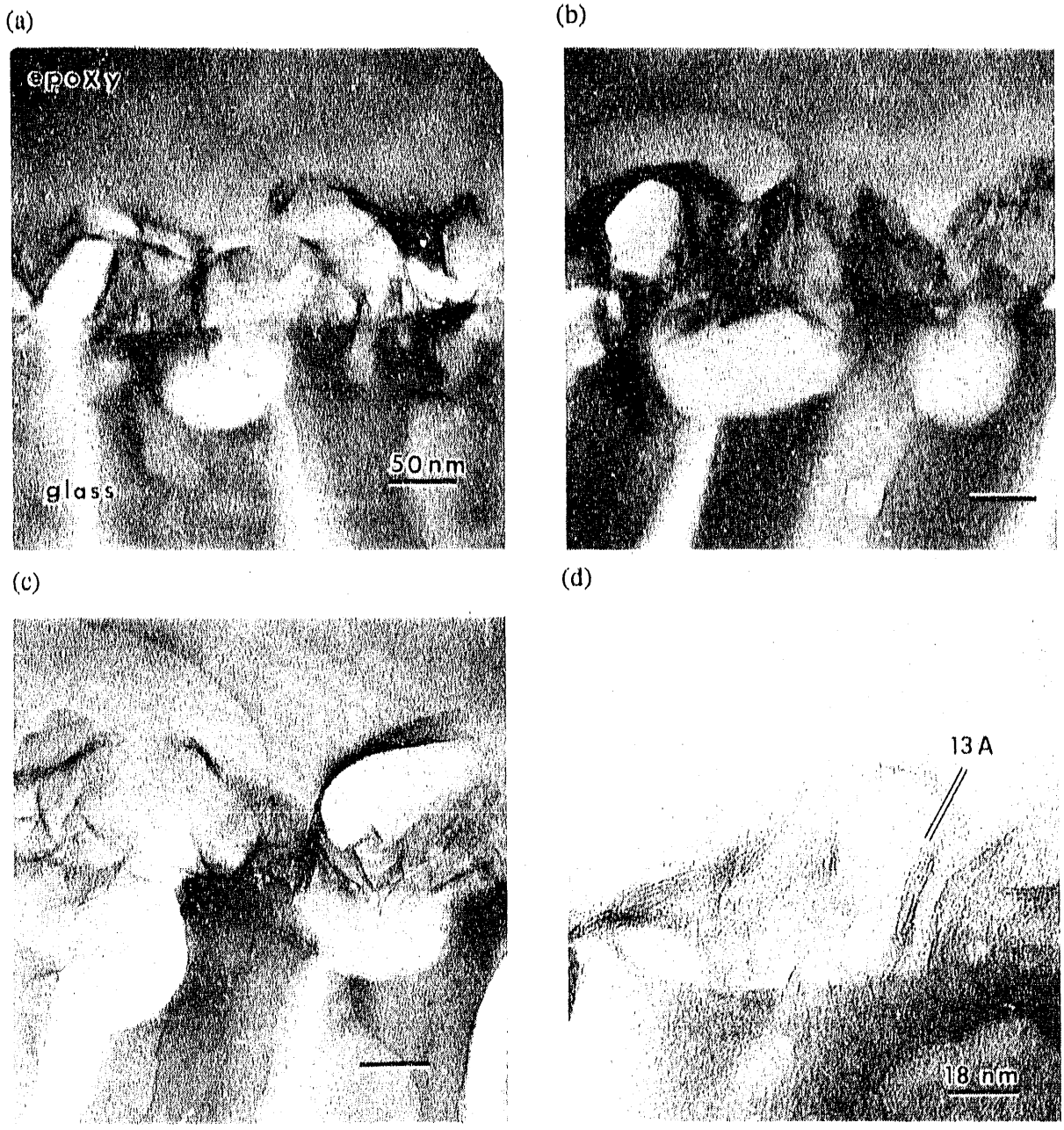

Fig. 6. 131/11S Glass Reacted at SA/V = 2000 m^{-1} for (a) 30 Days, (b) 70 Days, and (c) 140 Days, and (d) the Outer Reaction Layer (Sample DP21, 30 Days). The developing clay layer can be seen as wisps of parallel fringes. A lattice spacing of approximately 13 Å is observed. In a, b, and c, the tic mark is 50 nm.

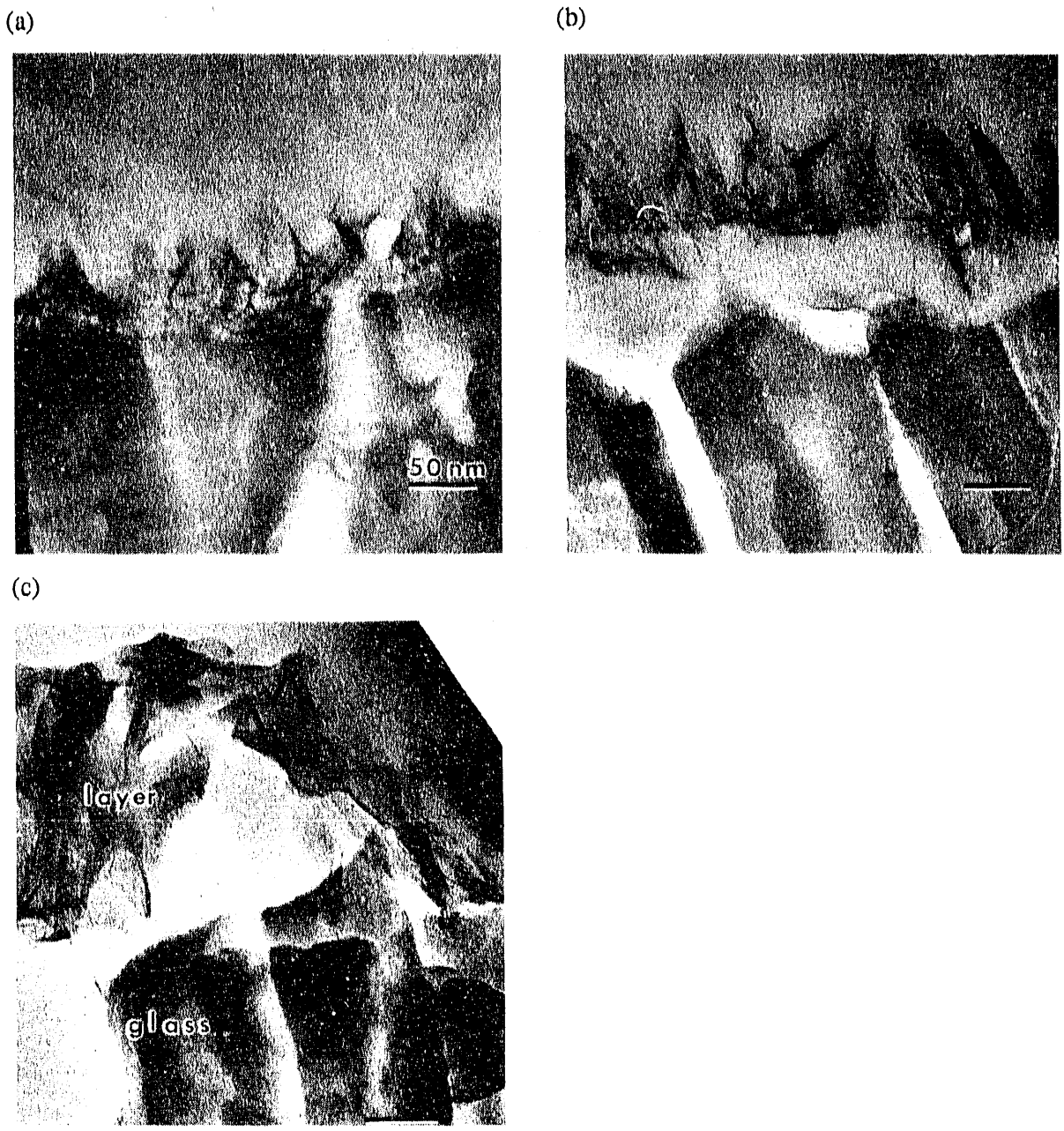

Fig. 7. 200S Glass Reacted at SA/V = 2000 m^{-1} for (a) 3 Days, (b) 14 Days, and (c) for 70 Days. The tic mark is 50 nm.

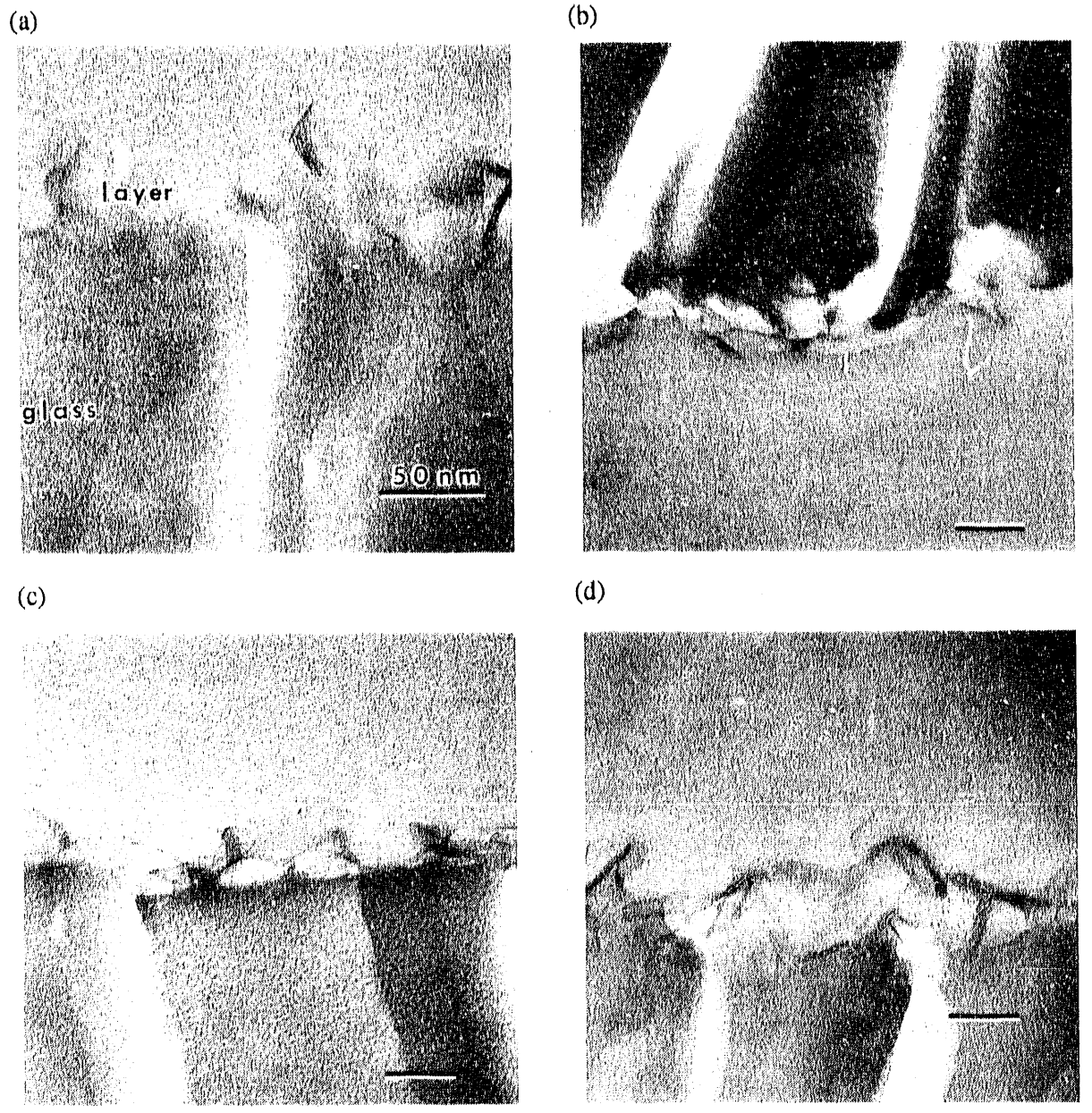

Fig. 8. 165/42S Glass Reacted at SA/V = 2000 m^{-1} for (a) 30 Days, (b) 70 Days, (c) 140 Days, and (d) 280 Days. The tic mark is 50 nm.

Table 5. Results from TEM Survey of Reacted Glass Samples

Glass	Duration, d	SA/V, m^{-1}	Sample ID	Layer Thickness, nm
SRL 165S	30	2000	DP72	5-10
SRL 165S	70	2000	DP74, DP75	~20
SRL 165S	140	2000	DP76, DP77	15-40
SRL 165S	280	2000	DP78, DP79	50-80
SRL 131S	30	2000	DP20	50-90
SRL 131S	70	2000	DP21	80-120
SRL 131S	140	2000	DP22	120-160
200S	3	2000	DP138, DP139	50-90
200S	14	2000	DP140, DP141	~120
200S	70	2000	DP142, DP143	~200
200S	15	20,000	DP174, DP175	50-80
200S	14	340	DP104	90-170
SRL 131S	28	340	DP7	20-50
SRL 131S	91	340	DP8	50-110
SRL 165S	28	340	DP41	5
SRL 165S	91	340	DP43	30-70
SRL 165S	360	340	DP45	70-120

Tests at high SA/V usually generate concentrated leachate solution after shorter reaction times, and the reaction affinity is reduced more than similar tests at lower SA/V. The reacted layers of the tests at higher SA/V are, therefore, usually thinner than those for tests at lower SA/V for the same length of time. For 200S glass, the reacted layer thickness decreased when the SA/V of the tests was increased from 340 m^{-1} to 20,000 m^{-1}. Similar comparisons for 131/11S and 165/42S compositions are not yet available.

vii. Conclusion

The leaching behavior between simulated and fully radioactive glasses is being compared through long-term testing in this study. The data discussed above reveal a difference in the leaching behavior for each pair of glass compositions. Table 6 is a schematic representation of the leachability of all the glass types at different SA/V ratios, where the leachate pH values and the normalized leachate concentrations of the major components of the radioactive glasses are compared to those of the simulated glasses.

Although differences in normalized releases were observed between fully radioactive and the simulated glass of the same type, analyses of the solution data indicate that each type of glass tested generally follows the same controlling mechanism in the glass reaction. The dominant

Table 6. Comparison of pH and Leach Rates between Radioactive and Simulated Glasses[a]

Glass Type	SA/V, m^{-1}	pH	B	Li	Na	Si
131/11	340	<	< - >	< - >	< - >	<
	2000	> - <	<	<	<	<
165/42	340	<	< - >	< - >	>	< - =
	2000	< - >	>	>	>	>
200	340	<	<	<	<	<
	2000	<	<	<	<	<
	20,000	<	<	<	<	<

[a]Comparison was made with normalized weight loss, g/m^2, radioactive vs. simulated glass. The greater than (>), less than (<), and equals (=) signs indicated that the pH and elemental normalized loss for a fully radioactive glass are larger than, less than, and equal to those of a simulated glass, respectively.

release process for both 165/42R and 165/42S is preferential alkali release, and the normalized lithium concentrations in the leachates are always the highest. The reaction of 200R and 200S is more characteristic of matrix dissolution, and the normalized boron and sodium concentrations are usually higher than the corresponding lithium concentrations, which may also suggest the incorporation of lithium into secondary phase. The 131/11R and 131/11S glasses show a reaction characteristic of matrix dissolution for the extended time periods and an ion-exchange-dominated reaction in the early test period, where normalized lithium concentrations fall between those of sodium and boron. The relative glass durability observed for the simulated glasses is 165S > 131S > 200S. The same order of glass durability is preserved for the fully radioactive glass in terms of both glass leach rates and the thickness of the reacted layers.

The pHs for the radioactive glasses are usually lower than those for the simulated glasses due to the radiolysis-induced formation of nitrogen-related acids and other acids in the leachates. This reduction in solution pH of the radioactive glasses, combined with the controlling mechanisms revealed above, helps explain the observation that the radioactive glass reacts less than the corresponding simulated glass for both 131/11 and 200 glasses, but more for 165 glasses. The controlling reaction mechanism for 131/11 and 200 glasses is matrix dissolution, where the dissolution rates are proportional to the concentration of the nucleophilic species, hydroxide. The pHs are lower in the solutions of the radioactive glasses, and therefore, lower reaction rates are observed for 131/11R and 200R glasses. On the other hand, for the time period reported, 165-type glasses are leached mainly through an ion-exchange reaction mechanism, where the reaction rate depends on the hydronium ion concentration. As the pH is lowered for 165/42R glass due to the radiation effect, the increased concentration of hydronium ions promotes the ion exchange process between hydronium ions in solution and the alkalis in glass, resulting in a faster release. Thus, as opposed to the 131- and 200-type glasses, the 165/42R glass reacts more rapidly than the 165/42S.

The results demonstrate that, under conditions of the reported tests, a radiation effect exists, mainly in terms of its influence on the leachate pH, which, in turn, affects glass reaction. The differences in reactivity between the radioactive and simulated glasses can be reasonably explained if the controlling reaction mechanism is taken into account. The reactivity differences are glass-composition and leaching-mechanism dependent, and while the difference in reactivity reaches a maximum of 400% for selected elements, the overall difference in reactivity is small.

c. Future Progress

The ongoing static tests will be continued. The emphasis will be placed on analysis of the reacted samples. This includes the detailed surface examination on simulated glass and the initiation of the surface analysis on radioactive samples. Data will be generated to compare the identities and sequences of secondary phases of radioactive and simulated glasses. The radionuclides will continue to be analyzed from unfiltered, filtered, and acid strip solutions, and the data will be analyzed to identify the temporal trends and distribution of the radionuclides. The solution data, combined with surface analysis results, will be used to further compare the reactivity of the radioactive and nonradioactive glasses and to provide a data base for validation of glass performance models.

2. Long-Term Intermittent Flow Tests at High SA/V

The long-term intermittent flow tests are being conducted using the Unsaturated Test (UT) procedure developed by the YMP to assess glass performance in an unsaturated environment [BATES-2, -6]. The standard UT matrix was modified to include effects of aging both the glass and metal components to make the results more relevant to an actual storage environment. The tests are being performed with 200R glass, and the objectives of the tests are to provide (1) data that describe the release of radionuclides from a specifically designed waste package under strictly controlled test conditions and (2) information concerning synergistic effects that may occur between waste package components. Since the tests are performed with 200R glass, all preparation for these tests was done in a hot cell.

a. Status

The test matrix is shown in Table 7. There are two sets of five replicate tests and one blank test.

The first set of five tests is being done with aged components. The glass was aged by contact with water vapor at 200 °C. This reaction accelerated hydration of the glass such that the outer surface of the glass was transformed into stable crystalline phases. Two degrees of hydration aging were obtained by reacting the glass samples for two and four weeks. Two tests (one batch and one continuous) are being done with the four-week hydrated glass, and three tests (one batch and two continuous) are being done with the two-week hydrated glass. The hydration of glass in a vapor environment is not only a process that can be used to age the glass in the laboratory, but also a process that likely will occur in the repository. Glass aging could occur in a steam environment if containment breach occurs before the temperature of the waste package cools below 95 °C. It could also occur in a vapor environment if a breach occurs at a temperature below ~95 °C prior to ingress of liquid water. The latter case is the expected environment for the unsaturated repository; thus the present tests are being done to induce a degree of vapor hydration aging that likely will occur in the repository.

Table 7. Test Matrix for Long-Term Intermittent Flow Tests at High SA/V

Test Designation[a]		Components[b,c]	Test Duration, yr						
			0	0.4	0.8	1.0	1.5	2.0	2.5	3.0
N4	#1 Batch	4-week aged glass, 304L SS holder								
	#2 Continuous	4-week aged glass, 304L SS holder								
	#3 Batch	2-week aged glass, 304L SS holder								
	#4 Continuous	2-week aged glass, 304L SS holder								
	#5 Continous	2-week aged glass, 304L SS holder								
	#6 Batch	glass, 304L SS holder								
	#7 Batch	glass, 304L SS holder								
	#8 Continuous	glass, 304L SS holder								
	#9 Continuous	glass, 304L SS holder								
	#10 Continuous	glass, 304L SS holder								
	#11 Continuous	blank								

	No. Analyses Required						
Total radionuclide (solution and metal)	7	7	9	7	12	7	7
Total matrix element (solution Li, B)	7	7	8	7	10	7	7
Wt loss and surface analyses			1		3		
Interaction of stainless steel			1		3		

[a]The continuous tests are sampled every four months for the first year and every six months thereafter and continue until termination.
[b]In tests 6-10, the 304L SS holder will be partially sensitized; in tests 1-10, the 304L SS holder will be partially sensitized and then subjected to an aging process along with the glass.
[c]In tests 6-10, the glass will be as-prepared. In tests 1-5, the glass will be aged as indicated.

The second set of five tests is being performed with unaged or as-cast glass, and the results will be comparable with previous test series using the UT method [BATES-6]. These tests represent the scenario whereby the container and pour canister are breached at a time after liquid water has penetrated the waste package environment and liquid water immediately passes through one breach, contacts and reacts with the glass, and passes out through a second breach. This scenario is unlikely; nevertheless, it represents a bounding condition with fresh glass, and the results will form a basis for comparison with tests done with aged components.

To begin the tests, 11 cast glass forms were produced. This was done by homogenizing a 300 g batch of 200R glass by grinding, then melting 100 g batches to cast the waste forms. The cast waste forms were made by pouring the glass into specially manufactured Pt-5% Au molds and annealing for a short period of time. The cast forms were released from the molds and cut to size, cleaned, examined, and introduced for testing. The entire matrix of 11 tests was initiated on 6/27/91 and 7/1/91, and the first four-month sampling period has been completed.

b. Results and Discussion

To determine the conditions to be used in the hydration aging process, two practice hydration runs were done using nonradioactive start-up frit. This frit has a composition similar to 200R glass, and while detailed reaction kinetics for the hydration process cannot be derived from these tests, it is necessary to demonstrate that (1) the hydration process can be done in a full-sized test vessel (standard hydration tests are performed in 22 mL Parr vessels, while the UT is performed in specially designed 100 mL 304L type stainless steel vessels), and (2) a measurable degree of hydration occurs with this glass.

The practice hydration runs were done in duplicate for a five-week period. The runs were successful in that the test vessel maintained pressure and the glass was heavily hydrated, yet still intact, at termination. The hydrated glass was examined, and its reaction is similar to that reported for 202U glass (see Sec. VI of this report). Based on the results of the practice hydration runs, hydration periods of two and four weeks were chosen for the 200R glass.

The 200R glass was hydrated according to schedule, and the aged radioactive glasses had the same general appearance as the hydrated practice glasses. The outer glass surface had transformed into stable secondary phases, which were loosely associated with the glass monolith. These hydrated glasses were transferred to new test vessels immediately after the aging process was completed, and the testing was initiated.

The first sampling period was completed on 11/4/91, and the test solutions were analyzed for pH, carbon, anions, cations, and radionuclides. Additionally, the test solutions were wicked through "holey" carbon grids to trap particulate material suspended in solution for TEM analysis, and an aliquot of solution was sequentially passed through varying pore size filters to study the size distribution of potential radionuclide-bearing colloids.

To date, only the results of the pH measurements are available. The tests done with aged glass all have solution pH values in the 11.5 range, while the tests with as-cast glasses had pH values in the 8.5 range. Most likely, alkalis leached from the glass during the aging process and not incorporated into stable phases were rinsed from the surface during the initial water contact. The other solution analyses should evaluate the differences in the release of radioactive components.

c. Future Progress

The ongoing drip tests will be terminated as scheduled, and analyses performed with emphasis on radionuclide release. It is anticipated that partial results will be available for the first draft of the Critical Review and Compendium, as needed.

3. Long-Term Repository Environment Tests

The laboratory analog test has been developed [BATES-7] to relate the performance of glass as observed in the Unsaturated Test with a more repository-relevant environment. In the laboratory analog test, the waste package assemblage (WPA) as used in the Unsaturated Test is placed within a bored-out cavity in a tuff core. The dimensions of the WPA and the cavity are similar to those used in the Unsaturated Test. A sketch of the apparatus is shown in Fig. 9. The tuff core and WPA are assembled, and an unsaturated flow of water is forced through the core by using a vapor pressure slightly above ambient.

The objective of this test is to evaluate glass performance in an environment that closely matches that expected in the repository. Emphasis is placed on measuring glass reaction by examining the reacted glass and surrounding tuff rock at the test termination and by monitoring the radionuclide content of the groundwater as it is released from the test vessel.

a. Status

Two analog tests have been started using 200R glass. One is using unaged glass and a sensitized 304L stainless steel retainer, and one is being done with three-week-aged glass and stainless steel. As with the drip tests, the preparation of these tests had to be done in a hot cell due to high levels of radioactivity associated with the glass.

b. Results and Discussion

The hydration reaction produced aged glass similar in appearance to that used in the drip tests. The aged glass was transferred to the tuff core without incident, and both tests are ongoing. However, no water has yet been collected from the output line; thus no measurement of radionuclide release has been measured. Based on past experience, it takes about one month before liquid is released from the test, and the water collection rate is ~0.01 mL/h. Enough liquid is available for analysis after several months of testing.

c. Future Progress

The tests will continue, with periodic monitoring of the effluent.

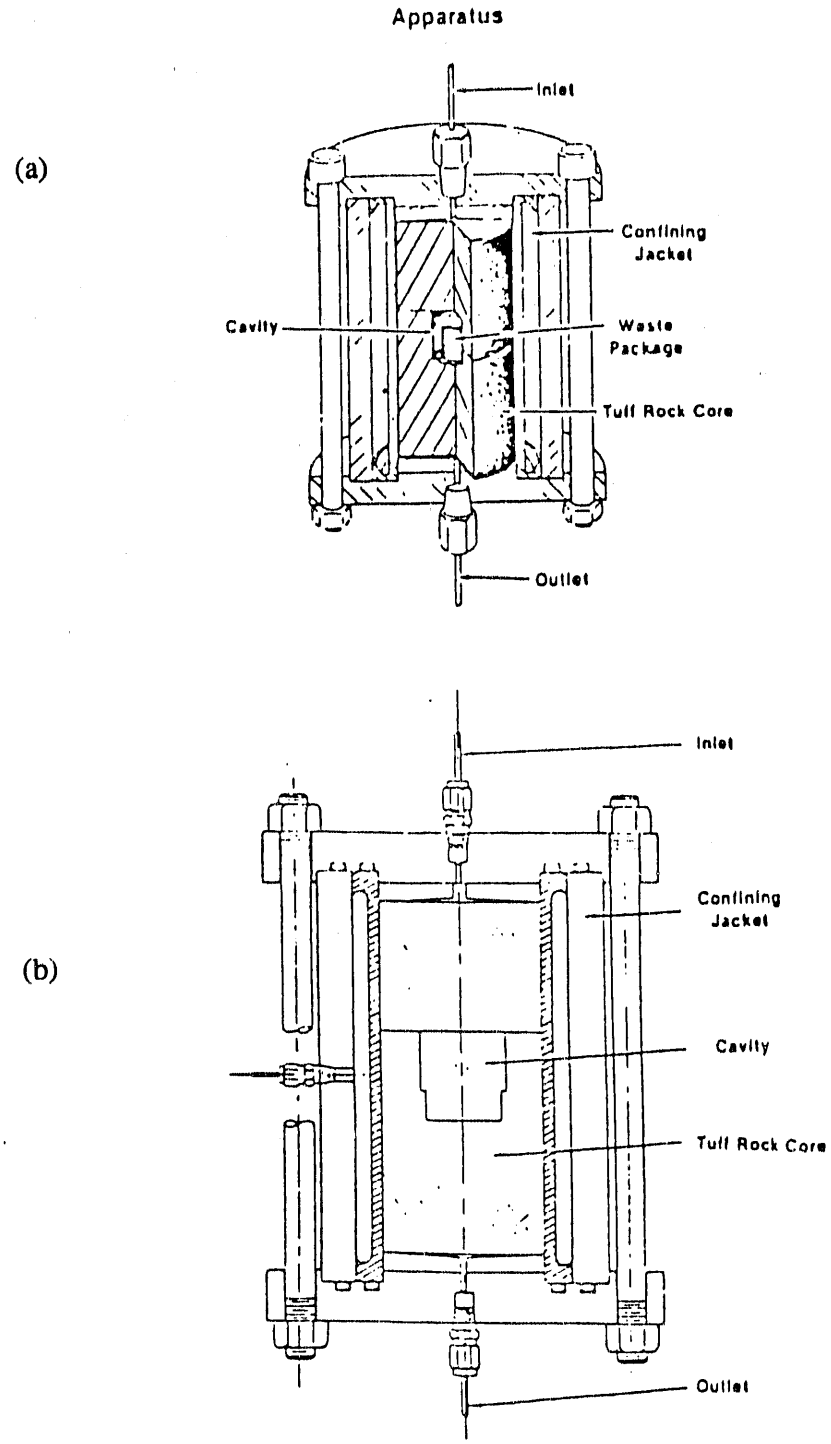

Fig. 9. Representation of the Laboratory Analog Test Apparatus (a) with Glass as the Waste Form and (b) without the Waste Form. Note that the waste form does not rest on the bottom of the test cavity but on a shelf situated above the cavity, as shown in Fig. 9b.

VI. EFFECT OF RADIATION ON GLASS REACTION AT LARGE SA/V

A. Introduction and Background

Many studies have been conducted to investigate the effects of radiation on glass leaching in air-water systems. Notable decreases occur in the pH of deionized water in the presence of an irradiated air system [BARKATT-1, McVAY]. This acidification is attributed to the radiolytic decomposition of molecular nitrogen and carbon dioxide, and a several-step recombination of the dissociation products with oxygen and water to produce nitrogen and carboxylic acids [LINACRE, BURNS, VAN KONYNENBURG]. Exposure of simulated borosilicate waste glass monoliths to such an acidified system may result in significant increases in glass reactivity.

In similar experiments conducted with tuff groundwater exposed to ionizing radiation, large decreases in the leachate pH were buffered by bicarbonate in solution, or the radiogenic acids were readily diluted under the relatively low SA/V conditions of the tests [BATES-4, -8; ABRAJANO-1; EBERT-2, -3]. The resultant glass reaction rates do not display any increase when bicarbonate is present in the leachate.

Under the geologically unsaturated conditions expected at the proposed Yucca Mountain repository, the most likely scenario for water contact with the waste glass, in the event of container breaching, is by condensation of thin films of water on the glass surface. Rapid concentration of radiolytic products may thus occur in the limited amount of water present on the glass. In such a high SA/V type environment, the bicarbonate present in the small volume of leachant may be quickly overwhelmed by nitric acid produced in radiolysis reactions. Any nitric acid that subsequently condenses on the glass surface is likely to react with the glass and may significantly alter the degradation of this waste form.

The limited quantity of solution expected to condense on the glass surface will also preclude any volumetric dilution of the radiolytic and the glass dissolution products. Rapid concentration increases of glass dissolution products will also result in saturation of leachate with respect to certain secondary alteration minerals, accelerating the eventual precipitation of secondary phases. This process may promote rapid dissolution of the glass as secondary phases sequester elements from the leachate and lower the activity of certain ions in solution, thereby promoting additional dissolution of the glass [EBERT-4]. The present experiments are thus designed to examine the effects of radiolysis and the formation of radiolytic products on the performance of glass in an unsaturated repository environment (high SA/V conditions).

At the time of glass production, the dose rate of gamma radiation from a container of glass will be approximately 8×10^3 rad/h [BAXTER]. Experimental evidence obtained during gamma irradiation of a two-phase air/water system indicates a reaction efficiency (G value) of ~2 molecules of NO_3^- produced for each 100 eV of energy absorbed at ~80°C [LINACRE]. Using this G value, the G/L ratio, the dose rate, and the concentration of N_2 in the gas phase, the amount of nitric acid produced in the system can be calculated by using an equation presented by Burns et al. [BURNS]. The gamma field will decrease by more than three orders of magnitude during the first 1000 years of storage. Thus, the effects of gamma radiation on glass performance will be important only under unanticipated conditions of premature canister breach and water ingress.

The glass will also contain long-lived alpha-producing actinides, such as Pu-239 and Pu-240. The initial concentrations of these two radionuclides are 3.48×10^{-3} and 2.34×10^{-3} Ci/lb glass, and the half life is 24,110 and 6560 yr, respectively [BAXTER]. Due to their long half-lives, the radiation field produced by alpha emitters is expected to dominate during the later stages of the service life of the repository.

Only alpha particles produced within approximately 10^{-4} cm of the glass surface may escape from the waste and contribute to radiolysis reactions. Using the actinide concentration data for a 1000-year-old glass waste form [AINES], an alpha dose rate of 20 rad/h is expected to be emitted and absorbed within a 4-cm air layer above the glass. Any alpha particles escaping the glass would also only escape into the air if the film of water adsorbed on the glass is less than 4×10^{-3} cm in thickness. The HNO_3 production by alpha particles in moist air is expected to be the same as for gamma radiation [LIND], although the high G/L ratio experimental data are not sufficient to support this theory.

B. Objectives

The overall purpose of this task is to determine if radiation has any significant effect on glass durability under the high SA/V conditions that are expected for an unsaturated repository site. Data will be collected to examine three main objectives. The first objective examines the effect of radiation on moist air systems, without the presence of glass (blank experiments), and the locations and concentrations of radiolytic products. Variables to be tested include radiation type (alpha vs. gamma), temperature, dose rate, and gas/liquid (G/L) volume ratio. The second objective examines glass reaction rates in unsaturated conditions as a function of glass composition and SA/V ratios. Comparisons of alteration profiles from glasses reacted in irradiated vs. nonirradiated conditions will be used to characterize the influence of irradiation on alteration rates. The final objective examines the influence of radiation and the radiolysis environment on the stability and formation of secondary phases. Detailed SEM/EDS, AEM, and XRD comparisons between alteration assemblages developed on glass in irradiated vs. nonirradiated conditions will be used to characterize the influence of irradiation on mineral phase development.

C. Technical Approach

Blank experiments have been carried out in several sample configurations, with each test conducted in duplicate. Gamma blank tests were conducted in 22 mL stainless steel Parr test vessels, with enough deionized water (DIW) added to achieve a G/L volume ratio of 100 at 25°C. These tests will be used as a comparison between NO_3^- yields in a high SA/V environment, as is expected for an unsaturated environment, relative to results previously obtained at lower SA/V ratios (0.1 to 18; LINACRE). The present experiments also allow an evaluation to be made of NO_3^- yield differences, if any, that will result from the use of a γ-radiation source with the present tests, relative to the neutron-dominated source of the Linacre and Marsh study. The gamma blank tests were irradiated with an external gamma source of $\sim 3 \times 10^3$ rad/h, and elevated temperature experiments were maintained in thermally controlled ovens. Gamma blank experiments will also be run at an external dose rate of 1×10^5 rad/h. Results from these tests will allow a comparison to be made of the effect of variable dose rate on NO_3^- production.

Alpha blank tests utilized a 1500 μCi ^{241}Am foil attached to either a lucite or stainless steel support rod. The measured dose rate from these samples is also $\sim 3 \times 10^3$ rad/h. This assembly was inserted and sealed into a two-quart glass vessel with enough DIW added to achieve a G/L volume ratio of 100. These

tests will also allow a comparison of the effects of different types of ionizing radiation when results are correlated with the previously described gamma-blank tests and the neutron source tests of Linacre and Marsh. Upon completion of both types of blank tests, solution aliquots were taken for pH, carbon, and anion analyses. The surfaces of the test vessels and the alpha foils and support rods in the alpha blank tests were next sprayed with DIW to collect any radiolytic products that had collected on these surfaces. Aliquots of this "rinse" solution were also submitted for pH, carbon, and anion analyses.

Experiments with glass monoliths were also performed in the same type of 22 mL stainless steel test vessels used in the gamma blank tests. The glass samples for these tests were cut into 0.1-cm thick by 1.0-cm diameter glass disks. Several different glass compositions were tested, including uranium-doped SRL 131 and 202 compositions, and actinide- and technetium-doped SRL 131, 165, and 202 composition glasses. The 202 composition glass is similar to that projected for waste disposal, while the 131 and 165 compositions represent glasses that are less and more durable, respectively, relative to the 202 glass.

Two types of SA/V tests are being conducted with glass monoliths present, with all tests conducted in duplicate to quadruplicate. The first test type involves the immersion of four glass monoliths in 2 mL of EJ-13 water at an SA/V ratio of 340 m^{-1} and a temperature of 90°C. This batch monolith test design allows for the highest SA/V ratio attainable with the glass monoliths completely immersed in water, and also allows for the collection of enough solution aliquots to complete all desired analyses. As with the gamma blank tests, these experiments will be exposed to an external gamma source of ~3 x 10^3 rad/h. Solution aliquots will be taken from these tests to analyze for pH, carbon, cation, anion, and filtered size distributions of actinides.

The second test type is conducted at a much higher SA/V ratios (~4000 m^{-1}). The exact SA/V ratio of these vapor hydration tests is difficult to constrain because the adsorption of fluids on the glass may vary as a function of the composition of the solution in contact with the glass surface. These tests will be performed with two slotted glass monoliths suspended in each vessel by a Teflon or platinum support thread. Each vessel will have 0.25 mL of DIW added, and experimental temperatures will range from 150 to 200°C. The elevated temperatures of these experiments are used to accelerate the glass reactions to reasonably short experimental time frames. Previous testing [ABRAJANO-1] indicated that the glass reaction mechanism and sequence of secondary phases produced will not change under the range of temperatures examined. These tests will either be conducted in the absence of radiation or at an external gamma source of ~3 x 10^3 rad/h. Comparisons between irradiated and nonirradiated glasses will indicate what influence the irradiated environment has on glass reaction. Because of the small amounts of solution present in these tests, it will not be possible to take aliquots for analysis. Instead, extensive solid phase characterizations will be made of altered surface material by optical microscopy, SEM/EDS, XRD, and AEM. Alteration profile development and secondary phase genesis will be utilized as a gauge of the reaction rates.

1. Matrix

The experimental matrix is displayed in Tables 8 to 10. A minimum of two tests was carried out in each configuration, although in some instances up to four identical tests have been carried out. These multiple evaluations allow for a comparison of the precision of the testing method. For tests utilizing glass monoliths, the composition of the initial glass frit is given in Table 1. The composition of the EJ-13 solution used in batch leach tests is given in Table 2.

Table 8. "Effects of Radiation" Sampling Matrix for Alpha and Gamma Blank Tests

Expt. Number	Radiation Type	Temp., °C	Test Length, days	Dose Rate, MR/hr	Gas/Liquid Ratio, L/L	Status of Experiment Group
IV9000	Gamma	25	14, 28, 56, 120	0.100	100	To be initiated, dosimetry tests started
IV9000	Gamma	25	14, 28, 56, 120	0.003	100	Tests completed
IV1000	Gamma	90	56, 120, 180	0.003	100	Tests completed
IV2000	Gamma	200	56, 120, 180	0.003	100	Tests completed
IV9000	Gamma	25	56, 120	0.100	10	To be initiated, dosimetry tests started
IV9000	Alpha-Lucite Support	25	14, 28, 56	0.003	100	Tests completed
IV9000	Alpha-SS Support	25	14, 28, 45, 56, 85, 110, 129	0.003	100	85- and 110-day tests in progress, all others completed

Table 9. "Effects of Radiation" Sampling Matrix for Vapor Hydration Tests

Expt. Number	Glass Type	Temp., °C	Water Type	Test Length, days	Status of Experiment Group
IVE202A	202A	200	DIW	7, 14, 21, 35, 56	All completed, reruns planned
IVE202U	202U	200	DIW	7, 14, 21, 35, 56	All completed
IVE165A	165A	200	DIW	7, 14, 21, 35, 56	Tests under preparation
IVE131A	131A	150	DIW	7, 14, 21, 35, 56	Tests under preparation
IVE131U	131U	150	DIW	3, 5, 7, 14, 28, 56, 91, 180	Most completed, 180-day tests active

Table 10. "Effects of Radiation" Sampling Matrix for Saturated Batch Leach Tests

Expt. Number	Glass Type	Temp., °C	Water Type	Test Lengths, days
IV9202A	202A	90	EJ-13	14, 28, 56, 91, 180, 360, 540,[a] 720[a]
IV9165A	165A	90	EJ-13	91, 180, 360, 720[a]
IV9131A	131A	90	EJ-13	14, 28, 56, 180, 360,[a] 720[a]

202A Scheduled sampling dates: 540 d, 2/8/92; 720 d, 8/6/92

165A Scheduled sampling dates: 720 d, 9/3/92

131A Scheduled sampling dates: 360 d, 3/5/92; 720 d, 9/15/92

[a]These tests are in progress; all other completed.

2. Status

All of the 14 initially planned alpha blank experiments have been completed; however, four additional tests have been initiated to fortify the present results. Twenty of the original 32 gamma blank tests have been completed, with results being tabulated for the standard and elevated temperature experiments. Dosimetry tests have been initiated to identify suitable locations for the remaining 12 gamma blank experiments at higher dose. All 45 of the batch monolith leach tests have been initiated, with 29 of the tests being completed. Anomalous results in four of the experiments will warrant additional reruns (see discussion below). For the nonirradiated vapor hydration tests, 25 of the 34 experiments have been terminated, and 19 samples have undergone extensive surface examinations. For the irradiated vapor hydration experiments, 10 of the 30 tests have been completed; however, these tests will be rerun again with platinum support wires replacing the Teflon wires used previously. These replicate experiments are being undertaken due to some concern that Teflon will degrade in the irradiated environment of the tests, and possibly influence the experimental results by reacting with the glass wafers. Only limited surface analyses of these tests have been performed to date.

D. Results and Discussion

1. Blank Tests

Results presented previously [BATES-4] indicate that significant amounts of nitrate and carbon (both inorganic and organic) were produced during the alpha blank tests. Only minor amounts of Cl^-, F^-, SO_4^{2-}, and NO_2^- were detected, either in the surface rinse fraction or bulk solution. Nitrate and nitrite were concentrated in the surface rinse fraction, with the total production of NO_3^- resulting in a $G(NO_3^-)$ value of 2.0 ± 0.7 (Fig. 10). These results indicate that alpha irradiation of an air atmosphere saturated with water vapor culminates in the concentration of nitrate and nitrite in the thin films of water covering the solid surfaces and, to a lesser extent, in standing water at the bottom of the test vessel.

The carbon results display a larger degree of scatter than those for nitrate. Both organic and inorganic carbon concentrations increase with time in alpha irradiated tests using lucite support rods. Results from the tests using stainless steel support rods do not show any consistent temporal variations, yet increases are noted in inorganic and especially organic carbon concentrations of the rinse fraction. These results suggest that some of the carbon in the tests with a lucite rod is being derived from the lucite rods themselves. The increase in organic carbon in the stainless steel rod supported tests, however, indicates that some organic carbon is being produced in these experiments from CO_2. Both formate and oxalate were detected in solutions analyzed from alpha and gamma blank tests, although the concentrations of these species do not display any linear relationship with absorbed dose. These carboxylic acids may play an important role in the transport of radionuclides; thus their occurrence in these tests will be more fully evaluated in the future.

The amounts of nitrate and nitrite are also greatest in solutions rinsed from the vessel walls in the gamma blank tests. This pattern is the same as that found in the alpha blank experiments. At 25 °C, the nitric acid produced by radiolysis and dissolved into the condensed water is predicted to result in a pH of about 3.9 after 7 days.

Gamma radiolysis blank tests run at 25, 90, and 200 °C measure the formation of radiolytic products as a function of temperature. Results indicate that NO_3^- production varies inversely with temperature, with the lowest quantities being detected for the higher temperature experiments (Fig. 11). The $G(NO_3^-)$ values for the 25, 90, and 200 °C experiments are 3.2 ± 0.8, 1.4 ± 0.7, and 0.47 ± 0.10, respectively. The 90 °C yields are comparable to the $G(NO_3^-) = 1.9$ value obtained by Linacre and Marsh

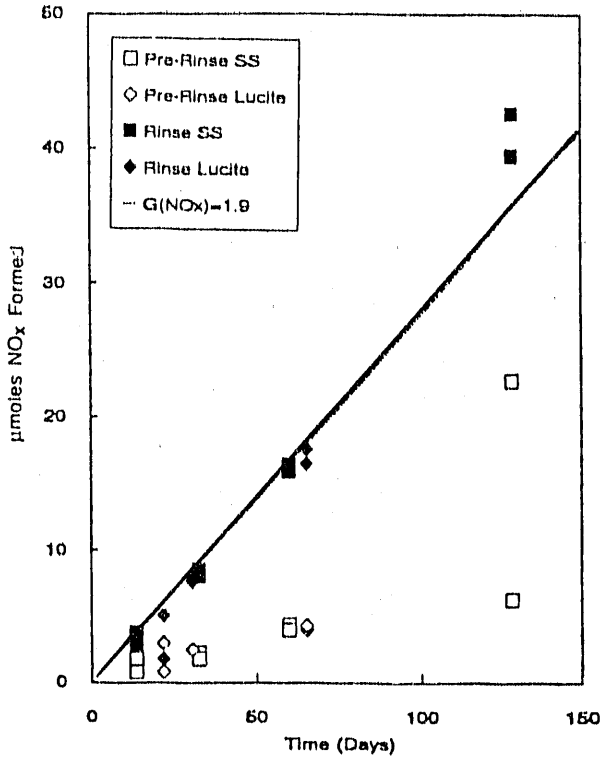

Fig. 10.
Nitrate plus Nitrite Formation in Alpha Blank Tests. $G(NO_x) = 1.9$ from ~80°C data of [LINACRE]. Dose rate ~3 x 10^3 rad/h.

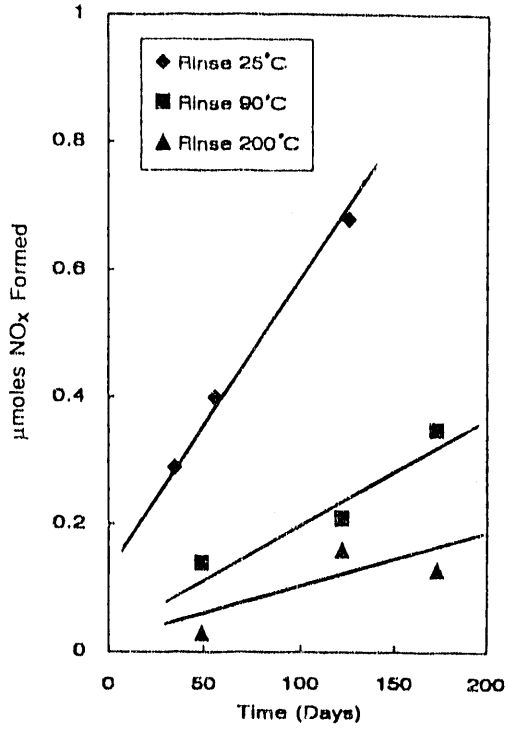

Fig. 11.
Average Nitrate plus Nitrite Formation in Gamma Blank Tests. Dose rate ~3 x 10^3 rad/h.

in tests conducted at 80°C. The results indicate that NO_3^- yields for the 90°C experiments are ~40%, while the 200°C yields are ~15% of those that characterize the 25°C results, respectively. These results are important in that the highest gamma dose rates will occur when the repository temperature is also the highest. Thus, the elevated temperatures early on in the repository may buffer the repository environment from large decreases in pH.

2. Tests with Glass Monoliths

For the second objective of these experiments, the cumulative effects of these radiolytic products on the alteration of a simulated borosilicate waste glass were examined. Glasses of identical compositions were reacted under variable SA/V conditions in both radiation and nonradiation fields. Water vapor contact with the glass may result in hydration aging and alteration, which may ultimately affect the release of radionuclides when the hydrated glass is contacted by liquid water. The reaction occurs in a thin film of water sorbed onto the glass surface. The result of hydration is the formation of an in situ hydrated layer penetrating into the glass and the precipitation of secondary mineral phases on the reacted surface. The goal of the initial vapor hydration studies is to determine if ionizing radiation will influence the hydration aging of glass. Previous investigations note the formation of secondary phases during exposure of glass to water vapor in a radiation field [YOKAHIMA], but comparative studies between irradiated and nonirradiated conditions have not been made. The present study compares the reactivities of various SRL 202 frit-based glass compositions doped with the transuranic isotopes ^{237}Np, ^{239}Pu, and ^{241}Am and a uranium-containing analog (for example, 202A and 202U, respectively).

a. Vapor Hydration Tests

The thin films of water in contact with glass wafers in the irradiated vapor hydration tests with 202A glass turned out to be so corrosive that the samples had reacted completely through their ~1 mm thicknesses between 35 and 56 days of exposure. By contrast, the 35- and 56-day samples reacted in a nonirradiated environment have in situ hydration layer thicknesses of 51 ± 9 and 132 ± 15 μm, respectively, as measured by SEM of cross-sectioned altered glasses (Fig. 12). The overall reaction rates

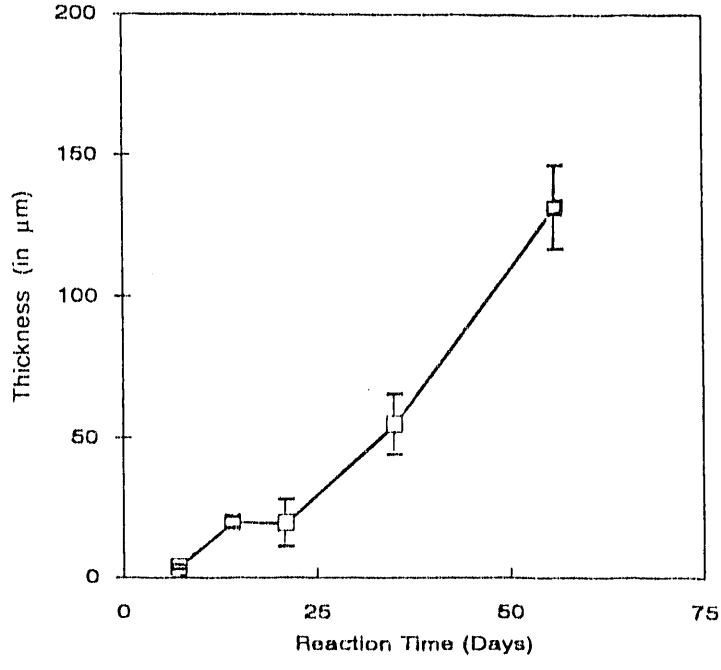

Fig. 12.
Alteration Layer Thickness of 202U Glasses Reacted at 200°C. Error bars indicate ±1σ standard deviation on alteration layer measurements.

determined in these experiments indicate an alteration rate of 2.4 μm/day for the nonirradiated samples, while the irradiated samples had reaction rates of approximately 10-15 μm/day. This preliminary comparison suggests that glass reaction rates in a vapor-dominated radiation field exceed those in a nonradiation field by a factor of about five.

Reaction layer measurements were also made on 131U glasses reacted in a vapor environment for up to 14 days at 150°C. Alteration layer thicknesses of 5.1 ± 0.9 μm were measured for the 14-day glass. Additional 131U glass tests have been initiated, so that long-term alteration effects on glass durability can be quantified (Table 10). Comparative tests of these glasses in an irradiated field have yet to be initiated.

The radiation field also appears to have influenced the development of secondary mineral precipitates on the glass surfaces exposed to a vapor environment. Samples reacted in a radiation field (Fig. 13) develop thick precipitate layers that contain analcime [$NaAlSi_2O_8 \bullet H_2O$], weeksite [$K_2(UO_2)_2(Si_2O_5)_3 \bullet 4H_2O$], and an acicular calcium silicate phase (tobermorite?: $Ca_5(OH)_2Si_6O_{16} \bullet 4H_2O$). By contrast, samples reacted in the absence of a radiation field develop a relatively thin and discontinuous precipitate cover.

A complete paragenetic sequence has been worked out for the alteration mineral assemblage of the 202U glasses for reaction times of up to 56 days (Fig. 14). This sequence indicates the following temporal paths for the major cations leached from the glasses (major phases in bold letters):

Sodium. Incorporated early into herschelite, and later into **analcime**.

Potassium. Incorporated early into herschelite, followed by phillipsite, and in the later stages, distributed among **adularia**, **illite**, weeksite, and mordenite.

Calcium. Path is dominated by phase believed to be **gyrolite**.

Uranium. Incorporated early into unidentified Na-K-Ca-U-Si webbed shaped phases, followed by the formation of a discontinuous U-K-Si surface layer, and finally into weeksite.

These minerals may incorporate some radionuclides into their structures and may control radionuclide release during subsequent glass leaching. Thus, radiation may be an important parameter affecting both the rate of glass hydration and the stability of secondary phases formed. The observed experimental results display large discrepancies with the paragenetic sequence identified by the EQ3/6 model code. Differences between the experimentally observed and modeled results may arise from the consideration of several factors, including mineral kinetics, inadequate pressure-temperature stability of mineral phases, or differences between the leachant chemistry of the experiments and simulations.

b. Batch Leach Tests

Anion and cation solution analyses have been received for batch leach tests conducted with 202A, 165A, and 131A glasses (340 m^{-1}) at 90°C, under a gamma/alpha irradiation field, for time periods between 14 and 360 days. Results show invariant temporal paths for most anions (F^-, Cl^-, NO_3^-, SO_4^{2-}, $COOH^-$, and $C_2O_4^{2-}$) in solutions in contact with 202A, 165A, and 131A glasses, although some increases in the NO_2^- concentrations are noted after 180 days of testing.

(a)

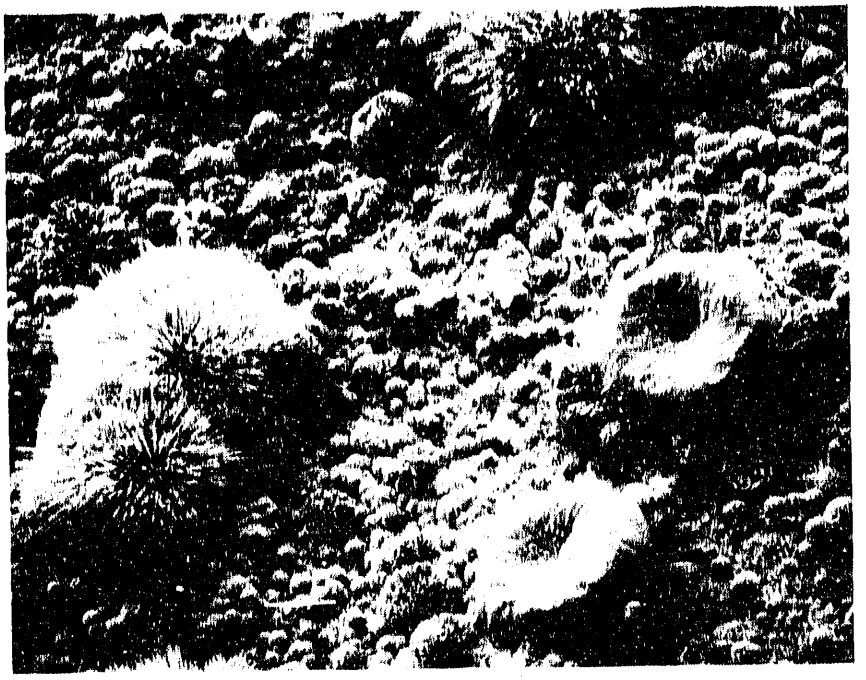

(b)

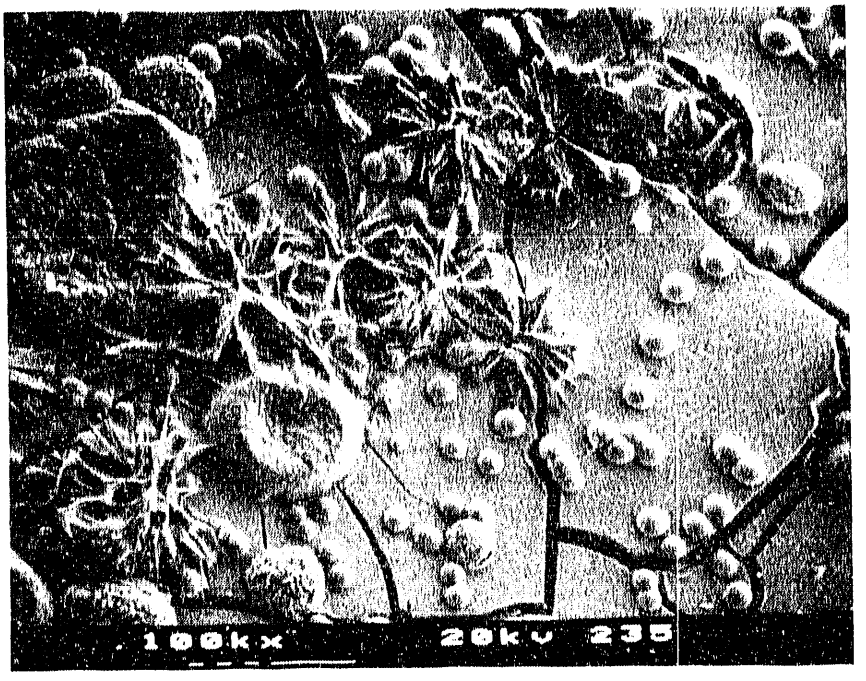

Fig. 13. SEM Photomicrographs of (a) the Surface of 202A Glass Hydrated at 200°C in a Gamma Radiation Field of ~3000 rad/h and (b) 202U Glass Hydrated at 200°C without Radiation. The experimental duration of both samples was 35 days. Note that the 202A glass has developed a thick alteration cover with a relatively dense overgrowth of secondary precipitates, while the 202U glass has developed a thin alteration cover with a sparse overgrowth of secondary mineral phases. Both photomicrographs at 100X, with scale bars equivalent to 100 μm.

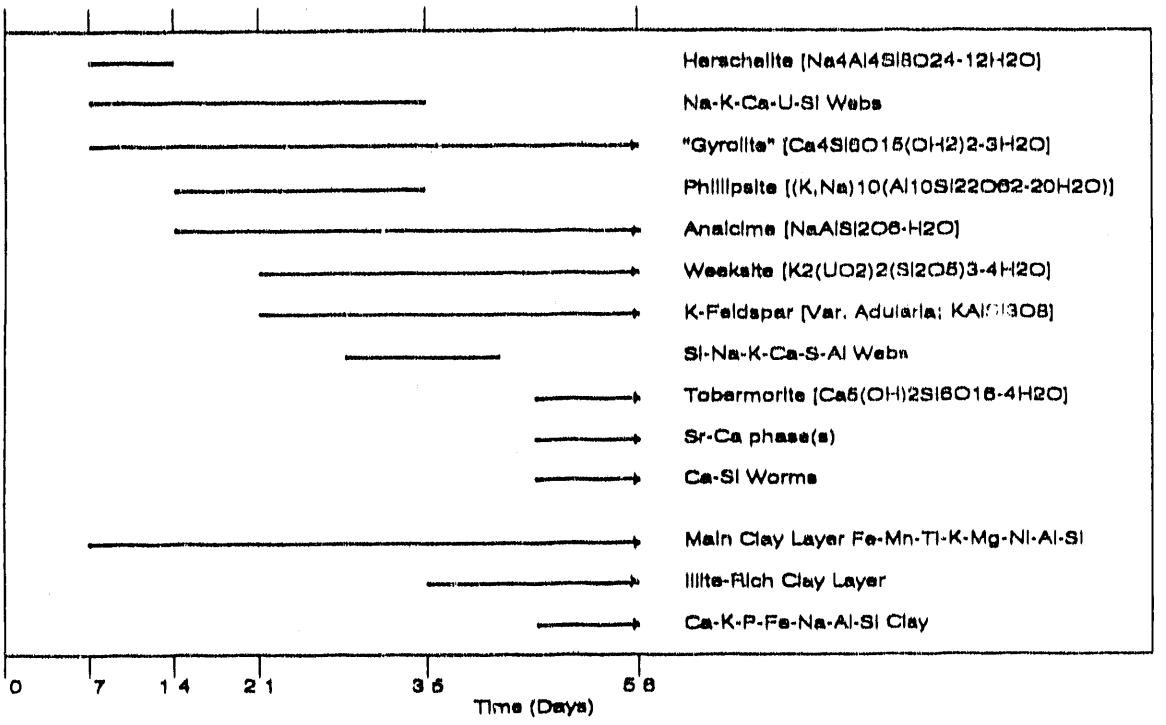

Fig. 14. Schematic of 202U Mineral Paragenesis for Reaction of 202U Glass up to 56 Days

Cations released during glass alteration may be useful in determining the overall extent of glass reaction. The net influx of various cations into solution will depend on a variety of parameters, including leachability from the glass or residual alteration layer, solubility in the leachant, and reprecipitation rate into secondary phases on the glass surface.

Figure 15 displays the log concentrations of the various cations normalized to the concentration of each element in the starting EJ-13 solution. Sodium, potassium, lithium, and boron exhibit parabolic release trends from the 202A and 131A glasses, with early rapid releases decreasing to a nearly flat rate after 91 days. These patterns may reflect a decrease in the rate of dissolution of glass components as solution concentrations increase. Calcium displays a parabolic release trend for the 131A glass, whereas Ca and Mg release rates from the 202A glass increase to 91 days, and then decrease thereafter. With the 165A glass samples, all alkali (except sodium), alkaline earth, and boron release patterns display progressive decreases in release rates between 91 and 360 days of reaction. Decreases in solution concentrations after an initial increase may indicate a decrease in the solubility product of a particular element in response to the presence of a newly formed secondary mineral phase.

Silicon release trends vary widely between the different glass types being examined (Fig. 15). The silica release patterns for 202A are parabolic, while the Si and Na releases for 165A decrease between 91 and 180 days, and then flatten out. The 131A samples display an increase in Si release during the first 56 days, and then a decrease thereafter. Uranium analytical results for 202A glasses display a considerable amount of scatter, but the overall trend indicates a fairly constant or slightly

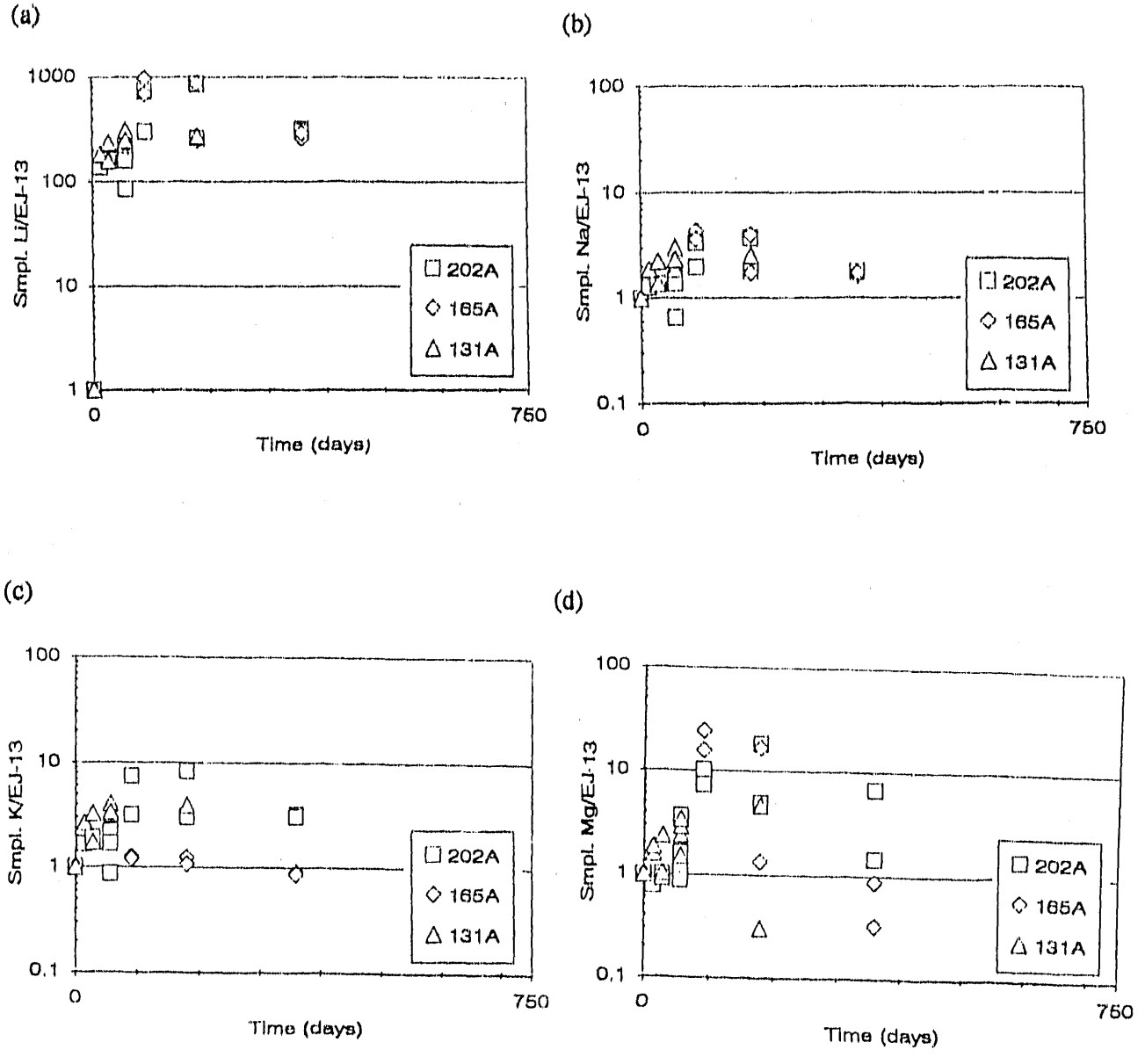

Fig. 15. Log Normalized Release Patterns of Various Cations in Solution Relative to the Concentration of the EJ-13 Starting Solution: (a) Li Release, (b) Na Release, (c) K Release, (d) Mg Release, (e) Ca Release, (f) Sr Release (concentrations in 202A and 131A tests were below detection limit), (g) B Release, (h) Si Release, and (i) U Release.

(e)

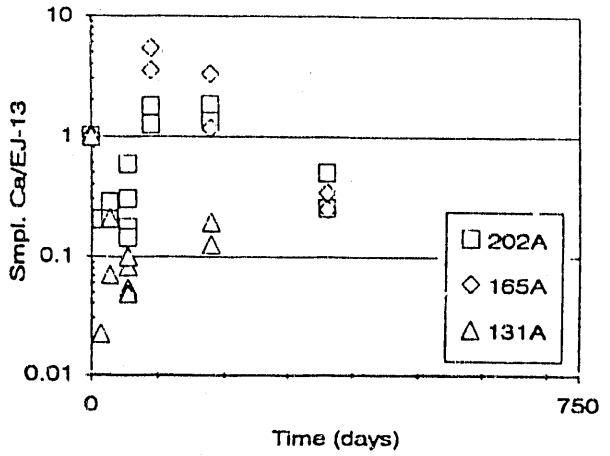

(f)

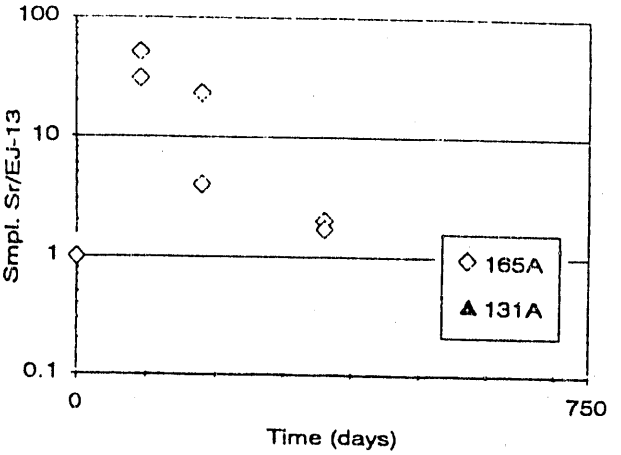

(g)

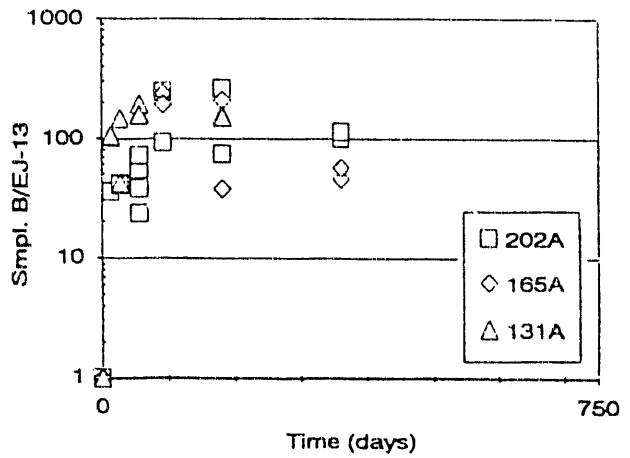

(h)

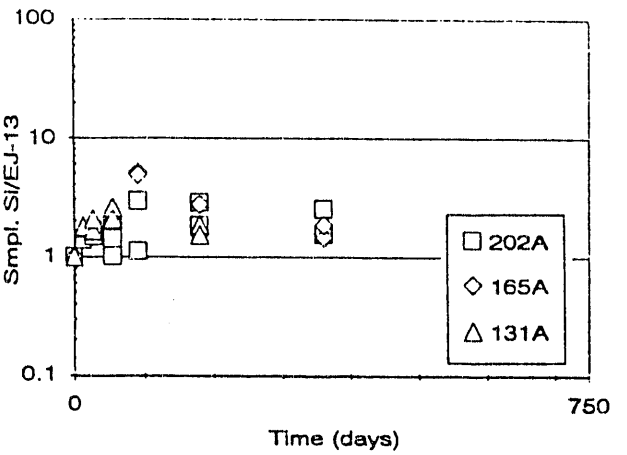

(i)

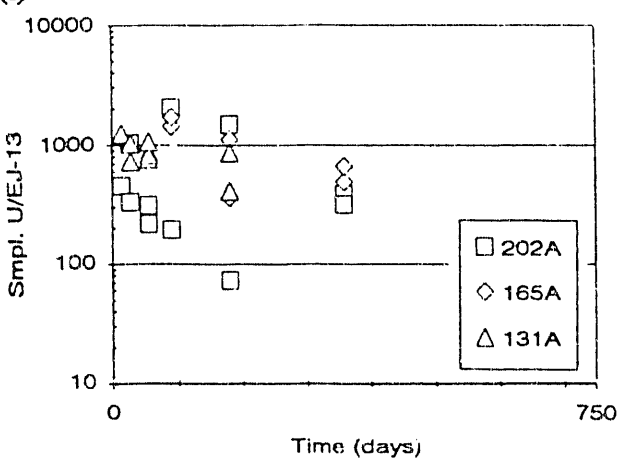

Fig. 15 (Cont'd)

depleted trend with time. Release patterns for the 131A and 165A glasses display a consistent decrease up to 180 and 360 days, respectively. These decreasing release rates may result from the precipitation of secondary uranyl phases on the altered glass surface and suggest that radiation may not significantly affect glass reactivity under conditions of total submersion. A comparison between the present results and those generated elsewhere in this program (Sec. VII) should definitely address this issue.

E. Future Progress

Glass behavior in an irradiated environment will be better characterized as more tests are terminated over the next year, and the results are more thoroughly analyzed. Additional alpha and gamma blank tests will be added to strengthen the analytical data base from this portion of the task. The batch leach tests experiments will be completed within the next year, allowing a comparison between the relatively high and low SA/V tests within this task. Vapor hydration tests and SEM/EDS-XRD surface examinations for all 131U and 202U samples should be completed shortly. The AEM analyses of the clay layers from these samples will continue, and should allow a more detailed analyses of the reaction process to be made within the upcoming year. Vapor hydration sampling of actinide-doped glasses exposed to external gamma irradiation will be completed as will detailed surface examinations. These analyses will allow a detailed evaluation to be made of the differences between glass reaction in an irradiated and nonirradiated environment.

VII. RELATIONSHIP BETWEEN HIGH SA/V EXPERIMENTS AND MCC-1

A. Introduction and Background

Static leach tests are being performed at various SA/V ratios to assess their effect on the glass reaction. Both leachate solutions and reacted glass surfaces are analyzed to characterize the extent and nature of the glass reaction. Two short-term static leach tests, MCC-1 and the Product Consistency Test (PCT), have been used by glass producers to monitor product durability and production consistency. The MCC-1 leach test measures glass durability as the response of glass monoliths upon exposure to DIW at 90°C and an SA/V of 10 m^{-1}. The PCT is also performed in DIW at 90°C. The PCT utilizes powdered specimens to achieve an SA/V of 2000 m^{-1}. Because of the different solution chemistries generated, the glass response will be different in the two systems and different relative durabilities within a series of glass compositions may result. A clear understanding of the effects of the SA/V is necessary to compare MCC-1, PCT, and other test results.

The influence of the SA/V on the glass reaction is also important when projecting short-term experimental results to predict long-term glass durabilities. The approach of the YMP to long-term projection of glass performance in the Yucca Mountain repository is to develop a computer model that can simulate glass reaction under various scenarios throughout the repository service life, including different SA/V conditions. The results of tests such as the MCC-1 and PCT are being used to generate the algorithm for computer simulation of the glass reaction. The effects of the SA/V on the test results must be clearly understood to correctly model the glass reaction and to relate short-term experimental results to long-term behavior.

The primary effect of the SA/V is through dilution of released species. In the simplest case, tests at SA/V differing by a factor of ten, for example, will generate solution concentrations that also differ by a factor of ten after an equal amount of glass has reacted. Conversely, ten times as much glass must react in the test at the lower SA/V to generate an equivalent solution concentration. Various authors have proposed that tests at different SA/V ratios can be scaled using the parameter (SA/V) times the reaction time. That is, equivalent solution compositions are predicted at equivalent products of (SA/V)•t. What is assumed in this simplistic scaling procedure is that the glass reaction is similar at all SA/V ratios. As the tests in this task will show, different solutions are generated due to initial reactions, primarily those which increase the pH, which may complicate the simple scaling of solution results at longer reaction times. Changes in the reaction mechanism occurring at different SA/V ratios will be evidenced by changes in the structure and composition of secondary solids at the reacted glass surface and changes in the leachate chemistry and release patterns of glass components such as doped actinides. A knowledge of how the SA/V affects the results of laboratory tests is required both to understand the results of durability tests and to properly account for the SA/V in computer simulations of glass performance under likely environmental conditions over long periods of time.

B. Objectives

The purpose of this task is to compare the nature and extent of glass reaction at various SA/V ratios as characterized by analyzing both the leachate solution and the reacted glass surface. Tests are designed to monitor changes in both the solution and the glass surface as a function of SA/V, reaction time, leachant composition, and vessel material. The results of these tests will provide insight into comparison of tests performed at low and high SA/V, including those of the MCC-1 and PCT tests, and the influence

of SA/V on the glass reaction mechanism with regard to the solution chemistry and secondary phases. Results will be employed to validate models of glass behavior used to project the reaction to very long times.

C. Technical Approach

In this task, two glass compositions are reacted at four different SA/V ratios at 90°C. A glass composition that has been shown to have low durability in previous MCC-1 type leach tests (SRL 131) was selected to demonstrate a large SA/V effect within a short time period. A second, more durable glass (SRL 202) was also selected. The SRL 202 simulates the glass to be produced by the DWPF for disposal in the repository. The glasses were doped with actinide elements and are referred to as SRL 131A and SRL 202A glasses. A nondoped analog of the SRL 202 glass was used in tests with Teflon vessels. This is referred to as SRL 202U. Tests in Teflon are performed to measure the effect of the vessel material on the reaction and to provide data for comparison to computer simulations. These data will provide modelers with solution data and characterize secondary solids in a system that is nearly free of vessel interactions. The tests are conducted to supply the necessary data for validation of the submodel describing the glass reaction rate.

Samples were prepared as both monolith disks (diameter ~1 cm, thickness ~1.5 mm, 600-grit finish) and as crushed glass (-100 +200 mesh, washed to remove fines). Monolith samples are reacted at SA/V = 10 and 340 m^{-1}, and granular (powdered) glass samples are reacted at 2000 and 20,000 m^{-1} in EJ-13 or DIW at 90°C. The values of SA/V selected for testing include those used in the MCC-1 test (10 m^{-1}) and the PCT (2000 m^{-1}). Tests are also performed at SA/V ratios which use minimum solution volumes and still completely submerge the samples and allow for complete solution analyses for tests with monoliths (340 m^{-1}) and powdered glass (20,000 m^{-1}). The reaction times were selected to provide a description of the temporal reaction trend, to permit direct comparison of the results at several equivalent (SA/V)•t values, or to compare test results with those obtained in other tasks.

The task matrix (leachant, vessel material, and SA/V) is shown in Table 11. This matrix provides comparison of tests at different SA/V ratios, in different leachants, and in different reaction vessels. Tests with different glass compositions can also be compared. Blank tests are performed to provide background values for all test series. Tests are performed for various durations in each of the test series and the blanks, as shown in Table 12, where the nominal value of the product SA/V•t is also given. In addition to the reaction times listed, two tests with unspecified reaction times are conducted in each series to serve as replacement tests if any of the scheduled tests are deemed to have failed or to provide an additional duration time. The status of the test series in this task is shown in Table 13.

Table 11. Task Matrix Overview[a]

Leachant	Vessel Material	SA/V, m^{-1} 10	340	2000	20,000	Blank
DIW	Teflon		202U	202U	202U	None
EJ-13	Teflon		202U		202U	None
EJ-13	304L stainless steel	202A 131A	202A 131A	202A 131A	202A 131A	None

[a]Tests performed in other tasks may be utilized.

Table 12. Reaction Times for Tests with Glass and Blank Tests

	Reaction Time,[a] days			
SA/V•t	10 m^{-1}	340 m^{-1}	2000 m^{-1}	20,000 m^{-1}
70	7[a]			
280	28			
940	94			
2,380	238			
4,760		14		
6,000	600		3	
9,520		28		
14,000	1400		7	
19,040		56		
28,000			14	
30,940		91		
60,000			30	3
61,200		180		
122,400		360		
140,000			70	7
183,600		540		
224,800		720		
280,000			140	14
560,000			280	28
1,120,000			560	56
1,960,000			980	98
3,640,000			1820	182
7,280,000				364
14,560,000				728
TBD	TBD[b]	TBD	TBD	TBD

[a]Duplicate tests performed at each duration.

[b]Test durations to be determined.

Table 13. Status of Tests to Determine Effects of SA/V (as of 9/16/91)

Test Series[a]	Glass	Leachant	SA/V, m^{-1}	Test Durations, days		
				Completed	In Progress	To Be Initiated
BX	SRL 202A[b]	EJ-13	10	7, 28, 94, 238	600, 1400, 2800, TBD	
BY	SRL 202A	EJ-13	2000	3, 7, 14, 30, 70, 140, 280	560, 980, 1820, TBD	
BZ	SRL 202A	EJ-13	20,000	3, 7, 14, 28, 56, 98, 182, 364	728, TBD	
BW	SRL 202A	EJ-13	340		180, 360, 540, 720	14, 28, 56, 91, TBD
PX	SRL 131A[b]	EJ-13	10	7, 28, 94, 238	600, 1400, 2800, TBD	
PY	SRL 131A	EJ-13	2000	3, 7, 14, 30, 70, 140, 282	560, 980, 1820, TBD	
PZ	SRL 131A	EJ-13	20,000	3, 7, 14, 28, 56, 98, 182	364, 728, TBD	
PW	SRL 131A	EJ-13	340		91, 180, 360, 540, 720	14, 28, 56, TBD
TW	SRL 202U[c]	DIW	340	14, 28, 56	91, 180, 360, 540, 720	TBD
TW	SRL 202U	EJ-13	340	14, 28, 56	91, 180, 360, 540, 720	TBD
TY	SRL 202U	DIW	2000	3	140, 280, 560, 980	7, 14, 30, 70, TBD
TZ	SRL 202U	DIW	20,000	3, 7, 14, 28, 56	91, 182, 364	TBD
TZ	SRL 202U	EJ-13	20,000	3, 7, 14, 28, 56	91, 182, 364	TBD
DIT	None[d]	DIW	N/A	3, 7, 14, 28, 56	91, 182, 280, 364	TBD
EJT	None[d]	EJ-13	N/A	3	91, 182, 280, 264	7, 14, 28, 56, TBD

[a]Test series designation of glass type and SA/V for each test series.

[b]Tests with SRL 202A or SRL 131A glass performed in 304L stainless steel vessels.

[c]Tests with 202U glass performed in Teflon vessels.

[d]Blank are performed in Teflon vessels.

D. Results and Discussion

The reactions are characterized by the solution chemistries (pH, and anion and cation concentrations) and by analysis of the reacted solids. Special attention is given to the distribution of released actinide species between dissolved and colloidal fractions that appeared in the leachate, that sorbed onto the vessel walls, and that left an insoluble residue on the glass surface or incorporated into secondary phases. The amount of actinides in each fraction is quantified using appropriate sampling procedures. These and other analytical procedures are performed in accordance with the data needs of modelers.

Aliquots of the leachate are removed for carbon and actinide analyses. The leachate solutions are then filtered through 0.45 μm (or larger) filters to remove any glass particulates from the solution. The filtration is performed at the reaction temperature to prevent temperature-induced precipitation of secondary phases from solution prior to filtration. Analyses of the solution for cations, anions, actinides, and pH are then performed on the cooled filtrate. A subsequent filtration through filters with an approximate pore size of 60 Å is performed on some leachates to remove suspended material smaller than about 0.45 μm. and the filtrate is analyzed for selected cations.

The reacted glass is analyzed using optical microscopy, SIMS, SEM/EDS, and AEM. The surfaces and cross sections of reacted particles are examined to quantify the extent of reaction by the thickness and composition of a reaction layer formed on the surface and by the secondary products formed.

Test series with SRL 202A and SRL 131A glass at 10, 2000, and 20,000 m^{-1} have been completed through 364 days, and the solution results of these tests are discussed below.

1. pH Analyses

The leachate was filtered through 0.45 μm filters at the reaction temperature, and the filtrate was analyzed for pH at room temperature. The measured pH values are plotted against the reaction time in Figs. 16a and 16b for tests with SRL 131A and SRL 202A glasses, respectively, performed at SA/V values of 10, 2000, or 20,000 m^{-1}. The initial leachant had a measured pH of 8.18 for all tests. Tests at 10 m^{-1} show only a small increase in pH from the initial leachant, while tests at 2000 and 20,000 m^{-1} show a large increase at all reaction times tested. Tests with SRL 131A attain higher pH values than tests with SRL 202A glass after equivalent reaction times at all SA/V ratios.

The difference in the leachate pH at different SA/V ratios is due, in a large part, to dilution effects. If the same amount of glass is reacted at 2000 and 20,000 m^{-1}, for example, the pH should be one unit higher at 20,000 m^{-1} because the total solution volume per unit glass area is a factor of ten smaller than at 2000 m^{-1}. Through about 200 days, tests with SRL 131A glass at 20,000 m^{-1} have pHs more than one unit higher than tests at 2000 m^{-1} after equal reaction times. This suggests that more glass has reacted at 20,000 m^{-1} than 2000 m^{-1} after equal reaction times. The pH values in tests with SRL 202A glass at 2000 and 20,000 m^{-1} differ by about one unit through about 200 days. This result suggests that the extent of glass reaction is similar.

In Fig. 16, the pH for SRL 131A at 2000 m^{-1} has a pH higher after 280 days than the trend shown in previous tests at 2000 m^{-1}. The corresponding tests with SRL 202A glass also show a small increase with respect to previous tests. This pH rise suggests an acceleration of the reaction, perhaps due to the formation of stable secondary phases which affect the pH. Analyses of the reacted solids to identify differences in the secondary phase assemblages before and after the pH increase are in progress.

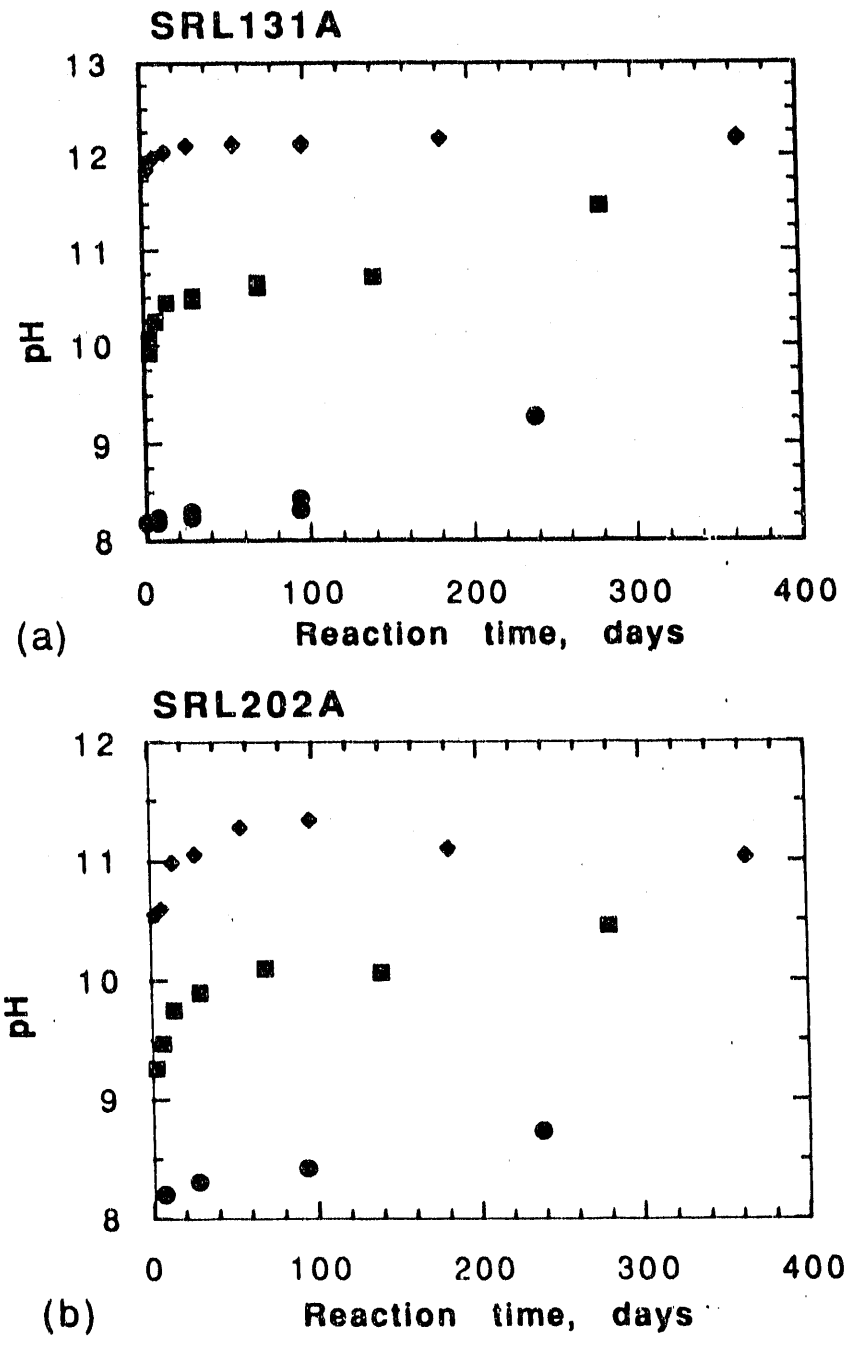

Fig. 16. Final Leachate pH (Measured at Room Temperature) vs. Reaction Time for Tests with (a) SRL 131A Glass and (b) SRL 202A Glass at SA/V of (●) 10, (■) 2000, and (◆) 20,000 m^{-1}

The pH change at short reaction times is due primarily to reactions which release alkali metals from the glass and consume protons. Because the solubility limits of the alkali metals are high, the reactions to release alkali metals proceed at a high rate at short reaction times. A limiting pH is apparently reached after several weeks. This suggests that the reactions releasing the alkali metals have been quenched. The pH attained due to these early reactions then strongly influences hydrolysis reactions, which dominate the overall glass reaction rate as the reaction continues. Tests at 20,000 m^{-1} appear to reach limiting pH values of about 12.1 for SRL 131A and 11.2 for SRL 202A glasses, and tests at 2000 m^{-1} approach pH values of about 10.7 and 10.2, respectively, through about 200 days. Thus, an important effect of the SA/V ratio is to establish the solution pH through initial ion-exchange reactions, which drive the pH up. Different pH values are attained at different SA/V ratios because of the different dilutions, although it is not clear why the pH reaches apparently limiting values (at least through 200 days) and does not increase to a single value for tests at all SA/V ratios. Part of the reason may be that water diffusion into the glass to allow alkali to be leached slows with the reaction time and thus limits the reactions primarily responsible for the pH rise. This issue should be clarified by solids analyses, which are in progress.

2. Cation Analyses

The filtrate from filtration through 0.45 μm filters was analyzed for major components of the glasses. Figures 17a and 17b show the log of the measured boron concentration plotted against the log of (SA/V)•t. Such a plot is often presented to demonstrate the applicability of (SA/V)•t scaling of leach data, where tests at equivalent (SA/V)•t are predicted to generate similar solution concentrations. The plots in Figs. 17a and 17b show that similar solution concentrations are not generated at equivalent (SA/V)•t for these tests. The differences in concentrations at different SA/V ratios are probably due to the differences in the leachate pH. Boron is usually assumed to be released through a hydrolysis reaction with hydroxide ions. The boron release rate is expected to increase with the pH, and differences in the leachate pH at different SA/V ratios will result in different reaction rates. For example, the boron concentration is greater after reacting 7 days at 20,000 m^{-1} than 70 days at 2000 m^{-1} (both tests performed for log(SA/V)•t = 5.15) for both glass types, because the pH is higher in tests at 20,000 m^{-1} than 2000 m^{-1}. The difference is less for the less reactive SRL 202A glass, which also showed a smaller pH difference.

The leachates of some tests were filtered to assess the amount of suspended and colloidal material. Results of analyses of the unfiltered leachate, leachate filtered through 0.45 μm filters, and leachate filtered through approximately 60 Å filters for two tests are presented in Table 14. Boron is considered to be a good indicator of the extent of glass reaction because it has a very high solubility limit at all pH values. Filtration through 0.45 μm filters did not remove significant amounts of any glass component (not more than 10%). Filtration through approximately 60 Å filters did reduce the measured concentrations of some species. Similar levels of boron and alkali metals are measured before and after filtration. Some elements, including Al, Fe, and Mn, were almost completely removed by the 60 Å filters. These elements are present in the leachate primarily as suspended material. Filtration through 60 Å filters did not remove a significant amount of silicon, however. This is in contrast to tests with other glasses (PNL 76-68 and R7T7), which showed a correlated decrease of iron and silicon by filtration. This suggests that silicon is not associated with iron in the suspended material in the present tests. The presence of suspended material is important because released actinides may sorb onto this material and be transported away from the glass. Analysis of the suspended material in tests with SRL U using AEM is in progress.

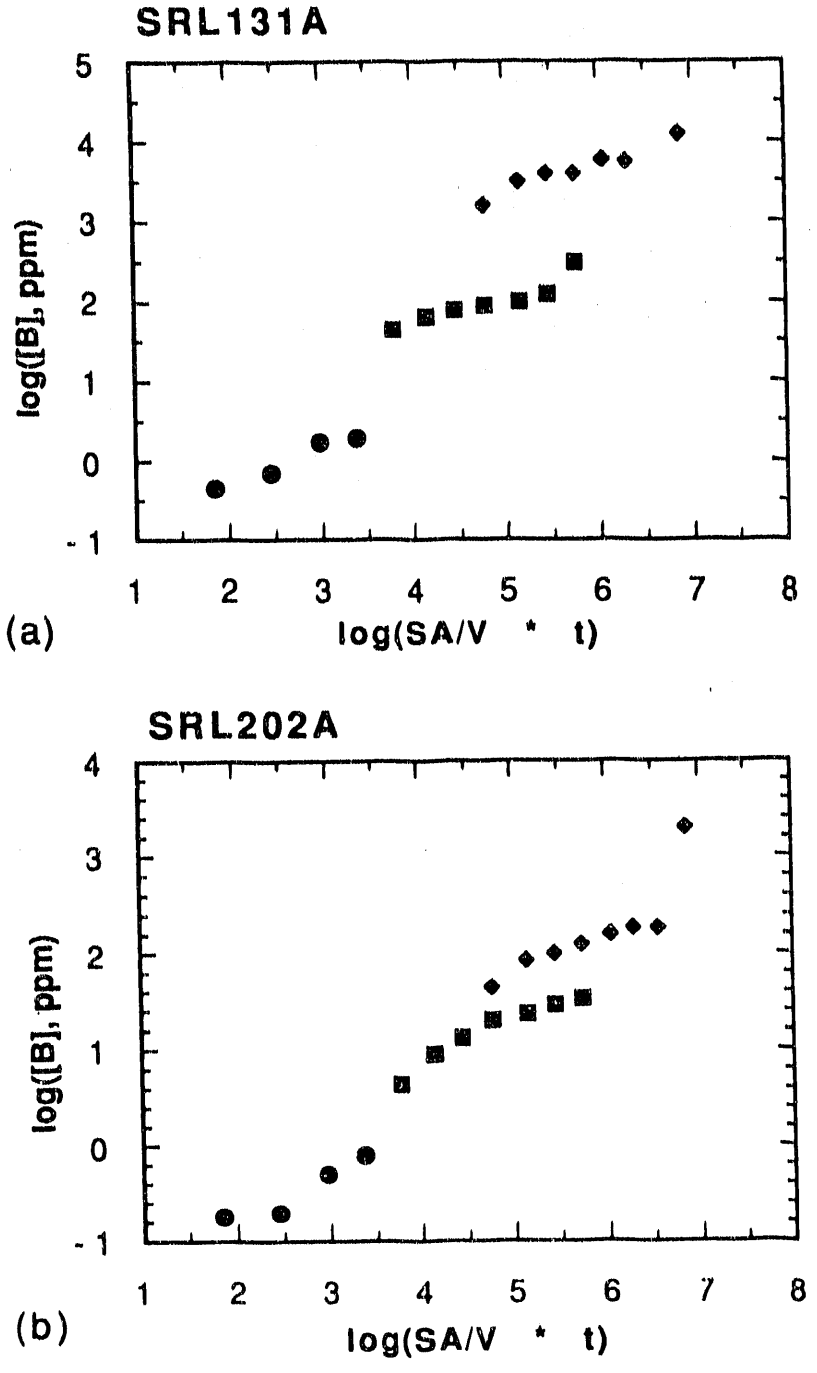

Fig. 17. Log Boron Concentration (ppm) vs. Log SA/V•time (days/m) for Tests with (a) SRL 131A Glass and (b) SRL 202A Glass at SA/V of (●) 10, (■) 2000, and (◆) 20,000 m^{-1}

Table 14. Cation Concentrations (ppm) in Unfiltered Leachate (UF), Filtrate from 0.45 μm Filtration (F.45), and Filtrate from 60 Å Filtration (F60)

	BY11[a]			PY11[b]		
	UF	F.45	F60	UF	F.45	F60
Al	4.0	3.7	2.2	3.1	2.9	1.5
B	28	29	29	120	130	130
Ba	<0.16	<0.13	<0.17	<0.13	<0.13	<0.07
Ca	<0.16	0.33	1.5	<0.13	<0.13	0.60
Cr	0.74	0.80	0.71	0.64	0.66	0.60
Cu	0.82	0.60	0.13	0.13	0.13	0.07
Fe	6.4	5.9	0.17	12	9.7	0.11
K	29	30	32	74	76	73
Li	30	30	30	44	46	42
Mg	0.57	0.53	0.24	0.71	0.65	0.7
Mn	1.1	0.93	<0.03	2.3	1.8	<0.04
Na	150	160	-	400	420	-
Ni	0.25	0.27	<0.10	0.39	0.39	0.11
Si	150	150	140	240	250	240
Th	<0.41	<0.33	<0.17	<0.32	<0.33	<0.18
Ti	0.33	0.33	<0.07	0.26	0.20	<0.07
Zn	<0.16	<0.13	0.17	<0.13	<0.13	<0.07
Zr	<0.41	<0.33	<0.17	<0.32	<0.33	<0.18
U	3.2	3.1	2.5	3.8	3.9	3.4

[a]SRL 202A; EJ-13; 2000 m^{-1}; 280 d.

[b]SRL 131A; EJ-13; 2000 m^{-1}; 280 d.

The measured boron concentrations are used to compare the extents of reaction in tests at different SA/V ratios. The normalized elemental mass losses for boron vs. the reaction time are shown in Figs. 18a and 18b, which give the loss of boron as g/m^2 of glass surface. The normalized elemental mass loss accounts for differences in dilution and is proportional to the amount of glass reacted. The results for tests with SRL 131A glass show the release of boron to increase with SA/V as $10\ m^{-1} \sim 2000\ m^{-1} < 20{,}000\ m^{-1}$. Tests with SRL 202A show the releases to be similar for all three SA/V ratios through about 200 days. The observation that the rate of boron release is greatest at 20,000 m^{-1} with SRL 131A but similar at all SA/V ratios with SRL 202A may be due to the different pH values achieved or to differences in the reaction mechanisms.

Notice the increased boron release in the tests with SRL 131A at 2000 m^{-1} after 280 days. This is consistent with the pH jump seen earlier and indicates a sudden increase in the reaction rate. Similar jumps in the boron levels are seen for both glass types after 364 days at 20,000 m^{-1}. The pH did not increase in these tests, presumably because the pH was already at the maximum achievable value for both glass types.

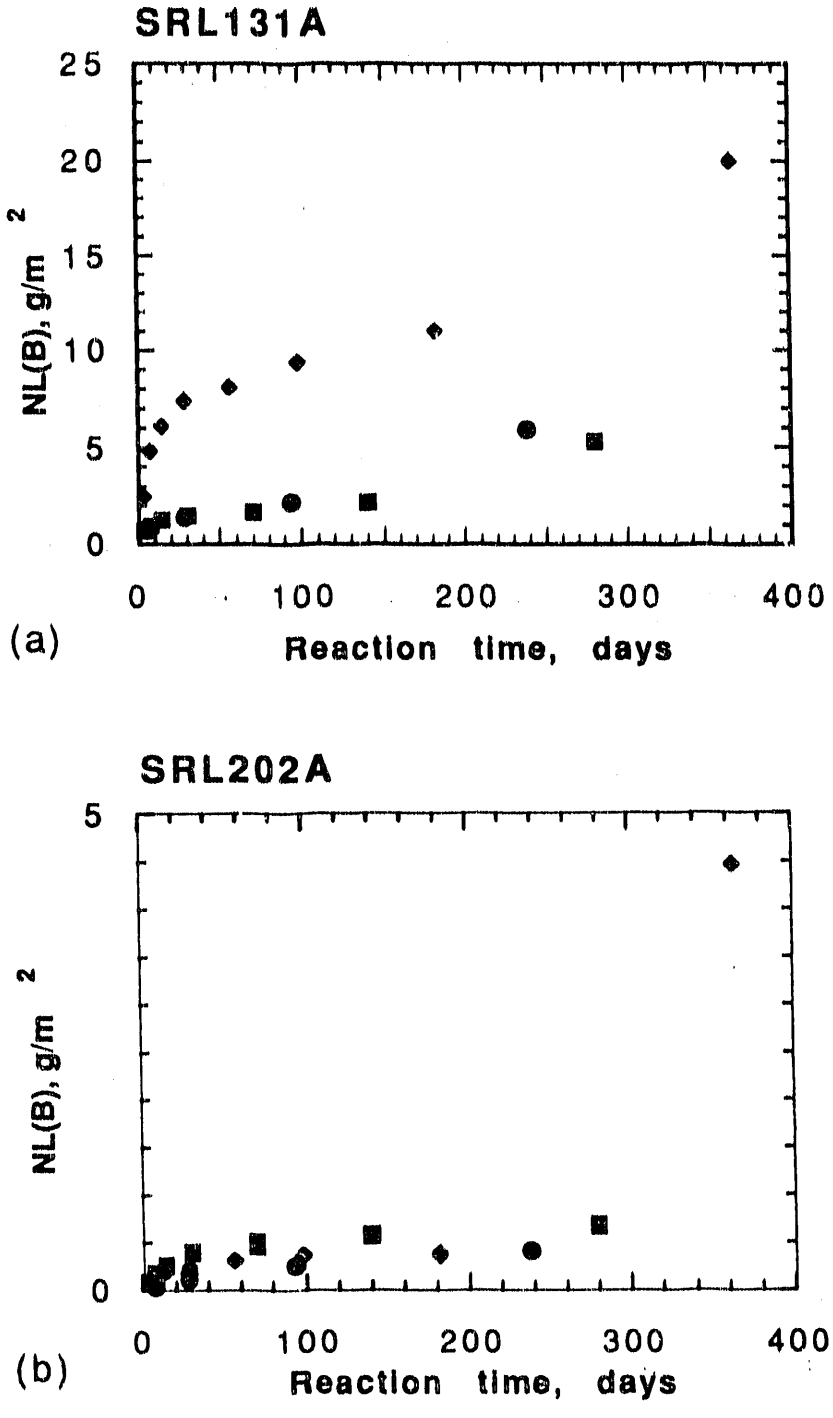

Fig. 18. Normalized Boron Mass Loss (g/m^2) vs. Reaction Time for Tests with (a) SRL 131A Glass and (b) SRL 202A Glass at SA/V of (●) 10, (■) 2000, and (◆) 20,000 m^{-1}

The mechanism of glass reaction is characterized, in part, by the relative release rates of different glass components. Initially, the dominant reaction step is ion exchange to release alkali metals. As the pH increases, the ion-exchange reactions are quenched, and base-catalyzed hydrolysis becomes the dominant reaction. The solution concentrations of soluble species reflect the glass reaction mechanism. Figures 19a and 19b show the normalized elemental mass losses of several elements for tests with SRL 202A glass at 2000 and 20,000 m^{-1}. These results show the release to be nonstoichiometric at all times tested and to decrease initially as Li > Na > B > K > Si. The release of alkali metals reflects typical ion-exchange selectivity observed in glass dissolution tests as Li > Na > K. Boron is released intermediate between Na and K, though through a different reaction. Boron cannot be released any faster than lithium because the reaction to release boron requires the hydroxide produced by the ion-exchange reaction. Silicon is also released via base-catalyzed hydrolysis but is released about one-half as fast as boron. This is due to the greater number and strength of Si-O bonds that must be broken to free a silicon-bearing species than to release a boron-bearing species.

A similar nonstoichiometric release is seen for tests at 20,000 m^{-1} through about 98 days. After about 182 days, however, the lithium concentration decreases, presumably due to the incorporation of lithium into a secondary phase. (Note that the silicon level also decreases slightly at 180 days.) The release of the alkali metals and boron increases significantly by 364 days. The silicon concentration increases only slightly. At 364 days, the normalized mass losses follow the order Si < Li < K < Na < B. The observation that boron has the greatest normalized mass loss indicates that Li and Na have been incorporated into secondary phases. The increase in boron release between 182 and 364 days indicates that the glass reaction has been accelerated upon secondary phase formation.

A similar, sudden increase in the reaction rate has been observed in other tests performed in our laboratory in a vapor environment upon the formation of stable secondary minerals. The increase in the reaction rate upon mineral formation in tests in vapor has been attributed to a decrease in the solution concentrations of critical (as yet unidentified) species, such as silicon, which affects the affinity for the glass reaction. These observations are important to the long-term modeling of the glass reaction necessary for performance assessment of the repository. We have shown that the observed acceleration upon secondary phase formation is entirely consistent with the models of glass reaction currently used in the LLNL computer simulation. The present tests offer valuable insight into the observed acceleration because both solution and reacted solids are analyzed. For example, Fig. 19b clearly shows that the silicon content of the solution is similar at 364 days to shorter times, although the boron release increases about an order of magnitude. Analyses of the reacted solids in tests run 182 or 364 days are in progress to identify changes that may have occurred concurrent with the apparent acceleration of the reaction. These observations show that both solution and solids analyses are required to completely characterize the reaction.

3. Actinide Release

To characterize the nature of the actinide release, several solution aliquots from each test were analyzed using alpha spectroscopy. The following aliquots were analyzed: unfiltered leachate, the filtrate from filtration with 0.45 μm polycarbonate filters, and the filtrate from filtration with approximately 60 Å fiber filters. In addition, a solution was generated by filling the reaction vessel with an approximately 1 M HNO_3 solution to dissolve any actinides that may have sorbed or plated onto the vessel walls. This is referred to as the "acid soak" solution. The purpose of these analyses is to determine the amounts of each radionuclide dissolved in solution, suspended in solution, or plated onto the steel vessel walls. Analysis of the reacted solids will also indicate the amounts of these nuclides that remain associated with the glass.

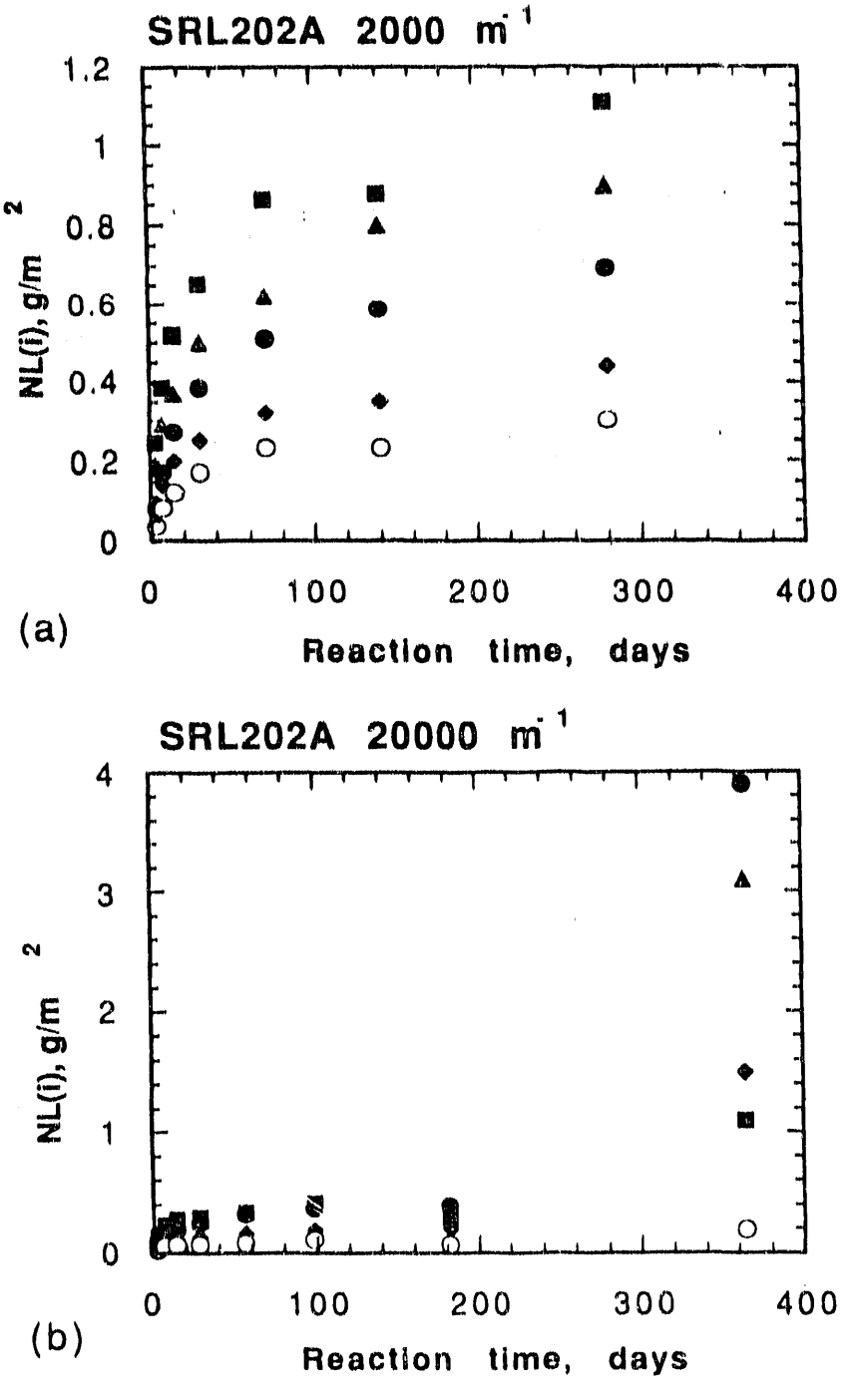

Fig. 19. Normalized Elemental Release from SRL 202A vs. Reaction Time at (a) 2000 m^{-1} and (b) 20,000 m^{-1} for (■) Li, (▲) Na, (●) B, (◆) K, and (○) Si

Analyses of tests running 364 days or less show that ^{237}Np, ^{239}Pu, and ^{241}Am are released into all three fractions at all SA/V ratios for both glass types. The amounts of ^{237}Np, ^{239}Pu, and ^{241}Am in solution either as dissolved, suspended, or sorbed material are sensitive to the SA/V ratio (or to the leachate pH). Figures 20a through 20f show the total amounts of each actinide in the filtrate from 0.45 μm filtration, 60 Å filtration, and the acid soak for tests with SRL 202A glass at 2000 and 20,000 m^{-1}. Although there is significant scatter, general trends of actinide release and distribution were determined. Tests at 2000 m^{-1} show a generally increasing release trend. Neptunium is predominantly in a filterable fraction, and very little is sorbed to the vessel. Both Pu and Am are found suspended in the filterable fraction and sorbed onto the vessel with very little dissolved. These findings are consistent with the solubilities of these actinides.

Tests at 20,000 m^{-1} showed very different trends. Large amounts of all three actinides were found in the leachates of short-term tests but the amounts decreased at longer reaction times. Neptunium was found on the vessel walls of some tests, mostly at shorter reaction times. Both ^{239}Pu and ^{241}Am were primarily associated with the vessel walls, with very little in the leachate.

The different distributions of actinides seen in tests at 2000 and 20,000 m^{-1} are attributed to the generation of secondary phases at 20,000 m^{-1}. Released actinides are presumed to sorb onto this material and be removed from the leachate either by settling out during reaction or during filtration using a 0.45 μm filter. Tests at 2000 m^{-1} do not generate a significant amount of secondary material through 280 days, although the decrease in neptunium seen at 280 days may be due to secondary phases.

Suspended material generated in tests with SRL 202U is being analyzed using AEM to correlate with the solution results. These analyses may identify suspended phases which may sorb actinides.

E. Future Progress

Tests are in progress in all test series, as shown in Table 13. Short-term tests in series reacted in Teflon vessels will be completed through one year at the end of FY 1992. Long-term tests in all series will continue through the next several years. Detailed analyses of the reacted solids are in progress and will represent considerable upcoming effort. An example of the type of information available through solids analysis is given in Sec. VIII on Analytical Support. Solution analyses available to date are being compiled into an interim report. The results of these tests provide valuable data and insight into the glass reaction mechanism itself, in addition to the influence of SA/V on the reaction. The observation of accelerated reaction rates within one year of reaction at 2000 and 20,000 m^{-1} indicates that these tests will provide a valuable link to other tests performed in the glass studies program at ANL, especially novel tests in water vapor where abundant secondary phases are generated. The minerals identified in those tests will provide guidance in identifying minerals which may also form in the present tests.

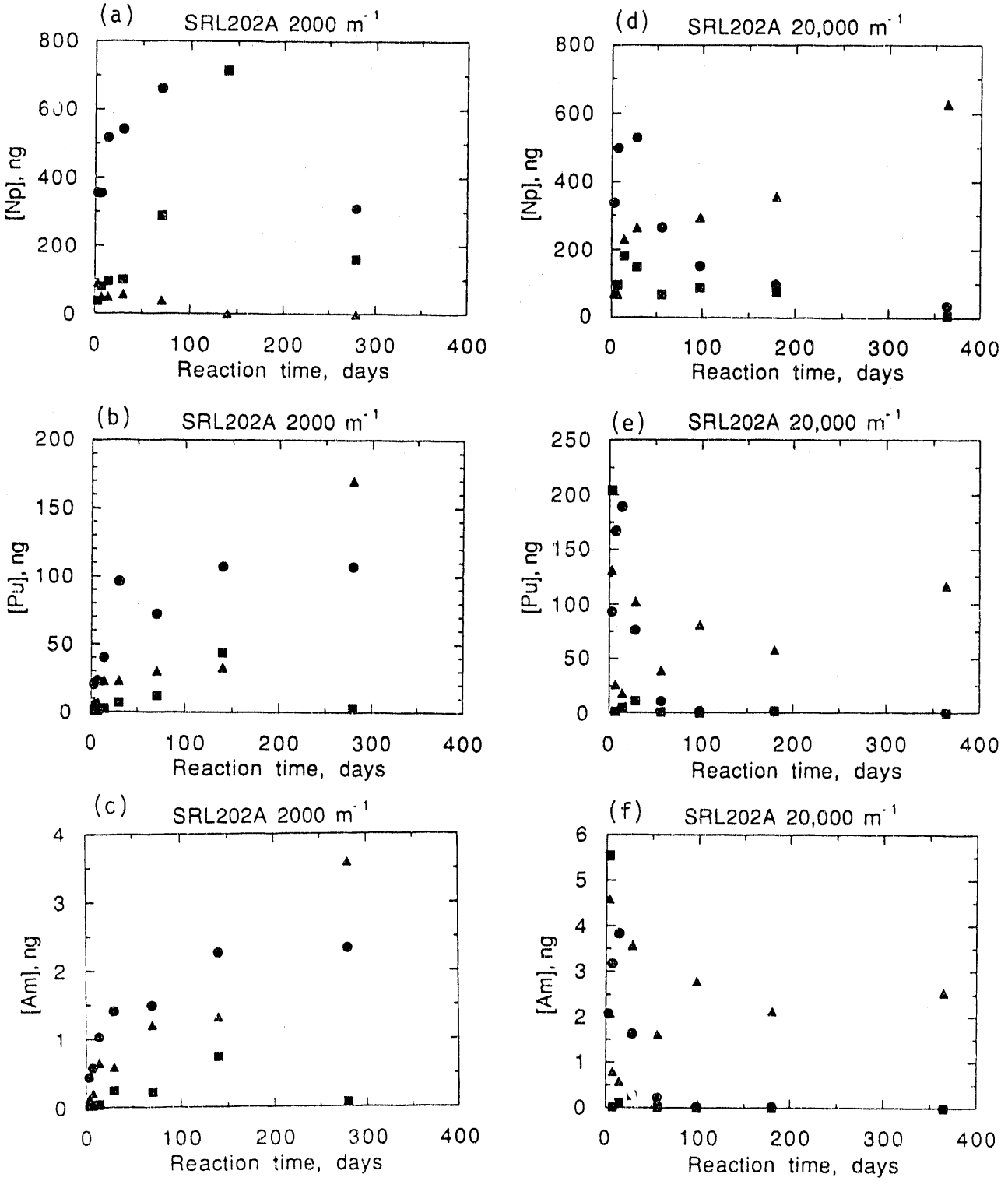

Fig. 20. Total Mass Actinides (Np, Pu, and Am) Measured to Be in (●) F.45 Filtrate, (■) 60 Å Filtrate, and (▲) Acid Soak Solution for Tests at 2000 m^{-1} and 20,000 m^{-1} vs. Reaction Time

VIII. ANALYTICAL ELECTRON MICROSCOPY SUPPORT

A. Introduction and Background

Analytical electron microscopy (AEM) is a combination of transmission electron microscopy (TEM), energy dispersive X-ray spectroscopy (EDS), electron energy loss spectroscopy (EELS), and electron diffraction (ED). Point-to-point resolution for images obtained with the TEM approaches 3 Å, and the smallest region that can be investigated using ED, EDS, and EELS is about 200 Å. The AEM is a very powerful tool for the investigation of inhomogeneous samples--very small inclusions, small crystallites, colloidal size particles, and thin reaction layers.

Samples for AEM studies must be extremely thin, and considerable effort is required to prepare the electron transparent (500- to 800-Å thick) specimens that are required. Sample preparation is an integral, nontrivial part of the work. Sample size, however, is really a benefit in that very little material is required to produce a specimen. This has been important when only small amounts of material are produced in a reaction and will take on added significance when work begins with fully radioactive glasses. During the past year, staff from the WSRC and the University of New Mexico have visited ANL to learn how TEM samples of the reacted glasses are produced at ANL. Small-particle handling techniques, sectioning, and surveying procedures were demonstrated.

B. Objectives

The Analytical Support staff collaborates with other members of the Technical Support Program to investigate and identify reaction products produced from corrosion of nuclear waste glass during testing under simulated environmental conditions. These structural studies provide information necessary to understand the reaction processes. This information will contribute to the development of the models needed for prediction of glass behavior.

C. Technical Approach

Much of our work is concerned with reaction layers that form on the surfaces of reacted glasses. These layers are frequently 50 μm or more thick and can be extremely fragile. As mentioned above, to identify secondary phases using AEM, one must have extremely thin self-supporting samples. Transverse cross sections of these reaction layers are prepared by ultramicrotomy, in which thin sections of small particles are mounted in epoxy blocks using a diamond knife. This is a difficult process which frequently requires several attempts before success is achieved. During this past year, particles from approximately 70 bulk samples have been mounted in about 250 epoxy blocks, producing over 500 TEM sample grids, each holding about 40 sections. After the particles are sectioned, each grid is examined in the electron microscope to ascertain whether or not sample preparation has been successful. The micrographs produced in this initial survey are used for more than quality control of the sample preparation process. They are often very helpful in interpreting the glass reaction mechanism and are frequently incorporated into publications generated by the group. The most intact of the TEM sections from a particular reacted glass sample will be used for more detailed analysis.

Tables 15 through 18 present an overview of the results of sample surveys this year. The tables are organized according to the task which generated the sample and include some brief comments describing the reaction layers observed. More information about the reaction conditions and the compositions are available in the appropriate Task Plans.

Table 15. Results of Sample Surveys for "Long-Term Testing" Glass (Sec. V)

Sample	Description
DP-7	Some reasonable areas. 75-nm-thick clay layer. The electron beam caused damage in this sample rapidly.
DP-8	Sectioning results have been mixed, but since the reaction layers are thin and several attempts have been made, it has been possible to find small intact regions, extending from the epoxy to the glass in all the powdered samples except DP-8. DP-8 has adequate material to analyze but is not intact.
DP-20	A good section of several particles of glass bound together with clay layers was produced. A good section showing an extremely thin reaction layer was obtained.
DP-21	A good section showing an extremely thin reaction layer was obtained, and in another case sections showed several particles of glass bound together with clay layers.
DP-22	One good sample and one reasonable sample were produced, and these have been used for detailed analysis. The layer was thin, about 20 nm.
DP-43	A few samples were well intact with an outer layer thickness of 50-60 nm. Some small regions possessed more disordered layers, which were around 100-nm thick.
DP-45	One good sample. The layer was 100-150 nm thick.
DP-78	Steel particle was sectioned in one instance.
DP-79	Samples were intact with a layer around 20-nm thick. Lattice fringes were visible.
DP-104	A number of good samples. The clay layer was 100-nm thick.
DP-138	In one block, the clay layer on one side of glass particle was relatively thick (~200 nm). Elsewhere it was around 50-75 nm. The glass was electron beam sensitive.
DP-139	Two good samples were produced from this test. The clay layer was 5-nm thick.
DP-140	The layer was found to be 50-100 nm thick. Some samples had cracks in them, which had then reacted. A number of the specimens were intact.
DP-141	Samples were mainly not intact. The layer was ~50-nm thick.
DP-142	Clay layer was 100-300 nm thick. Two good samples were produced.
DP-143	A 100-200 nm thick clay layer was observed. One out of three of the blocks yielded good sections.

Cont'd

Table 15 (Cont'd)

Sample	Description
DP-174	The layer was 50-nm thick. Lattice fringes were observed in many cases.
DP-175	In some regions the layer was at least 120-nm thick, and a backbone was visible. However, on average the layer was 50-nm thick. A number of intact specimens were found for both DP-174 and DP-175.
DP-176	A number of good samples were produced. A 50-100 nm thick clay layer was observed.
DP-177	At least one good sample was produced. The clay layer was 50-150 nm thick.
DP-178	Generally, sectioning of this glass produced poor samples. It possessed a 200-nm thick clay layer.

Table 16. Results of Sample Surveys for "High SA/V" Glass (Sec. VI)

Sample	Description
SVT75	A 100-200 nm clay layer was visible along with a 500-800 nm alteration layer. One good sample was produced from this test and has been used for detailed compositional analysis of this sample.
SVT77	This sample consisted of a 150-200 nm thick outer clay layer and a 400-600 nm alteration layer. At least two of the five blocks produced had good sections. These have been used for detailed layer analysis.
SVT127	The layer consisted of at least five bands: an outer layer about 150-nm thick, an iron-rich thin band, an alteration layer around 250-nm thick, a lath-rich region about 100-nm thick, and then a clear glass region. Detailed layer analysis has been performed on this sample.
SVT128	This sample consisted of a reaction layer, 400-nm thick, and an outer layer, 500-nm thick. Some good sections.
SVT129	This sample consisted of good sections, showing an extremely thin reaction layer.
SVT133	The layer consisted of an outer layer 100-nm thick, an iron-rich band, an alteration layer 100-nm thick, a mottle or lath-rich region another 100-nm thick, and then clear glass. Detailed analysis has been carried out on this sample.
SVT134	This sample consisted of good sections, showing an extremely thin reaction layer, in all about 150-nm thick.
SVT135	The sample consisted of some reasonable sections with an outer layer 50-nm thick and total reaction layer thickness of 200 nm.

Table 17. Results of Sample Surveys for West Valley Glass

Sample	Description
WV 50 925	A grid with good sections of the outer layer was obtained. A CaTh PO_x phase was found and tentatively identified as brabantite $[CaTh(PO)_4]_2$.
WV ATM-10	An attempt was made to mount and section a large piece of the $CaThPO_x$ phase. Sections were not good and primarily consisted of Si and O. There was no detectable Th.

West Valley Survey Results for pH/SA/V Tests

Test	Clay Layer, nm	Alteration Layer, nm	Comments
D85	<10	300	Good samples.
D852	20-50	200	Cracks in glass. No samples available for accurate detailed analysis.
H85	50-100	200-300	Precipitates of Fe, Ni, Cr oxide.
H852	20-50	150-200	Precipitates of Fe, Ni, Cr oxide. Not suitable for detailed analysis.
D10	300-400	2500	Some reasonable samples.
D102	300	800	Good samples.
H10	200-300	>400	Poor quality samples produced. The unreacted glass was not visible.
H102	400-500	>2000	Some reasonable samples.

Table 18. Results of Selected Sample Surveys

Sample	Description
"Effects of Radiation" Glass, ATM Glass, and Parametric Glass	
IVE202U-14	Good results were obtained for two of the outer layers. No glass layer interface has been prepared as yet. In some cases, remnants of a precipitate on the outer surface have been observed. No clear precipitate layer interface has been prepared.
IVE202U-14	Some cases produced good sections of the layer parts of the precipitate, and some distorted the interface; however, further effort will be required to obtain an undistorted interface in a section.
ATM-1C 567	Heavy chatter, some layer. Relationships between layer and glass unclear.
ATM-1C 568	Mostly glass. Shattered layer, Na-depletion in "grainy" layer.
ATM-1C 572	Reaction layers, but relationships between layer and glass unclear. Sodium depletion.
ATM-1C 575	Heavy chatter, thin reaction layer. Glass often plucked out; sodium depletion.
ATM-1C 579	Many plucked out, some shards remain. The clay layer is just beginning to form. Extensive disruption, suggestion of possibly three layers. The clay layer was around 300-nm thick with an alteration layer of 1.5 μm. A complete layer structure was not found.
P-VII	Several grids of the colloids suspended in the liquid phase were prepared. In general, these were thick, and the density of particles on the substrate was too high to be useful. This was a first attempt to prepare samples of the colloids; better results should be achievable with some experience.
P-150-2	Reaction layers on all of these are quite thin. A thin (20-50 nm) reaction layer was observed.
Natural Analogue Glass	
Tektite	Layer and glass interface not intact. Only the layer was visible.
IC2010-04	These sections showed a reaction layer, a second layer where glass had been grossly etched, and possibly a third layer of subtly modified glass. Further work will be required to determine whether this third layer is real or an artifact of sample preparation.

Cont'd

Table 18 (Cont'd)

Sample	Description
IC1710-02	(Lab-reacted tektite.) No outer layer was visible either with bright-field or dark-field imaging.
IC20210-03	(D1-90-296 lab-reacted tektite.) Fringes from a 25-nm thick layer were visible.
SRL Glass	
1099 165/TDS	This was a brine-reacted sample from SRL.
SRL 165/16	A small region of etched glass; no layers of reaction products. Glass, etched glass, and small clay-like particles distributed on the surface of the etched glass were observed. Some samples were nearly all glass; others had a small region of etched glass.
SRL U 421	A backboned layer was visible: a gap, etched glass, and then fresh glass.
Other Samples	
U1,U2,U3	These were various uranium oxide samples. They sectioned well to yield samples which will be used to investigate whether the Parallel Electron Energy Loss (PEELS) system can provide oxidation state data.
Sandstone	The result of sectioning samples of a sandstone was largely successful. However, because the sample was ground up before sectioning, it was not possible to provide much more data than SEM analysis. The sandstone was found to contain phases typical of this sedimentary rock, namely, quartz, K-feldspar, muscovite, and smectite.

In some cases, the usual technique of mounting a small particle of reacted glass was not successful because the reaction layer was very thick and delicate, and the manipulations that were required to mount the ample result in disruption of the layer structure. Special techniques of preparing particles from these glasses for sectioning have also been developed during the last year [BRADLEY].

In addition to the reaction layers that adhere to the glass, colloidal particles are spalled from the glass reaction layers into the reaction effluent or form from solution. These colloidal particles may carry radionuclides or other undesirable elements into the environment. Colloidal samples have been collected by wicking the reaction effluent through a "holey carbon" grid. These grids are coated with specially prepared carbon films, approximately 200 to 400 Å thick, and perforated with an array of very small holes. Most of the fluid passes through these holes, leaving the particles dispersed on the film where they can be analyzed with the TEM. With the TEM one obtains size and compositional information, and if the particle is crystalline, diffraction patterns are also recorded. Colloidal particles have been collected from the leachate of many samples. Results of analyses of these particles are discussed in more detail later in this section and are briefly summarized in Table 19.

D. Ongoing Tasks

A short description of work being performed in support of the program tasks along with selected results is given in this section.

1. Analysis of Long-Term Test Glass

The task involving the long-term testing of fully radioactive glass (made from actual waste sludge) seeks to evaluate the long-term performance of fully radioactive glass and compare this performance with that of nonradioactive glasses with the same nominal composition (Sec. V). Samples have been prepared of all nonradioactive tests terminated to date in this test matrix. Detailed analyses have begun [BATES-9], and efforts to develop a method for profiling the sodium distribution in the first micron of glass below the reaction layer are underway. The sodium profile near the surface is indicative of which reaction mechanism, ion exchange or matrix dissolution, is dominant. Analysis by SIMS gives good depth profiles for sodium but assumes a uniform surface and cannot be used with powdered glass (high SA/V) samples, where the reaction progress is most advanced. Profiling the sodium distribution, especially in these cases, would be very useful in determining the dominant glass reaction mechanism. Colloidal particles have been collected from the leachate of these glasses, and detailed analysis of these particle assemblages is also underway.

Using the AEM we have prepared and analyzed sections from the long-term test matrix. The first aspect of that matrix to be investigated with the TEM are sequences of nonradioactive analogs reacted for different periods of time and with different SA/V•t. Sequences of high magnification photographs showing the temporal development of reaction layers for each type of glass and at each SA/V have been produced (see, for example, Figs. 1 through 8). All of these reactions were carried out at 2000 m^{-1} at 90°C in deionized water. These types of photographs show the progress of the reaction, the relative durability of the glasses, and the overall effect of other variables (e.g., surface area to leachate volume) on the reaction.

Table 19. Results of the AEM Colloidal Particle Investigations

Test	Phases Identified	Heavy Elements Found
200R Glass		
DP90 (56 d)	Nontronite, Fe-silicate, chlorite	Ti, Fe, U, Pb, Ni, Cr, Mn, Zn
DP160/1 (98 d)	Smectite, nontronite, kaolinite	Hg, Zn, Au, Mn, Ni, U
DP92 (182 d)	Calcium-phosphate, montmorillonite, kaolinite	U, Fe, Cr, Zn, Ni
DP162 (182 d)	Smectite	U, Pb, Hg, Fe, Mn, Ni
200S Glass		
DP142/3 (70 d)	Fe,Ca-silicate, smectite, montmorillonite	U, Ni, Ti, Mn
DP178/9 (98 d)	Sodium silicates, kaolinite	Fe, U, Mn, Ti
DP181 (182 d)	Phosphates, silicates	Sn, Ni, Fe, Cr, Ti
DP108 (182 d)	Nontronite	Mn, Cr, Fe
165/42 Glass		
DP32 (364 d)	Smectite, kaolinite, rutile	Hg, Fe, Zn, Ti, Ni
131/11 Glass		
DP3 (364 d)	Rutile, nontronite, Mg, Ca, Al silicates, trace phosphates	Fe, Mn, Ti, Cr
"Effects of SA/V" Glass (20,000 m^{-1}, SRL 202)		
TZ3.1 (DIW, 7 d)	Smectite, nontronite	U, Fe, Mn, Ni
TZ42 (EJ-13, 91 d)	Kaolinite, phosphates, CaO, SiO_x	U, Fe, Pb, Zn
"Effects of Radiation" Glass (reacted at 90°C)		
165 λ Glass (91 d)	Fe colloids	
202 λ Glass (360 d)	Nontronite, FeO, Ca- and Mg-rich phases	Zn, Fe, Mn, Ni, Ti, Cr, Pb
131 Glass (180 d)	Mg-rich colloids	Fe, Cr, Mn, U

Detailed analysis of the identity of the reaction layers has also begun. Electron diffraction, lattice images, and compositional information from the reaction layers of DP20, DP21, and DP22 (131/11S glass reacted at 2000 m^{-1} for 30, 70, and 140 days, respectively) are consistent with a poorly developed smectite layer. The thickness of the reaction layer increases as the reaction proceeds and it is easier to find regions of lattice fringes in the samples which have been reacted for a longer period of time which suggests that the crystallinity is more advanced. Detailed analysis of other glass types and different SA/V is in progress. Further analysis of samples in this sequence will be performed as tests are terminated.

2. Analysis of Radiation Effects Glass

Another task seeks to elucidate the effect of radiation on leaching and vapor phase aging of DWPF glass under conditions anticipated for an unsaturated repository and a third task examines the relationship between high glass surface area to leachate volume experiments and MCC-1 tests (a standard leach test). Sample preparation of glasses from these matrices is underway and samples of colloidal particles have been prepared.

3. Analysis of SA/V Effects Glass

Detailed analysis of samples from another matrix examining the effects of surface area to volume ratio on glass reactions is well underway [MAZER-2]. In this experiment, samples of a 131 glass with different surface to leachate volume ratios have been reacted to the same SA/V•time product in order to test the validity of using SA/V to accelerated glass reactions without modifying the reaction mechanism. We have observed a close correspondence of secondary phases for many, but not all of these samples reacted to the same SA/V•t.

A similar matrix of samples has been reacted by X. Feng, formerly of the Catholic University of America (CUA) and now working at ANL. These CUA samples are of West Valley glass and the matrix is designed to investigate the effect of pH on the reaction progress as well as SA/V scaling. These samples have been analyzed and the results will be incorporated in a forthcoming paper.

4. Analysis of Tektite

Detailed analysis of laboratory reacted tektites (glasses formed as the result of a meteoritic impact) and naturally reacted tektites has been performed [MAZER-3]. This is an important set of data. Models developed on the basis of experiments that last only a few years may be criticized when used to predict glass performance over periods of tens of thousands of years. Natural analogues allow one to examine glasses that have been reacted for millions of years and compare predictions based on the results of "short-term" laboratory reactions with the actual result of long-term reaction.

A hydration layer is visible in tektites as a thin rim of birefringent material on the surface of the glass and can be measured with an optical microscope. An attempt was made to observe this hydration layer in the AEM; this attempt was partially unsuccessful. Dark-field imaging techniques, under certain conditions, have revealed a strained amorphous region corresponding to this birefringent area.

5. Formation and Characterization of Colloids in Nuclear Waste Glass Reactions

The potential formation of colloids in nuclear waste glass dissolution and the role of these colloids in transporting radionuclides are important issues in evaluating the behavior of nuclear waste glass (and, indeed, other waste forms) after disposal in a geologic repository. In particular, the assumption that the mobile concentrations of most sparingly soluble radioelements would be "solubility limited" needs to be checked. A study was, therefore, initiated to examine the formation and characteristics of colloidal particles formed under a variety of waste glass testing conditions.

a. Actinide Behavior

Samples of waste glasses, in the form of monolithic disks or crushed (sieve size 100-200 mesh) powders, were leached in J-13 well water under the test conditions shown in Table 20. A leachate sample from each test was filtered sequentially through a series of Nuclepore (polycarbonate) and Amicon Diaflo (YM-cellulose) filters. In general, the filter pore size sequence was 5, 1, 0.1, and 0.015 μm for the Nuclepore filters and approximately 3.8 nm for the Amicon YM30. The filters were placed and sealed in a Gelman filter housing. The leachate solution was forced through the filters by using a syringe to supply the leachate and the necessary filtration overpressure. After filtration, the amount of filtrate collected was weighed, and an aliquot was deposited and dried on a stainless steel planchette for alpha counting. Also, the filters were removed from the filter housing and mounted on steel planchettes in a configuration suitable for alpha counting.

The filters and filtrate aliquots were counted using a calibrated Ortec model 576 alpha spectroscopy system. The observed count rates for the alpha peaks characteristic of Np-237, Pu-239, Pu-238, Am-241, and Cm-244 were used to calculate the filterable and nonfilterable concentrations for each isotope. Samples suitable for TEM examination were prepared from selected leachate solutions by carefully wicking a small droplet of the leachate through a holey carbon TEM grid.

Table 20. Matrix of Test Conditions[a] for Colloid Particle Investigations

Test Number	Glass Type/Form	SA/V, m^{-1}	Test Duration, days
DP16	131/11-powder	2000	280
DP61[b]	165/42-powder	2000	280
DP62[b]	165/42-powder	2000	280
DP122[b]	200R-powder	2000	14
DP123[b]	200R-powder	2000	14
DP158	200R-powder	2000	14
PY11[b]	131A-powder	2000	140
PY12[b]	131A-powder	2000	140
BY11	202A-powder	2000	140
G523	ATM-8-disk	30	1460
G537[c]	ATM-8-disk	30	1460

[a]All tests were conducted at 90 °C.
[b]Duplicate tests.
[c]Test similar to G523, with tuff disk included.

The data for neptunium indicate that less than 15% of the solution concentration is filterable, even at the 3.8-nm filter pore size. This result is consistent with neptunium results previously reported [CUNNANE]. In contrast to Pu, Am, and Cm, the neptunium data are consistent with the expectation that the concentration is dominated by the material truly dissolved in solution, and that colloidal formation and transport may not play an important role in Np release from the waste packages and engineered barrier system.

The data indicate that most (up to 100%) of the Pu, Am, and Cm concentration in the glass leachate solutions is associated with particulate material in the colloidal size range. The size distribution changed significantly from test to test. The TEM results, e.g., those shown in Fig. 21, show two distinct types of particles. The larger particles (see Fig. 21b) are believed to result from exfoliation of the reacted layer on the glass surface. The particles illustrated in Fig. 21a are believed to be typical of those that account for the filtration results and may be formed and grown in the leachate solution. The size distributions are probably influenced by a broad range of factors, including glass type, test duration, and test conditions, which are not well understood at this point. However, the distribution of these elements (i.e., Pu, Am, Cm) associated with the different size fractions do not appear to be element specific. Where data are available for more than one of these elements, they appear to follow the same trend.

Although the work reported here is preliminary, the results indicate that the performance assessment assumption that groundwater concentrations of actinide elements will be solubility limited should be reexamined. This conclusion applies particularly to modeling the release of Pu, Am, and Cm isotopes from waste packages containing nuclear waste glass.

b. Colloid Characterization

Samples of the leachate from the EM and related tasks have also been examined with AEM. Table 19 outlines the glasses examined and some of the analysis results. Specimens were produced by placing a drop of unfiltered leachate onto a "holey" carbon grid and wicking the solution through with ethanol. Figure 22 shows a typical low magnification micrograph of an area of leachate (DP90). The agglomeration of a number of colloids is visible. Characterization of colloidal particles was accomplished by ED and EDS.

Clay colloids can be readily identified in the TEM, as they produce oblique textured electron diffraction patterns (OTED) when tilted. Only layered materials such as clays produce these diffraction patterns. They result when clay crystallites precipitate onto the "holey" carbon grid with **c*** perpendicular to the carbon film. The resulting reciprocal lattice is a series of concentric circles on top of one another, and when tilted produces an ellipse [GARD]. A library of colloidal clay samples examined in the AEM is being established so as to allow rapid and consistent identification of clay colloids within leachates.

Figure 23 is an example of an OTED pattern of a smectite-type colloidal particle. At 0° tilt (Fig. 23a) the pattern is circular, but as the grid is tilted (Fig. 23b) an oblique pattern appears. The slight rotation around the **c*** axis, which results in the cylindrical reciprocal lattice, can occasionally cause the formation of Moire fringes in clay colloids (see Fig. 24). This is the most common type of colloidal clay morphology observed during these investigations; however, other arrangements have been observed.

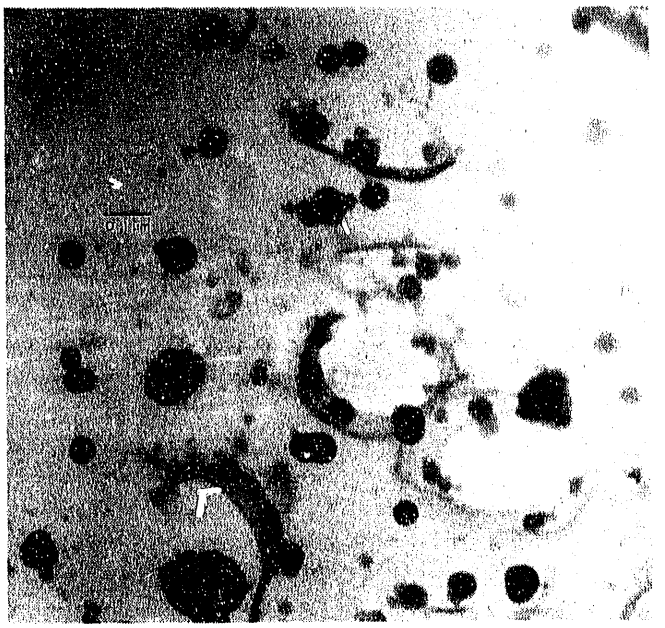

(a)

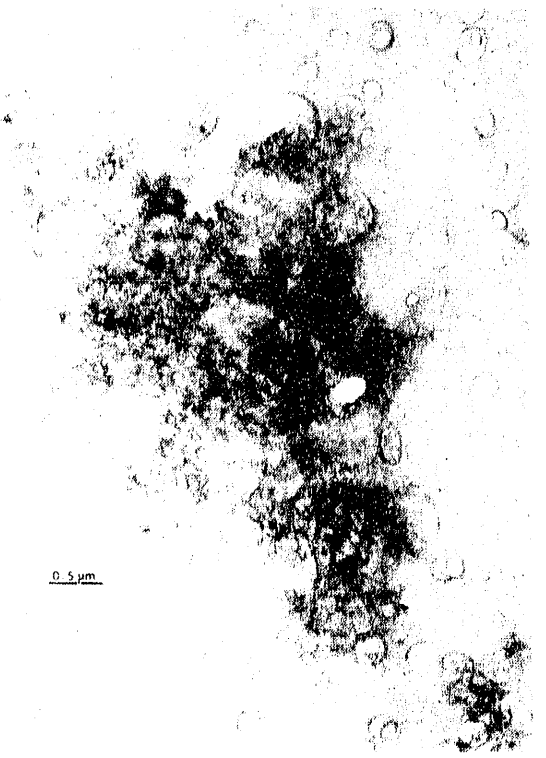

(b)

Fig. 21. TEM Micrographs of Particulate Material Isolated on a Holey Carbon TEM Grid. (a) Colloids formed from solution and (b) material in solution spalled from the glass surface.

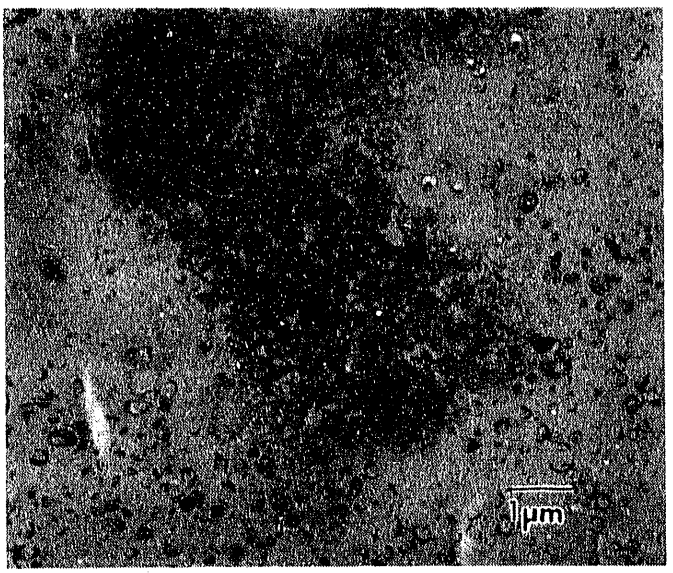

Fig. 22. Micrograph Showing the Distribution of Colloids in DP90

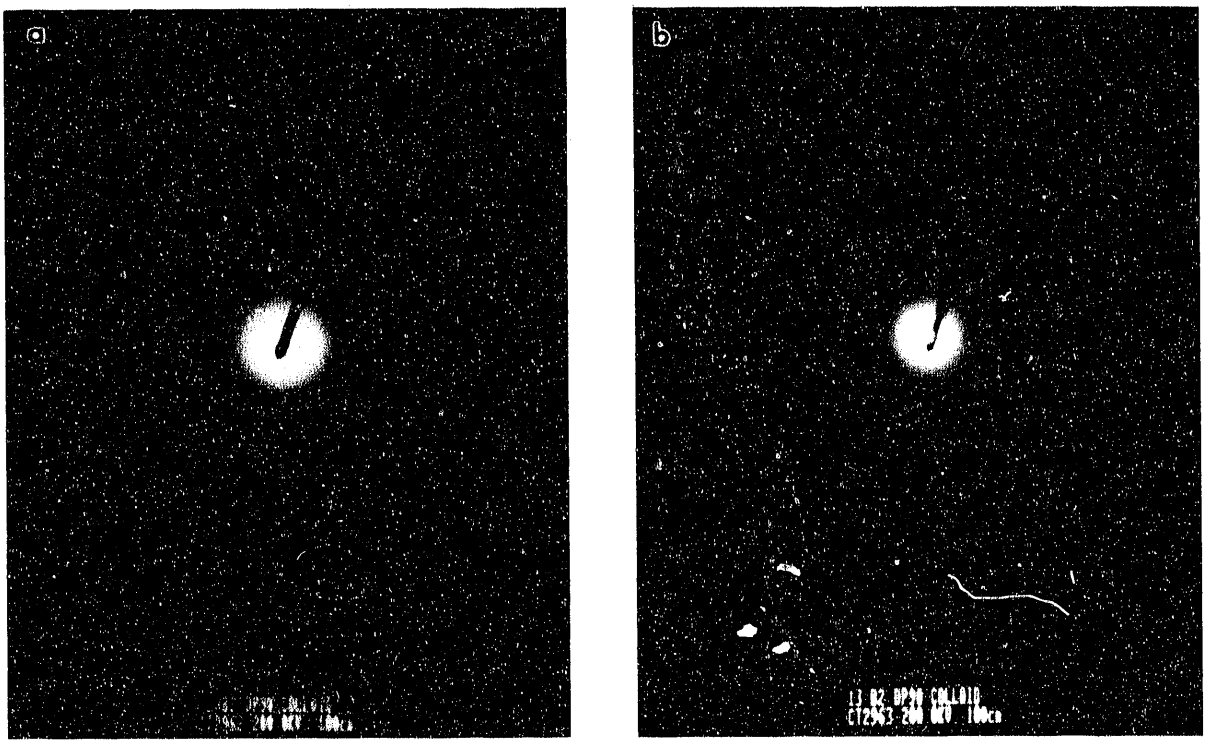

Fig. 23. Electron Diffraction Patterns of a Smectite Clay Taken at (a) 0° and (b) 35° of Tilt

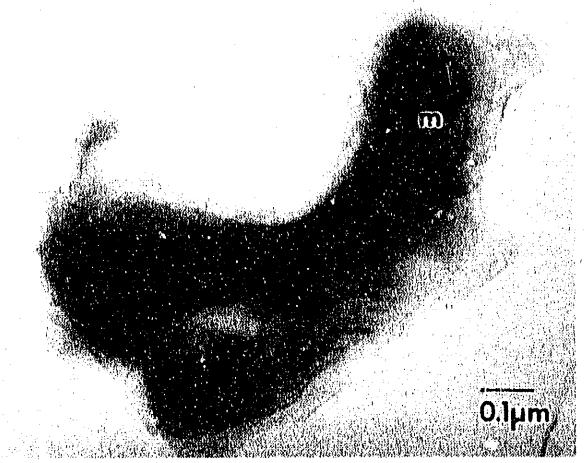

Fig. 24.
An Example of Moire (m) Fringes on a Clay Colloid Caused by the Rotation of a Few Degrees between Crystallites

In Fig. 25, the striped ribbon-like contrast of the clay colloids results in small bend contours. Small regions of the clay are at the Bragg reflection position and are, therefore, darker than the rest of the colloid. It may be possible to identify clay colloids on the basis of their morphology. For example, chrysotile is known to form tubular crystals and something similar to that has been observed in the leachate of DP143 (see Fig. 26).

Analysis of filtered leachates from some reacted glasses has shown that these were depleted in aluminum and iron. Examination of the colloid particles of these tests has revealed the presence of Al- and Fe-rich colloids.

Concentrations of particular elements within colloids were often greatly increased and colloids rich in Hg, Pb, Cr, Fe, U, and Sn have all been observed. Figure 27 is an EDS spectrum of a colloid which demonstrates the presence of a significant concentration of mercury.

Many different phases have been identified, such as phosphates, oxides of magnesium, and calcium; some of these phases may have the potential to take up actinides. Rutile (TiO_2) has been found within clay colloids (Fig. 28). Figure 29 is an example of the sorption of Fe- and Ca-rich particles onto a silicate. The most common types of clay colloidal particles found appeared to be smectite and kaolinite; however, many other types of phases have been observed. Many of these were unidentifiable.

At present, trends are difficult to see, yet a few tentative conclusions can be drawn. Smectites are the most common type of colloid found, and colloidal phosphate phases seem to appear only in samples reacted over the longer periods of time. A number of phases identified are somewhat surprising. Some of these phases have not been detected within the surface layers and have, therefore, not been included in the computer models for waste glass behavior. In addition, the concentrating of hazardous elements within colloids is another effect that has not been predicted. Hence, these studies clearly show the need to carry out investigations with fully radioactive production glasses, so that the leach rate of radionuclides away from the proposed repository can be predicted.

Fig. 25.
Ribbon-Like Clay Colloids from IV9165-A-91. The contrast is due to parts of the colloid being at the Bragg reflection position.

Fig. 26.
Tubular-Type Colloids from the Leachate of DP142/3

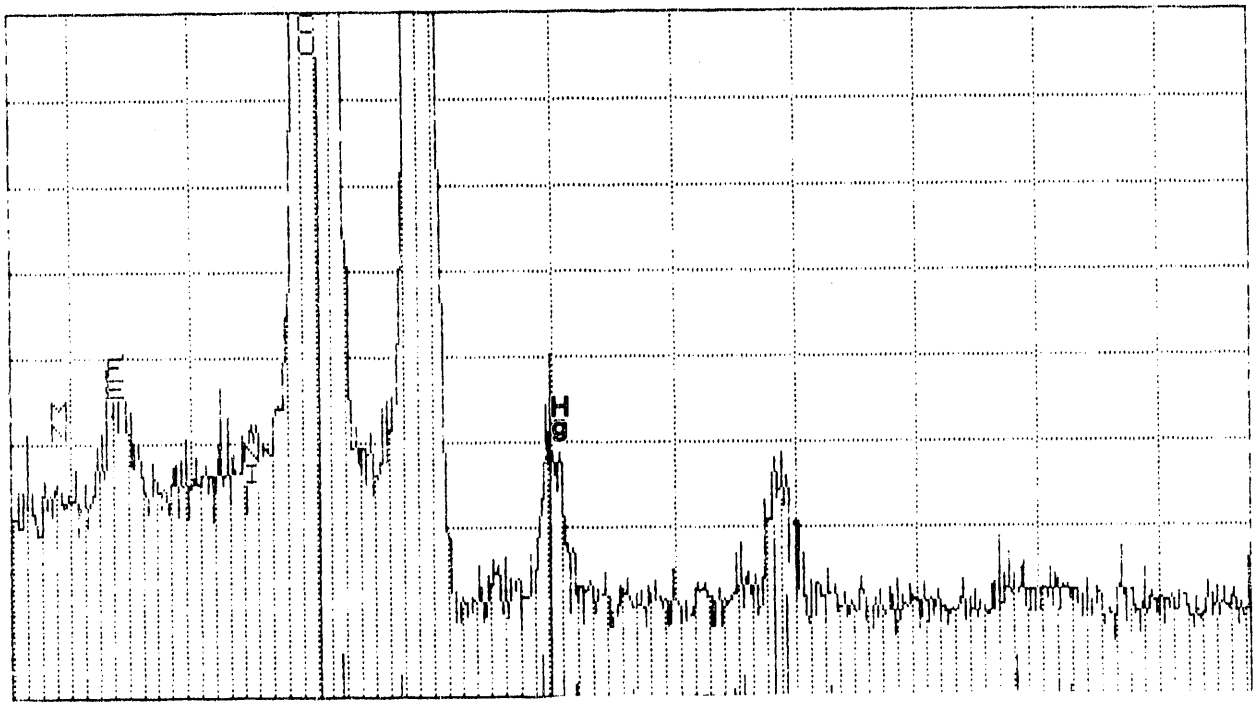

Fig. 27. EDS Spectrum of a Colloid Containing Mercury in DP160/1

Fig. 28. Brightfield Micrograph of a Particle of Rutile Attached to a Clay Colloid from Sample DP3

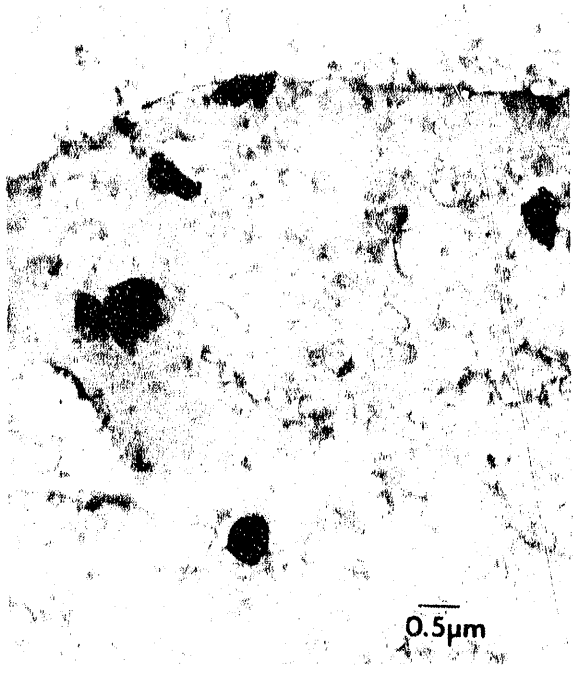

Fig. 29. Micrograph of Iron- and Calcium-Rich Particles Sorbed onto a Larger Colloid from DP142/3

E. The Use of AEM in Characterizing the Glass Reaction Mechanism

A goal of these studies is use AEM in characterizing the reaction mechanism of glass and the effects of experimental variables and possible environmental conditions on glass behavior during disposal in a geologic repository. An understanding of the glass reaction mechanism is necessary to assure that waste glasses produced for repository burial will meet performance standards. The long-term behavior of waste glass in a geologic repository will be simulated using computer codes based on the understanding of the glass reaction mechanism gained through laboratory tests. The understanding of the glass reaction mechanism under different test conditions has benefited greatly from AEM analyses of reacted solids. Coupled with analyses of the leachate solution, high-resolution AEM is being used to derive a reaction scheme for glass, to assist in the interpretation of test results, and to refine the computer simulations used to predict long-term behavior.

1. Analysis Results

Samples were prepared in thin section for AEM analysis of the reacted layers by chipping a small wedge of layer plus glass from the sample and mounting it in epoxy for microtomy. Samples where the layer/glass interface remained intact were analyzed. Figure 30 shows high resolution images of the layers from samples reacted 56, 91, and 280 days. These micrographs clearly show the progression of the layer development from an amorphous, homogeneous, gel-type structure to a crystallized, heterogeneous clay layer. After 56 days, the layer is distinct from the glass and has an amorphous appearance. A few lattice fringes exist in the outer half of the layer, but the layer is predominantly amorphous. Analysis by SIMS shows iron to be evenly distributed throughout the layer at 56 days [EBERT-2].

Segregation of iron to the center of the layer to form an iron-rich rib is seen to have occurred as the outer layer crystallized after about 91 days. This rib is amorphous and distinct from the layer material above and below it. A similar rib was seen in the layer in the cracks in the SEM analysis of cross-sectioned samples as a bright feature in the center of the layer [EBERT-2]. The layer material between the glass and the rib looks very much like the gel layer seen after 56 days of reaction, while the layer outside the rib is highly structured and crystalline. Lattice fringes are abundant in the outer layer, and electron diffraction shows most of the material to be crystalline. The entire layer appears to be in the process of separating from the glass at 91 days; at this point, most of the inner layer material remains attached to the iron band but some is still attached to the glass.

After 278 days of reaction, the inner layer crystallized to form a phase identical to the outer half of the layer. The iron-rich rib remains near the center, and the inner layer is completely separated from the glass. The separation is not due to sample preparation, and no inner layer material is found attached to the underlying glass after 278 days. The crystallized layer outside the iron band is not changed in appearance from 91 days.

The EDS analyses of the different layers show compositional changes to occur with the observed structural changes. Table 21 gives the compositions of the 56-day gel layer, the inner and outer layers at 91 and 278 days, and the unreacted glass (all normalized to 100%) as analyzed in the AEM. The iron-rich rib was excluded from the analyses. Notice the similarities among the unreacted glass, the gel layer at 56 days, and the inner layer at 91 days. Also note the similarities between the outer layer at 91 days and both layers at 278 days. Generation of the gel layer due to the leaching of the alkalis and boron early in the reaction results in an enrichment of insoluble species, such as Al and Fe. This analysis is consistent with leachate and SIMS results and with results of EDS in the SEM. Transformation of the

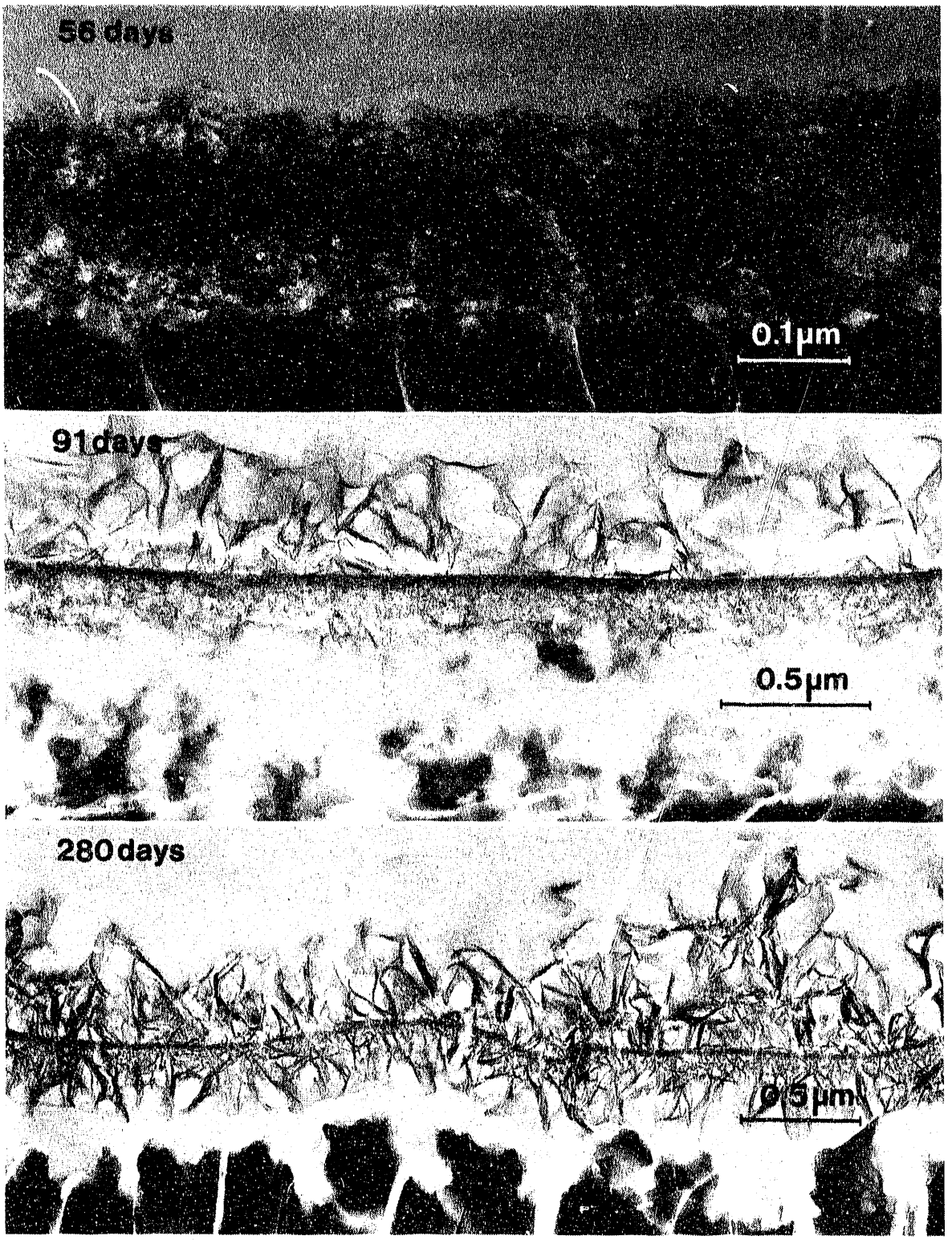

(a)

(b)

(c)

Fig. 30. Brightfield Electron Micrographs of Cross Sections of Glass Reacted for (a) 56 Days, (b) 91 Days, and (c) 278 Days

Table 21. Cation Weight Percent in Unreacted and Reacted SRL 165 from AEM Thin Sections

	Unreacted Glass	56 days	91 days		278 days	
			Inner	Outer	Inner	Outer
Mg	1.0	-	0.4	2.1	3.4	3.7
Al	5.5	8.2	12.5	13.4	14.9	15.7
Si	63.1	45.5	51.4	41.8	40.4	40.2
Ca	2.9	2.8	2.8	0.2	0.2	0.1
Ti	0.2	0.3	0.1	-	-	-
Mn	4.5	1.1	5.2	8.6	8.8	8.9
Fe	20.9	41.9	25.9	29.5	28.8	28.2
Ni	1.7	0.1	1.4	4.3	3.2	3.2

gel into the crystallized outer layer between 56 and 91 days results in an enrichment of Mg, Al, Mn, and Ni and a depletion of Si, Ca, Ti, and Fe in the outer layer, relative to the gel. Iron, calcium, and uranium have segregated to the rib formed when the outer layer crystallized. Magnesium was adsorbed from solution as the layer crystallized, as suggested by the leachate results. Thus, the behavior of various elements in the original gel layer is strongly influenced by the crystallization of a clay phase having a limited composition range. Silicon, iron, and calcium in excess of the phase's stoichiometry are expelled from the clay as it crystallizes and form other secondary phases adjacent to the crystallizing phase. The observation of small precipitates rich in Si, Ca, and U both on the outer parts of the clay and near the iron rib is consistent with the expulsion of these elements from the gel as the layer crystallized. The limited solubilities of these species resulted in secondary phases, in addition to the clay layer being formed as the glass reacts. Other minor components of the glass, such as actinide elements, may either be sorbed into the clay or excluded as it forms. Tests have shown uranium and neptunium to be leached from the reacted layer. Plutonium and americium have low solubilities at the alkaline pH values attained in tests with glass and so remain in the layer as insoluble residue. Americium appears to be concentrated on the outer surface of the layer, while plutonium is found predominantly sorbed onto stainless steel vessel surfaces.

2. Proposed Mechanism

These analyses allow a temporal description of the glass reaction to be proposed in terms of the release of individual glass components as the reaction progresses. The initial reaction is dominated by the behavior of the alkali metals and the inward diffusion of water. When the glass is first exposed to the leachant, terminal alkali silicate groups that are accessible to water molecules undergo an ion-exchange reaction with water to form silanol and to release alkali into solution. This reaction may occur with a hydronium ion or a water molecule. In either case, the pH increases due to the removal of hydronium or generation of hydroxide.

The reaction can be written as

$$\equiv Si\text{-}O\text{-}M + H_3O^+ \longleftrightarrow \equiv Si\text{-}OH + M^+ + H_2O$$

$$\equiv Si\text{-}O\text{-}M + H_2O \longleftrightarrow \equiv Si\text{-}OH + M^+ + OH^-$$

Note that the forward reaction is quenched by high concentrations of alkali in the leachate and high pH values.

Water must diffuse into the glass to under an ion-exchange reaction with other terminal alkalis. In the simplest approximation, the diffusion follows a rate law proportional to the square root of time. The observed release rates of alkali metals depends on both the rate of water diffusion to the reaction site and the rate of ion exchange. The release of alkalis is observed to follow nearly $t^{1/2}$ kinetics in most leach tests. This suggests that the water diffusion is the rate-limiting step. Thus, the release of alkali is seen to slow with time due to the kinetics of water diffusion and due to the increase of alkali and hydroxide in the leachate.

As water continues to diffuse into the glass and ion-exchange reactions occur, a region is generated at the glass surface that is enriched in water and depleted in alkali metals. The pH in this region may be very high due to the hydroxide produced by the ion-exchange reactions. Hydroxide produced by the ion-exchange reactions can participate in hydrolysis reactions, which "depolymerize" the silicate network, as shown below:

$$\blacksquare Si\text{-}O\text{-}R\blacksquare + OH^- \longleftrightarrow \blacksquare Si\text{-}OH + {}^-O\text{-}R\blacksquare$$

or

$$\blacksquare Si\text{-}O^- + HO\text{-}R\blacksquare$$

$$\blacksquare Si\text{-}O^- + H_2O \longleftrightarrow \blacksquare SiOH + OH^-$$

where R = S, Al, Fe, or other network-forming cation. The anionic silicate can abstract a proton from a water molecule to regenerate a hydroxide ion, and the hydrolysis reaction can, therefore, continue. The rate of hydrolysis of particular bonds will depend on both the bond energies and the solution chemistry. The mechanism of the hydrolysis reaction includes nucleophilic attack of the hydroxide on, for example, a network silicon atom, as shown below:

$$OH^- + \blacksquare Si\text{-}O\text{-}Si\blacksquare \longleftrightarrow \left[\begin{array}{c} OH \\ | \\ \blacksquare Si\text{-}O\text{-}Si\blacksquare \end{array} \right]^- \longleftrightarrow \begin{array}{c} OH \\ | \\ \blacksquare Si \end{array} + {}^-O\text{-}Si\blacksquare$$

Electrons in the bond between the attacked silicon atom and the bridging oxygen shift toward the bridging oxygen to create a partial negative charge. This bond breaks as the hydroxide becomes bonded to the silicon atom to form silanol. If a monomer of $H_3SiO_4^-$ results, then this may be solvated and enter solution. If the nonattacked silicon is replaced by, for example, aluminum, then an aluminum species would be released. At high silicate (or $H_3RO_4^-$) concentrations in solution, the hydrolysis reactions will be slowed. Further dissociation at high pH values will decrease the solution concentration of $H_3SiO_4^-$, for example, and may increase the forward rate of reaction. The kinetics of this reaction is what is modeled in the computer simulations used for glass reaction. The strength of local bonds and the ability to stabilize a negative charge will differentiate the release rates of different network formers. Steric effects and the local glass structure will also affect the accessibility of the silicon atom to attack by the hydroxide.

Boron is usually observed to be leached from the glass to a similar extent as the alkali metals, although it is considered to be a network former. This suggests that silicates bonded to boron are most susceptible to nucleophilic attack, and borate species are readily released from the glass, for example, as

$$\blacksquare Si\text{-}O\text{-}B{=} + OH^- \longleftrightarrow \blacksquare Si\text{-}OH + {}^-OB{=}$$

The bonding of boron in borosilicate glasses is not fully understood, and it is possible that boron is not bonded to three bridging oxygens. Nuclear magnetic resonance results suggest that the ratio of "Si-O-B" groups to the boron content is much less than three. Thus, a reaction layer is formed at the glass surface early in the reaction due to release of alkali metals by ion exchange and boron by hydrolysis. Both the alkali metals and boron are leached from the glass as the reaction front penetrates the glass at a rate controlled by the rate of water diffusion. What remains behind the water diffusion/ion exchange front is a partially hydrolyzed glass phase depleted in alkali and boron. Hydrolysis reactions continually occur in this depleted region to break the glass network into smaller fragments. The reacted layer can, therefore, be described as an aggregate of partially connected fragments of leached glass. This is the layer formed after 56 days of reaction, as shown in Fig. VII-30a.

Hydrolysis at the outer surface of the reacted layer may result in the generation of monomers or dimers which may be solvated. The surface of the glass may, therefore, retreat from its original position as the reaction progresses. Elements can be released from within the layer if the reaction frees a species small enough to be solvated and released into solution. The leachate may reach the solubility limit of some species (e.g., iron) after very little glass has reacted. As the surrounding silicate network dissolves, iron-containing species and other insoluble species may remain associated with the surface as insoluble residue. Therefore, both the kinetics of hydrolysis and the solubility limits in solution determine the composition of the reacted layer as the reaction proceeds.

The behavior of specific cations observed in the static leach experiments as the reaction progresses is summarized below. Figure 31 shows the layers formed after 56 and 278 days in schematic cross section with representative release of alkali metals and boron, silicon, and iron. After 56 days, a mostly amorphous gel-like layer is observed on the surface. This layer is depleted in alkali metals and boron due to ion exchange and initial hydrolysis reactions. The degree of depletion is similar throughout the layer. The alkali metals and boron must, therefore, be released primarily at the glass/gel interface. Calculations comparing the solution concentrations and the initial glass compositions show that the alkali metals had to be released from about a 1 μm depth to generate the measured solution concentrations for tests of 56 days. Since the measured layer depth is only about 0.2-μm thick after 56 days, the outermost surface must have retreated from the original surface by about 0.8 μm. Transition metals such as iron have very low solubilities under the alkaline pH conditions attained during these tests. The transition metals and aluminum remain as insoluble residue within the gel layer as the silicon framework dissolves and the surface retreats. The gel layer may become highly enriched in these insoluble metals as the outer surface of the layer dissolves. After 56 days, these insoluble species are distributed throughout the gel layer. The behavior of doped actinides is of special interest. Doped actinide elements behave as follows: uranium and neptunium have relatively high solubility limits and are released into solution. The gel layer is found to be depleted in both U and Np. Plutonium is neither depleted nor enriched in the gel. Plutonium and americium have very low solubility limits under high pH conditions and have very low solution concentrations in these tests. Plutonium is released from the glass as the outer surface of the reaction layer dissolves and is found sorbed onto the stainless steel vessel walls. Americium is found in small quantities on the vessel walls but primarily remains in the gel layer as insoluble residue.

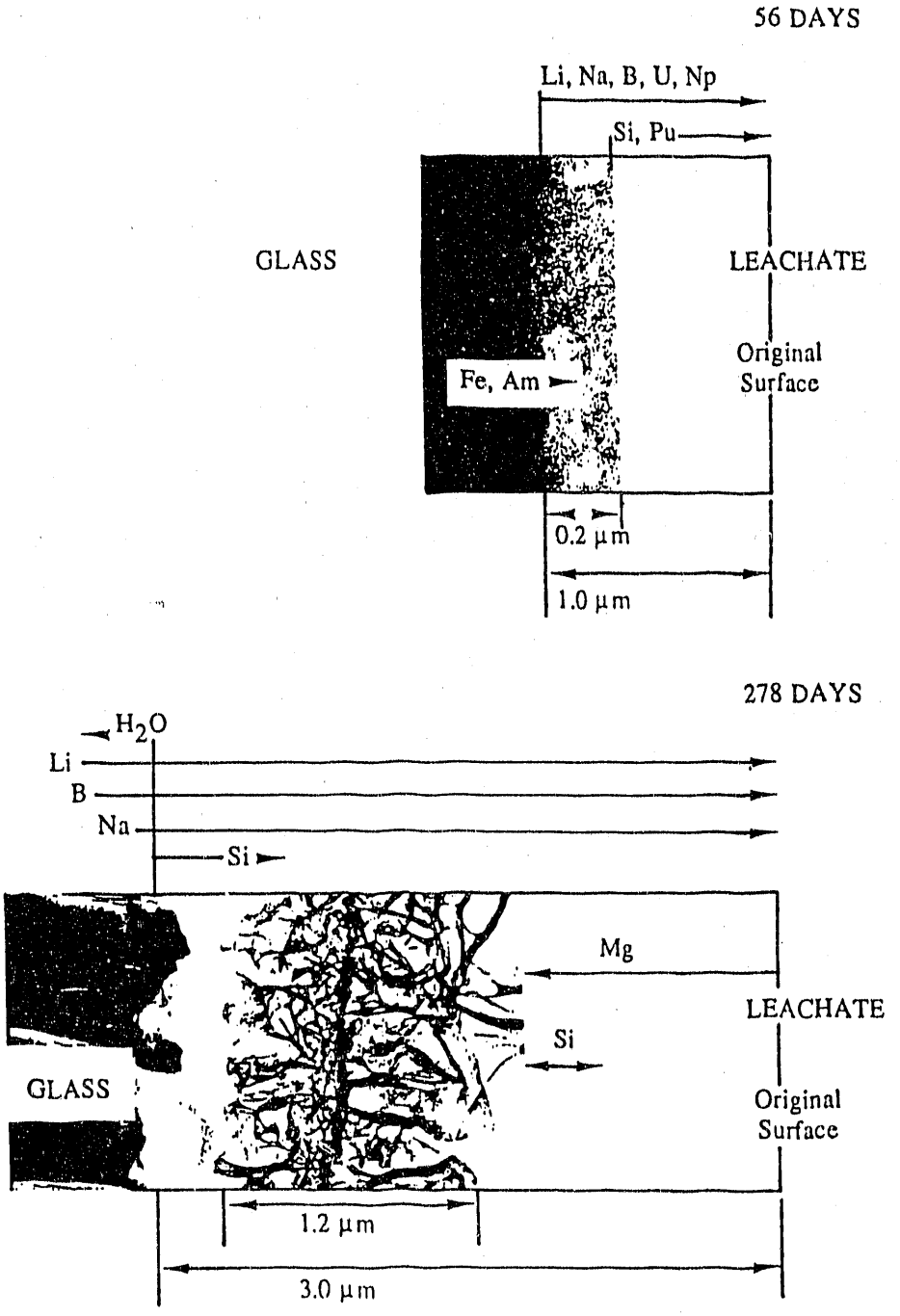

Fig. 31. Schematic View of Elemental Release Trends at (a) 56 Days and (b) 278 Days

Between 56 and 91 days of reaction, the gel layer nucleates to form small clay laths. The outer portion of the layer crystallizes before the inner layer because the silica network is more completely disintegrated in the outer portions of the layer, which have been exposed to water for longer times. As the gel crystallizes, some species are expelled due to the stoichiometry of the phase, for example, Ca and Fe, while other species, such as Mg, are incorporated into the crystallized phase from solution. As the outer layer crystallizes, the iron migrates away from the solution into the center of the layer where the silicon network has not sufficiently disintegrated to begin recrystallizing. The iron does not redistribute in the inner layer which has not yet crystallized, rather it accumulates at the interface of the crystallized and uncrystallized layers, forming a "backbone" structure from which the clay phases radiate. The "backbone" structure provides structural integrity to the layer as it forms and keeps the layer structures from collapsing onto the glass. Why the iron accumulates at the center of the layer is unclear. This may indicate that a hydrophobic iron species is formed and is repelled by the solution as it penetrates the layer.

As the reaction continues, the inner layer eventually crystallizes. More iron is excluded from the inner layer as the clay crystallizes and migrates to the center of the layer to complete the formation of the iron-rich rib. Material in the inner layer nucleates at the iron rib, and crystallization occurs from the rib to the glass. Gel-like material becomes completely dissolved from the glass as the inner clay layer forms. Because the "backbone" provides structural integrity and because selected elements go into solution as the glass reacts, a void develops between the layer and the glass. This void is filled with solution which facilitates the crystallization of the inner layer. The transformation from glass to reacted layer is not an isovolumetric process.

After 278 days the entire layer has crystallized into a clay phase(s), which is in near-equilibrium with the adjacent leachate solution. This is shown in Fig. 30, where the layer surface is positioned to display the continual retreat of the surface as the reaction proceeds. A retreat of about 3 μm is indicated from the solution concentrations of highly soluble elements. Elements which form the clay layer have their solubility limits determined by the clay phase. These include silicon, aluminum, iron, magnesium, and other elements included in Table 22. At 91 days, when the layer begins to crystallize, and at longer times, the measured solution concentration of silicon is nearly constant. This is because the crystallized outer layer is in near equilibrium with the leachate, and silicon has attained its solubility limit with respect to the clay or clays which comprise the outer layer. Other species, such as iron and aluminum, maintain low solution solubilities throughout the reaction. Presumably, secondary phases of iron and aluminum hydroxides, for example, set the solubility limits for these species early in the reaction. Magnesium, which was released into solution prior to clay formation, is removed from solution as the clay forms. This is seen in analysis of the layer composition (Table 21) and the leachate analysis [EBERT-2]. While magnesium had a high solubility limit prior to clay formation, the clay incorporates magnesium as it crystallizes and sets a lower solubility limit for magnesium.

While the leachate is in near equilibrium with the layer, it is not in equilibrium with the glass, and the glass continues to react. Species that had accumulated in the layer due to low solubilities are now associated with the clay, either being incorporated into the clay or deposited on the clay as different phases. No evidence of amorphous gel-like material is seen on either the clay or the glass surface. The clay is now a distinct phase and is no longer connected to the glass by amorphous gel. Alkali metals and boron continue to be released from the glass surface unimpeded by the porous clay layer, which is now completely separated from the glass. After the clay layer separates from the glass, leachate can attack the exposed glass beneath the layer, and the reaction continues. The layer offers no deterrence to either incoming water or released species. Species such as silicon, aluminum, and iron, which are components of the layer, are released from the glass and nucleate as additional clay on the layer or as part of the

Table 22. EDS Results (wt %) for Unreacted Glass and Reacted Layers Formed after 180 and 278 Days of Reaction

	Unreacted Glass		Layer after 278 Days (#423)			Layer after 278 Days (#425)		
	As Analyzed	Renormalized	As Analyzed	Renormalized	Ratio[a]	As Analyzed	Renormalized	Ratio[a]
Na	8.0	15.3	0.8	2.1	0.1	1.2	2.8	0.2
Mg	0.4	0.8	1.0	2.6	3.3	1.1	2.5	3.1
Al	2.2	4.2	1.7	4.4	1.1	1.8	4.1	1.0
Si	24.7	47.1	16.1	42.0	0.9	18.9	43.2	0.9
Ca	1.2	2.3	1.6	4.2	1.8	1.7	3.9	1.7
Mn	1.5	2.9	2.0	5.2	1.8	1.9	4.3	1.5
Fe	8.4	16.0	13.6	35.5	2.2	15.5	35.5	2.2
Ni	0.7	1.3	0.5	1.3	1.0	0.6	1.4	1.1
Zr	0.5	1.0	0.7	1.8	1.8	0.8	1.8	1.8
U	0.7	1.3	0.4	1.0	0.8	0.2	0.5	0.4
Li[b]	2.0	3.8	0	0	0	0	0	0
B[b]	2.1	4.0	0	0	0	0	0	0
Total Cations	52.4	100.0	38.35	100.0		43.7	100.0	

[a]Radio of wt % in layer/wt % in unreacted glass.

[b]Assumed totally depleted in layer as per SIMS results.

"backbone," and so the layer grows as the glass dissolves. The solution concentrations of elements which form the layer remain constant. Other species released from the glass which are either in excess of the clay composition or are not a part of the layer, such as calcium and uranium, may form other secondary phases on or in the layer as their solubility limits in the solution are reached. The clay may act to sorb other released species having low solubilities such as the actinide elements. Further analyses are required to describe the actinide behavior.

It is important to note that a new gel phase is not generated at the newly exposed surface. Careful analyses with AEM and SIMS suggest that the outer surface of the exposed glass is depleted in alkalis and boron only to a limited extent. This is probably because the solution composition in contact with the glass differs from the initial leachant composition. The high pH and alkali content quench the ion-exchange reactions, which generate the gel layer at earlier times. Thus, it appears that continued reaction of the exposed glass is stoichiometric. This has important ramifications for long-term modeling of the glass reaction, which are discussed later in this report.

Several issues regarding the interpretation of the AEM micrographs are worth emphasizing, and a brief discussion is included below.

(1) Why does the iron-rich "backbone" form in the center of the layer? The "backbone" is only seen after the outer layer crystallizes. The EDS analyses show the crystallized layer to have a reduced iron content compared to the gel layer; thus, iron is clearly driven from the layer as it crystallizes. Why it migrates toward the glass rather than to the outer surface can be interpreted as a retreat from the solution or as coalescence. By forming inside the layer, the exposed surface area is greatly reduced from what it would be as discrete particles at the outer edges of the clay laths. The iron stops in the center of the layer presumably because the clay has stopped crystallizing at that point. This may be because the material in the inner layer is not sufficiently disintegrated to restructure. The region near the iron "backbone" then becomes the nucleating site for the inner gel material later in the reaction when the gel is able to reconstruct. Iron expelled from the inner layer then migrates to the existing iron "backbone," since it would be initially energetically unfavorable to generate a second "backbone." This reduces the surface area of the iron "backbone" material and the surface energy.

(2) Why does the clay layer separate from the glass? The reason that the gel layer remains fixed to the glass prior to about 278 days is that the silicate network still exists linking the layer to the glass. As the gel disintegrates and restructures to form the inner clay layer, these bonds are broken. No bonds are formed between the clay layer and the glass because of structural and compositional differences. As the exposed glass reacts, the two phases become further separated. The region between them becomes filled with leachate, and the reaction of the glass continues.

(3) Why doesn't a new gel layer form on the exposed glass surface after about 180 days? The gel forms early in the reaction when the solution has intermediate pH values, and the ion-exchange reactions occur faster than the hydrolysis reactions, for reasons discussed in the text. The gel develops because of the different release rates of the alkalis, boron, and silicon; the dissolution of silicon lags behind that of the alkalis and boron. At the high pH values achieved later in the reaction when the layer separates from the glass, the ion-exchange reactions are slower than the hydrolysis reactions and so no gel forms. Hydrolysis reactions release silicates from the glass, which then become associated with the clay.

F. Future Progress

In the future, detailed characterizations of phases will continue on the samples from the long-term test task, the effect of radiation task, and the high SA/V task. Identification of the secondary phases produced on the surface of the glass and observation of compositional gradients within the glass caused by the reaction process have already begun. Observation of these compositional changes is quite a challenge because those elements that are mobile in the reaction process are frequently also mobile in the focused electron beam used for analysis.

Preparations to begin sectioning radioactive glasses are complete. A special hood for the microtome has been designed, fabricated, and installed. Sections of fully radioactive glass are being produced, and analyses of these samples will begin shortly.

Colloidal studies will continue, and as the number of analyses completed increases, trends should start to show themselves. Standards will be produced to make more reliable identifications of both the colloidal and sectioned samples. It will also be necessary to run standards of various heavy elements which have been found in colloidal particles so that a minimum detection concentration for these elements can be calculated.

Detailed analyses of suites of samples from the reaction matrices described above, which show the development of reaction products and compositional gradients as functions of experimentally controlled variables, will be the focus of activities in the coming year.

IX. TECHNICAL REVIEW OF ANALYTICAL ELECTRON MICROSCOPY OF GLASS REACTION

A. Introduction and Background

Analytical electron microscopy (AEM) analysis of the reacted glass samples is an important component of the ANL Technical Support Program. The objective of this project at the University of New Mexico (UNM), under the ANL-UNM Contract No. 10362402, is to provide peer review input by performing AEM and SEM analyses of reacted glass samples to confirm conclusions reached in the ANL program.

This section covers the extensive AEM and SEM analyses performed on samples IVE202U-14-1-2 and B-82 at UNM in the period from February 1991 to September 1991.

B. Technical Approach

1. Sample Preparation

The two samples were received from ANL for analysis in late March. As described in the guidance memo from ANL, sample IVE202U-14-1-2 was reacted in saturated water vapor at 200°C for 14 days, while sample B-82 was reacted in saturated water vapor at 200°C for 23 days. Both samples are 202U glass, so their compositions are identical. However, the surface of as-received IVE202U-14-1-2 had two distinct parts, one had a dark appearance and the other had a bright appearance, which could be identified by the naked eye. These two parts were separated and considered as different samples before further preparation and analysis.

For TEM and AEM analyses in cross section, which allow one to study phase distribution from the top of the reacted surface to the underneath unreacted glass, very thin sections of several hundred angstroms in thickness have to be cut perpendicular to the original sample surface. Ultramicrotomy slicing technique similar to that described in [BATES-4] was used to obtain these thin sections. In the process, small chunks containing the reacted surface layer and a thin layer of glass were first broken off from the sample, and each of these chunks was then embedded in "Eponate 12 Quik-Mix" resin to form a block. Finally, thin sections which are transparent to electron beam were sliced from these blocks and were then mounted on copper mesh grid supported holey carbon films for observation. About 50 of these thin sections were made and examined for each sample. The samples are so fragile and delicate that most of the primary reaction layer and secondary phases were found to be shattered and separated from the glass substrate and the embedding resin under TEM observation. That makes the study of layer thickness, physical relationship, and interface between phases very difficult. This was not a problem with the TEM samples prepared at ANL, in which the entire sample was still intact and surrounded with the embedding resin. It seems that the resin used for embedding at UNM might be too brittle, and the sample preparation technique at UNM needs to be improved.

2. Scanning Electron Microscopy

Scanning electron microscopy with energy dispersive X-ray spectroscopy (SEM/EDS) analysis has been performed on the sample surfaces to obtain morphological overview of the reacted glass surface and to determine the composition-morphology relationship of the secondary phases on the surface. The SEM analyses were conducted before the sample surface was damaged during the TEM sample preparation process. A Hitachi S-800 scanning electron microscope with a field emission electron source

and a windowless Princeton Gamma Tech (PGT) EDS system was used for the analyses. During the analyses, the electron energy was set at 10 or 15 keV. The PGT EDS system does have light element detectability. However, the elemental quantification capability of the system is poor. Also, since a low energy (10 keV) electron beam was used during EDS analysis with SEM for reducing the X-ray contribution from the glass matrix, the excitation efficiency for the higher atomic number elements was artificially reduced. Thus, the analyses only provided qualitative chemical information. Nevertheless, the qualitative information was very valuable for matching the TEM image of a specific phase to their SEM counterpart and understanding the physical relationship between phases, especially because most TEM samples were shattered.

3. Analytical Electron Microscopy

Analytical electron microscopy was performed using a JEOL JEM-2000FX microscope attached with a TN-5500 EDS system. The microscope was operated at 200 keV during analyses. Extensive TEM imaging, including high resolution electron microscopy (HREM), selected area electron diffraction (SAD), and EDS studies, was conducted on the thin sections supported by holey carbon films.

The magnification of the microscope at its higher end was calibrated using the 3.4 Å (002) lattice fringes from a graphitized carbon specimen at a set objective lens condition. However, due to small variations in specimen height and lens conditions, an error of ±5% may still be incurred in the magnification of the HREM images. The camera length used for electron diffraction was calibrated using a Si [111] zone axis pattern, and the error in measurement is within ±2%. Because electron diffraction gives better accuracy, spacing of lattice fringes in the micrographs was determined whenever possible by the corresponding spots in the electron diffraction pattern.

Many factors contribute to the errors induced in quantitative EDS analysis. First of all, since the EDS system used has a rather "thick" (7.5 μm) Be window, most low energy characteristic X-rays from light elements were absorbed. Elements with atomic number smaller than that of Na (11), which include O, B, and Li, cannot be detected, despite the fact that the oxides of B and Li constitute more than 12 wt % of the glass composition. Secondly, the quantitative software used, SQMTF, can only handle eight elements, while there are about 20 elements present in the glass samples. Also, no absorption corrections were made for the results of analyses mainly because local sample thickness cannot be accurately determined. Nevertheless, accuracy of quantitative analysis of the EDS spectra has been studied very carefully in this project.

The eight "major" elements included in the quantitative analysis of glass and primary reaction layers compositions are Si, Fe, Na, K, Al, Mn, Ca, and Mg. Although K factors used for these elements have been well calibrated in the past in the laboratory from simple minerals, they have been checked carefully using the nominal bulk composition as a standard for more than 15 spectra from the glass. A bulk TEM glass sample was prepared by Ar ion milling for this purpose. Large variation and relative error (more than 50% lower than nominal quantity) have been found in the analyses of Na and K, mainly because (1) ignored absorption is probably quite substantial for Na, and (2) K is depleted by the electron beam during analysis. Even in the ten spectra collected at -155 to -165 °C using a liquid N_2 cooling sample stage, the depletion of K during analysis was still obvious. Since these errors can induce further distortion in the results for other elements, and they cannot be simply corrected by adjusting K factors, accuracy of quantitative analyses for the remaining six elements was checked with Na and K

data excluded, and the total content of these elements was normalized. Errors in the quantity of these six elements are all less than 1 wt %, although the relative error can still be as large as 27.5% due to the small content of some elements. A trial-and-error experiment based on five spectra from the glass matrix indicated that, if the K factors for Al and Mn were adjusted both from about 1.1 to 0.85, the relative error in the resulting data could be reduced from 27.45% to 1.34% for Al and from 24.26% to 0.71% for Mn. However, such adjustments have not been applied to the other spectra collected in this study because the errors in absolute quantity are already so small, and it is still not certain that our old K factors are wrong without further calibration on simpler standards. For the spectra from phases other than unreacted glass, the total content of the detected elements cannot be normalized with the true value because of the unknown quantity of undetectable elements in the phase. The errors in these results could be much larger. The K factors are shown in Table 23.

C. Results

1. Results from IVE202U-14-1-2

Extensive SEM with EDS analyses have been done on the surface of IVE202U-14-1-2. Although both the dark and the bright sides of the surfaces are covered by a honeycomb-like primary alteration layer, much more secondary crystals have been found on top of the layer in the bright part of the sample. Figure 32 contains selected SEM micrographs of various observed phases from the bright part of the sample surface. In one particular region of the sample, just next to the spot where the wire on which the sample was hung during the leaching experiment, the density of the secondary minerals is much higher than in the other areas, as shown in Figure 32b. According to their morphology [WELTON] and qualitative composition, the primary alteration layer and the four secondary phases could roughly be identified even before the AEM study. They are the smectite primary layer with honeycomb morphology (marked with letter "S" in Fig. 32); well-developed cubo-octahedral zeolites (marked with "Z"); calcium silicate rosettes with little aluminum (marked with "C"); calcium silicate flakes with some aluminum (marked with "C*"); and asbestos-shaped uranium silicate (marked with "U").

Table 23. K Factors (C_z/C_{Si} vs. I_z/I_{Si}) Calibrated in the AEM Laboratory of University of New Mexico for Quantitative EDS Analysis

Na	2.888 ± 0.067
Mg	1.386 ± 0.023
Al	1.099 ± 0.099
S	1.04 ± 0.05
Cl	1.14 ± 0.05
K	1.107 ± 0.017
Ca	1.025 ± 0.012
Ti	1.180 ± 0.010
Cr	1.17 ± 0.05
Mn	1.114 ± 0.017
Fe	1.110
Zn	1.343 ± 0.027

Fig. 32. SEM Micrographs from the Bright Part of the IVE202U-14-1-2 Sample Surface. Letters marked on the micrographs represent: S--smectite; Z--zeolite; C--calcium silicate; C*--calcium silicate with aluminum; and U--uranium silicate.


E
S
Z
000010 10KV X2.00K 15.0um
F
S
U
C
000002 10KV X2.00K 15.0um
G
S
U
C
000011 10KV X3.00K 10.0um
H
S
U
Z
000009 10KV X2.00K 15.0um

Fig. 32 (Cont'd)

This AEM study confirmed the SEM observation and provided more detailed information. Figure 33a and 33b are cross-sectional TEM brightfield micrographs taken from two relatively intact thin sections from the dark and the bright part of IVE202U-14-1-2 sample, respectively. As seen in Fig. 33a, on the dark surface of the sample, only a crystalline primary layer is present above the glass. However, all the four secondary phases on top of the smectite layer seen in the SEM study on the bright side of the sample can be observed in Fig. 33b. The primary alteration layer is also much thicker at the bright side of the sample. These observations indicate that, during the leaching experiment, the reaction condition on the sample surface was not spatially uniform.

The composition and structure of the primary alteration layer have been carefully studied with AEM. Figures 34 and 35 show the typical EDS spectra and the corresponding results of quantitative analysis for the glass substrate and the layer, respectively. The only noticeable difference between the two compositions is that the alteration layer has less Na and K, but more Ca than in the glass. Many spectra have been collected across the thickness range of the layer; no systematic compositional change was detected. A low magnification brightfield TEM micrograph with SAD pattern and two HREM images from the layer are shown in Fig. 36. The major d spacings measured from the SAD pattern are 0.16, 0.27, and 0.47 nm. The HREM images present the typical curved lattice fringes from clay minerals. As shown in the figure, 0.47 nm and 1.4 nm lattice spacings were measured (0.47 nm spacing was calibrated using the spacing on the SAD pattern). These results confirmed that the primary alteration layer is smectite and also suggest that it is probably either nontronite Fe-containing saponite. Nontronite and saponite were found in the previous studies of both altered basaltic glasses [JERCINOVIC] and simulated nuclear waste glasses [ABRAJANO-2], and saponite's basal spacing can vary from 1.35 to 1.68 nm [GUVEN], depending on the exact composition. However, while observed d spacings from the smectite layer matches closely with those on nontronite and ferroan-saponite as indicated in Table 24, the chemical formulas of these two phases cannot be matched with the quantitative EDS results.

Figures 37a and 37b compare SEM image and TEM image of the calcium silicate rosettes. After comparing the d spacings measured from the SAD pattern in Fig. 37b and quantitative EDS data shown in Fig. 38 with all of the calc-silicate phases listed as secondary minerals associated with altered basaltic glasses in [JERCINOVIC], we found no specific match. One main problem is that the Ca/Si ratio in the spectrum is too low for any of those listed phases. The EDS data from the SEM study indicated that this phase also contains certain amounts of sodium, but its quantity is unknown.

Figure 39 shows the TEM images and a SAD pattern of the zeolite phase. A ~0.96 nm lattice spacing was measured both in the SAD pattern and the HREM image. Apparently, the large zeolite blocks seen in the SEM image were shattered during slicing by ultramicrotomy. The EDS spectrum and its quantitative analysis results are shown in Fig. 40 for the zeolite. The EDS spectra obtained during SEM study of this phase show a Na peak but not a Ca-K_α peak because the excitation efficiency of Ca was reduced due to the low electron energy used. Stilbite, $NaCa_2Al_5Si_{13}O_{36}\bullet 14H_2O$ with $d_{100} = 0.911$ nm, offers a relatively close match to the data from this zeolite phase. Some zeolite crystals contain less Al and Ca, and an example is shown in Fig. 41.

The EDS data and two single crystalline microdiffraction patterns from an uranium silicate particle are presented in Fig. 42. The weight percent ratio of uranium oxide to silicon oxide in this crystal is about 70 times that in the bulk glass. The formation of this uranium-rich phase should result in a retardation in uranium leaching rate.

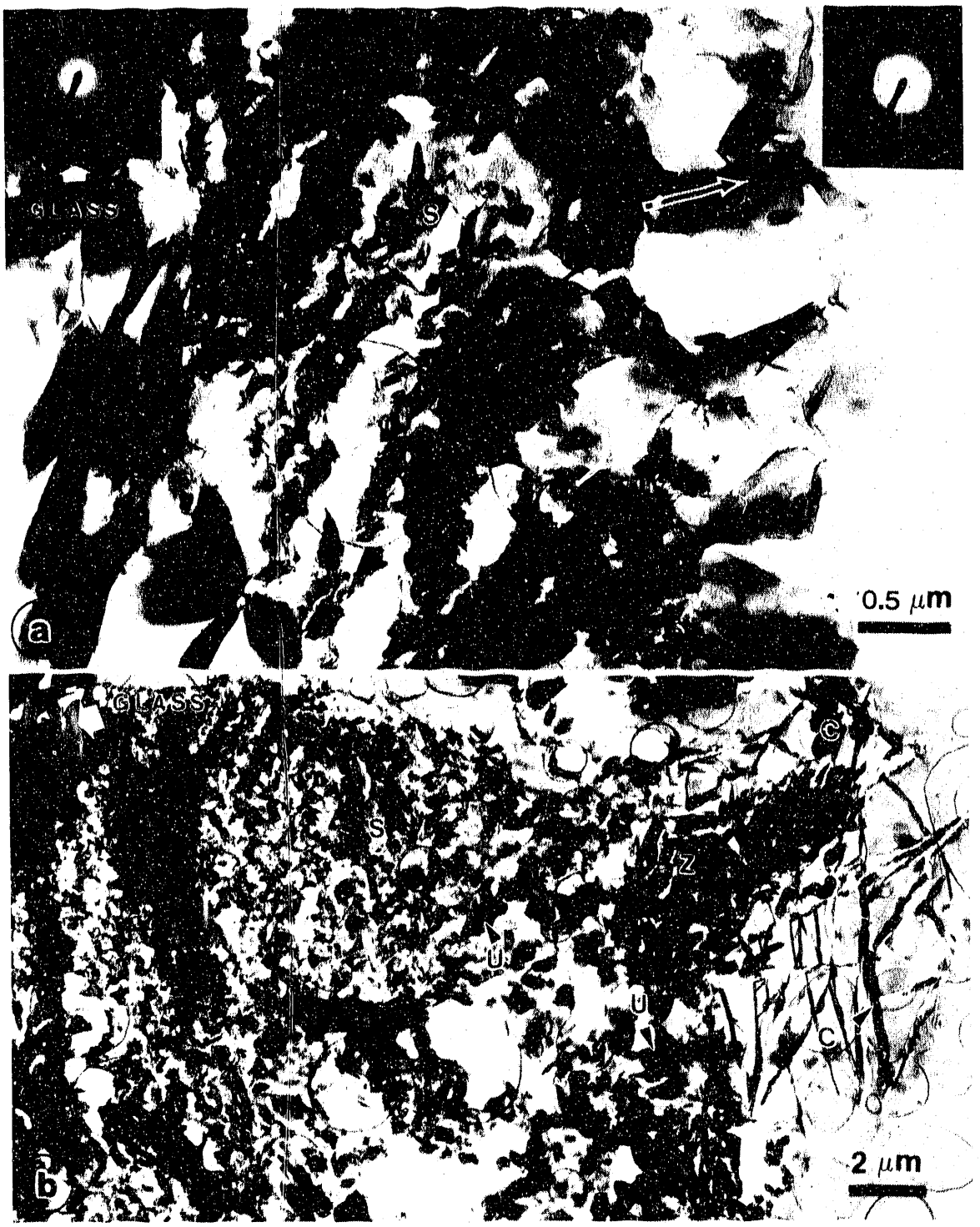

Fig. 33. TEM Micrographs Covering Entire Reacted Range (from Top Surface to Glass Matrix) of IVE202U-14-1-2 Sample. (a) Dark part of the sample, only smectite layer is observed; (b) bright part of the layer, secondary phases are present on top of the smectite layer. Letters marked on the micrographs represent: S--smectite; Z--zeolite; C--calcium silicate; C*--calcium silicate with aluminum; and U--uranium silicate.

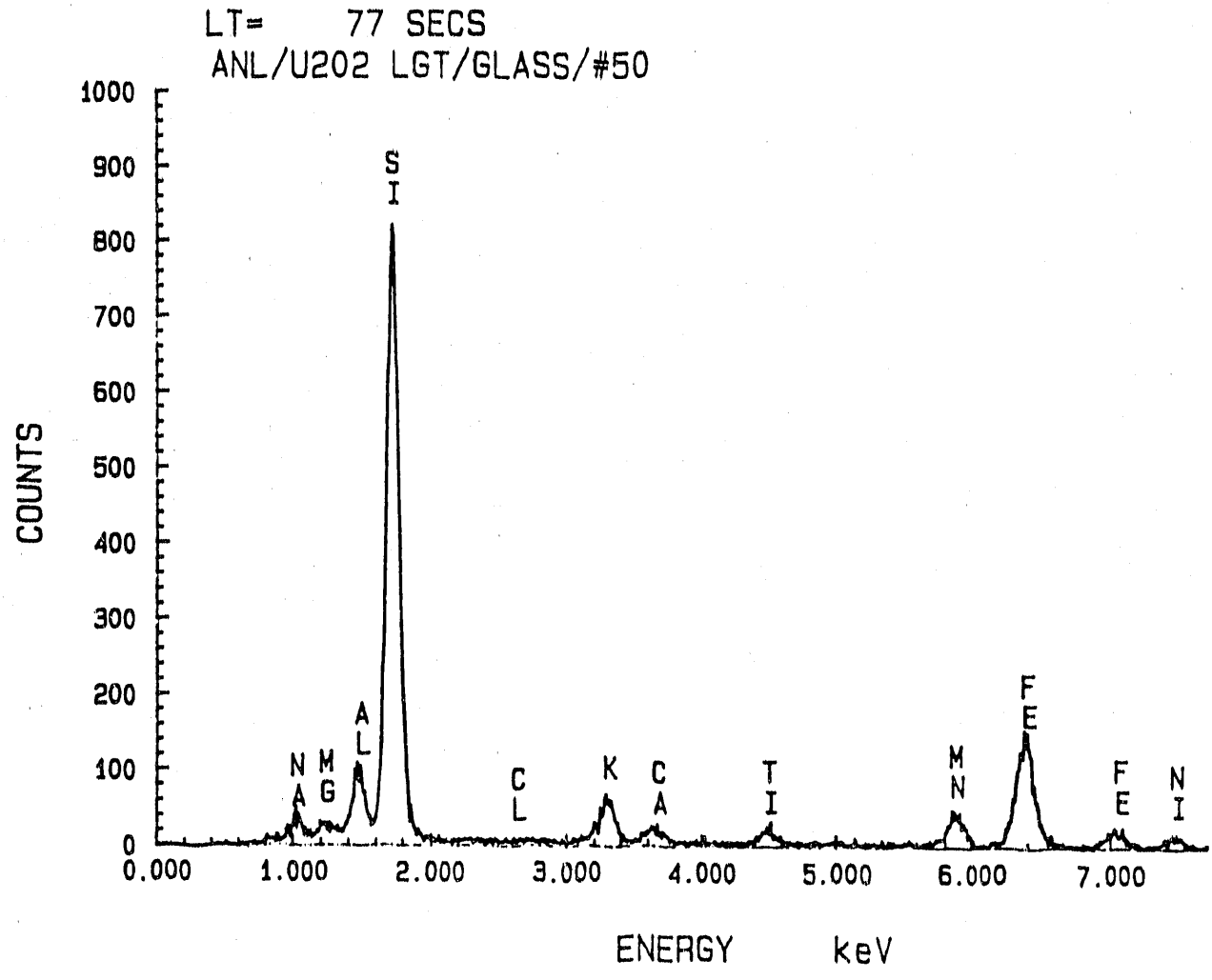

ANL/U202 LGT/GLASS/#50

EL-LINE	PEAK	K-FACTOR	CEL/CREF	ATOM%	EL WT%	WT%	FORMULA
SI-K	9525	1.000	1.000	24.53	31.55	±7.62	SIO2
AL-K	891	1.098	0.103	2.62	3.24	±.13	AL2O3
K-K	796	1.107	0.093	1.63	2.92	3.52	K2O
CA-K	348	1.024	0.038	0.64	1.18	1.66	CAO
MN-K	696	1.114	0.081	1.02	2.57	4.07	MNO2
MG-K	141	1.385	0.021	0.59	0.65	1.08	MGO
FE-K	2495	1.109	0.291	3.57	9.18	13.11	FE2O3
NA-K	218	2.887	0.066	1.96	2.09	2.82	NA2O
O			1.477	63.42	46.61		

Fig. 34. Typical EDS Spectrum (AEM) and Corresponding SQMTF Analysis Result from Unreacted 202U Glass Matrix

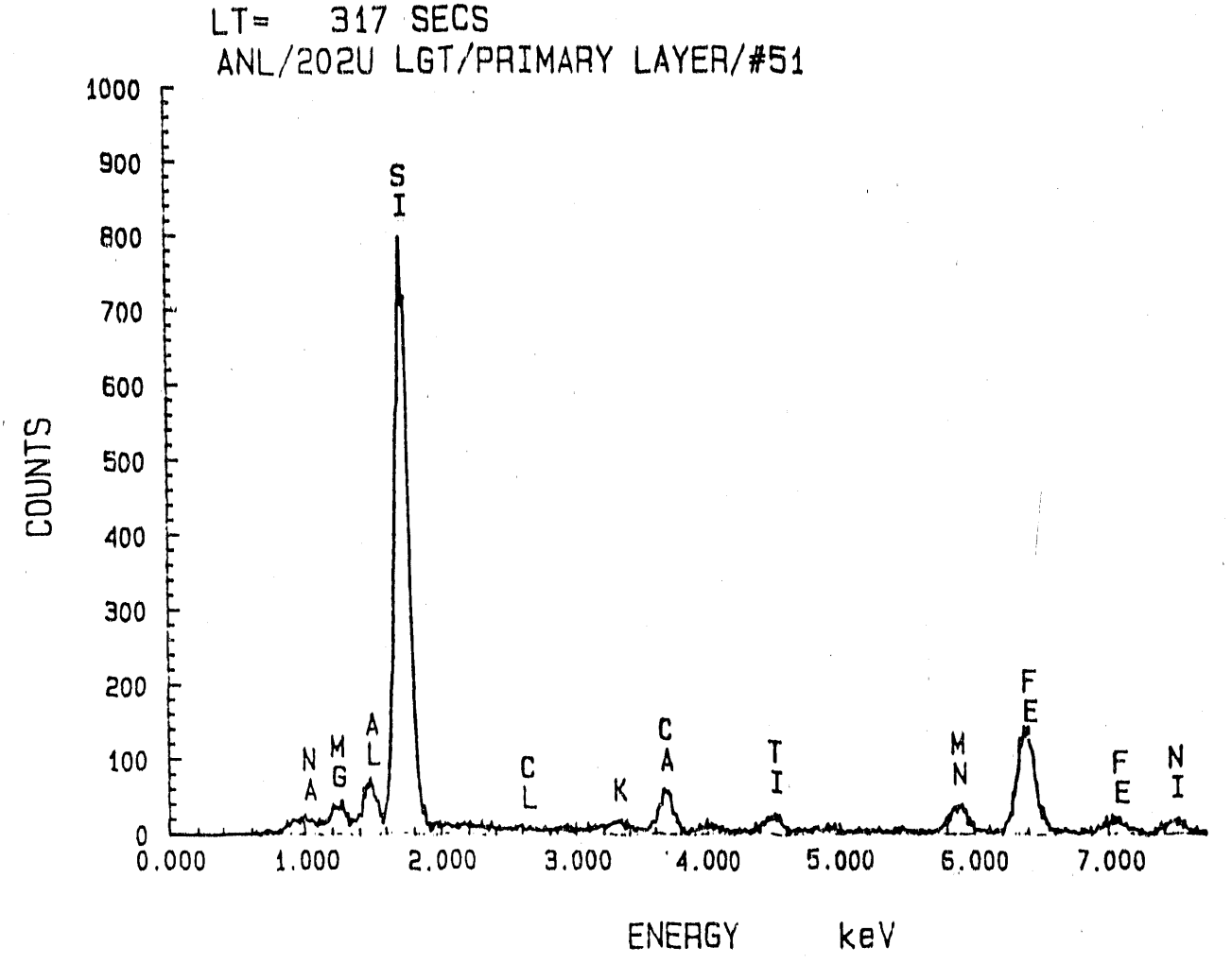

ANL/202U LGT/PRIMARY LAYER/#51

EL-LINE	PEAK	K-FACTOR	CEL/CREF	ATOM%	EL WT%	WT%	FORMULA
SI-K	9963	1.000	1.000	25.14	32.41	69.46	SIO2
AL-K	716	1.095	0.088	2.29	2.84	5.37	AL2O3
K-K	162	1.107	0.020	0.36	0.65	0.79	K2O
CA-K	823	1.024	0.094	1.66	3.05	4.27	CAO
MN-K	621	1.114	0.077	0.99	2.50	3.96	MNO2
MG-K	200	1.385	0.031	0.91	1.00	1.67	MGO
FE-K	2347	1.109	0.291	3.65	9.42	13.45	FE2O3
NA-K	72	2.887	0.023	0.72	0.76	1.02	NA2O
O			1.461	64.28	47.35		

Fig. 35. Typical EDS Spectrum (AEM) and Corresponding SQMTF Analysis Result from the Primary Alteration Layer--Smectite

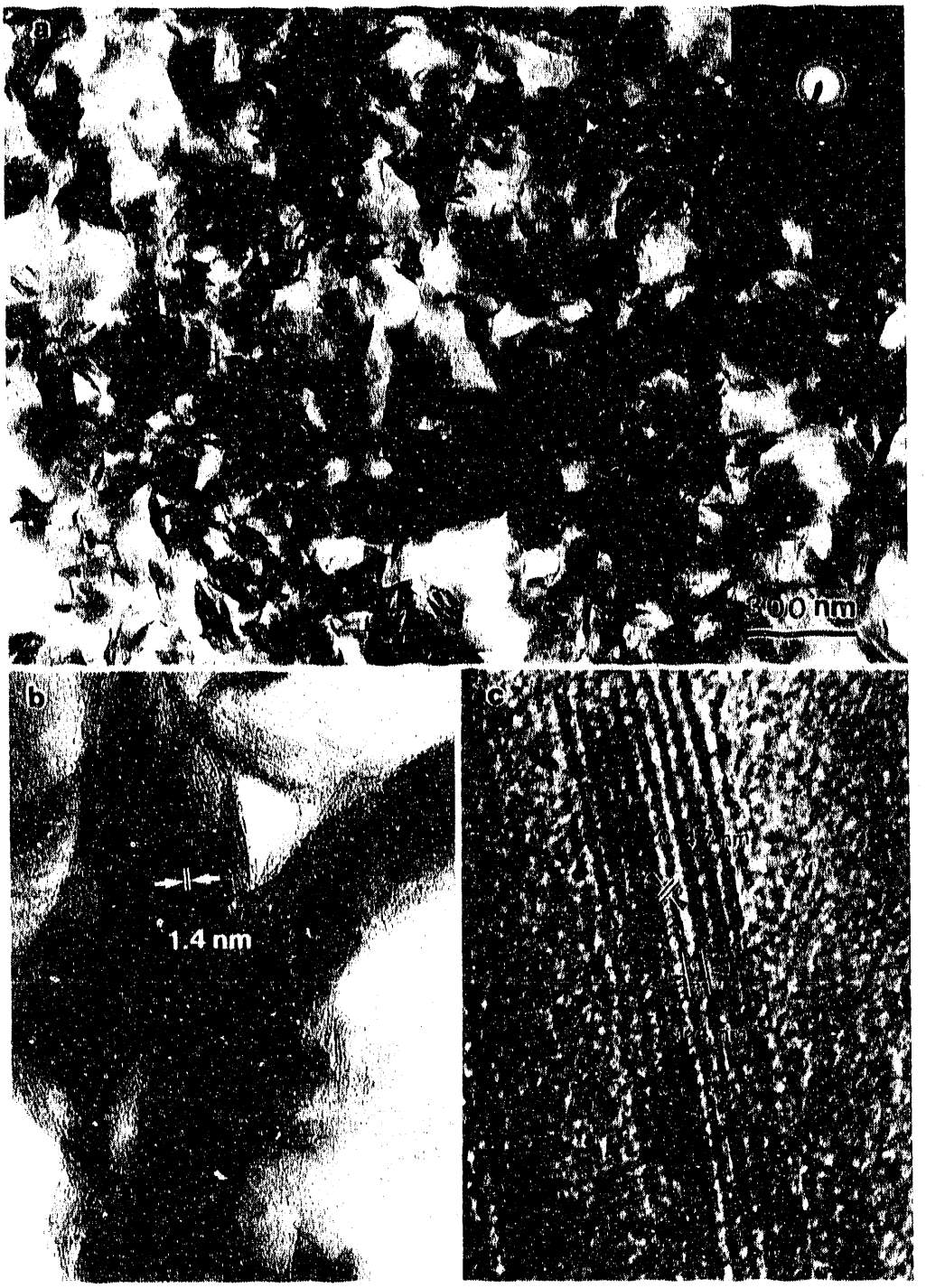

Fig. 36. Low Magnification TEM Micrograph with (a) SAD Pattern and (b and c) HREM Images from the Smectite Layer

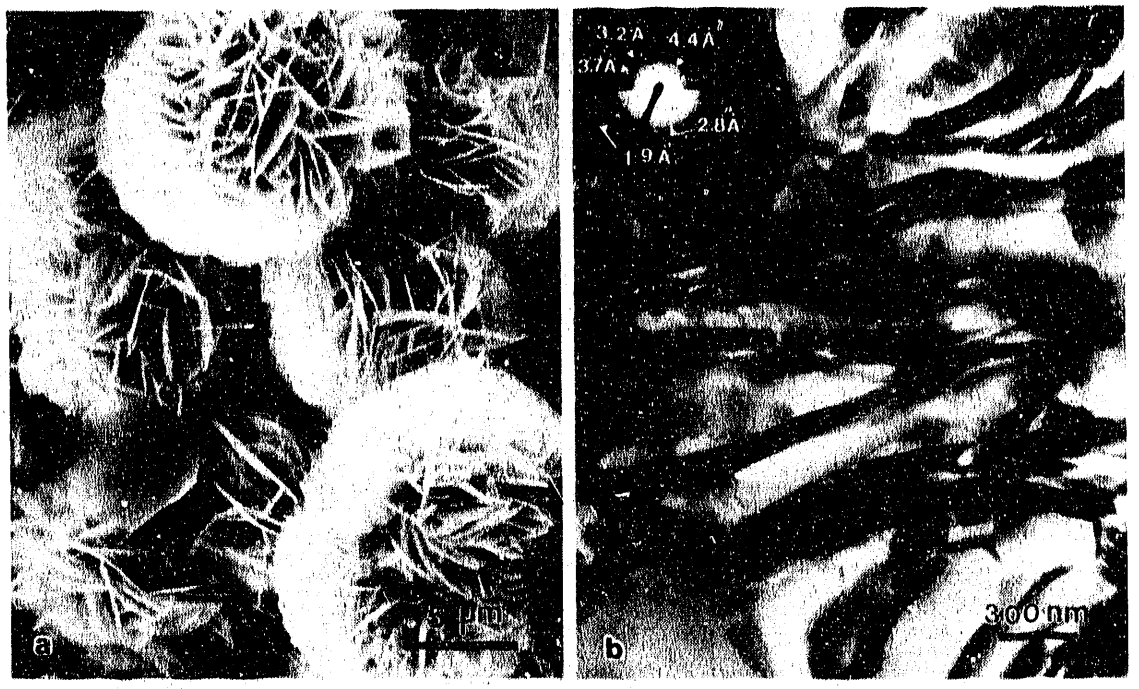

Fig. 37. Comparison of (a) SEM and (b) TEM Images from the Calcium Silicate Rosettes. A SAD pattern showing the major d spacings of the phase is included in (b).

Table 24. Major d Spacings (Å) of Selected Smectite Phases

Observed Smectite	Nontronite[a] (Glycolated)	Nontronite (Untreated)	Ferroan-Saponite[b]
14	15.4	13.5	15.4
-	-	-	7.9
4.7	4.51	4.51	4.6
3.2	3.29	3.49	3.13
2.7	2.59	-	2.648
1.6	1.69	1.79	1.541

[a]Nontronite: $Fe_2(Al_{0.33}Si_{3.67})O_{10}(OH)_2Na_{0.33}$.

[b]Ferroan-saponite: $Ca_{0.5}Na_{0.1}(Mg_{1.9}Fe_{0.5}^{2+}Fe_{0.4}^{3+}Al_{0.04})(Al_{0.8}Si_{3.2})O_{10}(OH)$.

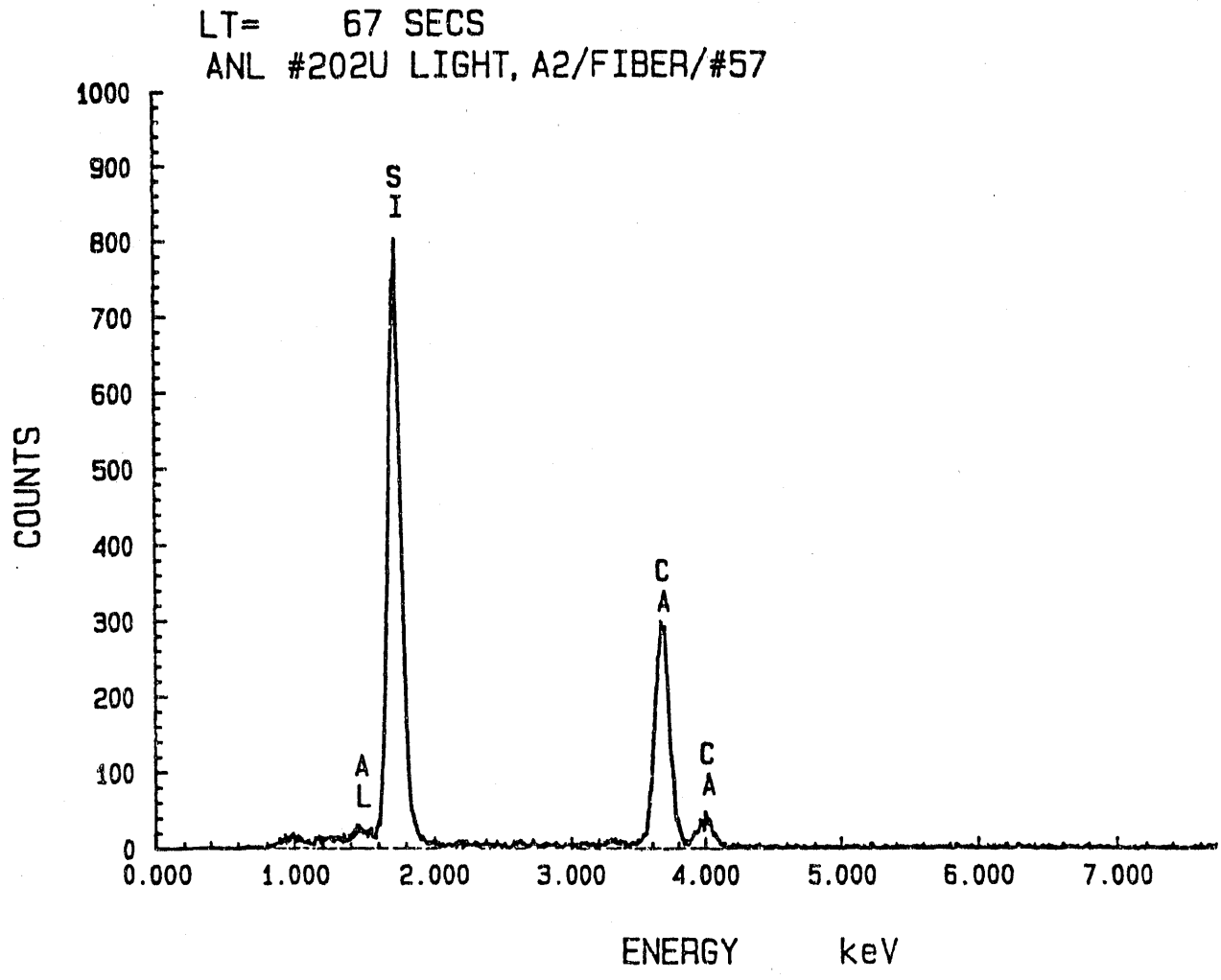

ANL #202U LIGHT,A2/FIBER/#57

EL-LINE	PEAK	K-FACTOR	CEL/CREF	ATOM%	EL WT%	OXI%	FORMULA
SI-K	9031	1.000	1.000	24.54	34.51	73.95	SiO2
CA-K	4526	1.034	0.514	9.54	17.73	24.82	CaO
AL-K	154	1.098	0.019	0.32	0.65	1.23	Al2O3
O			1.365	65.49	47.11		

Fig. 38. Typical EDS Spectrum (AEM) and Corresponding SQMTF Analysis Result from the Calcium Silicate Rosette Shown in Fig. 37b

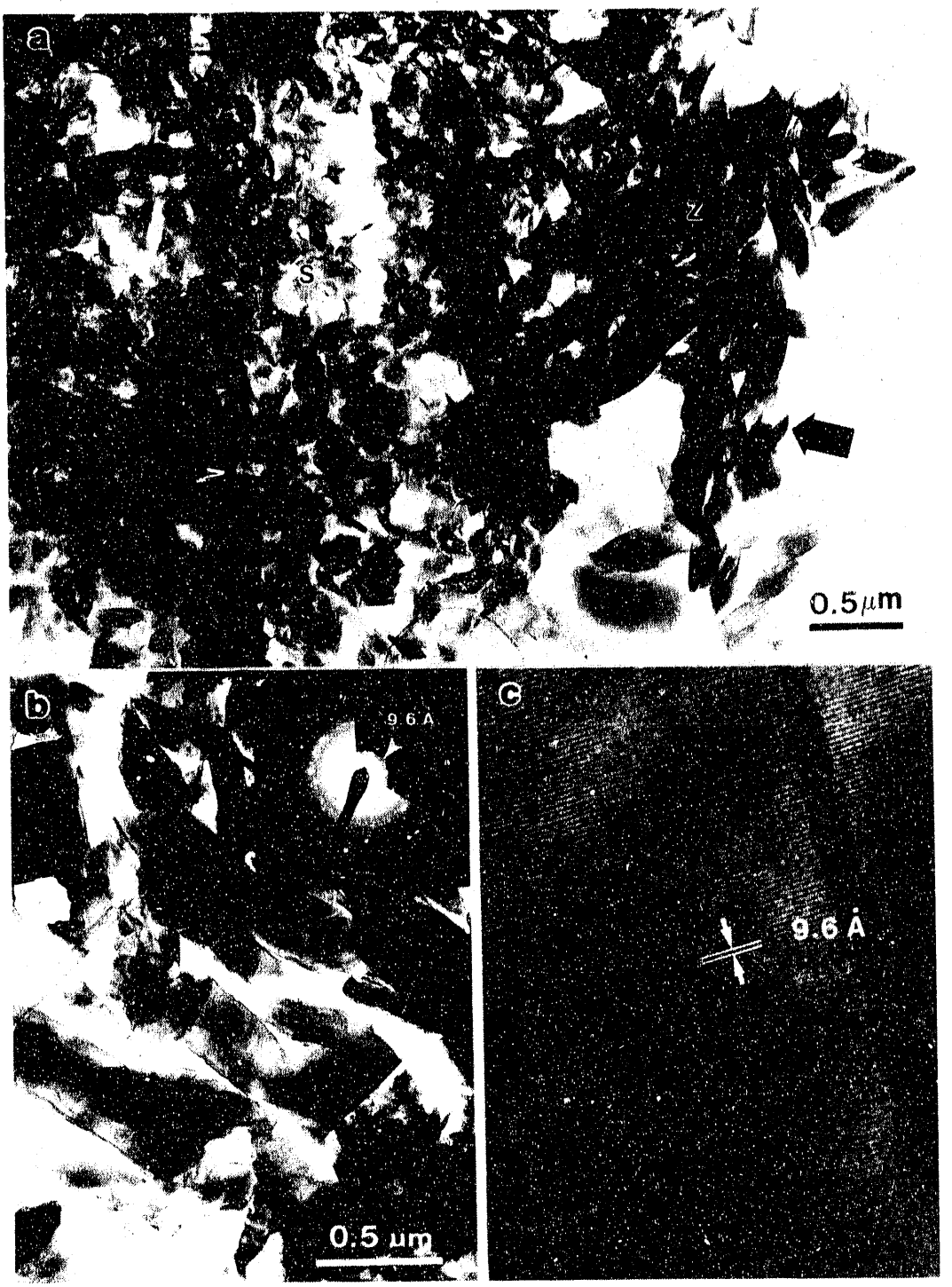

Fig. 39. Low Magnification TEM Micrographs with (a and b) SAD Pattern and (c) HREM Image from the Zeolite Crystal

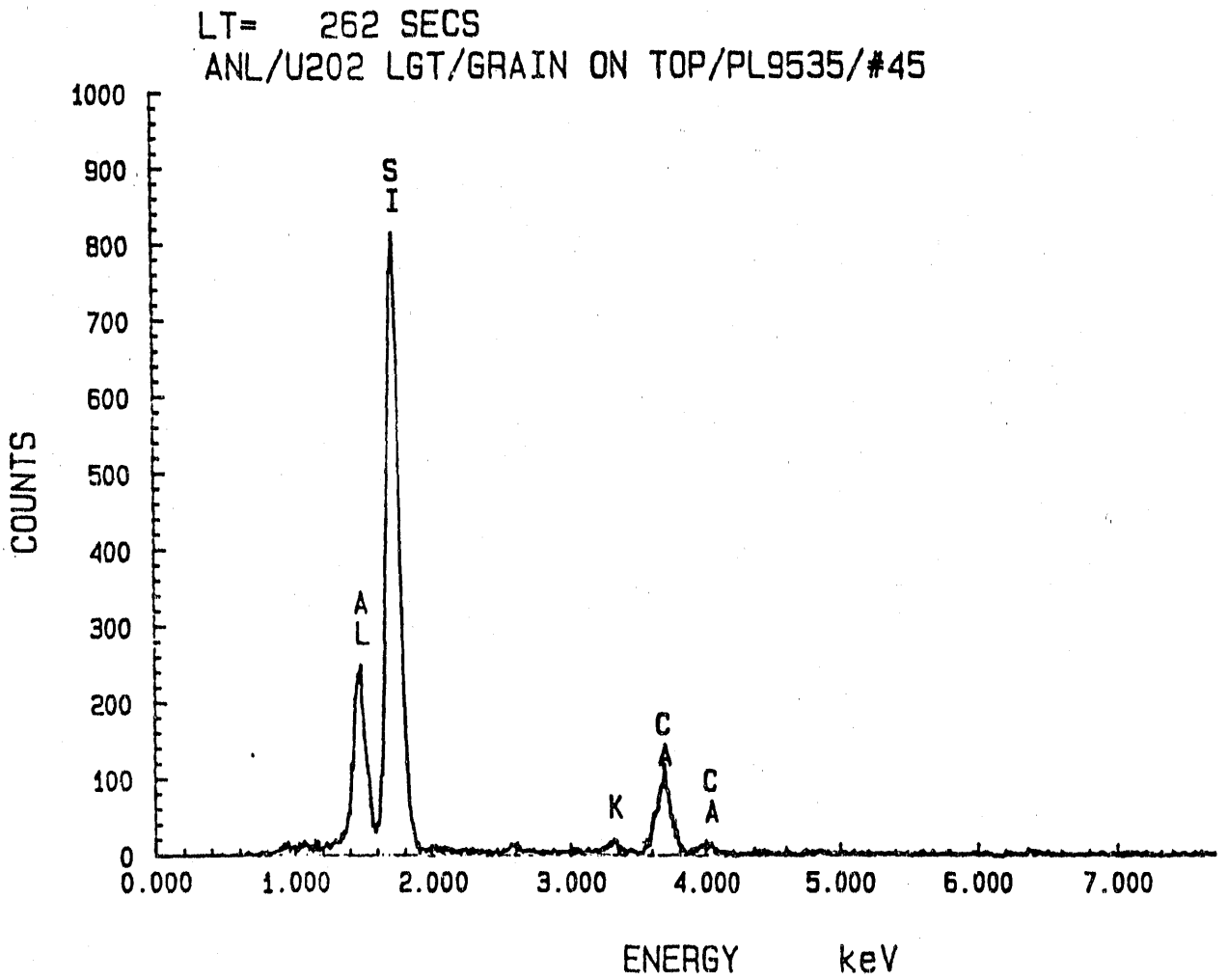

ANL/U332 LGT/GRAIN ON TOP/PL9535/#45

EL-LINE	PEAK	K-FACTOR	CEL/CREF	ATOM%	EL WT%	WT%	FORMULA
SI-K	9518	1.000	1.000	24.93	33.94	72.77	SIO2
AL-K	2614	1.098	0.302	7.80	10.25	19.36	AL2O3
CA-K	1408	1.024	0.152	2.65	5.15	7.21	CAO
K-K	137	1.107	0.016	0.29	0.54	0.65	K2O
O			1.475	64.34	50.10		

Fig. 40. Typical EDS Spectrum (AEM) and Corresponding SQMTF Analysis Result from the Zeolite Phase shown in Fig. 39

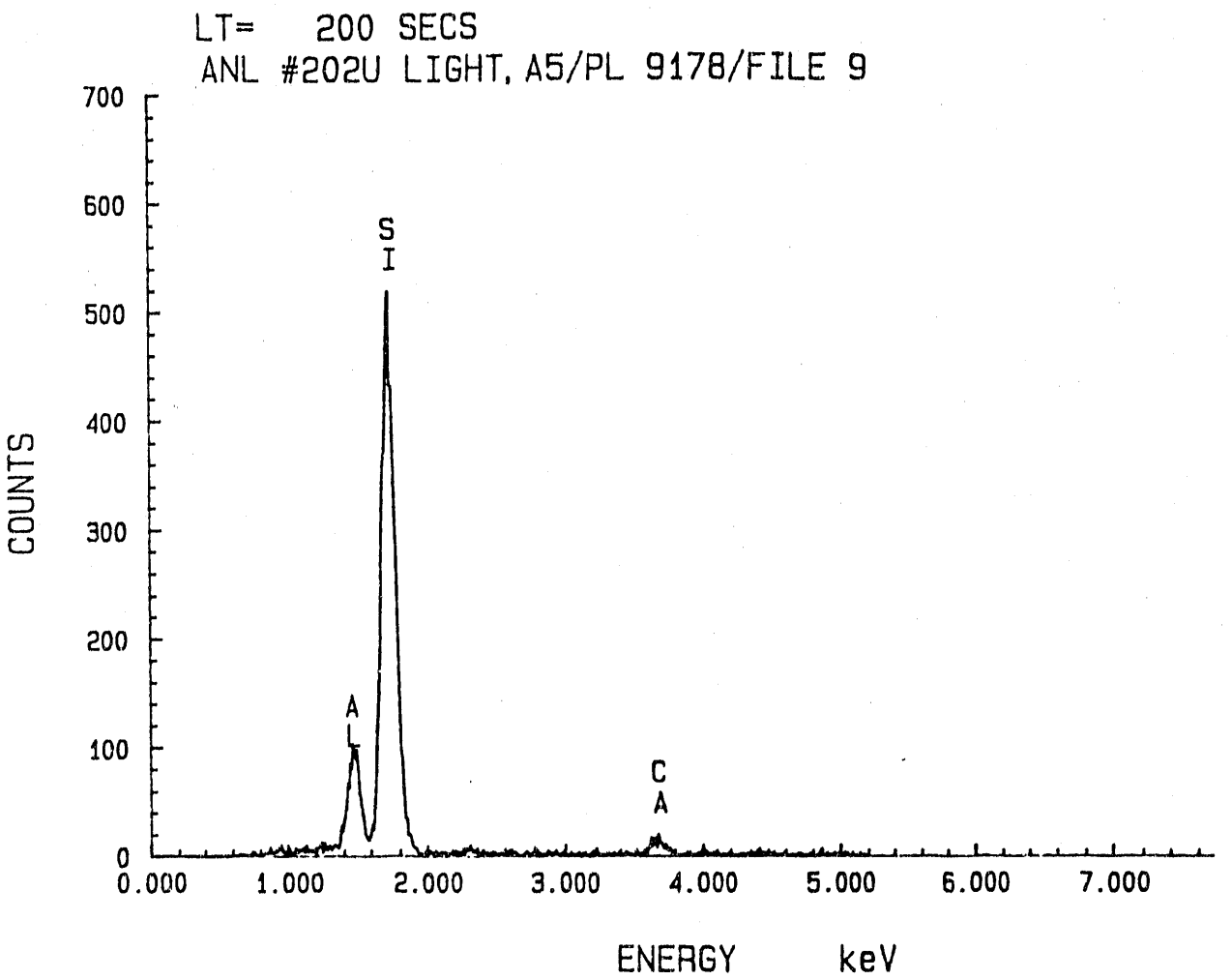

ANL #202U LIGHT,A5/PL 9178/FF

EL-LINE	PEAK	K-FACTOR	CEL/CREF	ATOM%	EL WT%	WT%	FORMULA
SI-K	5887	1.000	1.000	39.15	39.98	85.42	SIO2
AL-K	1045	1.095	0.191	5.77	7.72	14.58	AL2O3
CA-K	20:	1.024	0.006	0.71	1.42	1.98	CAO
O			1.334	68.47	51.98		

Fig. 41. EDS Spectrum (AEM) and Corresponding SQMTF Analysis Result from a Zeolite Crystal Containing Much Less Calcium than in the Crystals Shown in Figs. 39 and 40

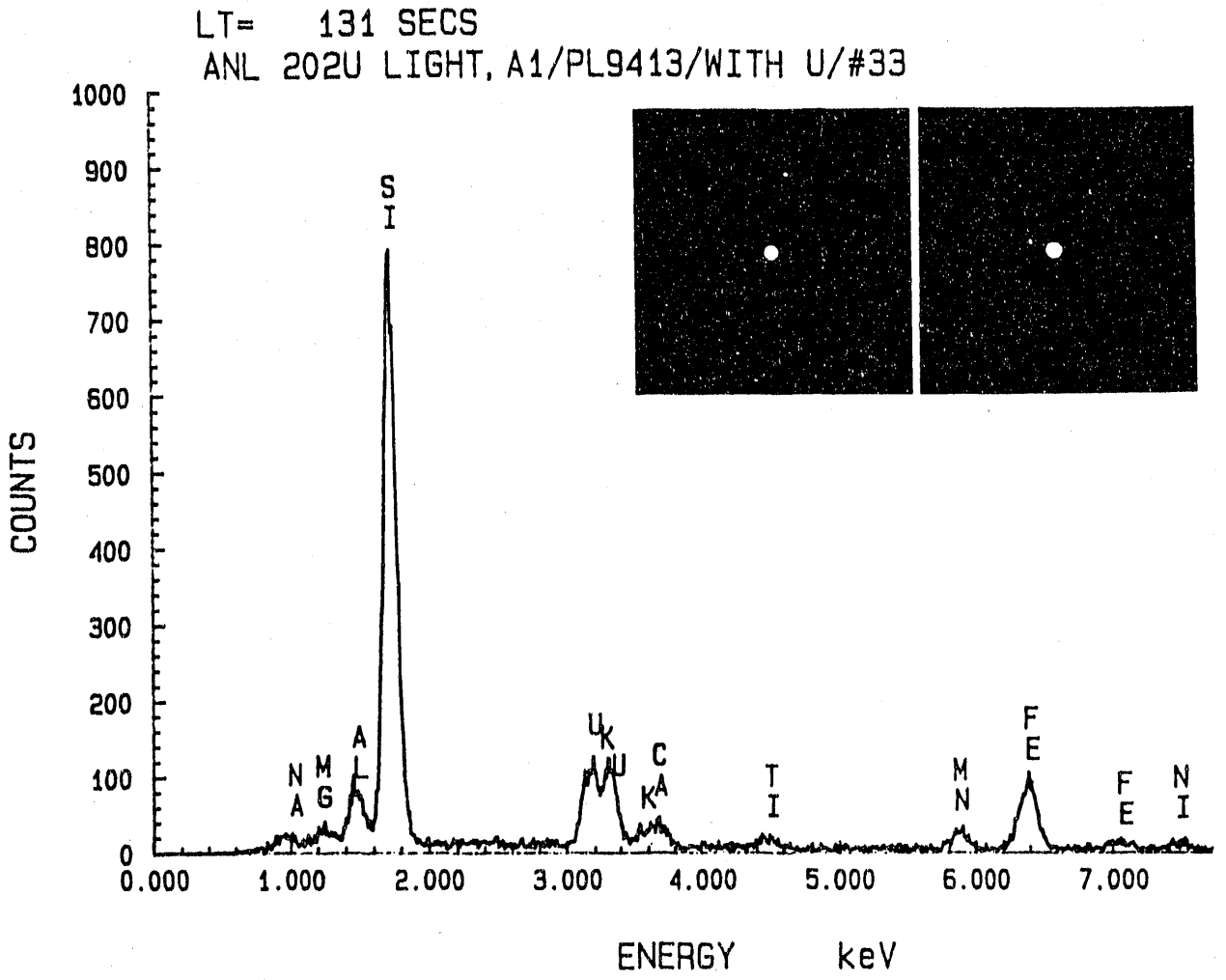

ANL 202U LIGHT,A1/PL9413/WITH U/#33

EL-LINE	PEAK	K-FACTOR	CEL/CREF	ATOM%	EL WT%	WT%	FORMULA
SI-K	9367	1.000	1.000	19.82	16.10	34.49	SIO2
AL-K	990	1.098	0.116	2.09	1.87	3.53	AL2O3
CA-K	527	1.024	0.059	0.80	0.93	1.30	CAO
K-K	615	1.107	0.073	1.06	1.17	1.41	K2O
U-M	2688	9.913	2.787	6.50	44.86	53.91	UO3
FE-K	1531	1.109	0.181	1.86	2.92	4.17	FE2O3
MN-K	399	1.114	0.048	0.48	0.77	1.21	MNO2
MG-K	245	1.385	0.036	0.84	0.58	0.97	MGO
O			1.913	66.35	30.80		

Fig. 42. EDS Spectrum (AEM) and Corresponding SQMTF Analysis Result and Two SAD Patterns from the Uranium Silicate Phase

In addition to the above-mentioned phases seen in both SEM and AEM studies, several crystals whose EDS spectra only contained Ca peaks were observed in the AEM study. Figure 43 gives an EDS spectrum and a SAD pattern of this phase. The electron diffraction pattern could not be matched with that of CaO, so this phase seems to be some sort of calcium hydrate.

2. Results from B-82

Although sample B-82 was reacted in the same conditions as IVE202U-14-2 for even longer time, the primary alteration layer observed on the glass surface was somehow thinner than that on IVE202U-14-1-2. Also, few secondary phases were seen on top of the layer. Figure 44 is a TEM micrograph taken from one of the best sections found. The electron diffraction and EDS data indicate that the primary layer is still smectite. One unique feature of the smectite primary layer on B-82 is that it consists of two sublayers, which are separated by a very obvious interface. This suggests that a fluctuation in the reaction rate may have occurred during the course of leaching experiment. This could have resulted from a fluctuation of temperature on the sample surface. Detailed EDS study of the two sublayers across the interface did not reveal any significant change in the layer composition. However, small uranium-rich particles (~30 nm in dimension) were found on the interface between the two sublayers of smectite. This is shown in Figs. 45 and 46. During the AEM study, reducing the size of the electron beam spot from ~30 nm to ~10 nm on these particles resulted in higher U and Ti peaks and lower Si and other peaks. This result indicates that the Si and other peaks are from the surrounding smectite, and the particles are U-Ti-O phase. Formation of such a phase on a similar glass was reported earlier [ABRAJANO-2].

Finally, a silica particle of ~300 nm in dimension was found on the top surface of the smectite layer. A low-magnification TEM brightfield image, a SAD pattern, and an HREM image of this particle are shown in Fig. 47. An EDS spectrum with corresponding quantitative analysis data is presented in Fig. 48. The measured lattice spacing matches very well with tridymite (d_{100} = 0.988 nm), one of the important SiO_2 polymorphs, which can contain appreciable aluminum and usually is only stable at higher temperatures [DEER]. However, in many cases, high-temperature polymorphs may be formed at low temperatures during silica glass crystallization because the transformation involves smaller reduction in free energy and thus is kinetically favorable [PUTNIS].

D. Summary

Both IVE202U-14-1-2 and B-82 sample surfaces are covered by a honeycomb-like smectite alteration layer after reaction in unsaturated water vapor at 200°C. Structurally and chemically simpler secondary phases, i.e., zeolite, calcium silicate, uranium silicate, and calcium hydrate crystals, formed on top of the smectite layer of IVE202U-14-1-2. However, their density and distribution are not uniform on the sample surface. The smectite layer on the surface of B-82 consists of two sublayers, which are separated by a very obvious interface. On the interface, small U-Ti-O particles are found. Also, a high-temperature silica polymorph, tridymite, has precipitated on top of the smectite layer.

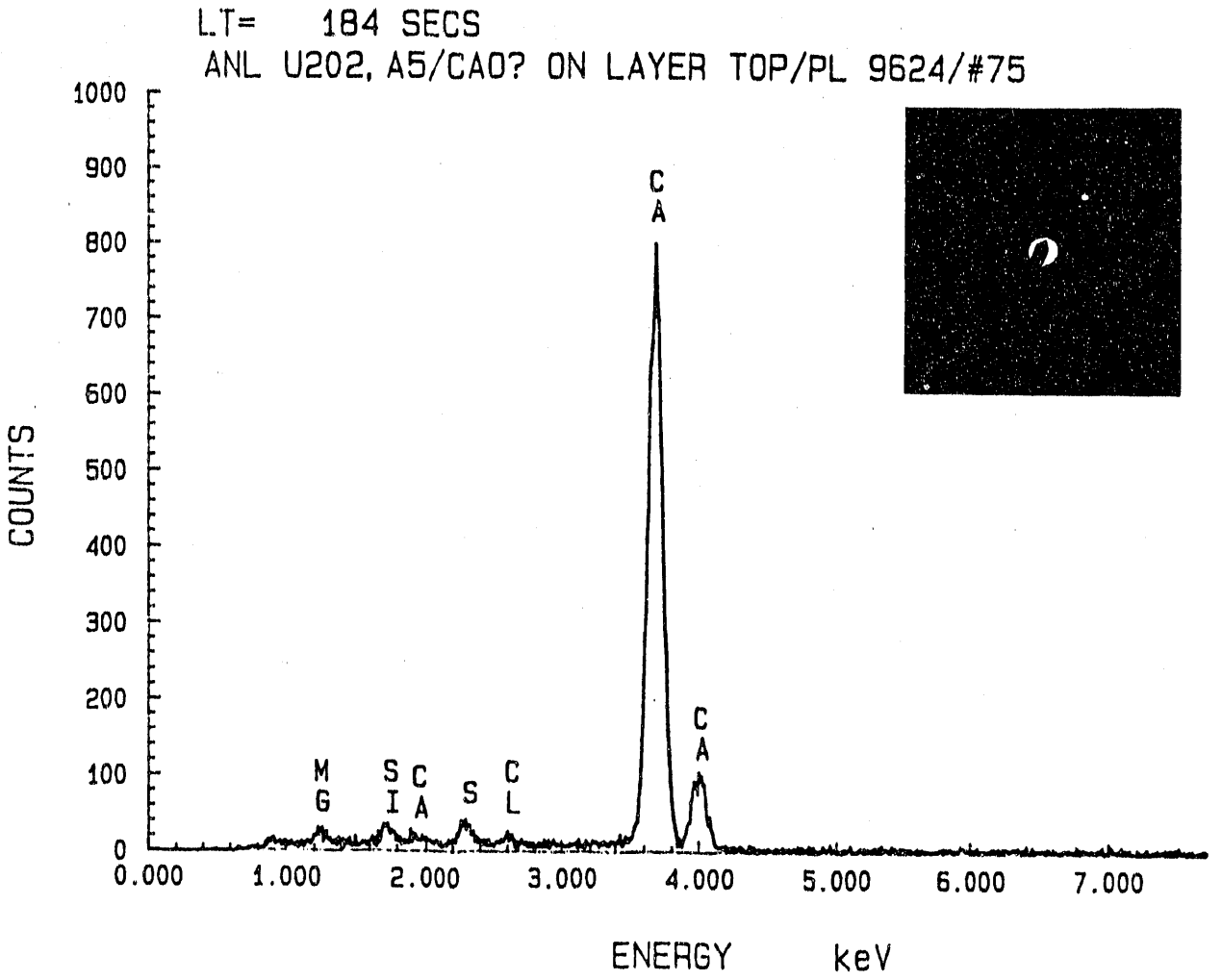

Fig. 43. EDS Spectrum (AEM) and SAD Pattern from a Calcium Hydrate Crystal

Fig. 44. TEM Micrographs Showing Entire Reacted Range (from Top Surface to Glass Matrix) of B-82 Sample. The secondary phases shown on the bright part of the IVE202U-14-1-2 sample surface are not observed in this sample.

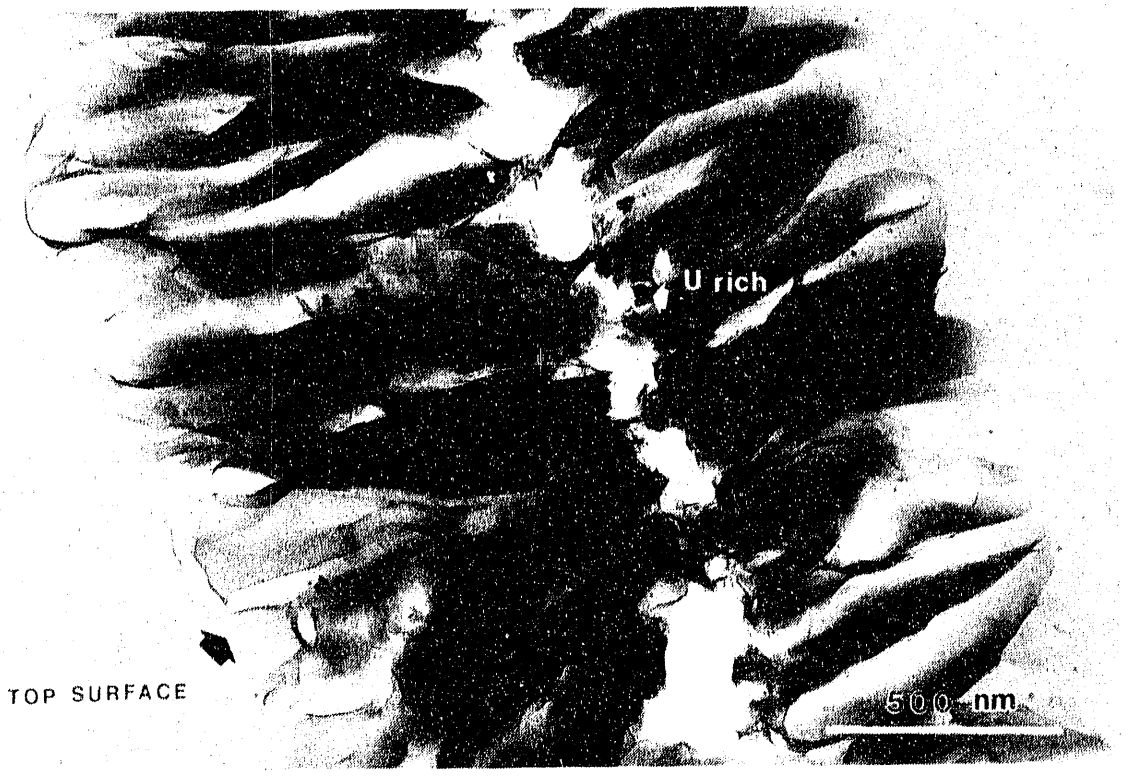

Fig. 45. TEM Micrograph of the Alteration Layer on the Surface of B-82 Sample. Note: There are two layers of smectite; small uranium-rich particles are observed at the layer interface.

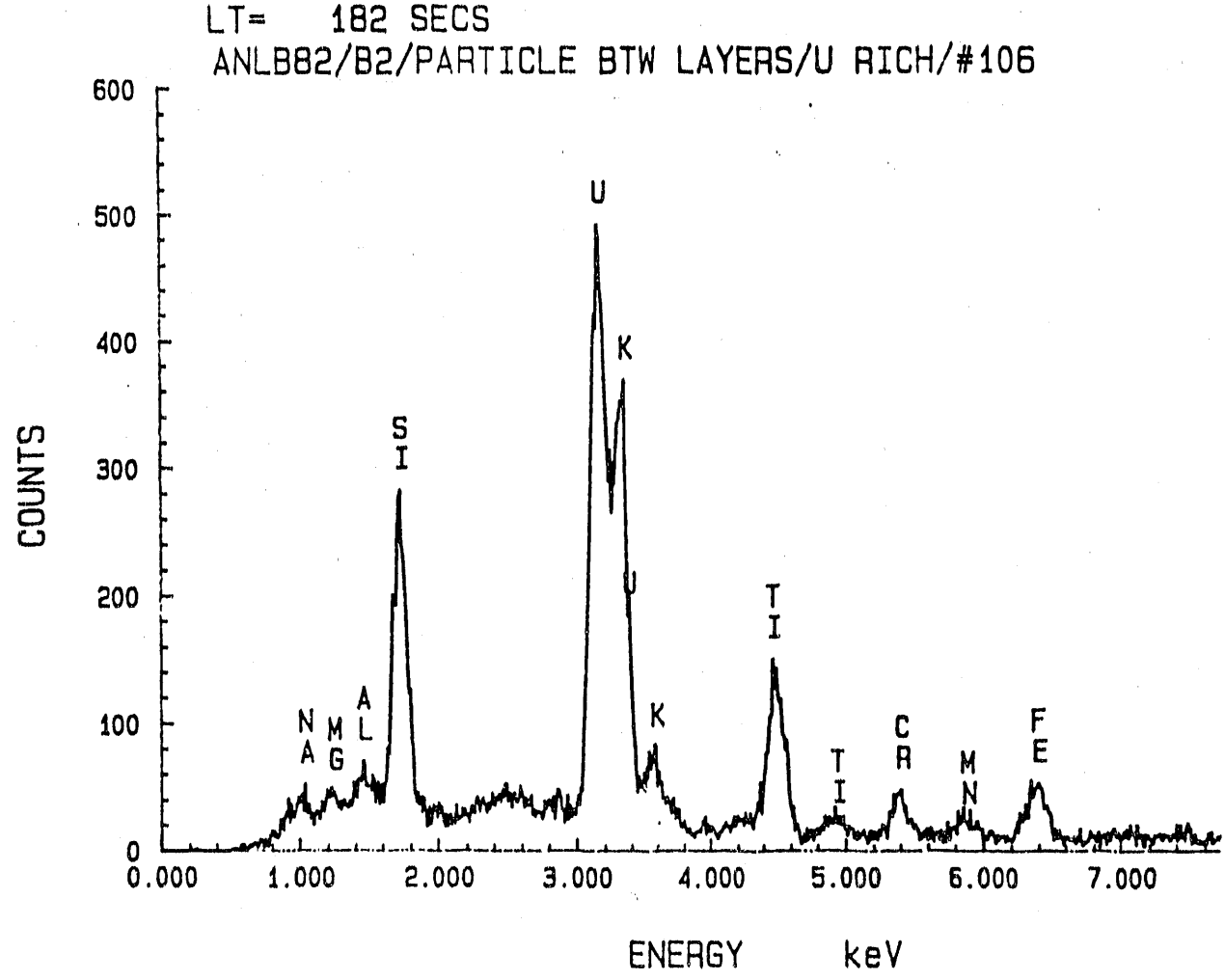

ANLB82/B2/PARTICLE BTW LAYERS/U RICH/#104

EL-LINE	PEAK	K-FACTOR	CEL/CREF	ATOM%	EL WT%	WT%	FORMULA
SI-K	2887	1.000	1.000	4.27	1.89	4.06	SIO2
AL-K	302	1.098	0.115	0.51	0.22	0.41	AL203
K-K	965	1.107	0.370	1.14	0.70	0.85	K20
U-M	11782	9.913	40.446	20.33	76.64	90.37	U3O8
FE-K	773	1.109	0.297	0.63	0.56	0.80	FE203
MN-K	250	1.114	0.097	0.21	0.18	0.29	MNO2
CR-K	502	1.169	0.204	0.47	0.39	0.56	CR203
TI-K	2053	1.179	0.839	2.09	1.59	2.65	TIO2
O			9.409	70.35	17.83		

Fig. 46. EDS Spectrum (AEM) with Corresponding SQMTF Analysis Result from the Uranium-Rich Particles at the Interface of Two Smectite Layers on the Surface of B-82 Sample, as shown in Fig. 45

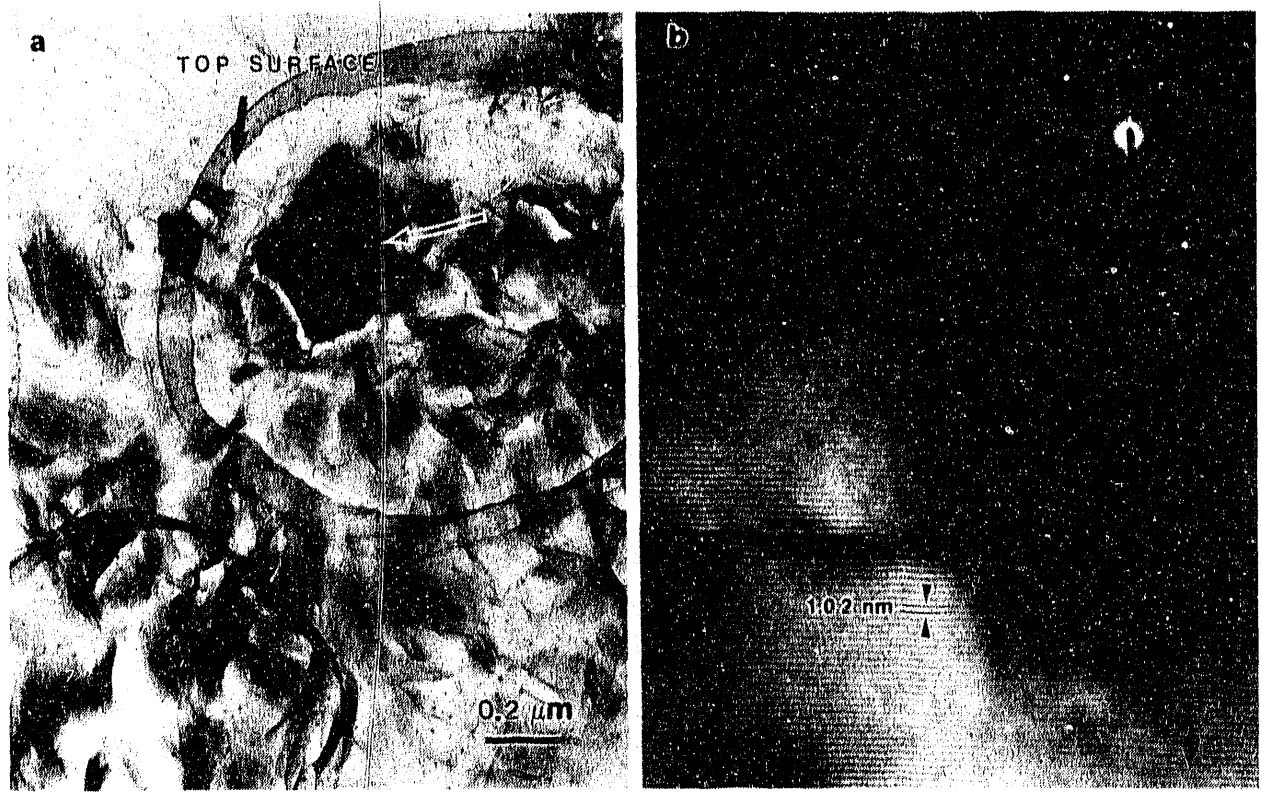

Fig. 47. TEM Brightfield (left) and HREM Micrographs (right) of a Tridymite Crystal on Top of the Smectite Layer Observed on Sample B-82

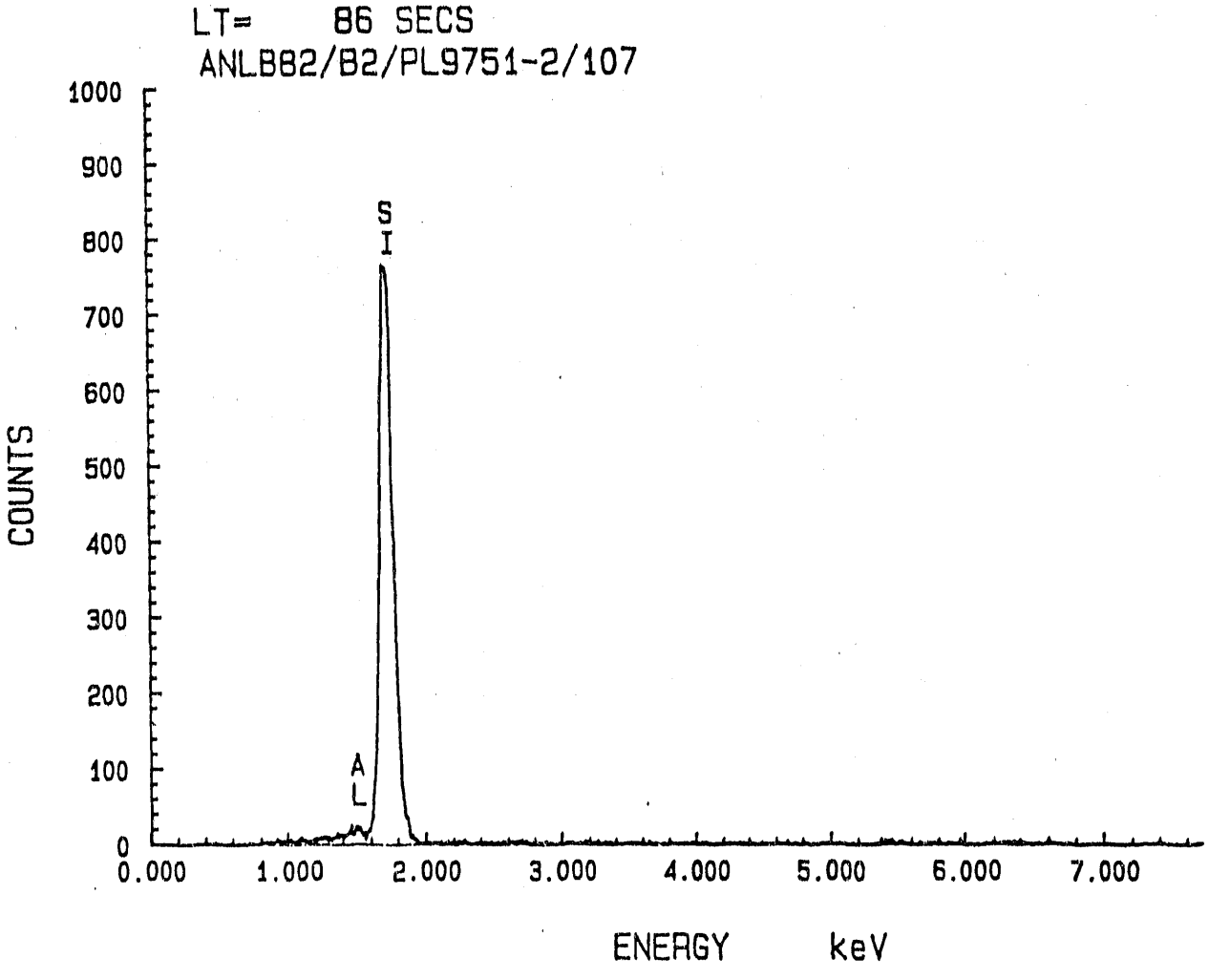

ANLB82/B2/PL9751-2/#107

EL-LINE	PEAK	k-FACTOR	CEL/CREF	ATOM%	EL WT%	WT%	FORMULA
SI-K	9395	1.000	1.000	32.92	46.68	98.75	SIO2
AL-K	122	1.098	0.014	0.49	0.66	1.25	AL2O3
O			1.156	66.58	53.25		

Fig. 48. EDS Spectrum (AEM) with Corresponding SQMTF Analysis Result from the Tridymite Crystal Shown in Fig. 47

X. WATER DIFFUSION OF NUCLEAR WASTE GLASSES

A. Introduction and Background

Glassification is one of the most promising methods for isolating high-level nuclear waste from the human environment. For this purpose, glasses with extremely good chemical durability are desired. In the past, most of the evaluation methods of the candidate waste glass compositions used the immersion of the samples in aqueous solution and the measurement of leached components. In recent years, it was realized that water diffusion from the vapor phase into glasses can have significant influence on the chemical durability of the glasses, for example, by accelerating dissolution of the glass into aqueous solution. Yet very few water diffusion data are available. Thus, it was decided to obtain water diffusion data for representative simulated nuclear waste glasses.

B. Objective

The objective of the present research is to obtain water diffusion coefficients for simulated nuclear waste glasses and evaluate the effect of water diffusion into the glasses on chemical durability.

C. Technical Approach

Three simulated nuclear waste glasses were chosen for the study: SRL 131U, SRL 165U, and SRL 202U. The main experimental tools for the water diffusion study are infrared spectroscopy and resonance nuclear reaction analysis. The former gives water uptake by glass specimens as well as water speciation (hydroxyl and molecular water), while the latter can determine the hydrogen profile near the surface layer of the glass specimens. By combining these two techniques and employing some simplifying assumptions, such as a concentration-independent diffusion coefficient, it is possible to determine the effective water diffusion coefficient into glasses. For example, the effective diffusion coefficient, D_e, can be obtained by

$$D_e = (\pi/t)\,(M/2C_i)^2 \qquad (2)$$

where t is the treatment time, M is the water uptake, and C_i is the water concentration in the surface layer of the glass. In this effort, C_i will be determined by nuclear resonance reaction analysis, and M will be determined by infrared spectroscopy. According to Beer's law, the infrared absorbance, A, is related to the water concentration, C, by

$$A = \log (T_0/T) = \varepsilon C d \qquad (3)$$

where T_0 is the base line transmission, T is the transmission at the absorption maximum due to water, ε is the extinction coefficient, and d is the specimen thickness. When water enters from the surface, water uptake, M, is related to the absorbance increase, ΔA, by

$$\Delta A = \varepsilon M \qquad (4)$$

Three glasses were cut into an approximate size of 10 mm x 10 mm x 1 mm, and the two large faces were then polished by using 600 grit SiC paper to the thickness of 350 μm-400 μm. This was followed by polishing with diamond pastes and CeO_2 paste. The polished surfaces were lightly etched by HF solution to remove the damaged surface layer.

Two experimental conditions were employed. The first method involved the exposure of the glass to high water vapor using a hydrothermal unit. This method resulted in a high water uptake and usually, because of the concentration dependence of the diffusion coefficient, resulted in a high diffusion coefficient. Consequently, it was possible to conduct measurements at comparatively low temperatures such as 150 and 250°C.

In addition to the diffusion measurement, optical microscope observation of the surface of the glass exposed to water vapor was made. Especially when the glass is exposed to high water vapor, various structural changes, such as crystallization, swelling, or flaking off can take place. These structural changes, in addition to property changes due to increased water content by diffusion, are expected to have a profound effect on subsequent chemical durability.

The second method involved the exposure of the glass specimens to a low water vapor pressure generated by 80°C water. In this method, water uptake was slow, and to be able to detect a sufficient water uptake by infrared spectroscopy in a reasonable time, the measurement had to be done at high temperatures, such as 500°C. The diffusion coefficient obtained at high temperatures will be extrapolated to low temperatures. The latter measurement is expected to provide a water diffusion coefficient undisturbed by surface layer cracking and give baseline data.

D. Results and Discussion

1. Diffusion Study at Low-Temperature and High Water Vapor Pressure

Infrared spectra of three glass samples with thickness of 350-400 μm are shown in Fig. 49. There are two infrared absorption peaks, one at 3500 cm^{-1} wave number due to free hydroxyl water, and the other at 2650 cm^{-1} wave number due to hydrogen-bonded hydroxyl. Corresponding nuclear resonance reaction analysis results are shown in Fig. 50.

Glasses were treated at 150 and 250°C in saturated water vapor as well as in liquid water using a digestion bomb. In Fig. 51, an example of the time variation of the infrared spectra is shown for SRL 165U exposed to the saturated water vapor at 150°C. The corresponding absorbance increase is shown in Fig. 52. It is clear that, predominantly, the free hydroxyl water increases, while the hydrogen-bonded hydroxyl remains unchanged. Also, it has been observed that the water uptake is faster in the sample exposed to liquid water than the one exposed to water vapor. In both cases, the uptake increases proportionately to the square root of the exposed time, indicating a diffusion-controlled process. An example of nuclear resonance reaction analysis after exposure to water vapor is shown in Fig. 53. Consistent with infrared spectra, the sample exposed to liquid water shows a greater water uptake compared with the specimen exposed to water vapor under the same temperature and pressure conditions.

Samples treated in a digestion bomb showed extensive surface layer alterations, such as microcracking and flaking off. Naturally, the higher temperature, 250°C, produced more extensive surface alterations. Also, different responses to water vapor and liquid water were noticed. Many flakes had fallen off the surface of the sample treated in water vapor during the treatment, while the surface layer started to flake off the sample treated in liquid water only when the sample was exposed to air. Microscope observations revealed the layer structures typical of reacted glass (see previous sections). The effect of these layers on the water uptake data shown in Figs. 51, 52, and 53 must still be considered.

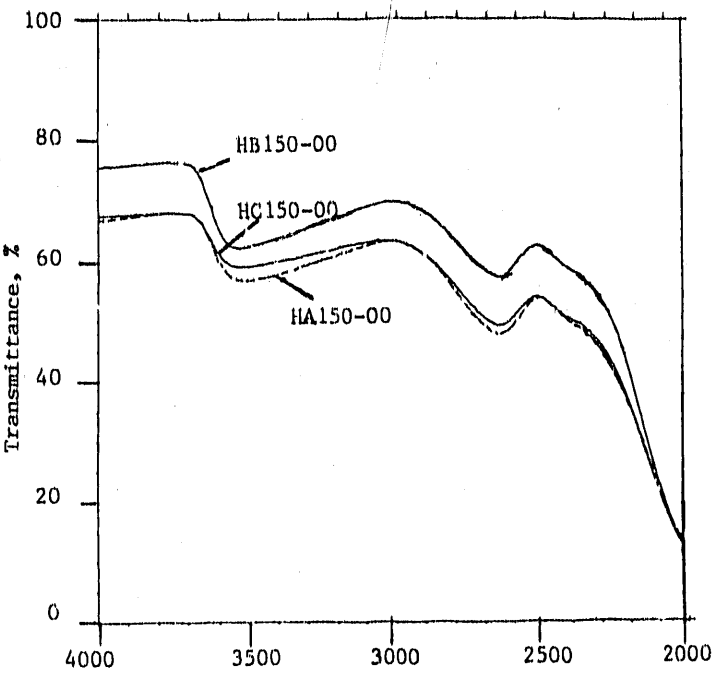

Fig. 49. IR Spectra of As-Received Simulated Nuclear Waste Glasses. Thickness of 350-400 μm. HA: SRL 131U, HB: SRL 165, and HC: SRL 202U.

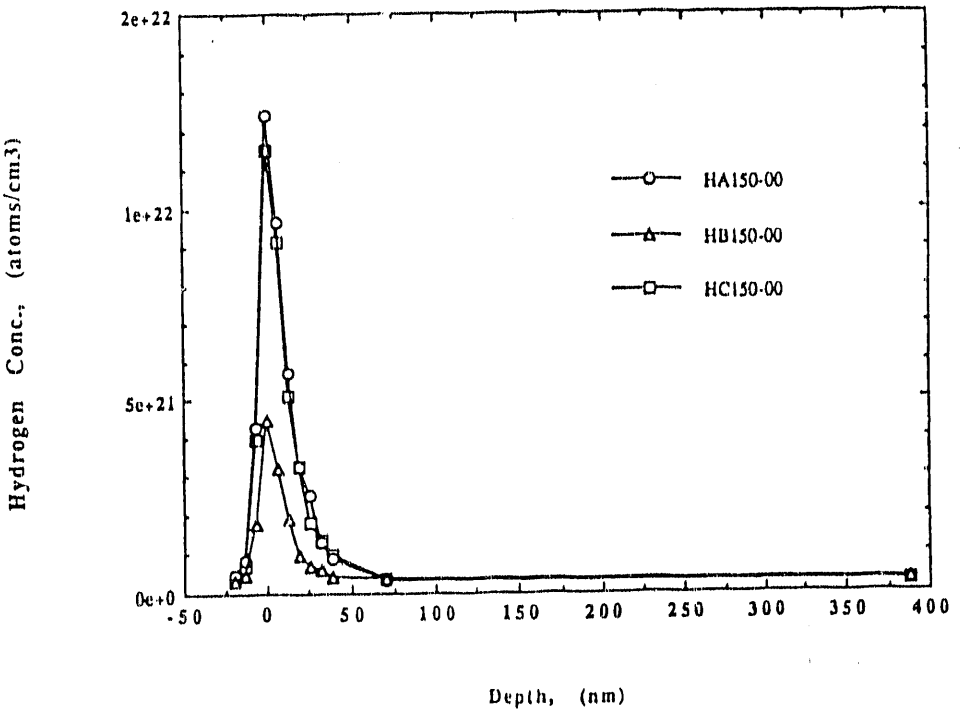

Fig. 50. Nuclear Resonance Analysis of As-Received SRL 131U, 165U, and 202U Glasses

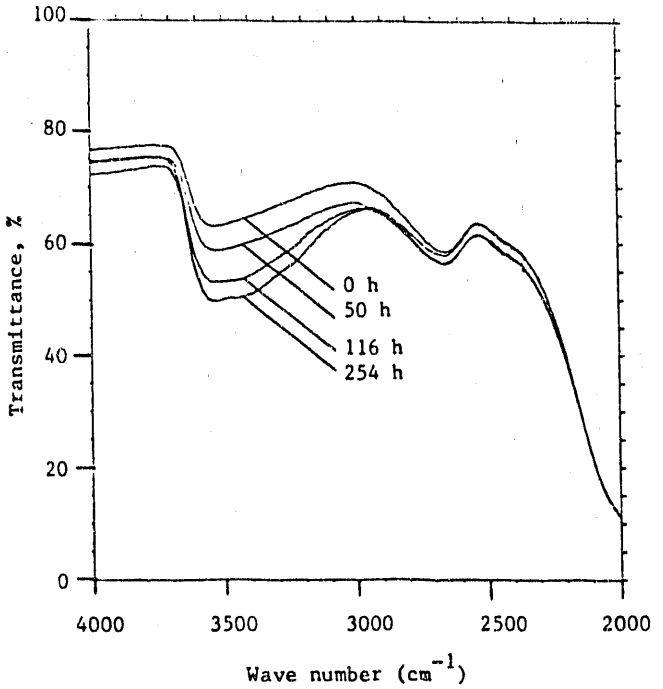

Fig. 51.
Selected IR Spectra for SRL 165U Glass after Hydrothermal Treatment in Water Vapor at 150°C for Various Lengths of Time

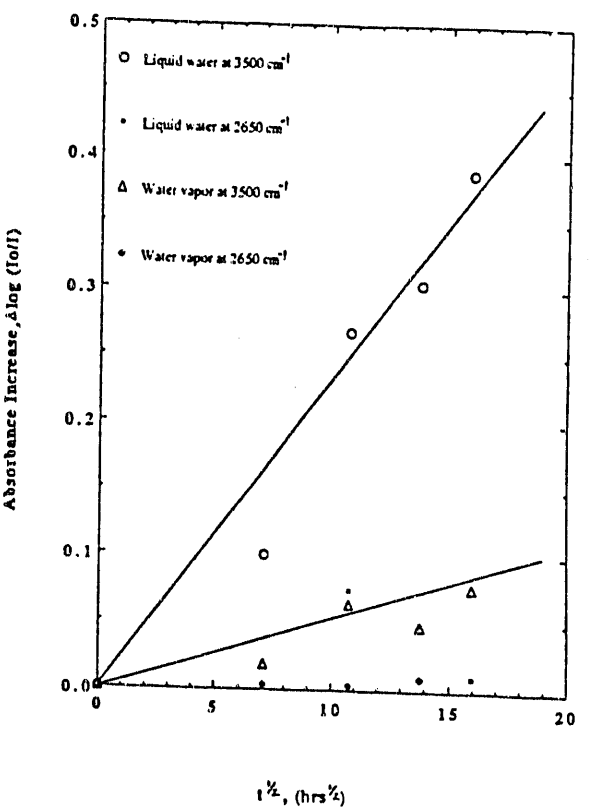

Fig. 52.
Absorbance Increase of SRL 165U Glass after Hydrothermal Treatment at 150°C as a Function of Time

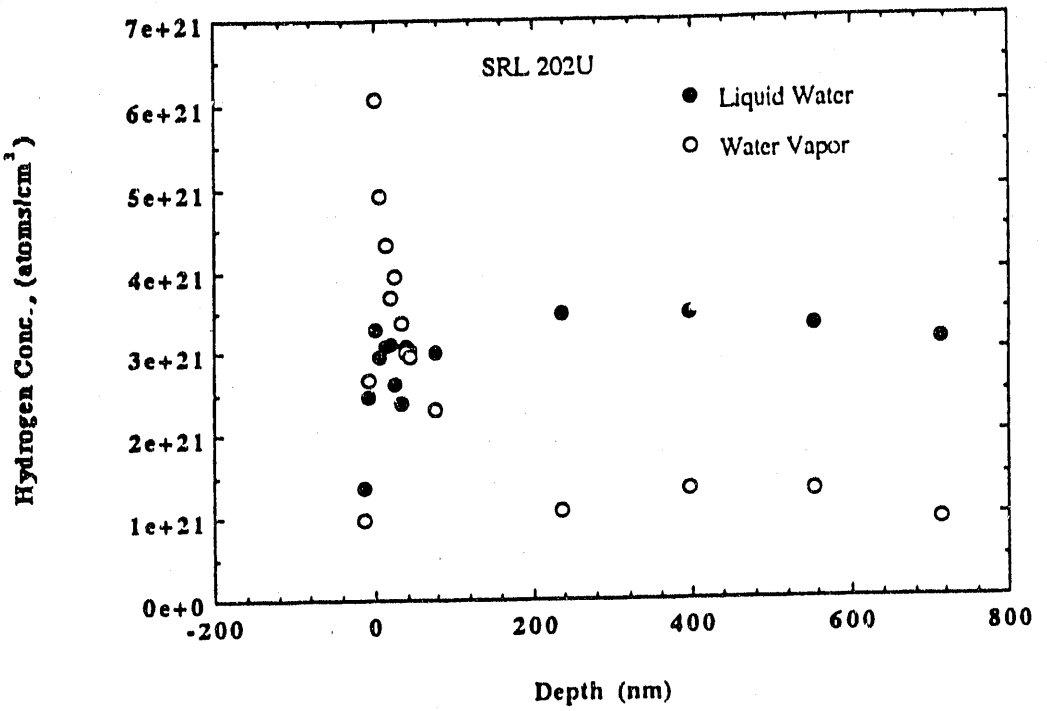

Fig. 53. Nuclear Resonance Analysis of SRL 202U Glass after Hydrothermal Treatment in Liquid Water and in Water Vapor at 250°C for 3.5 days

2. Diffusion Study at High-Temperature and Low Water Vapor Pressure

Figure 54 shows an example of water uptake of a glass specimen held at 500°C while being exposed to water vapor generated by 80°C water as a function of the square root of exposed time. Surface concentrations of three specimens treated at 500°C were determined by nuclear resonance reaction analysis and are shown in Fig. 55. To determine the diffusion coefficient from these data, one needs the extinction coefficient of the infrared peak, which is not yet known. Another problem to be solved is the data reproducibility. The reproducibility of the water uptake data was poorer compared with those of commercial glasses, such as SiO_2 glass, presumably because of the composition variation from sample to sample of a simulated nuclear waste glass. In fact, there were some specimens with visible streaks. In addition, we believe that the variation of oxidation state of the glass, e.g., Fe^{2+} vs. Fe^{3+}, can influence the water diffusion. Water diffusion in glass involves the diffusion of molecular water and its reaction with the glass to form immobile hydroxyl. The presence of a reduced element such as Fe^{2+} provides a site of easy reaction with H_2O.

E. Future Progress

The current effort will be continued. The extinction coefficient will be determined so that the diffusion coefficient can be evaluated from the obtained infrared and nuclear resonance reaction data. Efforts in the immediate future will be directed toward obtaining this constant and evaluating diffusion coefficients from the accumulated data. One of the problems is reproducibility of the data. It may become necessary to conduct numerous repeat measurements and obtain average values.

The water diffusion coefficient under low water vapor pressure will be obtained at two or three different high temperatures. This will enable us to extrapolate the data to low temperatures, which are more relevant to storage of the nuclear waste glasses.

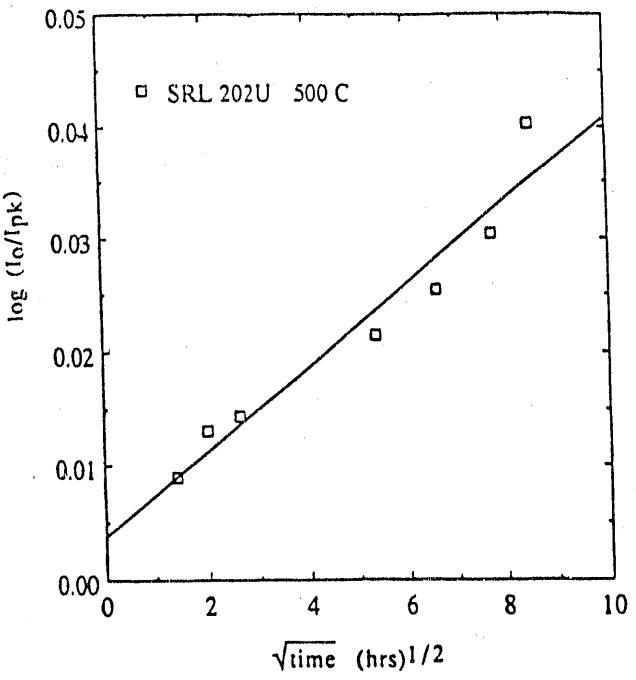

Fig. 54.
Absorbance Increase due to Water Uptake vs. Treatment Time at 500°C for SRL 202U Exposed to Water Vapor Generated by 80°C Water

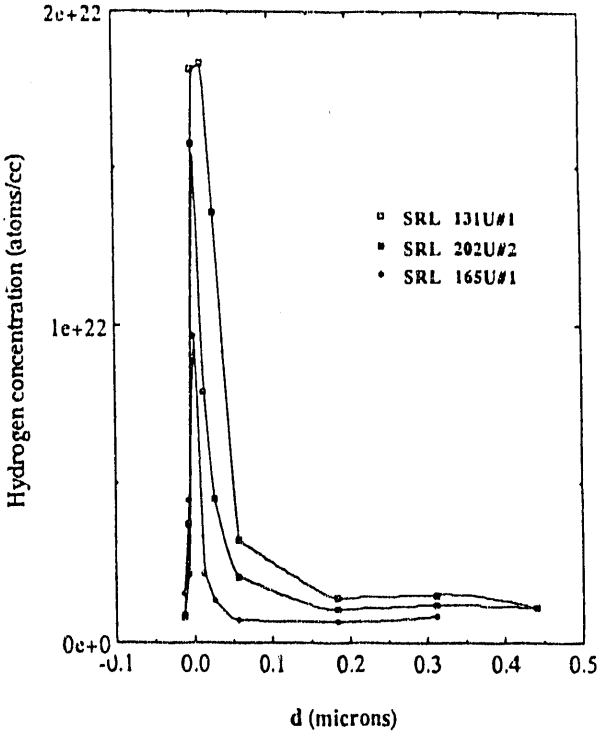

Fig. 55.
Hydrogen Concentration Profile Near the Glass Surface Determined by Nuclear Resonance Reaction Analysis after Treatment at 500°C in Water Vapor Generated by 80°C Water

Diffusion data at low temperature and high water vapor pressure will also be collected. From the comparison of the low vapor pressure data extrapolated to 250°C and 150°C and high vapor pressure data at these temperatures, vapor pressure dependence of both the solubility and diffusion coefficient of water will be obtained.

The effect of the formation of reacted layers on the measured profiles will be examined.

XI. MODELING TASKS AT LAWRENCE LIVERMORE NATIONAL LABORATORY

A. Experimental Support for Modeling

1. Introduction

The purpose of this task is to perform experiments that can be used to quantify the effects of glass composition and solution composition on glass durability. This information is fed directly into the glass dissolution model and used to perform simulations of site-specific tests, natural analogs, and performance assessment calculations of glass performance under repository conditions. Present long-term models for glass dissolution are limited because they rely on fitting parameters obtained through modeling short-term laboratory experiments. Our approach is to perform experiments that supply the necessary modeling parameters (such as temperature and pH dependence of glass rate constant) and validate the resulting model using site-specific test results and natural analog observations. The validated model can then be used with confidence to perform performance assessment calculations of glass behavior in a repository.

In FY 1991, we performed a series of flow-through tests with SRL 165U glass and CSG glass, an analog five-component glass (see Table 25). From the results of these tests, we determined the rate constant for SRL 165 glass as a function of pH. These data were incorporated directly into our glass dissolution model. We also determined the effects of dissolved calcium and magnesium on glass dissolution rate. These data will be combined with data from dissolution tests in progress involving Si, Al, and B to quantitatively determine the effects of solution composition on glass dissolution rates. These data will also be incorporated in our glass dissolution model.

This work is generic in the sense that is applicable to any given proposed repository. The effects of solution composition on glass dissolution rate, the effects of glass composition on glass durability, and the mechanistic model developed as a result of generic and site-specific testing can be applied to any given repository conditions, e.g., tuff, basalt, granite, or shale hosted. Few, if any, changes would be made to our experimental program if an alternative repository site were selected (the most changes would be made for a repository where brines may contact the waste form). Only minor amounts of additional work would be necessary to apply the glass dissolution model to alternative repository sites. In fact, our generic model would be useful in predicting glass performance in a variety of repository sites in order to provide input into site selection.

2. Technical Approach

Glass dissolution tests were performed in flow-through type reactors shown in Fig. 56. Powdered or monolithic glass samples of approximately one gram are reacted with pH-buffered fluids, some of which are doped with additional solution species. The fluids are pumped through the system at a rate adjusted to be low enough that dissolved species from the glass are above detection limits, but high enough that they do not exceed saturation with respect to alteration phases. The tests, therefore, measure the intrinsic dissolution rate of the glass unaffected by secondary phases either through their changing solution composition, or through their providing a transport barrier to dissolving species from the glass. Buffer compositions and dopant species used in the tests are listed in Table 26.

Table 25. Glass Compositions Used in Flow-Through Dissolution Tests

	CSG		SRL 165		SRL 202[a]	
Oxide	wt %	mol %	wt %	mol %	wt %	mol %
SiO_2	55.72	59.33	52.80	58.60	48.95	55.44
Al_2O_3	11.68	7.33	4.08	2.67	3.84	2.56
B_2O_3	8.43	7.75	6.76	6.47	7.97	7.79
Mn_2O_3			1.26	0.53	1.00	0.43
Fe_2O_3			11.30	4.72	11.41	4.86
ZnO			0.04	0.03	0.02	0.01
Na_2O	18.20	18.79	10.80	11.62	8.92	9.79
K_2O					3.71	2.68
Li_2O			4.18	9.33	4.23	9.63
Cs_2O			0.07	0.02		
FeO			0.35	0.32		
CaO	5.97	6.81	1.62	1.93	1.20	1.46
MgO			0.70	1.16	1.32	2.23
SrO			0.11	0.07	0.03	0.02
BaO			0.06	0.03	0.22	0.10
MnO			1.13	1.07	0.90	0.86
NiO			0.85	0.76	0.82	0.75
U_3O_8			0.96	0.08	1.93	0.16
TiO_2			0.14	0.12	0.91	0.78
ZrO_2			0.66	0.36	0.10	0.06
P_2O_5			0.29	0.14		
Totals	100.0	100.0	98.2	100.0	97.5	99.6

[a]Tests with SRL 202 glass are in progress.

Table 26. Buffer Compositions Used in Flow-Through Experiments. In all cases, buffer concentrations were 5 mM; dopants were 2.5 mM.

Composition	pH
Potassium Ortho-Phthalic Acid/HCl	4
Potassium Ortho-Phthalic Acid/KOH	6
Boric Acid/KOH	8
Boric Acid/KOH	10
KCl/KOH	12
Dopants	
Calcium Perchlorate	
Magnesium Perchlorate	

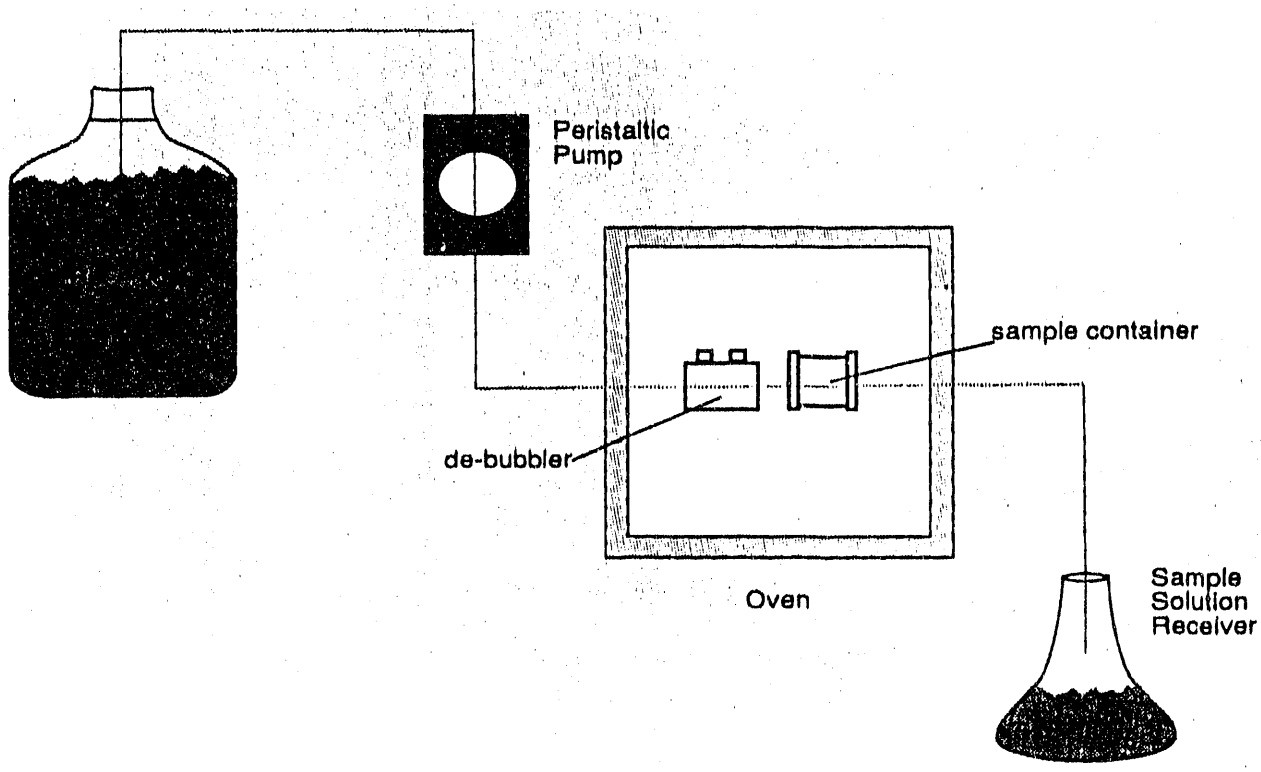

Fig. 56. Schematic of Flow-Through Glass Dissolution Test Apparatus

Initial flow rates were 50-60 mL/day. Once steady-state conditions were reached (where measured solution concentrations were constant with time), the flow rate was doubled and the tests continued until steady state was again achieved. In all tests so far, the second steady-state dissolution rates were approximately the same at both flow rates, indicating no complications due to unexpected flow conditions inside the reactor. The system, therefore, behaved as a continuously stirred reaction vessel.

Figure 57 is a connection diagram illustrating the experimental setup. Tests were performed at 70 °C in pH = 4, 6, 8, 10, and 12 solutions. The buffers were also doped separately with calcium perchlorate and magnesium perchlorate to investigate their effects on glass dissolution rates. The speciation program EQ3 was used to calculate the compositions of the pH buffers and to check for supersaturations with respect to secondary phases for the doped buffers; EQ3 was also used to calculate the pH values of the buffer solutions at 70 °C. Measured pH values at 25 °C compared favorably with those calculated using EQ3.

Two glass compositions were tested, SRL 165U glass prepared at ANL, and a simple analog of SRL 165, also prepared at ANL (see Table 25). The formula for the simple glass was derived from the formula for SRL 165 glass. The mole fractions of all monovalent ions in the SRL 165 glass that are believed to exist in the glass in a similar structural role as sodium were added together and used to determine the amount of sodium in the analog glass. A similar calculation was done for the other components. Based on the experimental results presented below, the analog glass dissolves at nearly the same rate and with the same pH dependency as the SRL 165 glass, indicating that our method for

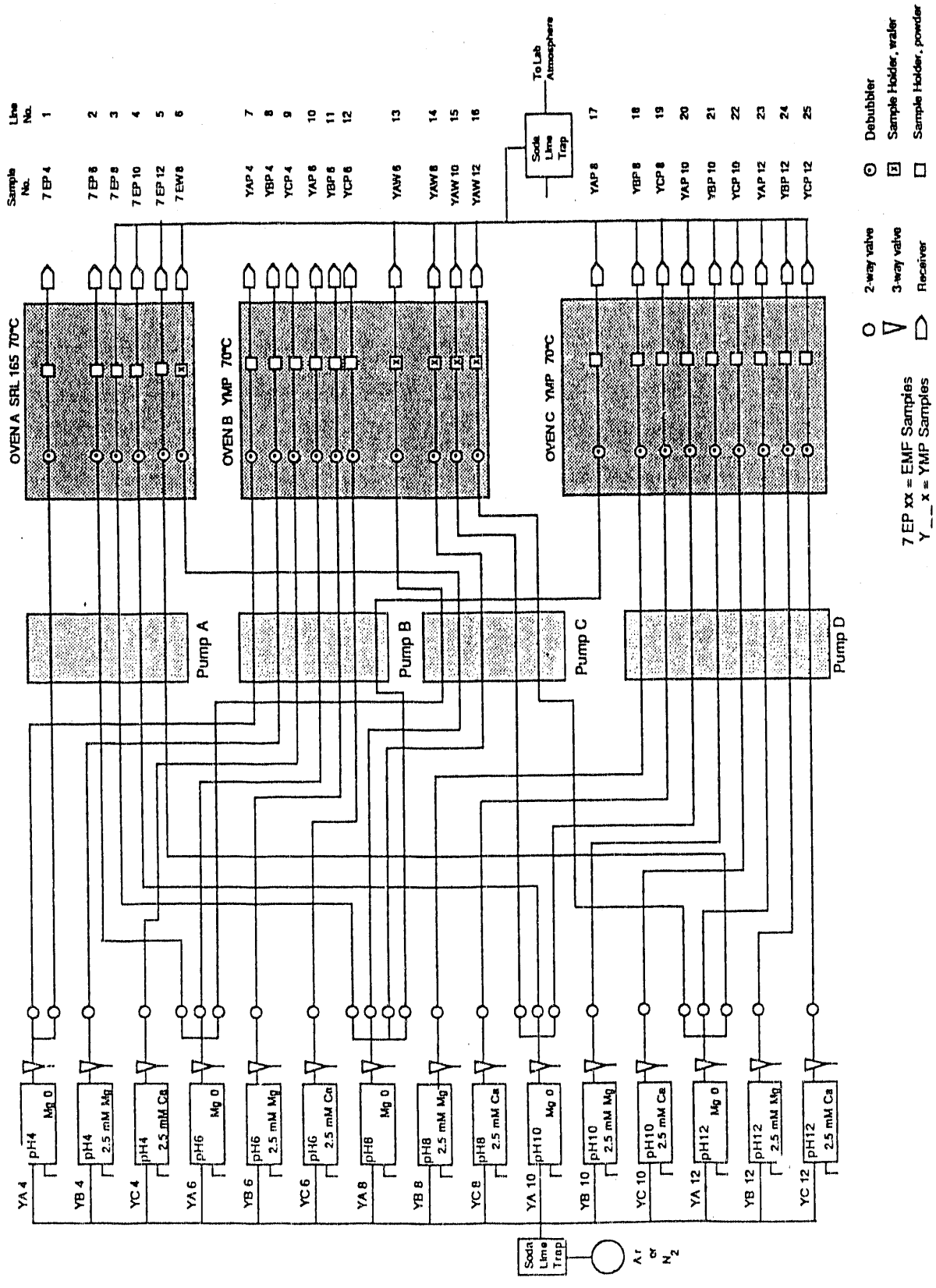

Fig. 57. Glass Dissolution Experiment Connection Diagram for Series 2 Flow-Through Tests

choosing an analog composition is valid. Analysis of the dissolution behavior of the simple glass is more certain than analysis of the results of the SRL 165 glass because of the lack of redox-sensitive elements, such as iron and manganese, in the simple glass. Glasses with significant amounts of redox-sensitive elements may undergo dissolution reactions that are linked to redox reactions, and it is difficult to decouple the two reactions in analysis of the data. For this reason we will continue to test both simple analog glasses and synthetic waste glasses in our test program.

3. Results and Discussion

The normalized steady-state concentrations of elements from the flow-through tests are used to compute the dissolution rate for the glass. Tables 27 and 28 show examples of the concentration vs. time data obtained for dissolution tests of CSG glass at 70°C in pH 6 (YAP6) and pH 10 (YAP10) buffers. The columns in Tables 27 and 28 are labeled as follows: "time" refers to time in days; "t1/2" is the averaged time for the sampling interval (the sum of the previous time plus the sampling time divided by 2), which is used as time in the plots and accounts for the fact that the sample was accumulating over an interval of time previous to the sampling time; "m/At" is the mass of reacted buffer solution divided by time; "pH" is the measured pH of the buffer solution at 25°C downstream from the glass; the columns labeled by elemental names are the concentrations, in mg/liter, of those elements; the columns labeled "RA1," "RB," etc., refer to normalized dissolution rates measured for each element. The "R" values are the release rates of constituents from the glass, in units of grams/m^2/day, calculated according to the formula

$$R_i = 10^{-6} (1/f) (1/\rho S) (m/\Delta T) \Delta ppm \qquad (5)$$

where f is the weight fraction of element i in the glass, ρ is the density of the solution, S is the measured surface area of the glass, ΔT is the elapsed time over which the glass was dissolving for the current sample, and Δppm is the change in elemental concentration of species i over the current time interval. The term of 10^{-6} converts ppm to mass fraction. The surface area of the 75-125 μ glass powder was determined to be 0.049 m^2/g using BET analysis.

When release is stoichiometric, the normalized release rates will be identical for all elements in the glass. Figure 58 shows such stoichiometric release for CSG glass leached at pH 10. Figure 59 shows nonstoichiometric release from CSG glass at pH 6. In general, release is nonstoichiometric below pH 8 and stoichiometric above pH 8 for the CSG glass at 70°C. The data for the plots in Figs. 58 and 59 were obtained from Tables 27 and 28. The rest of the raw data used for Figs. 59 through 65 will be incorporated in a topical report describing this series of flow-through tests and will not be included in the annual report because of its volume.

a. SRL 165U Glass

Flow-through tests of SRL 165 uranium-doped glass (composition given in Table 25) were performed in pH buffer solutions of 4, 6, 8, 10, and 12. Buffer compositions are given in Table 26. Figure 60 shows the normalized dissolution rate (R) values as a function of pH for eight of the elements in the glass (Al, B, Ca, Fe, Mg, Na, Si, and U). The rate is lowest at around pH 6 and increases as a function of pH in both directions from pH 6. Each symbol corresponds to a normalized release rate for an element in the glass. Release is stoichiometric when the symbols fall on top of each other. Nonstoichiometric release is primarily due to the formation of an alkali-depleted surface layer on the glass.

Table 27. Experimental Data for Flow-Through Tests of CSG Glass at pH 6. Column headings are defined and described in the text

Time	t1/2	m/At	pH	Al	B	Ca	Na	Si	RA1	RB	RCa	RSi	RNa	Timexact	t1/2
0														0	
1		59.382	6.86		2.79	4.54	15.23	1.73		0.127923	0.127739	0.007979	0.134419	0.625	0.313
2		53.536	6.14		2.42	3.83	11.67	0.83		0.100035	0.097153	0.003451	0.092859	1.625	1.125
3		49.453	6.02		2.24	3.42	11.49	0.91		0.085532	0.080137	0.003495	0.084454	2.625	2.125
4		53.811	6.1	0.09	2.4	3.62	13.39	1.25	0.001585	0.099718	0.092298	0.005224	0.107092	3.625	3.125
5		48.466	6.33	0.08	2.39	3.58	12.98	1.23	0.001269	0.089439	0.082212	0.00463	0.093501	4.625	4.125
7		56.631	6.27	0.07	2.08	3.18	11.15	1.08	0.001295	0.090791	0.085178	0.004742	0.093685	6.521	5.573
9		51.928	6.2	0.06	1.96	3.14	10.84	0.94	0.00102	0.078587	0.077258	0.003791	0.083664	8.541	7.531
13		48.283	6.28	0.06	1.98	3.09	10.95	0.8	0.000948	0.073816	0.070691	0.003	0.078581	12.521	10.531
16		55.67	6.23	0.06	1.56	2.53	8.82	0.57	0.001093	0.067056	0.066735	0.002465	0.072979	15.531	14.026
20		53.93	6.2	0.05	1.49	2.34	8.41	0.61	0.000882	0.062045	0.059794	0.002555	0.067411	19.531	17.531
24		53.815	6.16		1.39	2.22	7.77	0.6		0.057758	0.056607	0.002508	0.062149	23.531	21.531
29		53.9		0.05	1.22	1.97	6.84	0.52	0.000882	0.050774	0.050312	0.002177	0.054796	28.531	26.031
30		55.742		0.05	1.13	1.75	6.35	0.49	0.000912	0.048635	0.04622	0.002121	0.052609	29.552	29.042
31		65.617			0.96	1.65	5.47	0.41		0.048638	0.0513	0.002089	0.053347	30.531	30.042
32		73.296			0.86	1.46	4.86	0.35		0.048671	0.050705	0.001992	0.052945	31.635	31.083
33		74.123		0.05	0.87	1.42	4.86	0.35	0.001213	0.049792	0.049872	0.002015	0.053542	32.593	32.114
34		73.361			0.87	1.44	4.87	0.34		0.04928	0.050054	0.001937	0.053101	33.625	33.109
35		74.598			0.84	1.36	4.69	0.33		0.048383	0.048071	0.001912	0.052		
38				0.05	0.87	1.33	4.68	0.4							
41				0.06	0.82	1.31	4.61	0.42							

Table 28. Experimental Data for Flow-Through Tests of CSG Glass at pH 10. Column headings are defined and described in the text

Time	t1/2	m/At	pH	Al	B	Ca	Na	Si	RA1	RB	RCa	RSi	RNa	Timexact	t1/2
0														0	
1		61.724	9.87	2.81		1.97	7.43	11.8	0.056758		0.057615	0.056568	0.068163	0.625	0.313
2		59.056	9.86	4.01		2.76	8.66	16.5	0.07749		0.07723	0.075681	0.076013	1.625	1.125
3		59.6	9.89	3.45		2.83	8.33	14.06	0.067287		0.079918	0.065083	0.071133	2.625	2.125
4		58.796	9.88	4.4		3	10.11	18.23	0.084656		0.083575	0.083246	0.088348	3.625	3.125
5		58.55	10.19	4.44		3.05	10.23	18.36	0.08507		0.084614	0.08349	0.089024	4.625	4.125
7		64.704	10.16	3.89		2.55	8.58	15.96	0.082366		0.08155	0.080205	0.082513	6.521	5.573
9		60.989	10.13	3.78		2.32	8.31	15.43	0.075441		0.067043	0.073089	0.075328	8.541	7.531
13		54.606	10.27	3.72		2.53	8.54	15.28	0.066474		0.06546	0.064804	0.069311	12.521	10.531
16		55.267	10.18	3.55		2.38	8.2	14.59	0.064204		0.062324	0.062626	0.067358	15.531	14.026
20		59.769	10.18	3.39		2.16	8.22	14.13	0.066304		0.061171	0.065593	0.073022	19.531	17.531
24		59.754	10.29	3.41		2.02	8.27	14.09	0.066679		0.057192	0.06539	0.073448	23.531	21.531
29		62.008		3.18		2.12	7.58	13.14	0.064527		0.062287	0.063282	0.069859	28.531	26.031
30		64.013		3.05		2.11	7.38	12.72	0.06389		0.063998	0.06324	0.070215	29.552	29.042
31		74.689		2.83		1.85	6.95	12.02	0.069196		0.06547	0.069726	0.077152	30.531	30.042
32		76.788		3.02		1.94	7.13	12.5	0.075887		0.070584	0.074549	0.081375	31.635	31.083
33		76.872		3.11		2.14	7.3	13.05	0.078234		0.077946	0.077914	0.083406	32.593	32.114
34		76.322		3.19		2.15	7.43	13.26	0.079672		0.07775	0.078601	0.084284	33.625	33.109
35		76.868		3.23		2.18	7.43	13.45	0.081206		0.079358	0.080256	0.084843		
38				3.2		2.15	7.41	13.35		0					
41				2.96		1.98	6.65	12.37		0					

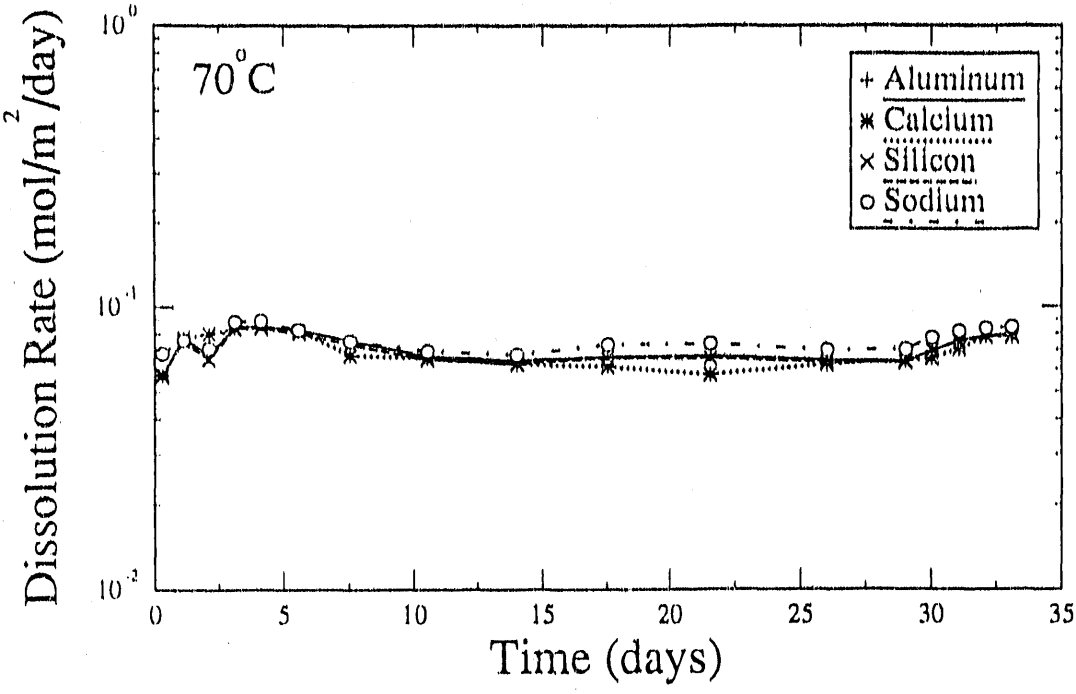

Fig. 58. Normalized Elemental Release Rates vs. Time for CSG Glass at pH 10 (YAP10). Glass dissolves stoichiometrically at pH 10.

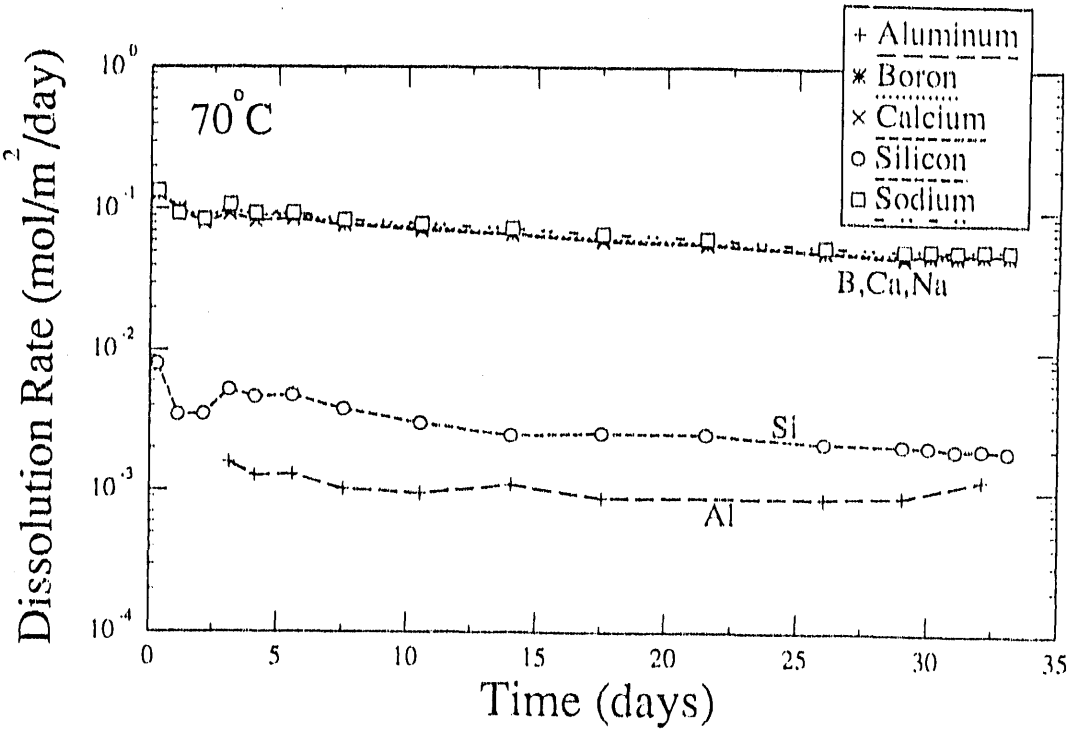

Fig. 59. Normalized Elemental Release Rates vs. Time for CSG Glass at pH 6 (YAP6). Glass dissolves nonstoichiometrically at pH 6.

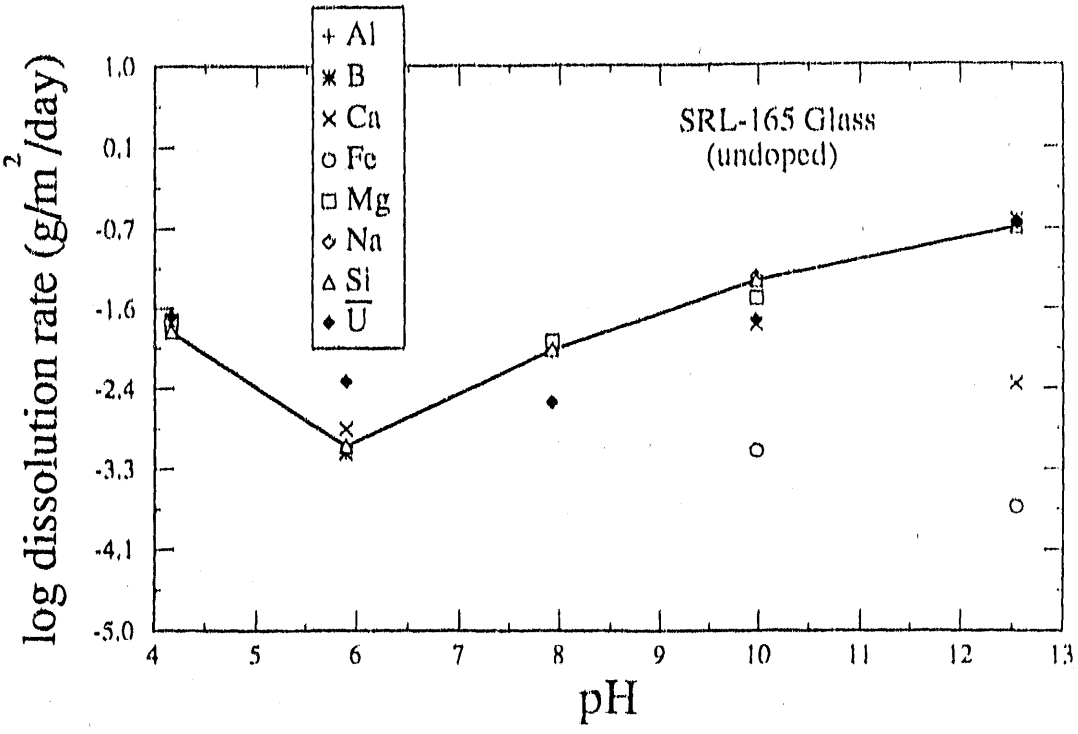

Fig. 60. Normalized Elemental Log Dissolution Rates vs. pH at 70°C for SRL 165 Glass. Line connects silica release data.

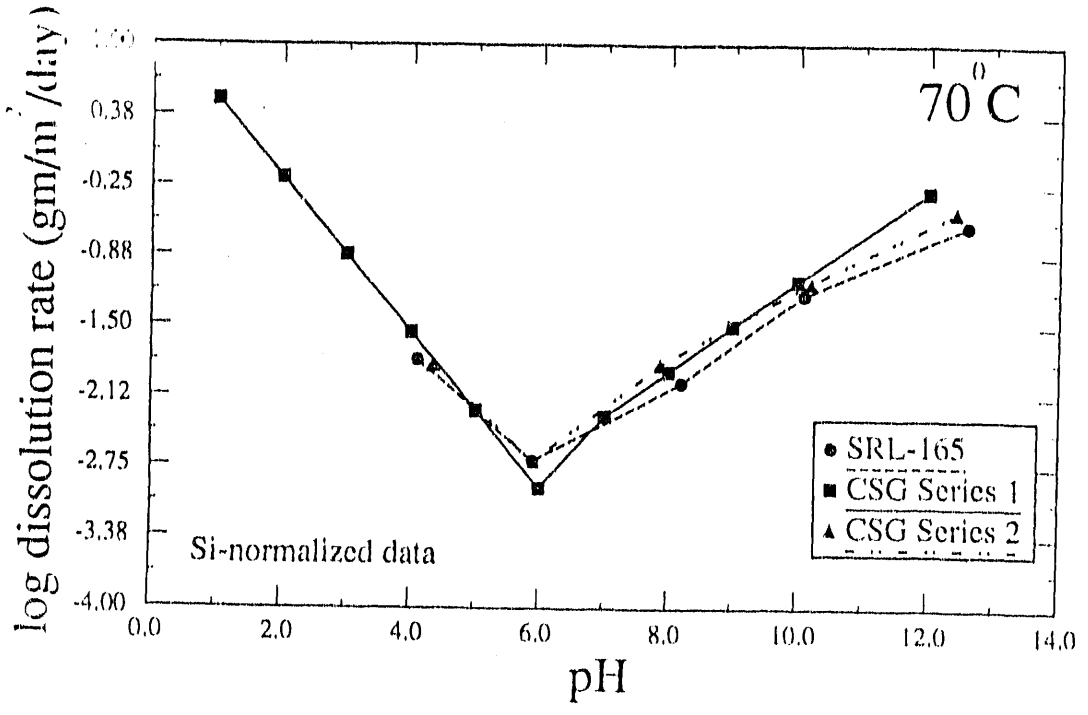

Fig. 61. Comparison of Dissolution Rates of SRL 165 Glass and CSG Glass Analog. Series 1 and 2 refer to replicate tests of CSG glass (see text).

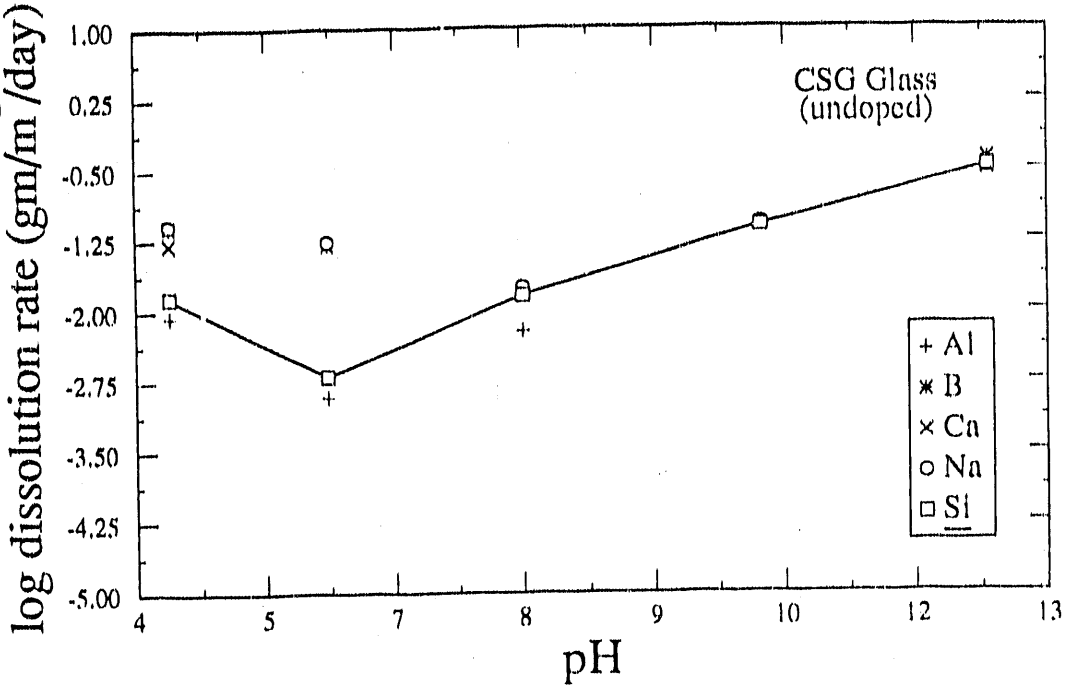

Fig. 62. Normalized Elemental Release Rates vs. pH for CSG Glass at 70°C. Above pH 8, all elements release at identical rates and release is stoichiometric.

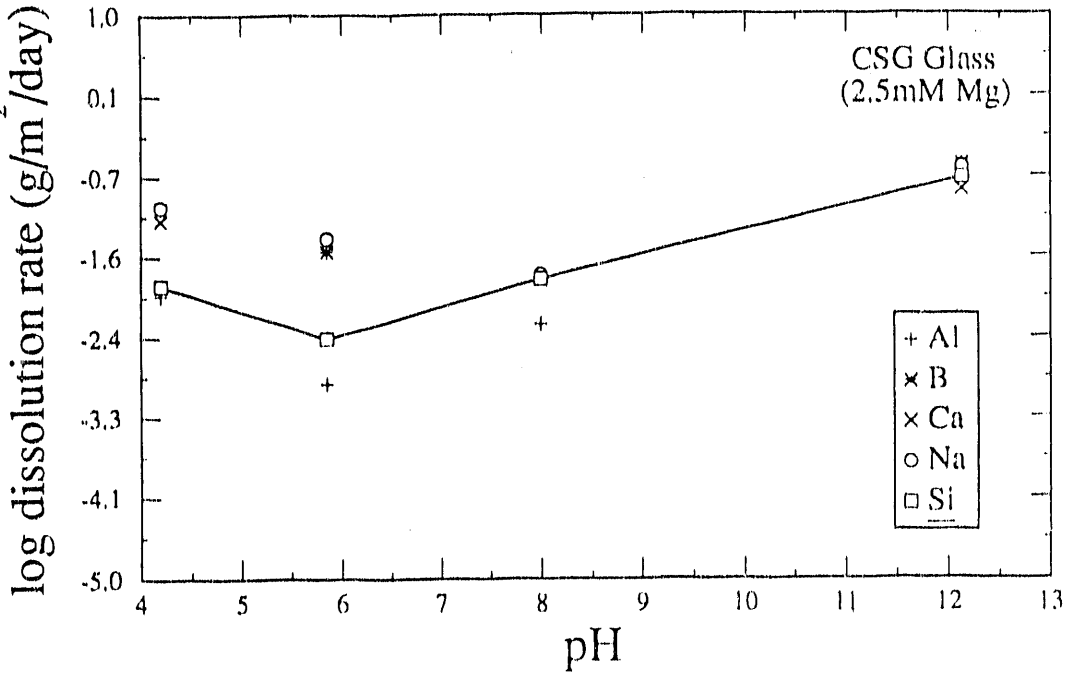

Fig. 63. Normalized Elemental Release Rates vs. pH for CSG Glass at 70°C in Calcium-Doped Buffer Solutions.

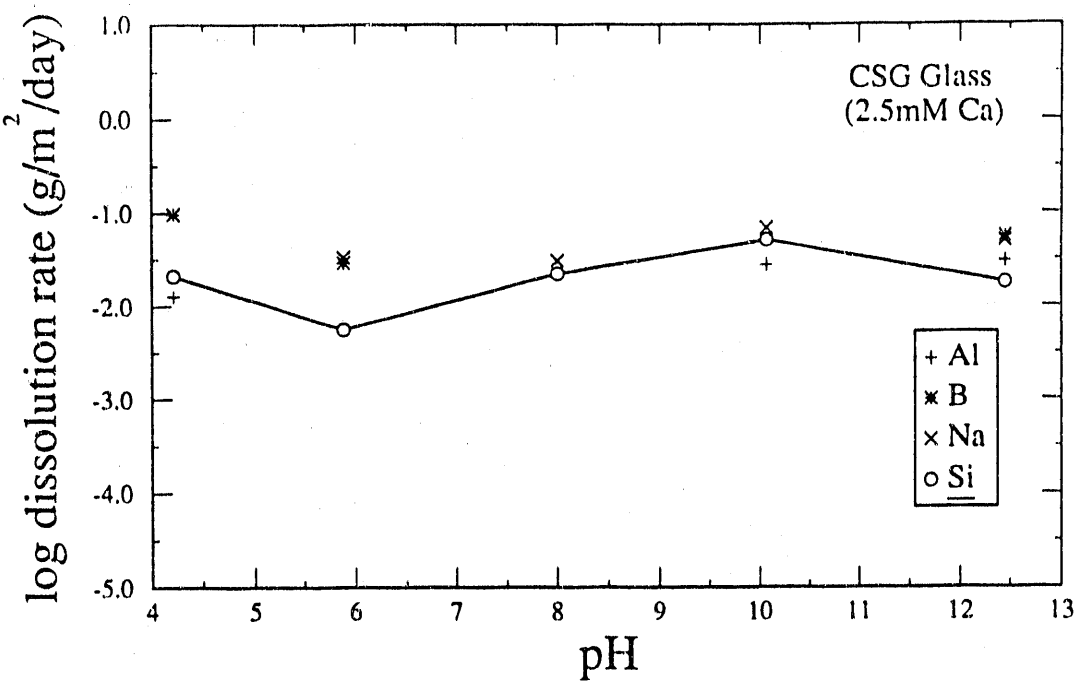

Fig. 64. Normalized Elemental Release Rates vs. pH for CSG Glass at 70°C in Magnesium-Doped Buffer Solutions.

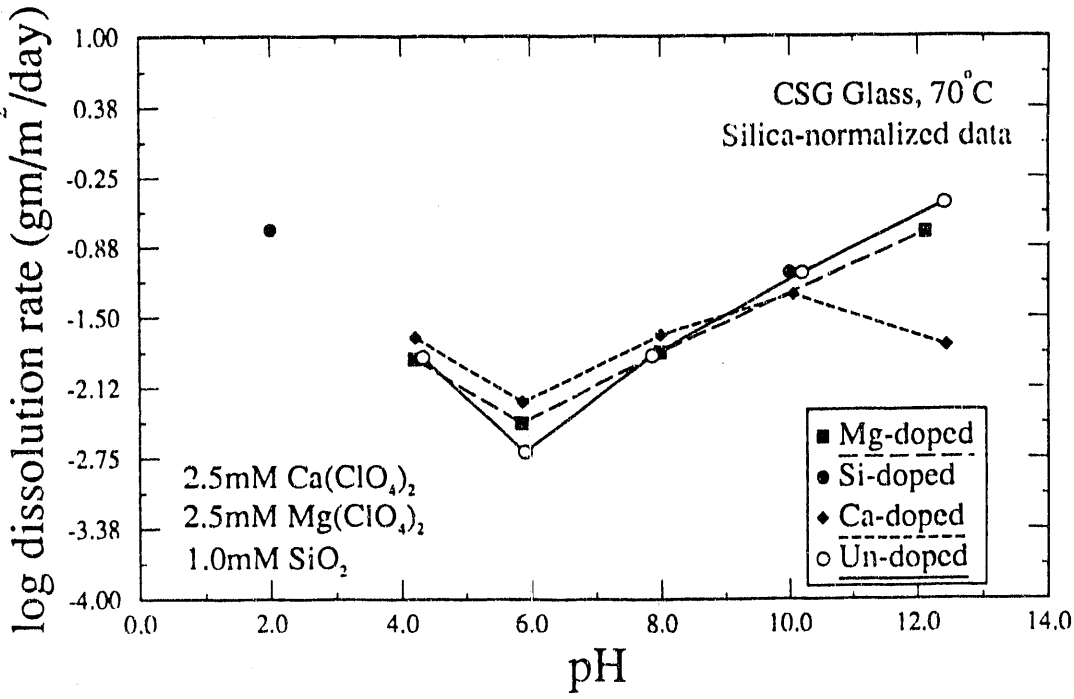

Fig. 65. Comparison of Dissolution Rate Data for Nondoped, Calcium-Doped, and Magnesium-Doped Buffer Flow-Through Tests.

At pHs of 10 and higher, the release rates for calcium and iron are significantly lower than those for the other elements. Calcium and iron may be precipitating in one or more secondary phases. The EQ3 calculations for these fluids indicate that calcium and iron oxide and hydroxide phases are supersaturated at these pHs and may have precipitated in the experiments. Uranium is released congruently at pHs of 4 and 12, is released more slowly than most other elements at pH 8 and 10, and faster than all other elements at pH 6. Apparently at pH 6, uranium is selectively extracted from the glass, perhaps due to a redox reaction in which uranium is oxidized to uranyl ion. Uranyl silicates may also be forming in pH 8 and 10 tests. The run products will be examined using X-ray, SEM, and electron microprobe techniques to identify any phases which have formed.

Figure 61 shows good agreement between silica-normalized data from tests of SRL 165 and CSG glasses. Both glasses have a minimum dissolution rate at around pH 6 (probably the zero point of charge of the glass in the buffer solution) and approximately the same rate dependence on pH. The dissolution rate of the SRL 165 glass is slightly smaller than that for the CSG analog glass above pH 6. This good agreement indicates that the primary controls on glass dissolution rate depend mainly on the major components of the glass and are less affected by minor and trace components. The data also support the validity of our methodology for choosing an analog composition from the composition of the SRL 165 glass, as discussed above.

In Fig. 61, the test results for CSG series one and two are data from two separate but similar tests of CSG glass performed in different laboratories by different technicians, 18 months apart. The CSG glass used in the first test was prepared at LLNL, the glass used in the second test was prepared at ANL. The data indicate that the tests are very reproducible using the experimental procedures that we have developed.

Future tests will be performed using both complex glasses, such as SRL 165 and SRL 202, and their simple analog counterparts. The simple glasses contain no redox-sensitive elements and highly insoluble elements such as iron and manganese, which make it easier to design tests where secondary phases do not precipitate. The use of simple glasses also avoids having to consider redox reactions during dissolution. Tests of the simple glasses will be used to better understand the fundamental dissolution reaction mechanisms. Tests of complex glasses can then be interpreted with more certainty using the framework generated from the simple glass dissolution tests. Our present data strongly support the idea that the simple glasses are accurate analogs for the complex glasses in terms of their fundamental dissolution mechanisms.

b. CSG Glass in Doped Buffers

The CSG analog glass was tested at 70°C and pH values of 4, 6, 8, 10, and 12 in three test series using nondoped buffers and buffers with added magnesium perchlorate and calcium perchlorate (Table 26). The 5 millimolal (mM) buffers were doped with an additional 2.5 mM of the dopants. The tests were performed to determine the effect of aqueous magnesium and calcium on the glass dissolution rate. Other workers have shown that dissolved silica decreases the overall dissolution rate. The effects of other glass constituents have not yet been determined.

Figure 62 shows the results for the nondoped tests for each element in the glass. The glass dissolves stoichiometrically above pH 8. Below pH 8, calcium, boron, and sodium are released more quickly than silicon and aluminum. Presumably, calcium and sodium are released in an ion exchange process. Although boron occupies tetrahedral sites in the glass, as does silicon, apparently the boron-oxygen bonds are much more susceptible to hydrolysis than the silicon-oxygen bonds, and the boron is

readily released from the glass. The fact that boron is generally one of the fastest-released elements indicates that little or no ion exchange can take place without some hydrolysis of structural bonds in the glass.

Another test series was performed at 70°C and pH 4, 6, 8, 10, and 12 with the buffers doped with 2.5 mM calcium perchlorate. These experiments were performed to determine the effect of dissolved calcium on glass dissolution rate. Our current model for glass dissolution predicts that all elements concentrated in the alkali-depleted surface layer can affect the glass dissolution rate through the affinity term in the rate equation. A high concentration of calcium in solution should lower the rate of glass dissolution similarly to the way dissolved silica lowers the rate.

Figure 63 shows the effect of calcium on dissolution rate. The rate is similar to that determined for CSG glass in nondoped buffer solutions, except at pH 12, where the rate in Ca-doped solutions is lower by about a factor of 10. The EQ3 calculations of these solutions show high degrees of supersaturation with respect to calcium-silicate and calcium hydroxide phases for these high-pH solutions. It seems likely that the decrease in rate is due to secondary phase formation, which causes the glass to be armored from further reaction. The run products will be analyzed to determine whether this is the case.

Previous workers have shown that magnesium can reduce the overall rate of glass dissolution by up to two orders of magnitude [BARKATT-2]. Magnesium was added to see if this effect, which has only been observed in closed-system tests where large degrees of supersaturation of magnesium silicate minerals are present, also occurs under flow-through test conditions. In terms of mechanisms, if magnesium acts to poison the dissolving glass surface through a surface chemical effect, it would be expected that both types of experiments with magnesium present would result in decreased dissolution rate. If secondary phase formation of magnesium silicate is responsible for lowering the dissolution rate, it would be expected to lower the dissolution rate only under closed-system conditions.

Figure 64 shows the results for the magnesium perchlorate-doped buffer tests. Comparison with the nondoped buffer results in Fig. 62 shows that magnesium has little effect on dissolution rates and little effect on the nonstoichiometric dissolution behavior at pHs less than 8. Figure 65 shows a direct comparison for silica-normalized data from the nondoped (open circles) and Mg-doped (filled squares) buffer test results. The rates are not significantly affected by the addition of magnesium. Data for the calcium-doped tests and previous data for silica doped tests are also shown in Fig. 65. These data indicate no significant surface chemical effect of magnesium on the glass dissolution rate for the concentrations used in these tests. Magnesium (and perhaps silica as well) apparently do not significantly affect glass dissolution rates under our flow-through test conditions.

Additional flow-through dissolution tests are underway for buffers doped with boron, aluminum, and silica. After the results of these tests are available, we should be able to better define the affinity term in the rate equation for glass dissolution.

B. Model Development

1. Introduction

The objective of this task is to develop and apply a computer model to the reaction of nuclear waste glasses in a repository environment. The model, once validated by successfully simulating laboratory experiments and selected natural systems, will be incorporated into a performance assessment model for the repository and used to estimate glass performance for a given set of repository conditions.

Currently, we are developing such a model in a four step process: (1) determine the important chemical processes that take place during glass dissolution; (2) develop a model which includes these processes; (3) perform experiments that provide the necessary constants to run the model; and (4) validate the model with laboratory experiments and observations from natural systems. A model has been developed [BOURCIER] (steps 1 and 2), and we are in the process of performing steps 3 and 4.

2. Work Summary

a. Collection and Estimation of Thermodynamic Data for Alteration Phases

Current simulations use as input the alteration (secondary) phases identified in a wide variety of glass dissolution experiments. Although the model can make predictions of which phases should form based on their thermodynamic properties, the predicted phases often do not match those observed in the tests. It is well known that the earliest phases to form during a reaction are often not the thermodynamically most stable. Instead, metastable phases precipitate first and may later transform into the more stable phases. Because the theory that could be used to make these predictions from first principles is not well developed, we prefer to directly use experimental results and observations from natural systems to identify secondary phase formation in the simulations.

The secondary phases observed in the glass tests performed at ANL are listed in Table 29, along with information as to whether thermodynamic data for these phases are in our current EQ3/6 data base or in the SUPCRT92 data base. We are beginning work to perform literature searches for appropriate data or estimate the needed data from available estimation techniques [CHERMAK, HOLLAND, TARDY, VIELLARD].

b. Modification of EQ3/6 and Gt Reaction Path Codes

Rate parameters generated by the flow-through tests have been incorporated into the EQ3/6 and Gt reaction path codes. At this time, we have determined the rate constants for SRL 165 glass and CSG analog glass as a function of pH and temperature. These data have been incorporated into the EQ3/6 code. Experimental work to provide the same data for SRL 202 glass is underway. This data will also be incorporated into the modeling codes.

We are incorporating the glass dissolution model into the Gt code. This involves additional minor coding for the pH dependence of the rate constant, as well as the addition of the glass alteration layer as a "fictive" mineral in the data base. Once completed, the Gt code can be used to perform rock-centered simulations of glass performance in the repository. The EQ3/6 code is limited to fluid-centered simulations. In the rock-centered mode, the code can simulate the reaction of the glass waste form (and other repository materials) as fluid flows in and past the waste form at any specified rate. We anticipate that most future modeling simulations will be performed using the Gt code in this mode.

Work to transform the EQ3/6 data base to a format readable by the Gt code was completed. We can now create customized data bases specific to glass dissolution modeling from our comprehensive data base for both EQ3/6 and Gt.

Table 29. Compilation of Secondary Phases or Chemical Compositions of Precipitates Observed (Both in Boldface) to Form during Nuclear Waste Glass/Water Interactions. Candidate phases that are compatible with observed compositions are tabulated in plain typeface. Also tabulated for each observed or candidate phase is the status of the EQ3/6 data base (data0.com.R7) and the SUPCRT92 data base with respect to whether or not the phase is included in the respective data base.

Phase	Ref.	In EQ3/6 Data Base?	In SUPCRT Data Base?	Comments
Acmite	7	No	No	
Aluminum Hydroxide	1			
Gibbsite		Yes	Yes	
Bayerite		No	No	
Doyleite		No	No	
Nordstrandite		No	No	
Boehmite		No	Yes	
Diaspore		Yes	Yes	
Apatite	1,5,6			
Chlorapatite		No	No	
Fluorapatite	6	Yes	No	
Hydroxyapatite	6	Yes	No	
Augite	7	No	No	
Birnessite	2	Yes	No	
Brabantite	2	No	No	
Brindleyite (Nimesite)	2	No	No	
Calcium Chloride	1			
Hydrophilite		Yes	No	
Calcium Oxide, CaO_4	2			CaO or $CaSO_4$?
Calcium Sulfate	1			
Anhydrite		Yes	Yes	
Gypsum		Yes	Yes	
Calcium Carbonate	6			
Calcite	1	Yes	Yes	

Cont'd

Table 29 (Cont'd)

Phase	Ref.	In EQ3/6 Data Base?	In SUPCRT Data Base?	Comments
Chlorite Group	4			
Clinochlore-7 Å		Yes	Yes	
Clinochlore-14 Å		Yes	Yes	
Daphnite-7 Å		Yes	No	
Daphnite-14 Å		Yes	No	
Chlorite-ss [model]		Yes	No	
Dolomite	1	Yes	Yes	
Eurcryptite	7	Yes	No	
Ferrihydrite	7	Yes	No	
Glauconite	2	No	No	
Gyrolite	3,5,7	Yes	No	
Gyrolite Polymorph	6	No		
Hematite	2	Yes	Yes	
Herschelite	3	No	No	
Illite	3	Yes	No	
Kaolinite	2,4	Yes	Yes	
Lithium Phosphate	6			
Magnesium Silicate	2			
Mordenite	3	Yes	No	
Oxides/Hydroxides	1			
Fe, Mn	1			
Cr, Fe, Mn	1			
Cr, Fe, Mn, Ni	1			
Potassium Chloride	1			
Sylvite		Yes	Yes	

Cont'd

Table 29 (Cont'd)

Phase	Ref.	In EQ3/6 Data Base?	In SUPCRT Data Base?	Comments
Potassium Feldspar		Yes	Yes	
Adularia	3	No	No	
Orthoclase	6	No	No	
Pyroxeroid group	4			Pyroxenoid?
Iron calcium silicate	4			
Reyerite	6	No	No	
Serpentine	1,4,5			
Chrysotile		Yes	Yes	
Lizardite		No	No	
Antigorite		Yes	Yes	
Silica	1			
Cristobalite		Yes	Yes	
Chalcedony		Yes	Yes	
Opal	1	No	Yes	
α-Quartz	1,2	Yes	Yes	
Smectite	1,4			
Smectite-high-Fe-Mg		Yes	No	
Smectite-low-Fe-Mg		Yes	No	
Smectite-di [ss mode]		Yes	No	
Montmorillonite	6			
Montmorillonite-Ca		Yes	No	
Montmorillonite-Cs		Yes	No	
Montmorillonite-K		Yes	No	
Montmorillonite-Mg		Yes	No	
Montmorillonite-Na		Yes	No	
Beidellite	2			
Beidellite-Ca		Yes	No	
Beidellite-Cs		Yes	No	
Beidellite-H		Yes	No	
Beidellite-K		Yes	No	
Beidellite-Mg		Yes	No	
Beidellite-Na		Yes	No	

Cont'd

Table 29 (Cont'd)

Phase	Ref.	In EQ3/6 Data Base?	In SUPCRT Data Base?	Comments
Nontronite	2,4,5,6			
Nontronite-Ca		Yes	No	
Nontronite-Cs		Yes	No	
Nontronite-H		Yes	No	
Nontronite-K		Yes	No	
Nontronite-Mg		Yes	No	
Nontronite-Na		Yes	No	
Saponite	5			
Saponite-ss		Yes	No	
Saponite-Ca		Yes	No	
Saponite-Cs		Yes	No	
Saponite-H		Yes	No	
Saponite-K		Yes	No	
Saponite-Mg		Yes	No	
Saponite-Na	2	Yes	No	
Sauconiteo	7	No	No	
Swinefordite	4	No	No	
Hectorite		No	No	
Stevensite	5	No	No	
Volkhonskoite		No	No	
Sodium Carbonate	1			
Natron		Yes	No	
Thermonatrite		Yes	No	
Trona-Na		No	No	
Wegscheiderite		No	No	
Sodium Chloride	1			
Halite		Yes	Yes	
Sodium Sulfate	1			
Mirabilite		Yes	No	
Thenardite		Yes	No	
Spinel	7	Yes	Yes	
Tinacalconite	6	No	No	

Cont'd

Table 29 (Cont'd)

Phase	Ref.	In EQ3/6 Data Base?	In SUPCRT Data Base?	Comments
Titantium Dioxide				
Anatase	1	No	No	
Brookite		No	No	
Rutile		Yes	No	
Rutile, iron-doped	2	No	No	
TiO_2(B)		No	No	
Tobermorite	3,5,6,7			
Tobermorite-9 Å		Yes	No	
Tobermorite-11 Å		Yes	No	
Tobermorite-14 Å		Yes	No	
Truscottite	7	No	No	
Uranophane	1	Yes	No	
Weeksite	3,6,7	Yes	No	
Zeolite	6			
Analcime	3,5,6,7			
Analcime-dehydrated		Yes	Yes	
Analcime-H_2O		Yes	Yes	
Chabazite	6	No	No	
Phillipsite	3,6	No	No	
Thomsonite	6	No	No	

1. J. Bates (ANL), pers. comm. to K. Knauss (LLNL), 7/12/91.
2. C. Bradley (ANL), pers. comm. to J. Bates (ANL), 7/10/91.
3. D. Wronkiewicz (ANL), pers. comm. to J. Bates (ANL), 7/8/91.
4. E. Buck (ANL), pers. comm. to J. Bates (ANL), 7/8/91.
5. J. Mazer (ANL), pers. comm. to J. Bates (ANL), 7/8/91.
6. W. Ebert (ANL), pers. comm. to J. Bates (ANL), 7/16/91.
7. R. D. Aines, Application of EQ3/6 to Modeling of Nuclear Waste Glass Behavior in a Tuff Repository, Lawrence Livermore National Laboratory report UCID-20895, p. 11 (1986).

Simulations using these modified codes in FY 1992 will concentrate on SRL 165 glass, which has the most diverse set of experimental test results of any glass. The experimental results will be obtained mainly from tests performed at ANL, although additional data are available from MCC and PCT tests from other laboratories. Successful simulations of this wide variety of tests are essential for validation of the model and data base. The more diverse the conditions under which the model makes accurate predictions, the more convincing it is that the mechanistic basis of the model is correct.

c. Preliminary Repository Performance Assessment Calculations

To test the capabilities of EQ3/6 to handle large multicomponent problems, we have performed scoping simulations of SRL 165 glass performance under conditions that may be found at the site for the potential Yucca Mountain repository. Three simulations were performed: J-13 groundwater with (1) glass alone, (2) glass plus tuff plus canister materials, and (3) glass plus tuff plus canister material plus cement. The purpose of these simulations is to investigate the effects of other repository materials on the behavior of glass. The other materials affect glass performance through their effects on solution composition, especially pH.

In this simple model, the glass is treated as two reactants. The first is the surface alteration layer, and the second is a "fictive" material that represents the mass of the original glass minus the components of the alteration layer. The alteration layer is used to calculate the glass dissolution affinity [BOURCIER]. The tuff is simulated by a mineralogic assemblage representative of the Topopah Springs tuff. It is represented by the minerals sanidine, plagioclase, quartz, biotite, and smectite. The effects of the corrosion of a stainless steel canister are approximated using the nickel-rich magnetite phase trevorite. The cement is represented by adding $Ca(OH)_2(s)$ to the system. All of these phases are entered as reactants in the system and allowed to dissolve or precipitate according to some rate law. The model is for a closed system where the dissolving glass and repository materials build up in solution and remain. This provides a simulation of repository conditions where the rate of fluid flow though the repository is low relative to the rate of materials dissolution/precipitation reactions. This simple treatment, therefore, provides a first approximation of how the chemical effects of all these reacting solids interact with each other, and ultimately affect glass performance in a repository.

Figure 66 shows the results of the three simulations where the rate of glass dissolution is plotted vs. time to 10,000 years. Rates of glass dissolution are predicted to be about three times higher with cement present than with either glass alone or glass with metal and tuff. The presence of tuff and metal is predicted to increase glass release rates by only a minor amount. The rates of dissolution are predicted to increase over time primarily due to the increase in the predicted pH. We have shown in our experiments that the rate of glass dissolution increases with pH above neutral pHs. Figure 67 shows the predicted pH values for the three simulations. The presence of cement increases the predicted pH by over 1.5 pH units and is the primary reason that glass is predicted to dissolve faster with cement present.

The current simulations are subject to several limitations. We have not allowed for precipitation kinetics of the secondary phases and have assumed that equilibration with the secondary phases is instantaneous. This forces the concentrations of dissolved species to lower levels than are actually observed experimentally and causes the model to predict higher release rates than would be predicted if precipitation kinetics were included. It is likely that dissolution rates are at least a factor of ten times higher than would be predicted using precipitation kinetics in the model. Future simulations will take this into account as best as possible with the existing rate data.

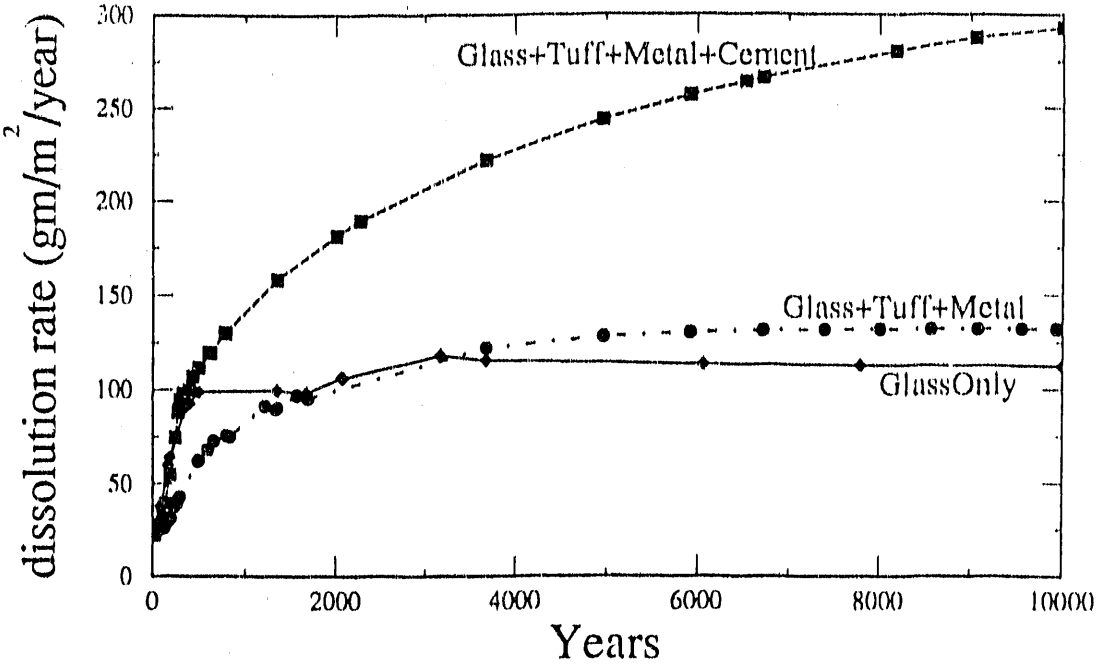

Fig. 66. Calculated Dissolution Rate of SRL 165 Glass in J-13 Water at 25 °C Using Glass Dissolution Model in EQ3/6 (see text).

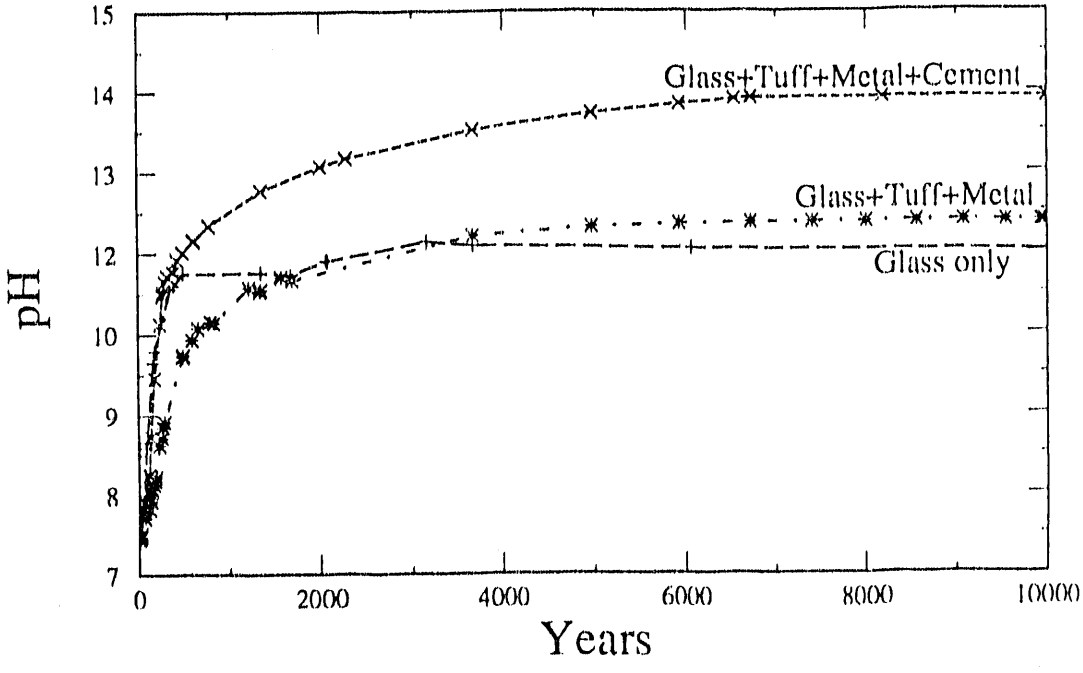

Fig. 67. Calculated pH of Solution in Contact with SRL 165 Glass and Various Repository Materials at 25 °C Using Glass Dissolution Model in EQ3/6 (see text).

We have not incorporated a rate law for metals dissolution but have simply included metals alteration minerals as reactants. A rigorous rate law for metal corrosion can be incorporated into the model which will better simulate the impact of a metal canister on the glass dissolution rate. It is unclear at this time whether the rate model for metal will increase or decrease the presently predicted glass dissolution rates. We hope to include a kinetic model for metal dissolution in our simulation at some point.

Finally, our glass dissolution model provides an approximate dissolution rate given the temperature and solution pH. We have not rigorously accounted for the effects of other dissolved species or redox state. We are performing experiments to collect these needed data. The simulation results will improve with time as these experiments are completed and their results incorporated into our model.

C. Data Evaluation and Assimilation

The scope of work for this task has not been defined in a test plan pending further guidance from the sponsor. However, we have initiated some work in this area by performing a statistical analysis of the Materials Characterization Center's compilation of glass leach test results. The analysis was performed to find correlations between glass composition and glass durability, and between solution composition and glass durability. This knowledge could then be used to develop an improved understanding of waste-glass leaching, which could be used in model development, and to form a basis for conducting further experiments.

We used an integrated package of two software programs from BBN Software Products Corporation. The basic program RS/1 allows for complex manipulation of tabular scientific data. The second program RS/Explore is an expert system that uses and builds on RS/1 capabilities to help analyze and interpret complex data. This includes correlations, linear and multiple regression, analysis-of-variance, and associated graphs. These programs run on a DEC VAX minicomputer. With considerable effort, the MCC data base was converted from its IBM PC format to RS/1 format on the VAX.

We did not receive any description of the purpose or history of the MCC data base with the package, only an explanation of how to access the information on a PC.

The MCC data base includes 1867 sets of data, each with up to 47 variables. This is a very large data base with almost 90,000 data values. These results come from 52 separate reports or compilations. It includes data that were taken under standard MCC test protocols. The data base includes sample compositions of 24 common constituent oxides. If available, SA/V ratios were given. Test duration, temperature, and ending pH were always included. Final leachate concentrations of the four common leachable constituents, silicon, sodium, boron, and lithium, were tabulated. The leachate concentrations were also normalized for the SA/V ratios and the mass fraction of the element in the glass. The data presented did not represent all of the data available in all of the reports. They seem to represent the "lowest common denominator" of the data in those reports.

We have examined the MCC data base to determine relationships between the variables and, in particular, to examine any effects of composition or test condition variables on the leaching properties of the glasses. We determined the leaching properties by the leachate concentrations reported. We looked at both the actual and normalized concentrations.

Our first attempt was to calculate correlations between all of the variables in the complete data base. We were particularly interested in the correlation of leach rates of the various species vs. chemical composition, time, temperature, and other MCC test procedure variables. A time-consuming examination of the entire data base showed little correlation (less than 0.4) between any of the variables.

The next approach was to look at individual glasses and reports to see if we could find more correlations within subsets that would likely have more commonality.

We initially looked at all of the results that had a MCC-1 test basis. That included 1248 samples. Since Carol Jantzen's work represented a large group of 212 samples with the MCC-1 test, we selected her work alone. We then looked at glass types. First was SRL 165, which is the most studied synthetic glass for waste storage purposes. A subset of 38 values was also looked at that included MCC-1 tests. We could only see correlations for Strachan's 1985 [STRACHAN] study of SRL 131 glass and were able to produce good graphs of leach rates vs. time at temperature.

These efforts encouraged us to look at the individual reports that included the most data. Five of the 52 reports accounted for almost half (929) of the values in the data base. These were examined more thoroughly. Twelve of the 52 data sets accounted for about 70% (1328) of the data.

Chick's 1984 [CHICK] report on West Valley glasses included the most data, 398 samples. Although this was a statistically designed study, we could not obtain good correlation coefficients between the variables using only the data base. We obtained a copy of the report. Chick et al. were able to develop models for their data. Except for the data from Strachan's 198_ report on SRL 131 glass, we were not able to see correlations between variables in the data base, viewed independent of the reports. Most of the 52 reports or compilations were not available to us. Several were private communications or interim reports, and thus not widely disseminated.

We did not look at every report individually, except for Strachan's 1985 report and the five reports containing the most data. Excluding these six reports, we did not attempt to break them apart according to certain variables, since this would have been extremely laborious, while working without the descriptive information for each study presumably given in each report. Such a detailed effort is the responsibility of each author.

Our purpose was to examine the data base as a whole to see if it provided any comprehensive picture of leach rates of various glasses under standard conditions. Unfortunately, it does not. It is best used as a reference for common data from several experimental studies.

ACKNOWLEDGMENTS

The authors gratefully acknowledge the contribution of Roberta Riel and Sy Vogler in providing Quality Assurance coordination and oversight to the program. Also the contribution of Roberta Riel in preparation of the report is greatly appreciated.

Work supported by the U.S. Department of Energy, Office of Environmental Restoration and Waste Management, under Contract W-31-109-ENG-38.

REFERENCES

ABRAJANO-1

T. A. Abrajano, Jr., J. K. Bates, T. J. Gerding, and W. L. Ebert, The Reaction of Glass During Gamma Irradiation in a Saturated Tuff Environment, Part 3: Long-Term Experiments at 1 x 10^4 rad/hour, Argonne National Laboratory Report ANL-88-14, (1988).

ABRAJANO-2

T. A. Abrajano, J. K. Bates, A. B. Woodland, J. P. Bradley, and W. L. Bourcier, "Secondary Phase Formation during Nuclear Waste-Glass Dissolution," Clay and Clay Miner. 38, 537-548 (1990).

AINES

R. D. Aines, "Estimates of Radionuclide Release from Glass Waste Forms in a Tuff Repository and the Effects on Regulatory Compliance," Am. Ceram. Soc., 3rd Int. Symp. on Nuclear Waste Disposal, Chicago, IL, (1986).

BARKATT-1

Aa. Barkatt, Al. Barkatt, and W. Sousanpour, "Gamma Radiolysis of Aqueous Media and Its Effects on the Leaching Processes of Nuclear Waste Disposal Materials," Nucl. Technol. 60, 218-227 (1983).

BARKATT-2

Aa. Barkatt, E. Saad, R. Adiga, W. Sousanpour, Al. Barkatt, and M. Adel-Hadadi, "Leaching of Natural and Nuclear Waste Glasses in Seawater," Appl. Geochim. 4, 593-603 (1989).

BATES-1

J. K. Bates, T. A. Abrajano, Jr., B. M. Biwer, C. R. Bradley, W. L. Ebert, J. J. Mazer, D. J. Wronkiewicz, and J. E. Young, "Critical Review of Parameters Affecting Glass Reaction in an Unsaturated Environment," draft submitted to DOE-HQ/EM (1990).

BATES-2

J. K. Bates and T. J. Gerding, One-Year Results of the NNWSI Unsaturated Test Procedure: SRL 165 Glass Application, Argonne National Laboratory Report ANL-85-41 (1986).

BATES-3

J. K. Bates, T. A. Abrajano, Jr., D. J. Wronkiewicz. T. J. Gerding, and C. A. Seils, Strategy for Experimental Validation of Waste Package Performance Assessment, Argonne National Laboratory Report ANL-90/21 (1990).

BATES-4

J. K. Bates, C. R. Bradley, J. P. Bradley, N. L. Dietz, W. L. Ebert, J. W. Emery, T. J. Gerding, J. C. Hoh, J. J. Mazer, and J. E. Young, Unsaturated Glass Testing for DOE Program in Environmental Restoration and Waste Management, Annual Report, October 1989-September 1990, Argonne National Laboratory Report ANL-90/40 (1991).

BATES-5

J. K. Bates, "Disposal of Vitrified Waste in an Unsaturated Environment," High Level Radioactive Waste Management, Proc. of 2nd Annual Int. Conf., Las Vegas, NV, April 28-May 1, 1991, Vol. 1, p. 700 (1991).

BATES-6

J. K. Bates and T. J. Gerding, Application of the NNWSI Unsaturated Test Method to Actinide Doped SRL 165 Type Glass, Argonne National Laboratory Report ANL-89/24 (1990).

BATES-7

J. K. Bates et al. "Annual Report to the Repository Technology Program," submitted to the Repository Technology Program (1990).

BATES-8

J. K. Bates, D. F. Fischer, and T. J. Gerding, The Reaction of Glass During Gamma Irradiation in a Saturated Tuff Environment, Part I: SRL 165 Glass, Argonne National Laboratory Report ANL-86-62 (1986).

BATES-9

J. K. Bates, X. Feng, C. R. Bradley, and E. C. Buck, "Comparison of Leach Behavior between Fully Radioactive and Simulated Nuclear Waste Glasses through Long-Term Testing. Part 2. Reacted Layer Analysis," to be presented at Waste Management '92, Tucson, Arizona, March 1-5, 1992.

BAXTER

R. G. Baxter, Description of Defense Waste Processing Facility Reference Waste Form and Canister, Savannah River Laboratory Report DP-1606 (1988).

BIBLER-1

N. E. Bibler, "Leaching of Fully Radioactive SRP Nuclear Waste Glass in Tuff Ground Water in Stainless Steel Vessels," Adv. Ceram. 20, 619 (1986).

BIBLER-2

N. E. Bibler, G. G. Wicks, and V. M. Oversby, "Leaching Savannah River Plant Nuclear Waste Glass in a Saturated Tuff Environment," Mater. Res. Soc. Symp. Proc. 44, 247-256 (1985).

BIBLER-3

N. E. Bibler and J. K. Bates, "Product Consistency Leach Tests of Savannah River Site Radioactive Waste Glasses," presented at the Fall 1989 Meeting of the Mater. Res. Soc., Boston, MA, November 26-December 1, 1989.

BIBLER-4

N. E. Bibler and G. Wicks, Leaching Savannah River Plant Nuclear Waste Glass in a Saturated Tuff Environment, Lawrence Livermore National Laboratory Report UCRL 91258 (1984).

BIBLER-5

N. E. Bibler and C. M. Jantzen, The Product Consistency Test and Its Role in the Waste Acceptance Process, Savannah River Laboratory Report DP-MS-88-188 (1989).

BIBLER-6

N. E. Bibler, "Characterization of Borosilicate Glass-Containing Savannah River Plant Radioactive Waste," Am. Chem. Soc. Symp. Ser. 246, 359-372 (1983).

BOURCIER

W. L. Bourcier, D. Peiffer, K. Knauss, K. McKeegan, and D. Smith, "A Kinetic Model for Borosilicate Glass Dissolution Based on the Dissolution Affinity of a Surface Reaction Layer," Mat. Res. Soc. Symp. Proc. 176, 209-216 (1990).

BRADLEY

C. R. Bradley, N. L. Dietz, and J. K. Bates, "Shaping Particles for Ultramicrotomy," presented at Materials Research Society Fall Meeting, Boston, MA, December 2-6, 1991.

BURNS

W. G. Burns, A. E. Hughes, J. A. C. Marples, R. S. Nelson, and A. M. Stoneham, "Effects of Radiation on the Leach Rates of Vitrified Radioactive Waste," J. Nucl. Mater. 107, 245 (1982).

CHERMAK

J. A. Chermak and J. D. Rimstidt, "Estimating the Thermodynamic Properties (ΔG_f° and ΔH_f°) of Silicate Minerals at 298 K from the Sum of Polyhedral Contributions," Amer. Min. 74., 1023-1031 (1989).

CHICK

L. A. Chick, A. M. Bowen, R. O. Lokken, J. W. Wald, L. R. Bunnell, and D. M. Strachan, West Valley High Level Nuclear Waste Development: A Statistically Designed Mixture Study, Battelle Pacific Northwest Laboratory Report PNL-4992 (1984).

CUNNANE

J. C. Cunnane and J. K. Bates, "The Role of Laboratory Analog Experiments in Assessing the Performance of Waste Package Materials," Mat. Res. Soc. Symp. Proc. 212, 885-892 (1991).

DEER

W. A. Deer, R. A. Howie, and J. Zussman, An Introduction to the Rock-Forming Minerals, Longman Group Limited, London, p. 340 (1966).

EBERT-1

W. L. Ebert, J. K. Bates, and W. L. Bourcier, "The Hydration of Borosilicate Waste Glass in Liquid Water and Steam at 200°C," Waste Mgmt. 11, 205-221 (1991).

EBERT-2

W. L. Ebert, J. K. Bates, and T. J. Gerding, The Reaction of Glass During Gamma Irradiation in a Saturated Tuff Environment, Part 4: SRL 165, ATM-1c, and ATM-8 Glasses at 1E3 R/h and 0 R/h, Argonne National Laboratory Report ANL-90/13 (1990).

EBERT-3

W. L. Ebert, J. K. Bates, T. A. Abrajano, Jr., and T. J. Gerding, "The Influence of Penetrating Gamma Radiation on the Reaction of Simulated Nuclear Waste Glass in Tuff Groundwater," Ceram. Trans. 9, 155-164 (1990).

EBERT-4

W. L. Ebert and J. K. Bates, "The Reaction of Synthetic Nuclear Waste Glass in Steam and Hydrothermal Solution," Mat. Res. Soc. Symp. Proc. 176, 339-346 (1990).

FENG-1
X. Feng, unpublished data, The Catholic University of America (1990).

FENG-2
X. Feng and I. L. Pegg, personal communication, The Catholic University of America (1991).

GARD
J. A. Gard, "Interpretation of Electron Diffraction Patterns," in Electron Microscopy in Mineralogy, ed. H.-R. Wenk, Springer-Verlag, Berlin, pp. 52-67 (1976).

GUVEN
N. Guven, "Smectites," Hydrous Phyllosilicates, ed. S. W. Bailey, Mineralogical Society of America, Washington, DC, Chapter 13 (1988).

HOLLAND
T. J. B. Holland, "Dependence of Entropy on Volume for Silicate and Oxide Minerals: A Review and a Predictive Model," Amer. Min. 74, 5-13 (1989).

JANTZEN
C. M. Jantzen, Glass Compositions and Frit Formulations Developed for DWPF, memo C. M. Jantzen to M. J. Plodinec, Savannah River Laboratory Report DPST-88-952 (1988).

JERCINOVIC
M. J. Jercinovic and R. C. Ewing, Basaltic Glasses from Iceland and the Deep Sea: Natural Analogues to Borosilicate Nuclear Waste Glass, JSS Project Technical Report 88-01 (1988).

JSS
JSS Project Phase II: Final Report of Work Performed at Studsvik Energiteknic AB and at Swiss Federal Institute for Reactor Research, Japanese, Swiss, Swedish Project Report JSS-85-01 (1985).

LINACRE
J. K. Linacre and W. R. Marsh, The Radiation Chemistry of Heterogeneous and Homogeneous Nitrogen and Water Systems, AERE Report R-10027 (1981).

LIND
S. C. Lind, Radiation Chemistry of Glasses, Am. Chem. Soc. Monograph Ser., Reinhold Publishing Corp., New York (1961).

LINEHAM
J. J. Lineham, U.S. Nuclear Regulatory Commission, personal communication (1989).

MAZER-1
J. J. Mazer, Temperature Effects on Waste Glass Performance, Argonne National Laboratory Report ANL-91/17 (1991).

MAZER-2

J. J. Mazer, J. K. Bates, B. M. Biwer, and C. R. Bradley, "AEM Analyses of SRL 131 Altered as a Function of SA/V," presented the Materials Research Society Fall Meeting, Strasbourg, France, November 4-7, 1991.

MAZER-3

J. J. Mazer, J. K. Bates, C. M. Stevenson, and C. R. Bradley, "Obsidians and Tektites: Natural Analogues for Water Diffusion in Nuclear Waste Glasses," presented the Materials Research Society Fall Meeting, Strasbourg, France, November 4-7, 1991.

McVAY

G. L. McVay and L. R. Pederson, "Effect of Gamma Radiation on Glass Leaching," J. Am. Ceram. Soc. 64, 154-158 (1984).

PUTNIS

A. Putnis and J. D. C. McConnell, Principles of Mineral Behavior, Blackwell Scientific Publications, London, Chapter 5 (1980).

SCHEETZ-1

B. E. Scheetz, W. P. Freeborn, S. Komarneni, S. D. Atkinson, and W. B. White, "Comparative Study of Hydrothermal Stability Experiments: Application to Simulated Nuclear Waste," Nucl. Chem. Waste Mgmt. 2, 229-236 (1991).

SCHEETZ-2

B. E. Scheetz, W. P. Freeborn, D. K. Smith, Ch. Anderson, M. Zolensky, and W. B. White, "The Role of Boron in Monitoring the Leaching of Boron Silicate Waste Glass Forms," Mat. Res. Soc. Symp. Proc. 44, 129 (1985).

SCP

Site Characterization Plan, U.S. Department of Energy, Office of Civilian Radioactive Waste Management, DOE Report DOE/RW-0199 (1988).

STRACHAN

D. M. Strachan, L. R. Pederson, and R. O. Lokken, Results from Long-Term Interactions and Modeling of SRL-131 Glass with Aqueous Solutions, Battelle Pacific Northwest Laboratory Report PNL-5654 (1985).

TARDY

Y. Tardy and R. M. Garrels, "Prediction of Gibbs Energies of Formation-I. Relationships Among Gibbs Energies of Formation of Hydroxides, Oxides, and Aqueous Ions," Geochim. Cosmochim. Acta 40, 1051-1056 (1976).

VAN KONYNENBURG

R. A. Van Konynenburg, Radiation Chemical Effects in Experiments to Study the Reaction of Glass in an Environment of Gamma-Irradiated Air, Groundwater, and Tuff, Lawrence Livermore National Laboratory Report UCRL-53719 (1986).

VIELLARD

P. Viellard and Y. Tardy, "Estimation of Enthalpies of Formation of Minerals Based on Their Refined Crystal Structures," Am. J. Sci. 288, 997-1040 (1988).

WELTON

J. E. Welton, SEM Petrology Atlas, The American Assoc. of Petroleum Geologists, Tulsa, OK (1984).

WCP

DWPF Waste Form Compliance Plan, U.S. DOE Report DPST-86-746 (1988).

WRONKIEWICZ

D. J. Wronkiewicz, J. E. Young, and J. K. Bates, "Effects of Alpha and Gamma Radiation on Glass Reaction in an Unsaturated Environment," Mat. Res. Soc. Symp. Proc. 212, 99-106 (1991).

YOKAYAMA

H. Yokayama, H. P. Hermansson, H. Christenson, I. K. Bjorner, and L. Werme, "Corrosion of Simulated Nuclear Waste Glass in a Gamma Radiation Field," Mat. Res. Soc. Symp. Proc. 44, 601-608 (1985).

Distribution for ANL-92/9

Internal:

J. K. Bates (25)
J. E. Battles
J. C. Cunnane
J. E. Harmon
J. E. Helt
M. J. Steindler
ANL Patent Dept.
ANL Contract File
TIS Files (3)

External:

DOE-OSTI (2)
ANL Library
Manager, Chicago Operations Office, DOE
A. Bindokas, DOE-CH
J. C. Haugen, DOE-CH
Chemical Technology Division Review Committee Members:
S. Baron, Brookhaven National Laboratory, Upton, NY
D. L. Douglas, Consultant, Bloomington, MN
N. Jarrett, Noel Jarrett Associates, Lower Burrell, PA
J. G. Kay, Drexel University, Philadelphia, PA
J. Stringer, Electric Power Research Institute, Palo Alto, CA
J. B. Wagner, Arizona State University, Tempe, AZ
R. G. Wymer, Consultant, Oak Ridge, TN
T. Ahn, U. S. Nuclear Regulatory Commission, Washington, DC
D. H. Alexander, USDOE, Civilian Radioactive Waste Management, Washington, DC
J. Allison, USDOE, Environmental Restoration and Waste Management, Germantown, MD
S. Bates, Idaho Falls, ID
H. Benton, B&W Fuel Company, Las Vegas, NV
A. Berusch, USDOE, Civilian Radioactive Waste Management, Washington, DC
N. E. Bibler, Westinghouse Savannah River Company, Aiken, SC
J. M. Boak, USDOE, Yucca Mountain Site, Las Vegas, NV
K. Boomer, Westinghouse Hanford Company, Richland, WA
W. Bourcier, Lawrence Livermore National Laboratory, Livermore, CA
A. Brandstetter, Science Applications International Corp., Las Vegas, NV
M. H. Campbell, Westinghouse Hanford Company, Richland, WA
K. A. Chacey, USDOE, Office of Waste Management, Germantown, MD
D. Chesnut, Lawrence Livermore National Laboratory, Livermore, CA
P. Cloke, Science Applications International Corp., Las Vegas, NV
M. O. Cloninger, Yucca Mountain Project Office, Las Vegas, NV
D. Codell, U. S. Nuclear Regulatory Commission, Washington, DC
S. Coplan, U. S. Nuclear Regulatory Commission, Washington, DC
S. P. Cowan, USDOE, Office of Waste Operations, Germantown, MD
J. Davidson, U. S. Environmental Protection Agency, Washington, DC
R. S. Dyer, Yucca Mountain Project Office, Las Vegas, NV
R. C. Ewing, Department of Geology, University of New Mexico, Albuquerque, NM

R. Fish, B&W Fuel Company, Las Vegas, NV
C. P. Gertz, Yucca Mountain Project Office, Las Vegas, NV
S. E. Gomberg, USDOE, Civilian Radioactive Waste Management, Washington, DC
T. Gutmann, USODE, Office of Waste Management, Germantown, MD
D. Harrison-Giesler, Yucca Mountain Project Office, Las Vegas, NV
B. Hastings, TRW Environmental Safety Systems, Fairfax, VA
C. Interrante, U. S. Nuclear Regulatory Commission, Washington, DC
C. Jantzen, Westinghouse Savannah River Company, Aiken, SC
L. J. Jardine, Lawrence Livermore National Laboratory, Livermore, CA
W. S. Ketola, USDOE, West Valley Project Office, West Valley, NY
D. A. Knecht, Westinghouse Idaho Nuclear Company, Idaho Falls, ID
W. L. Kuhn, Battelle Pacific Northwest Laboratory, Richland, WA
W. Lee, University of California, Berkeley, CA
J. C. Lehr, USDOE, Defense Waste and Transportation Management, Germantown, MD
H. Leider, Lawrence Livermore National Laboratory, Livermore, CA
D. Livingston, USDOE, Yucca Mountain Site, Characterization Project Office, Las Vegas, NV
J. J. Lorenz, USDOE, Yucca Mountain Site, Characterization Project Office, Las Vegas, NV
H. Manaktala, Southwest Research Institute, San Antonio, TX
J. M. Matusek, State of New York, Department of Health, Albany, NY
T. W. McIntosh, USDOE, Office of Waste Management, Germantown, MD
G. B. Mellinger, Battelle Pacific Northwest Laboratory, Richland, WA
R. Morissette, Science Applications International Corp., Las Vegas, NV
P. K. Nair, Southwest Research Institute, San Antonio, TX
J. L. Nelson, Westinghouse Hanford Company, Richland, WA
W. O'Connell, Lawrence Livermore National Laboratory, Livermore, CA
R. Palmer, West Valley Nuclear Services, West Valley, NY
U-Sun Park, Science Applications International Corp., Las Vegas, NV
W. D. Pearson, Savannah River Laboratory, Aiken, SC
C. Peterson, U. S. Nuclear Regulatory Commission, Washington, DC
T. H. Pigford, University of California, Berkeley, CA
M. J. Plodinec, E. I. DuPont, Savannah River Laboratory, Aiken, SC
W. G. Ramsey, Westinghouse Savannah River Company, Aiken, SC
C. G. Russomanno, USDOE, Civilian Radioactive Waste Management, Washington, DC
P. S. Schaus, Westinghouse Hanford Company, Richland, WA
J. Sproull, Westinghouse Savannah River Company, Aiken, SC
D. Stahl, B&W Fuel Company, Las Vegas, NV
R. Stout, Lawrence Livermore National Laboratory, Livermore, CA
D. Strachan, Battelle Pacific Northwest Laboratories, Richland, WA
V. Trice, USDOE, Office of Waste Management, Germantown, MD
C. N. Wilson, Westinghouse Hanford Company, Richland, WA
N. C. Garisto, Atomic Energy of Canada, Pinawa, Manitoba, CANADA
B. Grambow, Kernforschungszentrum Karlsruhe, GmbH, WEST GERMANY
W. Lutze, Hahn-Meitner-Institut, Gliennickerstrasse, GERMANY
P. Van Isegham, Boerecamp, BELGIUM
E. Vernaz, Centre d'Etudes Nucleares de la Valle du Rhone, Marcoule, FRANCE
L. Werme, Svensk Karnbranslehantering AB, Stockholm, SWEDEN

END

DATE FILMED

6/5/92